Introduction to Electrical Engineering II
Electrical Machines and Power Electronics

Bikash Sah

Universität Siegen / IAS Interconnected Automation Systems

Content

1. An initial overview of electrical machines and drives
2. Fundamentals- electrical, electromagnetic principles and magnetic materials
3. Transformers
4. DC machines
5. Induction machines
6. Synchronous machines
7. An initial overview of power electronics
   - Application examples
   - Energy, work, and power
   - Linear vs. switched power conversion
   - Course outline
8. DC-DC converters
   - Step-down converter
   - Step-down converter: output capacitor
   - Step-down converter: circuit realization and operation modes
   - Step-up converter
   - Buck-boost converter

Table of contents

An initial overview of electrical machines and drives

Bikash Sah

Universität Siegen / IAS Interconnected Automation Systems

Course Overview

The course will be in two parts with 3 modules each.

1. Electrical Machines
   - Module 1: Fundamentals
   - Module 2: Transformers
   - Module 3: Rotating machines
2. Power Electronics
   - Module 1: Fundamentals
   - Module 2: Power converter topologies
   - Module 3: Introduction to electrical drives

Pattern of class:
Day: Thursday, every week
Time: 8 am to 10 am (theory) and 10 am to 12 pm (tutorial) (ideally but it can change)
Holidays: 1st May, 29 May, and 19 June 2025. As required classes will be rescheduled.

The teaching team

Bikash Sah

Silas Florian Elter

Oliver Wallscheid**

Contact

- Email: see chair's homepage
- Offices: H-A building, 4th floor
- Individual appointments on request (remote or personally)
- Multiple relevant courses are offered by the Chair. Check link!

** The content of the slides for this course is based on 43IAS6000V and 43IAS1101V, prepared and delivered in past by Prof. Dr.-Ing Oliver Wallscheid.

Part I: Electrical Machines

What is an electrical machine?

Electrical machine

An electrical machine is a device that converts electrical energy into mechanical energy or vice versa.

- Electrical energy is routed via machine's external wiring connected to the terminal box.
- Mechanical energy is transferred via the shaft (if it is a rotatory machine).
- Historic timetable of the electrical machine development: KIT article (by M. Doppelbauer)

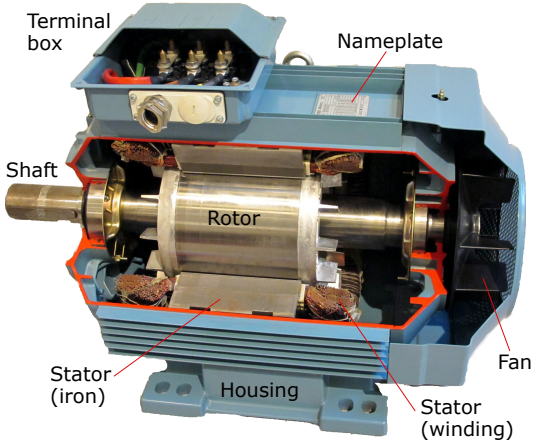

Fig. 1.1: Example of an electrical machine (source: derived from Wikimedia Commons, public domain)

Some exemplary electrical machines

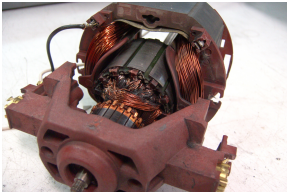

(a) DC machine (source: Wikimedia Commons, Marrci, CC BY-SA 3.0)

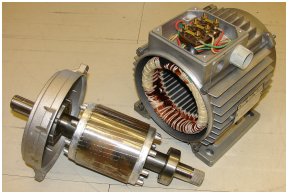

(b) Induction machine (source: Wikimedia Commons, Zureks, CC BY-SA 4.0)

(c) Permanent magnet machine (source: Wikimedia Commons, Andrez, CC BY-SA 4.0)

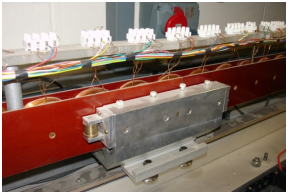

(d) Linear permanent magnet machine (source: Wikimedia Commons, Zureks, CC BY-SA 4.0)

The machine as an electrical-mechanical converter

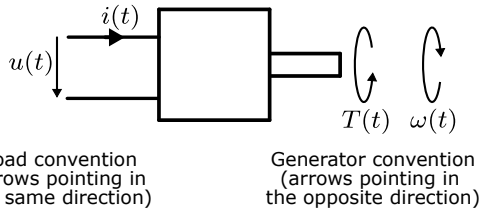

(a) Rotational converter

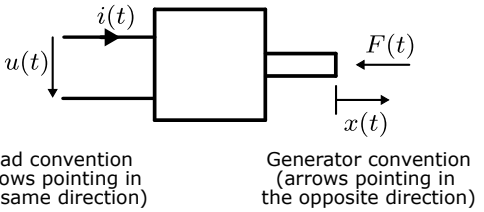

(b) Translational converter

Fig. 1.3: Electrically and mechanically free body diagrams of motors as energy converters with variable notation: time t, voltage u, current i, force F, displacement x, torque T and rational speed ω (adapted from J. Böcker, *Elektrische Antriebstechnik*, Paderborn University, 2020)

Some basic mechanical terms (recap)

	Translational converter	Rotational converter
Kinematic quantities		
Displacement / angle	x	ε
Velocity	$v = \dot{x}$	$\omega = \dot{\varepsilon}$
Acceleration	$a = \dot{v} = \ddot{x}$	$\alpha = \dot{\omega} = \ddot{\varepsilon}$
Jerk	$j = \dot{a} = \ddot{v} = \dddot{x}$	$\rho = \dot{\alpha} = \ddot{\omega} = \dddot{\varepsilon}$
Dynamical quantities		
Force / torque	F	T
Mass / inertia	m	J
Mechanical power	$P_{\mathrm{me}} = Fv$	$P_{\mathrm{me}} = T\omega$
Work	$W[t_0, t] = \int_{t_0}^{t} P_{\mathrm{me}}(\tau)\,\mathrm{d}\tau$	$W[t_0, t] = \int_{t_0}^{t} P_{\mathrm{me}}(\tau)\,\mathrm{d}\tau$
Momentum / rotational momentum	$p = mv$	$L = \omega J$
Kinetic energy	$E_{\mathrm{kin}} = \frac{1}{2}mv^2$	$E_{\mathrm{kin}} = \frac{1}{2}J\omega^2$

Tab. 1.1: Basic mechanical terms for translational and rotational converters

Work vs. energy (recap)

Work

Work is the integral of the power over a time integral (or force over distance) and is a measure of the energy transfer.

Energy

Energy is the capacity to do work, that is, a quantity depending on the state of a system at a given point of time.

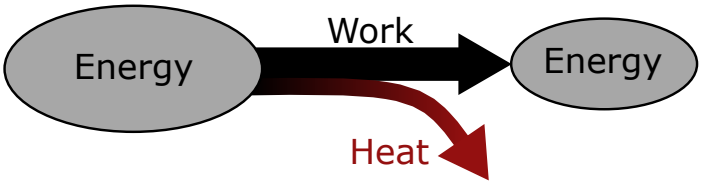

Fig. 1.4: Illustration addressing the work vs. energy terminology (simplified Sankey diagram)

Power balance of an electrical machine

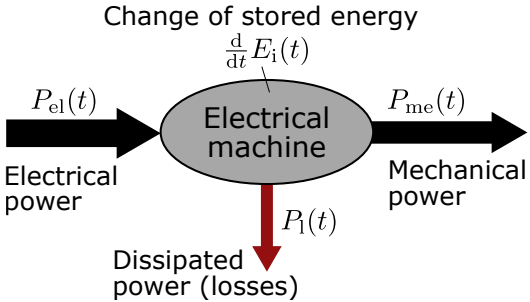

Fig. 1.5: Power balance of an electrical machine (illustrated in motoric operation)

The power balance

$$P_\mathrm{el}(t) = P_\mathrm{me}(t) + P_\mathrm{l}(t) + \frac{\mathrm{d}}{\mathrm{d}t}E_\mathrm{i}(t) \tag{1.1}$$

must hold for any point in time as energy is conserved, that is, not created or destroyed.

Four quadrants of machine operation

For the steady state ($\dot{E}_\mathrm{i}(t) = 0$), we define the machine efficiency as the ratio of the converted energy to the input energy:

$$\eta_\mathrm{mot} = \frac{P_\mathrm{me}}{P_\mathrm{el}} = 1 - \frac{P_\mathrm{l}}{P_\mathrm{el}}, \qquad (1.2)$$

$$\eta_\mathrm{gen} = \frac{P_\mathrm{el}}{P_\mathrm{me}} = 1 - \frac{P_\mathrm{l}}{P_\mathrm{me}}. \qquad (1.3)$$

Hence, we need to consider in which quadrant the machine operates as this will influence the power flow direction.

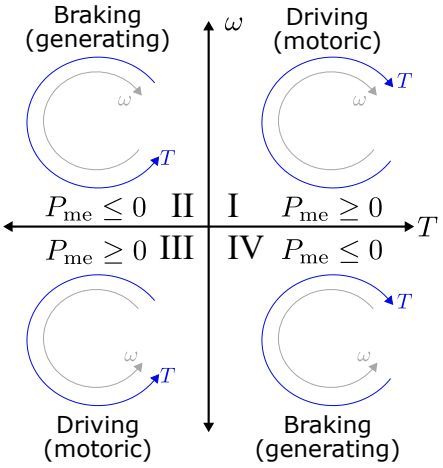

Fig. 1.6: Machine quadrants (derived from Wikimedia Commons, K. Pitter, CC BY-SA 3.0)

What is an electrical drive ?

Electrical drive

An electrical drive is a system that controls the torque, speed or position of an electrical machine connected to some mechanical process.

- Integrates the 'stupid' electrical machine into an 'intelligent' controlled system.
- The energy source and mechanical process ('load') are not part of the drive system.

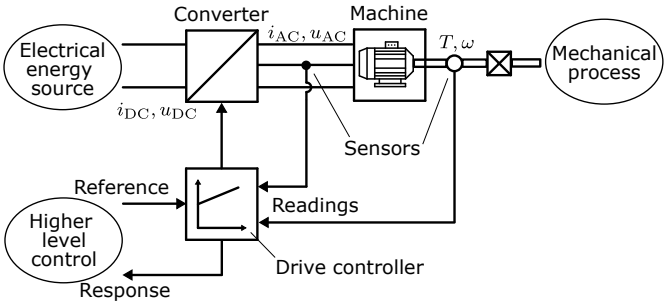

Fig. 1.7: Block diagram of an electrical drive (adapted from J. Böcker, *Elektrische Antriebstechnik*, Paderborn University, 2020)

Examples of electrical machine and drive applications (1)

(a) Electric cars (source: Wikimedia Commons, M. Movchin and F. Mueller, CC BY-SA 3.0)

(b) Wind turbine generators (source: pxhere.com, public domain)

(c) Factory robots (source: Wikimedia Commons, A. Reinhold, CC BY-SA 4.0)

(d) Electric tools (source: flickr.com, M. Verch, CC BY 2.0)

Examples of electrical machine and drive applications (2)

(e) High-speed trains (source: Wikimedia Commons, P. Elektro, CC BY-SA 3.0)

(f) Electric aircraft (source: Wikimedia Commons, M. Weinold, CC BY-SA 4.0)

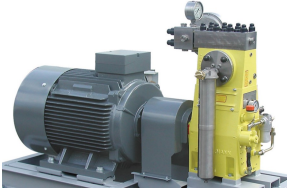

(g) Pumps (source: Wikimedia Commons, Hammelmann, CC BY-SA 3.0)

(h) Cranes (source: Wikimedia Commons, Belfast Dissenter, CC BY-SA 4.0)

A broad range of nominal power ratings

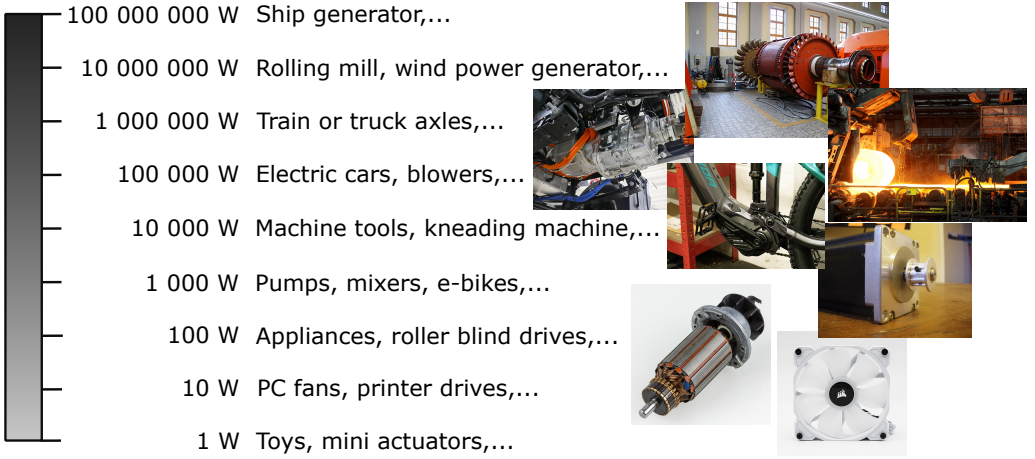

Fig. 1.9: Power range overview (inspired from A. Binder, *Elektrische Maschinen und Antriebe (lecture slides)*, Darmstadt University, 2022 with additional figure sources: A. Wolf, Asurnipal, M. Williams, R. Spekking, Foxcorner, A. Tredz and J. Halicki under varying CC licenses)

Why is knowledge about electric machines and drives important?

Electric machines and drives are an essential pillar of the modern society

Without electric machines and drives, our todays society would not be possible. Starting from providing electricity via electrical generators to powering electric vehicles, tools and entire factory production lines, electric machines and drives are everywhere, that is, they enable our today's living standard.

Energy efficiency and sustainability is key

Electric machines and drives utilize approx. 50 % of the global electricity with about 8 billion electric motors in use in the EU (source: European Commission and International Energy Agency). Therefore, improving their efficiency is an essential factor to reduce the global energy consumption and the associated CO_2 emissions.

Learning objectives

- Understand the basics of electrical and magnetics to build foundation of electrical machines.
- Understand the generation of magnetic fields, force formation and voltage induction in electrical machines.
- Differentiate the main types of electrical machines:
  - DC machines.
  - Induction machines.
  - Synchronous machines.
  - And their plentiful variants ...
- Understand their basic design and operation principles.
- Basic analysis on the operation of electrical machines
- Have fun learning about electrical machines and drives.

Necessary prior knowledge for this course

You should have a basic understanding of the following topics:

- Linear differential equations (modeling, solution techniques)
- Linear algebra basics (e.g., vector and matrix operations)
- Phasor algebra and complex numbers
- Basic signal theory knowledge (e.g., Fourier series, Laplace transform)
- Basic knowledge of electrical circuit theory
- Basic knowledge of basic physics (mechanics)

What we will not cover, but you do not need to know (covered in separate courses):

- Control engineering for electrical drive applications.
- Power electronics in depth involving analysis and controller design.

Recommended reading

- S. Chapman, Electric Machinery Fundamentals, Vol. 5, McGraw-Hill, 2011
- I. Boldea and S. Nasar, Electric Drives, Vol. 3, CRC Press, 2022
- A. Binder, Elektrische Maschinen und Antriebe (in German), Vol. 2, Springer, 2017
- D. Schröder and R. Kennel, Elektrische Antriebe: Grundlagen (in German), Vol. 7, Springer Vieweg, 2021
- PC Sen, Principles of Electric Machines and Power Electronics, International Adaptation. John Wiley & Sons, 2021.

Table of contents

Fundamental of Electrical Engineering (relevant topics)

Bikash Sah

Universität Siegen / IAS Interconnected Automation Systems

Basic Electrical Concepts

Phasors

- A phasor is a complex number representing a **sinusoidal** function.
- Sinusoid:

$$v(t) = V_m \cos(\omega t + \phi) \rightarrow \vec{V} = V_m e^{j\phi} \rightarrow V_m \angle \phi$$

  where, V_m is the peak amplitude, $\omega = 2\pi ft$, the phase in radians, t is seconds, and f is the frequency in cycles per second, and ϕ is the phase angle (angular difference or shift between the voltage and current waveforms in an AC circuit).
- Simplifies AC analysis using algebra.
- Addition/Subtraction: Vector addition.
- Multiplication/Division: Magnitudes multiply/divide, angles add/subtract.
- Example:

$$\vec{V_1} = 10\angle 30^\circ, \quad \vec{V_2} = 5\angle -10^\circ$$

$$\vec{V_1} + \vec{V_2} = ?$$

(Hint: convert to rectangular form)

Single-phase and three-phase systems

- **Single Phase**
- Consists of one alternating voltage source.
- Voltage expressed as:

$$v(t) = V_m \cos(\omega t + \phi)$$

- Used in residential and light commercial loads.

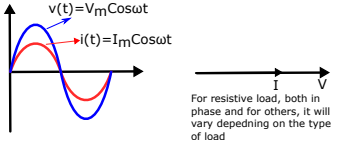

Fig. 2.1: Illustration of a single phase waveform

- **Three Phase**
- Composed of three sinusoidal voltages of equal magnitude and frequency, **120**$^\circ$ apart.
- Line voltages:

$$v_a(t) = V_m \cos(\omega t)$$
$$v_b(t) = V_m \cos(\omega t - 120^\circ)$$
$$v_c(t) = V_m \cos(\omega t + 120^\circ)$$

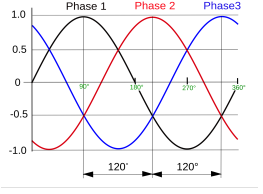

Fig. 2.2: Illustration of a three phase waveform (source: Wikimedia Commons, J JMesserly, CC BY 3.0)

Star/Wye Connection Basics

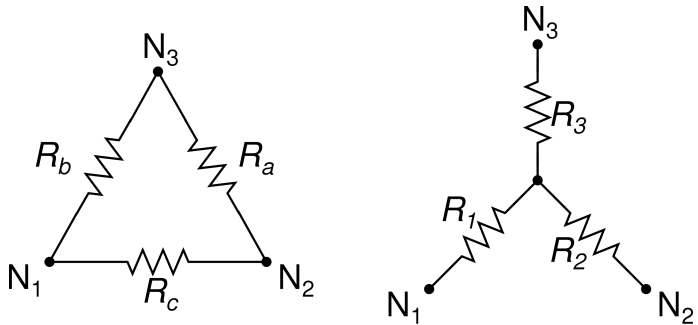

Fig. 2.3: Δ and Y circuits (source: Wikimedia Commons, CC BY-SA 3.0)

Star/Wye Connection Basics

- **Star (Y) connection**
- Each phase connected to a common neutral point.
- Line and phase voltages:

$$V_L = \sqrt{3} V_{ph}, \quad \angle 30^\circ$$

where V_L is the line voltage and V_{ph} is the phase voltage.

- Line and phase currents: $I_L = I_{ph}$ where I_L is the line current, and I_{ph} is the phase current.

- **Δ connection**
- Line and phase voltages: $V_L = V_{ph}$
- Line and phase currents:

$$I_L = \sqrt{3} I_{ph}, \quad \angle 30^\circ$$

where I_L is the line current and I_{ph} is the phase current.

- **Power** in both configurations (balanced load):

$$P = \sqrt{3} V_L I_L \cos \phi$$

where ϕ is the angle between voltage and current and P is the active power.

- Both configurations deliver the same power if balanced and same load impedance.

Phasors

- Active (Real) Power:

$$P = VI\cos\phi \quad \text{(Watts)}$$

- Reactive Power:

$$Q = VI\sin\phi \quad \text{(VAR)}$$

- Apparent Power:

$$S = VI \quad \text{(VA)}$$

- Relationship:

$$S^2 = P^2 + Q^2$$

- Power factor:

$$\text{pf} = \cos\phi = \frac{P}{S}$$

- Graphical representation using a power triangle.

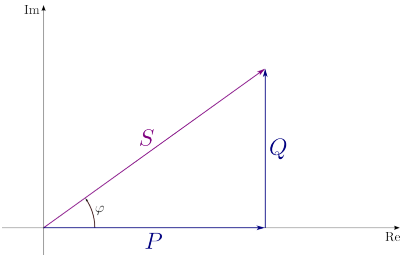

Fig. 2.4: Power triangle

Basic Magnetic Concepts

Ampère's circuital law: magnetic field strength

Relates the circulation of a magnetic field around a closed loop to the electric current passing through the loop:

$$\text{Integral form:} \quad \oint_{\partial S} \boldsymbol{H} \cdot \mathrm{d}\boldsymbol{s} = I_\mathrm{f}, \qquad (2.1)$$

$$\text{Differential form:} \quad \nabla \times \boldsymbol{H} = \boldsymbol{J}_\mathrm{f}. \qquad (2.2)$$

Here, $\boldsymbol{H}$ is the magnetic field strength, $\boldsymbol{J}_\mathrm{f}$ is the free current density, and I_f is the free current enclosed by the loop ∂S.

- Free current: current that is not bound to a material (i.e., without polarization and magnetization currents).
- SI-units: $[H] = \frac{\mathrm{A}}{\mathrm{m}}$, $[J] = \frac{\mathrm{A}}{\mathrm{m}^2}$

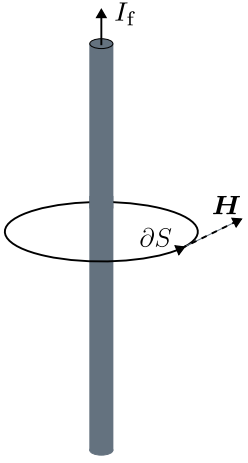

Fig. 2.5: Illustration of the magnetic field strength $\boldsymbol{H}$ around a simple conductor

Ampère's circuital law: free current example

What is the free current I_f enclosed by the loop ∂S?

- The current I_1 flows in the direction of the loop ∂S (according to right-hand rule).
- The current I_1 must be counted N times due to the N turns of wire around the loop ∂S.
- The current I_2 flows in the opposite direction of the loop ∂S (according to right-hand rule).
- Result:

$$I_\mathrm{f} = N \cdot I_1 - I_2.$$

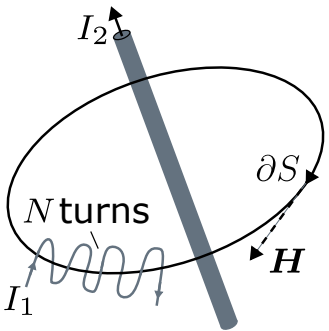

Fig. 2.6: Arrangement with two electrical conductors

Ampère's circuital law: simple solenoid example

Ampere's law for magnetic flux density $\boldsymbol{B}$ in vacuum:

$$\text{Integral form:} \quad \oint_{\partial S} \boldsymbol{B} \cdot \mathrm{d}\boldsymbol{s} = \mu_0 I, \tag{2.3}$$

$$\text{Differential form:} \quad \nabla \times \boldsymbol{B} = \mu_0 \boldsymbol{J}. \tag{2.4}$$

Here, μ_0 is the permeability of free space, $\boldsymbol{J}$ is the total current density and I is the total current enclosed by the loop ∂S.

- SI-unit: $[B] = \mathsf{T} = \frac{\mathsf{Vs}}{\mathsf{m}^2} = \frac{\mathsf{N}}{\mathsf{Am}}$
- Example contour ∂S on the right covering N turns and length l (flux density within solenoid):

$$\oint_{\partial S} \boldsymbol{B} \cdot \mathrm{d}\boldsymbol{s} = N\mu_0 I \Leftrightarrow B = \frac{N\mu_0 I}{l}$$

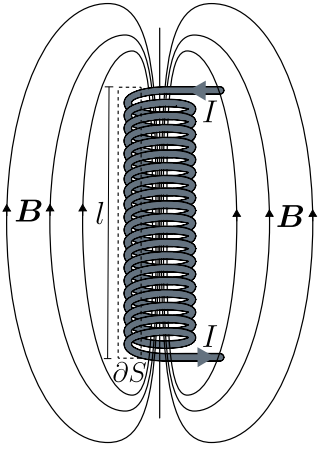

Fig. 2.7: Magnetic flux density evaluated at the contour $\partial \boldsymbol{S}$ (adapted from: Wikimedia Commons, Goodphy, CC BY-SA 4.0)

Shortcomings of the Ampère's circuital law

Applying Ampère's circuital law to a capacitor with a changing electric field $\boldsymbol{E}$ leads to a contradiction:

- Applying (2.2) to S_1 yields:

$$\oint_{\partial S_1} \boldsymbol{H} \cdot \mathrm{d}\boldsymbol{s} = I.$$

- In the case of S_2 we receive:

$$\oint_{\partial S_2} \boldsymbol{H} \cdot \mathrm{d}\boldsymbol{s} = 0.$$

- However, both surfaces share the same bounding contour ∂S.
- Issue: The magnetic field strength $\boldsymbol{H}$ is not able to describe the displacement current.

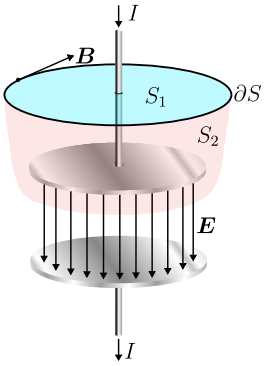

Fig. 2.8: Surfaces S_1 and S_2 share the same bounding contour ∂S. However, S_1 is pierced by conduction current, while S_2 is pierced by displacement current (adapted from: Wikimedia Commons, public domain).

Lorentz force

The force $\boldsymbol{F}$ acting on a particle of electric charge q with instantaneous velocity $\boldsymbol{v}$, due to an external electric field $\boldsymbol{E}$ and magnetic field $\boldsymbol{B}$, is given by

$$\boldsymbol{F} = q\left(\boldsymbol{E} + \boldsymbol{v} \times \boldsymbol{B}\right). \tag{2.5}$$

- The term $q\boldsymbol{E}$ is called the electric force.
- The term $q\left(\boldsymbol{v} \times \boldsymbol{B}\right)$ is called the magnetic force.
- In Cartesian coordinates, the Lorentz force is given by:

$$\begin{aligned} F_x &= q\left(E_x + v_y B_z - v_z B_y\right), \\ F_y &= q\left(E_y + v_z B_x - v_x B_z\right), \\ F_z &= q\left(E_z + v_x B_y - v_y B_x\right). \end{aligned} \tag{2.6}$$

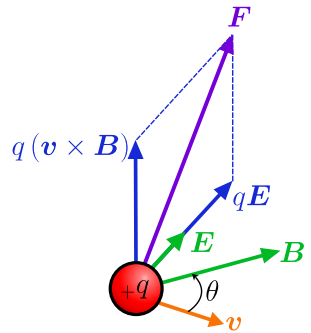

Fig. 2.9: Lorentz force $\boldsymbol{F}$ on a particle (of charge q) in motion (instantaneous velocity $\boldsymbol{v}$) with given $\boldsymbol{E}$ and $\boldsymbol{B}$ fields (adapted from: Wikimedia Commons, Maschen, CC0)

Hand rule of the magnetic Lorentz force

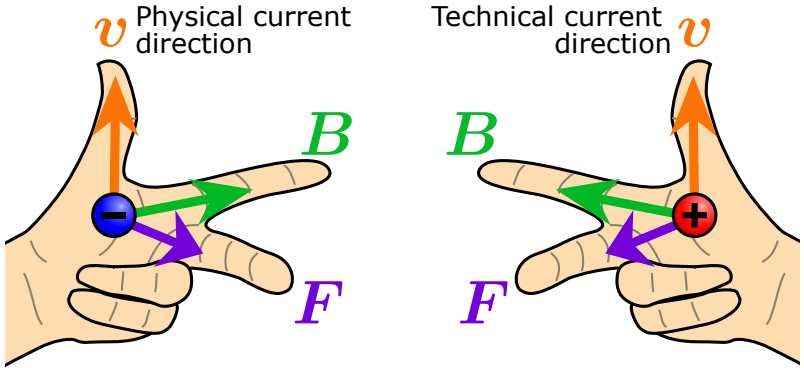

Fig. 2.10: Right and left hand rule for the magnetic Lorentz force $q\,(\boldsymbol{v} \times \boldsymbol{B})$ (adapted from: Wikimedia Commons, M. Run, CC BY-SA 3.0)

Lorentz force density for a continuous charge distribution

For a continuous charge distribution in motion, the Lorentz force density (force per unit volume) becomes:

$$\boldsymbol{f} = \rho\boldsymbol{E} + \boldsymbol{J} \times \boldsymbol{B}. \qquad (2.7)$$

- ρ is the charge density (charge per unit volume).
- $\boldsymbol{J} = \rho\boldsymbol{v}$ is the current density.

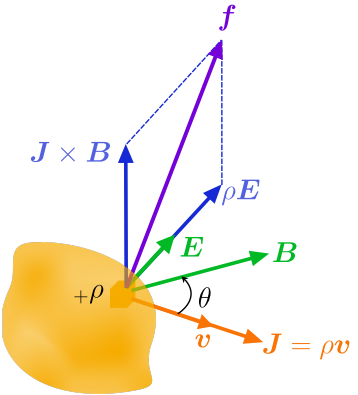

Fig. 2.11: Lorentz force density $\boldsymbol{f}$ on a continuous charge distribution (charge density ρ) in motion (adapted from: Wikimedia Commons, Maschen, CC0)

The Ampère – Maxwell equation

The charge of capacitor is:

$$Q = \oint_{S_2} \boldsymbol{D} \cdot \mathrm{d}\boldsymbol{S}.$$

If the electric field ($\boldsymbol{D} = \varepsilon_0 \varepsilon_\mathrm{r} \boldsymbol{E}$) changes, a displacement current results:

$$I_\mathrm{d} = \frac{\mathrm{d}}{\mathrm{d}t} \oint_{S_2} \boldsymbol{D} \cdot \mathrm{d}\boldsymbol{S}$$

- Is not a classical electric current (moving charges) but a term to describe the changing electric field.
- Above, ε_0 is the vacuum permittivity and ε_r is the relative permittivity of a material.

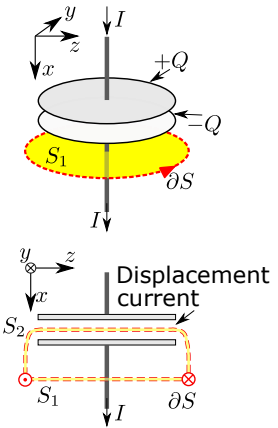

Fig. 2.12: Illustration for calculating the displacement current (adapted from: Wikimedia Commons, public domain).

The Ampère – Maxwell equation (cont.)

Adding the displacement current to (2.2) we receive the Ampère – Maxwell equation:

$$\text{Integral form:} \quad \int_{\partial S} \boldsymbol{H} \cdot \mathrm{d}\boldsymbol{s} = \iint_S \left(\boldsymbol{J}_\mathrm{f} + \frac{\mathrm{d}}{\mathrm{d}t} \boldsymbol{D} \right) \cdot \mathrm{d}\boldsymbol{S}, \tag{2.8}$$

$$\text{Differential form:} \quad \nabla \times \boldsymbol{H} = \boldsymbol{J}_\mathrm{f} + \frac{\partial \boldsymbol{D}}{\partial t}. \tag{2.9}$$

Above, $\boldsymbol{D}$ is the electric displacement field.

- SI-unit: $[D] = \frac{\mathsf{C}}{\mathsf{m}^2}$
- SI-unit: $[E] = \frac{\mathsf{V}}{\mathsf{m}}$
- $\varepsilon_0 \approx 8.854 \cdot 10^{-12} \, \frac{\mathsf{F}}{\mathsf{m}}$

Magnetic flux and flux linkage

The magnetic flux ϕ is the surface integral of the normal component of $\boldsymbol{B}$ over that surface:

$$\phi = \iint_S \boldsymbol{B} \cdot \mathrm{d}\boldsymbol{S}. \tag{2.10}$$

As there are no magnetic monopoles, the magnetic flux through a closed surface (which is covering a volume without holes) is always zero:

$$\oint_S \boldsymbol{B} \cdot \mathrm{d}\boldsymbol{S} = 0. \tag{2.11}$$

The flux linkage ψ is the product of the magnetic flux ϕ and the number of turns N of a coil:

$$\psi = N\phi. \tag{2.12}$$

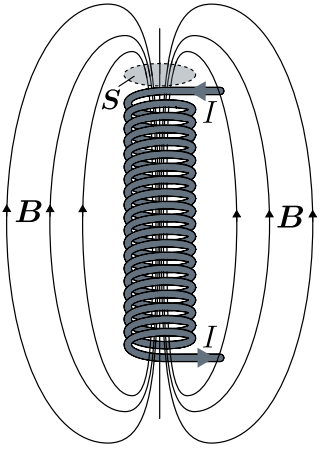

Fig. 2.13: Magnetic flux ϕ evaluated at the surface $\boldsymbol{S}$ (adapted from: Wikimedia Commons, Goodphy, CC BY-SA 4.0)

Magnetic leakage flux

- In the scenarios with multiple coils, the magnetic flux generated by one coil will influence also the other coils.
- Exception: two coils are perfectly perpendicular to each other.
- However, the magnetic flux typically does not fully couple with the other coils
- The difference is the leakage flux ϕ_σ.

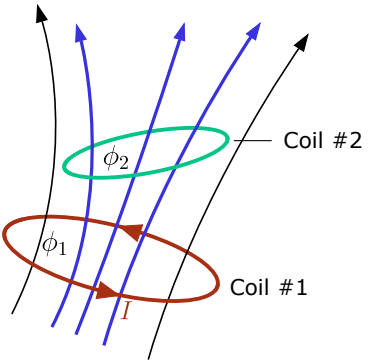

Fig. 2.14: The magnetic flux ϕ_1 generated by the current I does only partly couple with the second coil, while the difference $\phi_1 - \phi_2$ is the leakage flux (adapted from: Wikimedia Commons, M. Wacenovsky, public domain)

Inductance

The inductance L describes the ratio between the magnetic flux linkage $\psi(t)$ to the current $i(t)$:

$$\psi(t) = Li(t). \tag{2.13}$$

Example: From the solenoid in Fig. 2.13 we know that the magnetic flux linkage ψ is:

$$\psi = N \iint_S \boldsymbol{B} \cdot \mathrm{d}\boldsymbol{S} = \frac{1}{l} N^2 \mu_0 I \pi r^2$$

with r being the radius of the solenoid. Hence, the inductance L is:

$$L = \frac{\psi}{I} = \frac{N^2 \mu_0 \pi r^2}{l}.$$

- SI-unit: $[L] = \mathsf{H} = \frac{\mathsf{Vs}}{\mathsf{A}}$
- The inductance is an important parameter describing inductive systems.

Self and mutual inductance

Based on the inductive coupling between the two coils from Fig. 2.15, we can define the magnetic flux matrix:

$$\boldsymbol{\phi} = \begin{bmatrix} \phi_{11} & \phi_{12} \\ \phi_{21} & \phi_{22} \end{bmatrix}. \qquad (2.14)$$

- ϕ_{11}: magnetic flux component of coil 1 due to its own current i_1
- ϕ_{12}: magnetic flux component of coil 1 due to the current i_2 in coil 2
- ϕ_{21}: magnetic flux component of coil 2 due to the current i_1 in coil 1
- ϕ_{22}: magnetic flux component of coil 2 due to its own current i_2

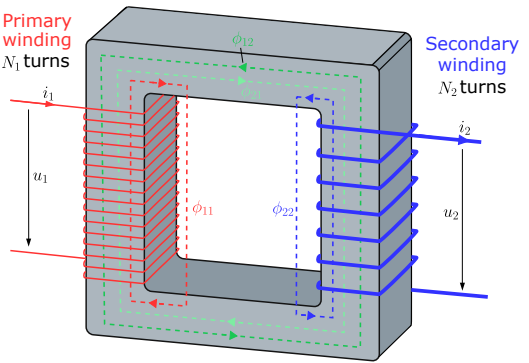

Fig. 2.15: Two coils coupled via a common core (adapted from: Wikimedia Commons, Bill C., CC BY-SA 3.0)

Self and mutual inductance (cont.)

Utilizing the permeance definition ("magnetic conductance")

$$\Lambda = \frac{\phi}{Ni}, \tag{2.15}$$

we can represent (2.14) as:

$$\phi_{11} = \Lambda_{11} N_1 i_1, \quad \phi_{12} = \Lambda_{12} N_2 i_2, \quad \phi_{21} = \Lambda_{21} N_1 i_1, \quad \phi_{22} = \Lambda_{22} N_2 i_2. \tag{2.16}$$

The resulting flux linkage per coil is then:

$$\begin{aligned} \psi_1 &= N_1 \left(\phi_{11} + \phi_{21} + \phi_{12}\right), & \psi_2 &= N_2 \left(\phi_{22} + \phi_{12} + \phi_{21}\right), \\ &= \underbrace{\left(\Lambda_{11} N_1^2 + \Lambda_{21} N_1^2\right)}_{L_1} i_1 + \underbrace{\Lambda_{12} N_1 N_2}_{M_{12}} i_2, & &= \underbrace{\left(\Lambda_{22} N_2^2 + \Lambda_{12} N_1^2\right)}_{L_2} i_2 + \underbrace{\Lambda_{21} N_1 N_2}_{M_{21}} i_1. \end{aligned} \tag{2.17}$$

Above, L_1 and L_2 are the self-inductances, M_{12} and M_{21} are the mutual inductances.

Self and mutual inductance (cont.)

Hence, we can define the flux linkages of both coils using the following inductance matrix:

$$\boldsymbol{\psi} = \begin{bmatrix} \psi_1 \\ \psi_2 \end{bmatrix} = \begin{bmatrix} L_1 & M_{12} \\ M_{21} & L_2 \end{bmatrix} \begin{bmatrix} i_1 \\ i_2 \end{bmatrix} = \boldsymbol{L}\boldsymbol{i}. \tag{2.18}$$

Due to the symmetry of the inductive coupling, the mutual inductances are identical:

$$M_{12} = M_{21} = M. \tag{2.19}$$

Based on (2.17), we can also split the self-inductance L_i of the i-th coil into the sum of the leakage inductance $L_{i,\sigma}$ and the magnetizing inductance $L_{i,\mathrm{m}}$:

$$L_i = L_{i,\sigma} + L_{i,\mathrm{m}} = \Lambda_{ii} N_i^2 + \Lambda_{ji} N_i^2 \quad \text{with} \quad i \neq j. \tag{2.20}$$

Finally, we can define the coupling coefficient k as:

$$k = \frac{M}{\sqrt{L_1 L_2}}, \qquad 0 \leq k \leq 1, \tag{2.21}$$

which indicates how strong or week the inductive coupling between the coils is.

Boosting the magnet field with ferromagnetic materials

While $\boldsymbol{H}$ depends on the currents applied to an object, $\boldsymbol{B}$ depends on the material properties of the object. In free space (vacuum), the relation is linear and represented by the magnetic constant μ_0:

$$\boldsymbol{B} = \mu_0 \boldsymbol{H} \quad \text{with} \quad \mu_0 \approx 4\pi \cdot 10^{-7} \, \frac{\mathrm{N}}{\mathrm{A}^2}. \tag{2.22}$$

To boost $\boldsymbol{B}$ for a given $\boldsymbol{H}$, ferromagnetic materials are typically used. These materials have a high relative magnetic permeability μ_r:

$$\boldsymbol{B} = \mu \boldsymbol{H} = \mu_0 \mu_\mathrm{r} \boldsymbol{H}. \tag{2.23}$$

Note that μ_r is a dimensionless quantity and that (2.23) assumes linear and isotropic material behavior.

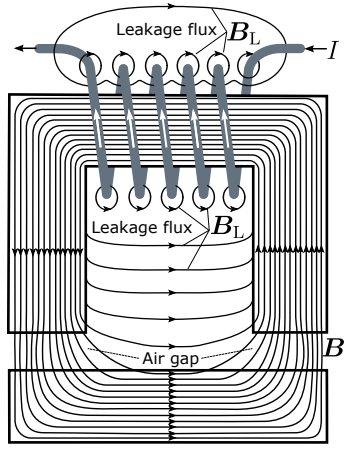

Fig. 2.16: Simplified magnetic field lines of an iron yoke with a coil (adapted from: Wikimedia Commons, public domain)

Relative permeability and magnetic saturation

Material	μ_r (range)
Air / copper / aluminum	($\approx$)1
Iron (99.8 % pure)	5000
Electrical steel	2000 - 35000
Ferrite	200 - 20000

Tab. 2.1: Typical relative permeabilities of materials

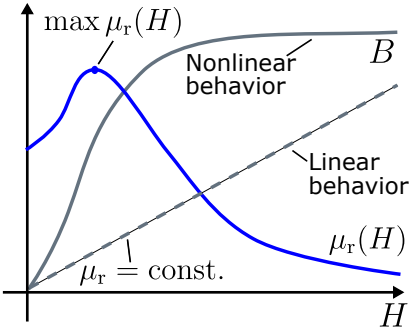

Fig. 2.17: Illustrative magnetization curves for ferromagnets (and ferrimagnets) and corresponding permeabilities (adapted from: Wikimedia Commons, public domain)

Linear magnetic behavior ($\mu_\mathrm{r} = \mathrm{const.}$) is only a local approximation. When considering larger H ranges, the (differential) permeability becomes nonlinear:

$$\mu_\mathrm{r}(H) = \frac{\mathrm{d}B}{\mathrm{d}H}. \qquad (2.24)$$

Magnetic domains (1)

- Magnetic domains are regions within a material where the magnetic moments of atoms are aligned ("mini magnets").
- The magnetization within each domain points in a uniform direction, but the magnetization of different domains may point in different directions.

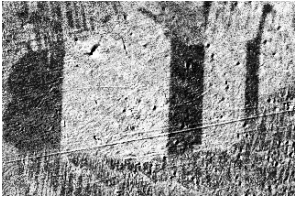

Fig. 2.18: Animation of moving domain walls (source: Wikimedia Commons, Zureks, CC BY-SA 3.0)

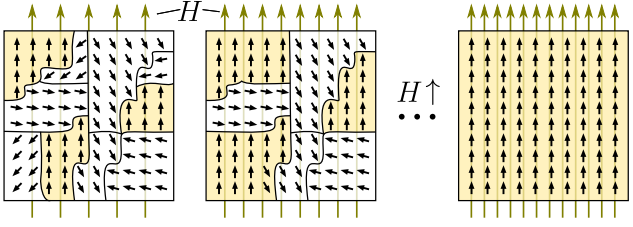

Fig. 2.19: Change of magnetic domains due to an external magnetic field (adapted from: Wikimedia Commons, M. Run, CC BY-SA 4.0)

Magnetic domains (2)

- A large region of material with a constant magnetization throughout creates a large magnetic field (diagram a) below). This requires a lot of magnetostatic energy stored in the field.
- To reduce this energy, the sample can "split" into two domains, with the magnetization in opposite directions in each domain which reduces the overall field (diagram b) below).
- To reduce the field energy further, each of these domains can split also, resulting in smaller parallel domains with magnetization in alternating directions, with smaller amounts of field outside the material (diagram c) below).

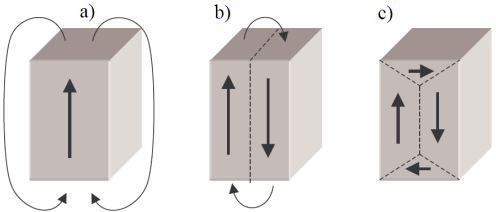

Fig. 2.20: Simplified representation of the formation of magnetic domains on the basis of energy minimization (source: Wikimedia Commons, public domain)

Hysteresis

- Material defects lead to small, random jumps in magnetization called Barkhausen jumps.
- Domain walls move irregularly.
- Process also depends on the history of the magnetization process (dynamic system).

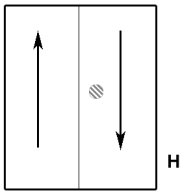

Fig. 2.21: Animation of the Barkhausen jump (source: Wikimedia Commons, public domain)

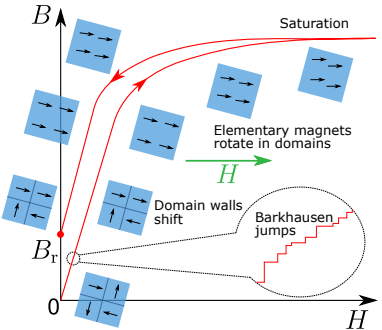

Fig. 2.22: Simplified hysteresis curve in first quadrant with magnetic domains illustration (adapted from: Wikimedia Commons, Fralama, CC BY-SA 3.0)

Hysteresis curve and losses

- With an external and varying field H, a closed hysteresis curve is obtained.
- Traversing through the curve requires to move the domain walls and rotate the elementary magnets within the domains.
- This process requires work and leads to heat dissipation (losses).
- The area enclosed by the hysteresis curve is identical to the relative remagnetization work (per volume, that is, $[w_\mathrm{h}] = \frac{\mathrm{J}}{\mathrm{m}^3}$):

$$w_\mathrm{h} = \oint \boldsymbol{H} \cdot \mathrm{d}\boldsymbol{B}. \qquad (2.25)$$

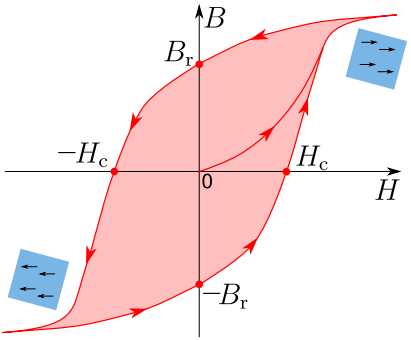

Fig. 2.23: Exemplary hysteresis curve with B_r being the remanence field density and H_c the coercivity field strength

How can we model the hysteresis losses?

1. **Data look-up table:** Measure the hysteresis curve and its losses directly on a test bench (cf. MagNet project data hub).
2. **Loss-fitted models:** Use empirical models to fit the hysteresis losses (e.g., Steinmetz model):

$$P_\mathrm{h} = k_\mathrm{h} f^a \max\{B\}^b.$$

3. **Curve-fitted models:** Use empirical models to describe the hysteresis curve and derive the losses (e.g., ODE as in the Jiles-Atherton model):

$$\frac{\mathrm{d}B}{\mathrm{d}H} = f(B, H).$$

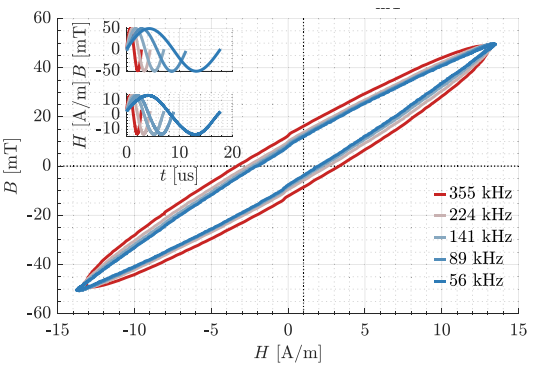

Fig. 2.24: Measured B-H loops for sinusoidal excitation at different frequencies (source: IEEE TPEL, Serrano et al., CC BY 4.0)

Alternative to boost the magnet field: permanent magnets (PMs)

- Create own persistent magnetic fields.
- Consist of hard ferromagnetic (or ferrimagnetic) materials.
- Nearly constant magnetiziation offset $\boldsymbol{B}_{\mathrm{PM}}$ in the usual operating range:

$$\boldsymbol{B} = \mu_0 \mu_{\mathrm{r}} \boldsymbol{H} \approx \mu_0 \boldsymbol{H} + \boldsymbol{B}_{\mathrm{PM}}. \qquad (2.26)$$

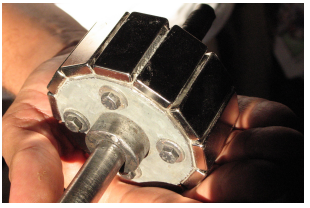

Fig. 2.25: PMs on a rotor (source: flickr.com, AIDG, CC BY-NC-SA 2.0)

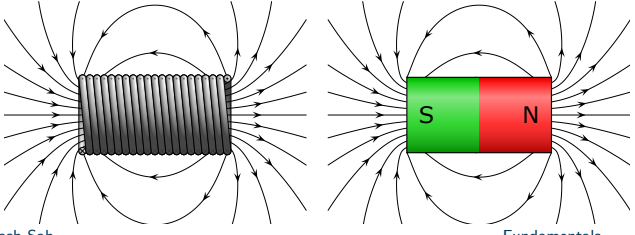

Fig. 2.26: Permanent magnets as alternatives to current-based excitation (source: Wikimedia Commons, M. Run, CC BY-SA 3.0)

Hysteresis curve of permanent magnets

- PM's magnetization is nearly completely saturated and constant in common operation area.
- The greater the coercivity H_c, the greater the resistance of the PM to demagnetization by external fields.
- Beyond the so-called knee point, PMs are (partially) demagnetized.
- Important figure of merit is the so-called energy product:

$$(BH)_\mathrm{max} = \max\{-BH\}\,. \qquad (2.27)$$

- The higher $(BH)_\mathrm{max}$ the less PM material is needed for an application.

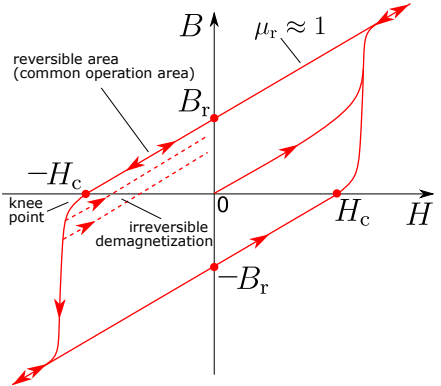

Fig. 2.27: Exemplary hysteresis curve of a permanent magnet

Hysteresis curve of permanent magnets (temperature dependence)

- Besides pressure and vibrations, PMs are also sensitive to temperature.
- The coercivity H_{c} and the remanence B_{r} decrease with increasing temperature.
- Hence, with higher temperatures, a PM gets more susceptible to demagnetization.

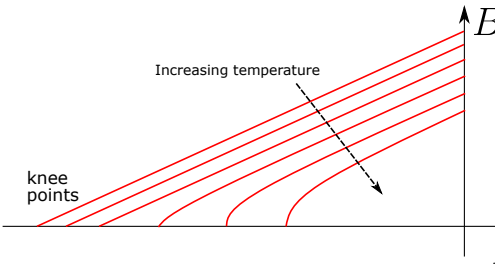

Fig. 2.28: Qualitative representation of the temperature dependence of permanent magnets

Energy product overview of permanent magnets

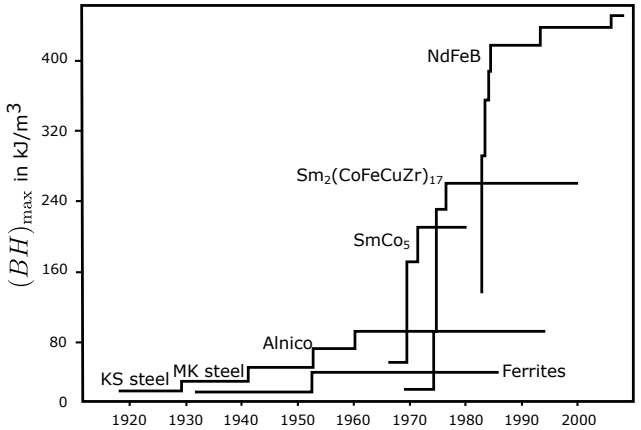

Fig. 2.29: Historic development of PM materials and their energy product (adapted from: Wikimedia Commons, Kopiersperre, CC BY-SA 4.0)

Manufacturing process of NdFeB permanent magnets

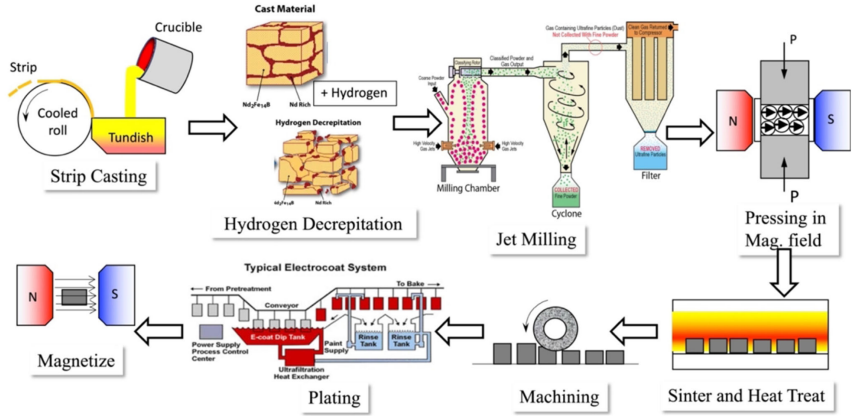

Fig. 2.30: Basic process steps for the NdFeB-based magnets (source: Springer JOM, J. Cui et al., CC BY 4.0)

Electromagnetic induction (Maxwell – Faraday equation)

A changing magnetic field induces an electric field according to the Maxwell – Faraday equation:

Integral form: $$\oint_{\partial S} \boldsymbol{E} \cdot \mathrm{d}\boldsymbol{s} = -\frac{\mathrm{d}}{\mathrm{d}t} \iint_S \boldsymbol{B} \cdot \mathrm{d}\boldsymbol{S}, \tag{2.28}$$

Differential form: $$\nabla \times \boldsymbol{E} = -\frac{\partial \boldsymbol{B}}{\partial t}. \tag{2.29}$$

Here, $\boldsymbol{E}$ is the electric field strength and $\boldsymbol{S}$ is the surface enclosed by the loop $\partial \mathcal{S}$.

- Lentz's law: The induced electric field opposes the change in magnetic field (negative sign above).

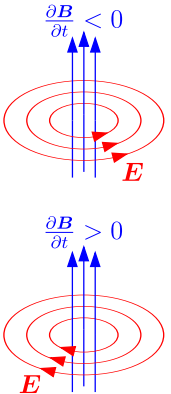

Fig. 2.31: Representation of the magnetic and electric field relation (adapted from: Wikimedia Commons, Qniemiec, CC BY-SA 3.0)

Electromotive force (EMF) and electromagnetic induction

If the integration path ∂S is identical to a conductor loop, the changing magnetic field induces a voltage u_i (electromotive force, EMF) according to Faraday's law:

$$u_\mathrm{i} = \oint_{\partial S} \boldsymbol{E} \cdot \mathrm{d}\boldsymbol{s} = -\frac{\mathrm{d}}{\mathrm{d}t} \iint_S \boldsymbol{B} \cdot \mathrm{d}\boldsymbol{S}. \qquad (2.30)$$

- Despite its name, the term EMF does not describe a force in the physical sense (as u_i is obviously a voltage).
- The term remains a historical artifact from the early days of electrical engineering, but is still frequently used in today's literature.

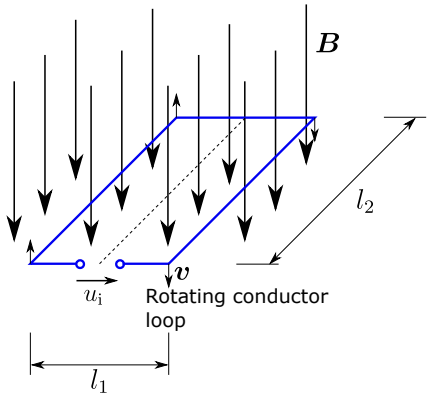

Fig. 2.32: Induced voltage / EMF in a rotating conductor loop (adapted from: Wikimedia Commons, M. Lenz, CC0 1.0)

Intermediate wrap up: electromagnetic principles and magnetic materials

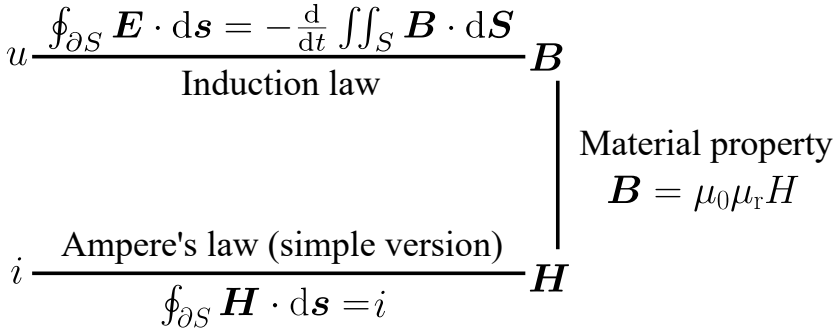

Fig. 2.33: Illustration of the connections between the phenomena discussed previously (derived from: Wikimedia Commons, M. Lenz, CC0 1.0)

Magnetic networks

- **Motivation**: Model magnetic systems with a simplified lumped-parameter approach and apply analysis techniques analogous to electric networks.
- **Assumption**: magnetic field is homogenous within a lumped element (cf. Fig. 2.34).
- The magnetic flux per element is:

$$\phi_k = A_k B_k. \tag{2.31}$$

- The magnetic voltage (magnetomotive force – MMF) per element is:

$$\theta_k = l_k H_k. \tag{2.32}$$

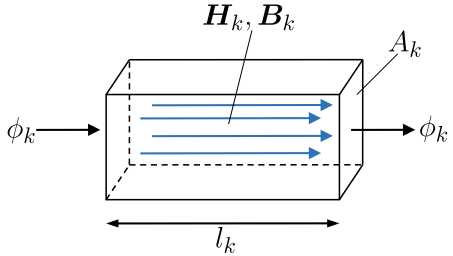

Fig. 2.34: Magnetic element with homogenous magnetic field (adapted from J. Böcker, Mechatronics and Electrical Drives, CC BY-NC-ND)

Magnetic networks (cont.)

- The magnetic reluctance per element is:

$$R_k = \frac{\theta_k}{\phi_k} = \frac{l_k}{\mu_0 \mu_{\mathrm{r}k} A_k}. \qquad (2.33)$$

- The magnetic conductivity (or permeance) per element is:

$$\Lambda_k = \frac{1}{R_k} = \frac{\mu_0 \mu_{\mathrm{r}k} A_k}{l_k}. \qquad (2.34)$$

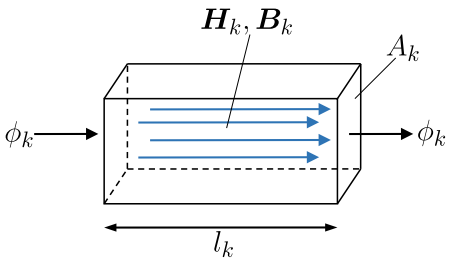

- As the magnetic field is free of sources ($\nabla \cdot \boldsymbol{B} = 0$), it follows (node rule – analogous to Kirchhoff's first law):

$$\sum_k \phi_k = 0. \qquad (2.35)$$

Magnetic networks (cont.)

Considering magnetostatic situations where the displacement current can be neglected, Ampère's law reads:

$$\oint_{\partial S} \boldsymbol{H} \cdot \mathrm{d}\boldsymbol{s} = I_{\mathrm{f}} = NI = \sum_k \theta_k = \sum_k l_k H_k. \tag{2.36}$$

So far, the equation has not the structure of the second Kirchhoff's law (loop rule). However, we can force this desired format by placing the term with the electric currents on the left-hand side of the equation:

$$\sum_k \theta_k - \theta_0 = 0 \quad \text{with} \quad \theta_0 = NI \text{ (MMF term)}. \tag{2.37}$$

Comparison: electric and magnetic network quantities

Electric network			**Magnetic network**		
Voltage	$u = \int \boldsymbol{E} \cdot \mathrm{d}\boldsymbol{s}$	V	Magnetomotive force	$\theta = \int \boldsymbol{H} \cdot \mathrm{d}\boldsymbol{s}$	A
Electric field	$\boldsymbol{E}$	$\frac{\mathsf{V}}{\mathsf{m}}$	Magnetic field	$\boldsymbol{H}$	$\frac{\mathsf{A}}{\mathsf{m}}$
Current	i	A	Magnetic flux	ϕ	Vs
Resistance	R	Ω	Reluctance	R	$\frac{1}{\mathsf{H}}$
Conductance	G	S	Permeance	Λ	H
Conductivity	σ	$\frac{\mathsf{S}}{\mathsf{m}}$	Permeability	μ	$\frac{\mathsf{H}}{\mathsf{m}}$
Ohm's law	$u = Ri$		Hopkinson's law	$\theta = R\phi$	
Kirchoff's first law	$\sum i_k = 0$		Equivalent first law	$\sum \phi_k = 0$	
Kirchoff's second law	$\sum u_k = 0$		Equivalent second law	$\sum \theta_k - \theta_0 = 0$	

Tab. 2.2: Electric and magnetic network quantities and their analogies

Magnetic network example: simple magnetic actuator

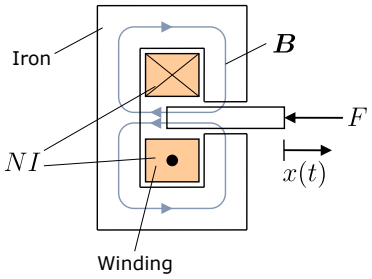

(a) Simple magnetic actuator

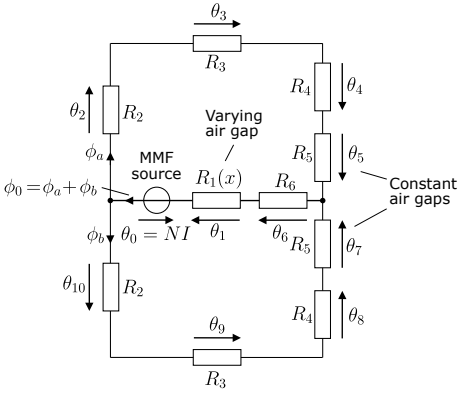

(b) Magnetic network representation of the actuator

Fig. 2.35: Example for a simple magnetic actuator and its magnetic network representation (adapted from J. Böcker, Mechatronics and Electrical Drives, CC BY-NC-ND)

Eddy currents

- A changing magnetic field induces a voltage.
- In bulky conductive materials (e.g., electromagnetic steel) this voltage drives currents called eddy currents.
- Eddy currents lead to energy losses and heat dissipation.
- To reduce eddy currents, laminated cores are used as they decrease the effective current path width and, therefore, increase the effective resistance per sheet.

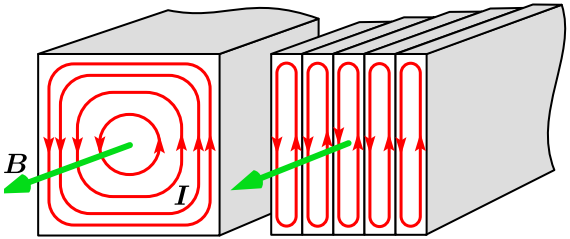

Fig. 2.36: Eddy current formations in solid and laminated steel cores (source: Wikimedia Commons, Chetvorno, CC0)

Eddy currents: single sheet example

Assumption

Sheet's thickness d is much smaller than the sheet's width w and the magnetic flux density $\boldsymbol{B}$ is homogenous in the normal direction of S and introduces a sinusoidal excitation $\boldsymbol{B}(x, y, t) = \hat{B}\sin(\omega t)$.

From (2.29) integrating over S, we get

$$2wE(x,t) = -\frac{\partial B}{\partial t} 2xw$$

with $2w$ being the effective contour length of ∂S and $2xw$ being the effective surface area.

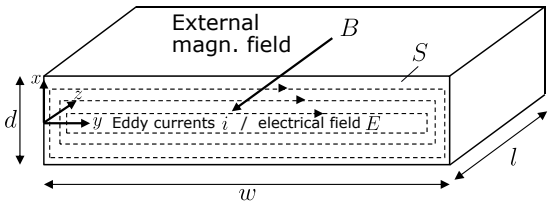

Fig. 2.37: Single sheet and induced eddy currents

Eddy currents: single sheet example (cont.)

With Ohm's law and the material conductivity σ, we get the current density J:

$$J(x,t) = \sigma E(x,t) = -x\sigma \frac{\partial B}{\partial t}.$$

Inserting the assumed magnetic flux density distribution it follows:

$$J(x,t) = -x\sigma\omega\hat{B}\cos(\omega t).$$

The relative power loss (per volume) density $p(x,t)$ results in:

$$p(x,t) = \frac{1}{\sigma}J^2(x,t) = x^2\sigma\omega^2\hat{B}^2\cos^2(\omega t).$$

The average power loss per volume (considering the x-direction) is:

$$p(t) = \frac{1}{d}\int_{-d/2}^{d/2} p(x,t)\mathrm{d}x = \frac{1}{12}\sigma\omega^2 d^2\hat{B}^2\cos^2(\omega t).$$

Eddy currents: single sheet example (cont.)

The average power loss per volume and time is then:

$$p = \frac{1}{T}\int_0^T p(t)\mathrm{d}t = \frac{1}{24}\sigma\left(\omega d\hat{B}\right)^2.$$

Although this is a simplified model, it shows the significance of

- the sheet's thickness d,
- and excitation conditions ω and $\hat{B}$.

This finding motivated empirical fitting approaches, like Bertotti's model for the eddy currents:

$$p_\mathrm{e} \approx k_\mathrm{e} f^2 \hat{B}^2.$$

Power loss types in electrical machines

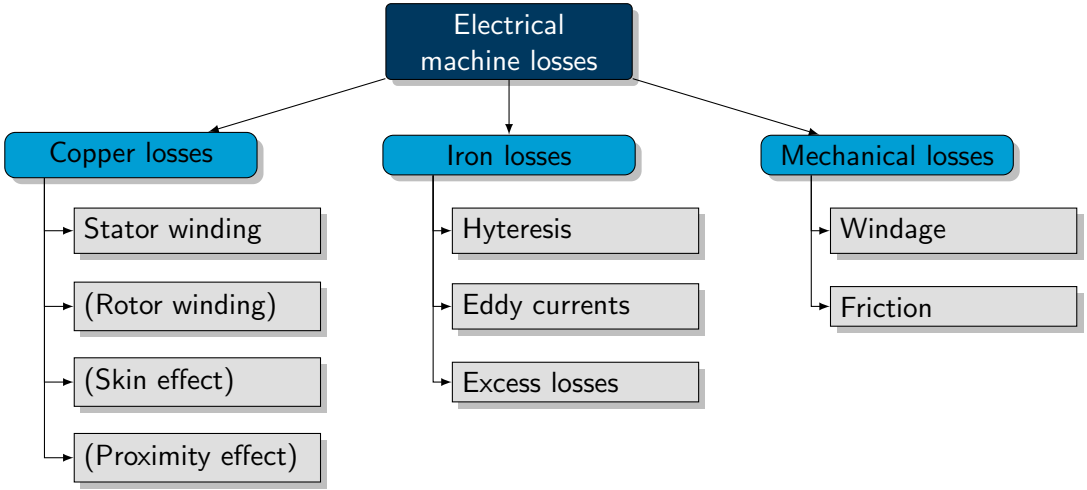

Fig. 2.38: Overview of power loss types in electrical machines

Table of contents

Transformers

Bikash Sah

Universität Siegen / IAS Interconnected Automation Systems

Transformer definition

Transformer

A transformer is a static device that transfers electrical energy between two or more circuits through electromagnetic induction. It converts the AC voltage levels between inputs and outputs.

- While a transformer is sometimes called a "static machine", it does not meet the formal definition of an electrical machine (compare first chapter).
- However, transformers share some working principles with electrical machines and are also often used as components of electrical power systems including drives.

Fig. 3.1: Transformer integrated at a utility pole (source: pxhere.com, public domain)

Function and example use of transformers

- Voltage level adjustment: Can help to make increase or decrease voltage level(**step-up** for increase and **step-down** for decreasing).
- Electrical isolation: Provides galvanic isolation between circuits, enhancing safety and reducing noise.
- Impedance matching: Helps in matching impedance between different electrical devices or systems to maximize power transfer and minimize losses (**Maximum power transfer theorem!**)
- Load sharing: Multiple transformers can share load in parallel operation,

- Example need of transformers- power systems
  - The wires in power systems have resistance $\rightarrow I^2R/$Joule losses eminent
  - Ohm's law (V=IR), increase "V" reduce "I" for same power.
  - So, at increased voltage, the same power can be delivered by a high-voltage transmission line in reduced current but higher efficiency.

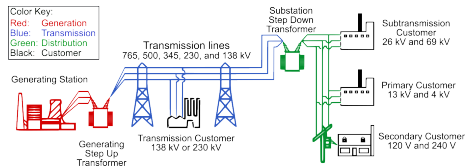

Fig. 3.2: Diagram of electric grid (source: United States Department of Energy, SVG version by User:J JMesserly, Public domain, via Wikimedia Commons, public domain)

Examples of transformers

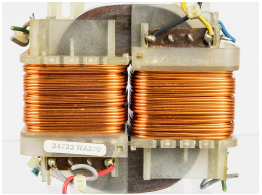

(a) Power supply transformer (source: Wikimedia Commons, R. Spekking, CC BY-SA 4.0)

(b) Single-phase transformer (source: Wikimedia Commons, Georg, CC BY-SA 4.0)

(c) Three-phase transformer (source: Wikimedia Commons, Asurnipal, CC BY-SA 4.0)

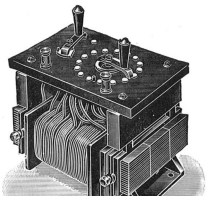

(d) Variable tapped transformer (source: Wikimedia Commons, public domain)

Types of transformers and working principle

- Based on voltage transformation- step up and step down.
- Based on number of phases- single phase, three phase, multi phase.
- Based on usage- power transformers typically used as generation transformer, transmission transformer, distribution transformers, current transformers (CT), voltage transformers (PT), isolation transformers, etc.
- Based on core medium- air core, iron/steel core, ferrite core, and nanocrystalline core.
- Based on construction- core type and shell type.

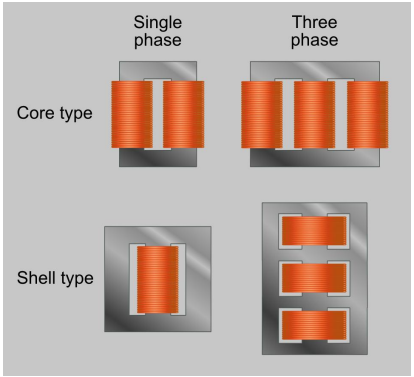

Fig. 3.4: Transformer winding formats (source: Wikimedia Commons, CC BY-SA 3.0)

Basic working principle- Faraday's Law of Electromagnetic Induction

- A changing magnetic flux in the primary coil induces an electromotive force (EMF) in the secondary coil.
- Mathematical expression: EMF $\propto \frac{d\psi}{dt}$, where ψ is the magnetic flux linkage through the core and $\frac{d\psi}{dt}$ is the rate of change of magnetic flux.
- An alternating current in the **primary winding** produces a time-varying magnetic field. This magnetic field links with the **secondary winding** through a magnetic core. The changing flux induces a voltage in the secondary winding.

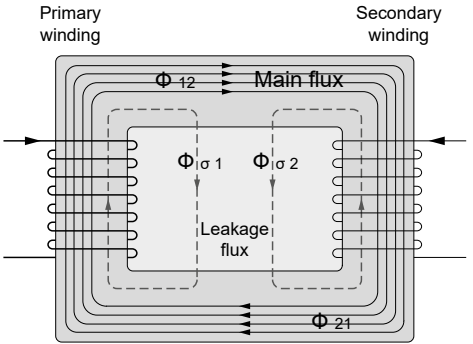

Fig. 3.5: Transformer flux linkage for working principle (source: Wikimedia Commons, Fred the Oyster, CC BY-SA 4.0)

Dot convention in transformers

- "Dot convention" or "Dot notation"- a method of indicating the relative polarity or phase relationship between the primary and secondary windings.
- **Purpose**: helps engineers and technicians understand the polarity of transformer windings.
- Dots mentioned– polarity important, else, does not matter.
- If current flows into the dotted terminal of one coil, the induced mutual voltage in the other coil will be positive at its dotted terminal. Conversely, if current flows out of the dotted terminal, the induced voltage will be negative at the dotted terminal.
- The polarity of the mutually induced voltage depends on the direction of current relative to the dot: current entering the dotted end of one winding results in a positive polarity at the dot of the coupled winding, while current leaving the dotted terminal results in a negative polarity at the other dot.

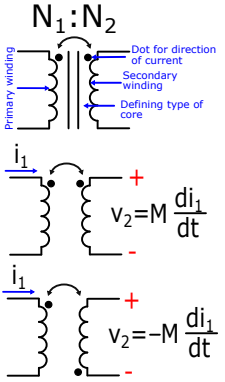

Fig. 3.6: Dot convention in transformer

Introduction to transformer- Ideal transformer

- Characteristics of an ideal transformer:
- **No resistance or reactance**: The transformer has no internal resistance or reactance, meaning that the primary and secondary windings have zero impedance.
- **Lossless**: No energy losses in the transformer (no copper or iron losses).
- **Perfect coupling**: All the magnetic flux produced by the primary winding links with the secondary winding (no leakage flux).
- **Linear**: The relationship between primary and secondary voltages and currents is linear (no saturation or non-linearity).
- **No phase shift**: The primary and secondary voltages are in phase (no phase difference).

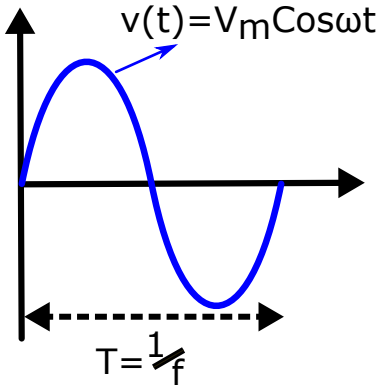

Fig. 3.7: A sinusoidal waveform or current or voltage in an ideal transformer

Voltage transformation in an ideal transformer

Using Faraday's Law:

$$e = -N\frac{d\psi}{dt} \tag{3.1}$$

For the primary and secondary windings:

$$e_1 = -N_1\frac{d\psi}{dt}, \quad e_2 = -N_2\frac{d\psi}{dt} \tag{3.2}$$

Dividing the two equations:

$$\frac{e_1}{e_2} = \frac{N_1}{N_2} \tag{3.3}$$

Assuming sinusoidal steady-state and ideal conditions (no losses):

$$\frac{U_1}{U_2} = \frac{N_1}{N_2} \tag{3.4}$$

Where:

- U_1, U_2: RMS voltages
- N_1, N_2: Turns in primary and secondary windings

Current transformation

For an ideal transformer:

$$\text{Input VA} = \text{Output VA} \tag{3.5}$$

$$U_1 I_1 = U_2 I_2 \tag{3.6}$$

From voltage transformation:

$$\frac{U_1}{U_2} = \frac{N_1}{N_2} \tag{3.7}$$

Substitute into power equation:

$$\frac{I_1}{I_2} = \frac{N_2}{N_1} \tag{3.8}$$

Where:

- I_1, I_2: Currents in primary and secondary
- Power is conserved under ideal conditions

Overview

Modelling of electrical machines helps in analysis, design, control, and simulation. Various modelling approaches are used depending on the application, complexity, and level of detail required.

- Steady-State Modelling
- Dynamic (Time-Domain) Modelling
- Electromagnetic (Field-Based) Modelling
- Equivalent Circuit Modelling
- Thermal Modelling
- Mechanical Modelling
- Data-Driven / Empirical Modelling
- Hybrid Modelling

Steady-State and Dynamic (time domain) Modelling

Steady state Modeling

- Assumes constant or periodic operating conditions.
- Useful for power flow, losses, voltage/current analysis under sinusoidal operation.
- Commonly used in:
  - Load flow studies
  - Motor rating selection
  - Efficiency estimation

Dynamic Modeling

- Captures transient and time-varying behavior.
- Based on differential equations and flux linkage dynamics.
- Common forms:
  - dq-axis model (Park's transformation)
  - State-space model
- Used in control design, simulation of startup/faults, and power electronics.

Electromagnetic and Equivalent Circuit Modeling

Electromagnetic (Field-Based) Modeling

- Solves Maxwell's equations using methods like FEM.
- Captures spatial variation of fields, core saturation, and parasitic effects.
- Used for:
  - Torque ripple/cogging analysis
  - Magnetic material optimization
  - Detailed design validation

Equivalent Circuit Modeling

- Simplified lumped-parameter model.
- Represents machines with resistances, inductances, and voltage sources.
- Used for:
  - Quick hand calculations
  - Educational and conceptual understanding
  - Basic control development

Thermal and Mechanical Modeling

Thermal Modeling

- Predicts temperature rise and heat dissipation.
- Models via lumped networks or FEM-based thermal simulations.
- Key for:
  - Overtemperature protection
  - Cooling system design
  - Electro-thermal coupling

Mechanical Modeling

- Models inertia, friction, damping, and mechanical loads.
- Integrated with electrical models in simulations.
- Applications include:
  - Speed/torque dynamics
  - Shaft vibration and failure analysis
  - Control loop tuning

Data-Driven and Hybrid Modeling

Data-Driven / Empirical Modeling

- Based on experimental data or system identification.
- No need for full physical understanding.
- Methods include:
  - Neural networks, lookup tables
  - Regression models, ML algorithms
- Useful when parameters are hard to measure or unknown.

Hybrid Modeling

- Combines multiple domains (electrical, thermal, mechanical).
- Balances accuracy and computational effort.
- Typical in:
  - Digital twin implementations
  - Real-time HIL simulators
  - Multi-physics co-simulation

Electromagnetic modeling of the single-phase transformer

Recap from (2.18): for some given current $\boldsymbol{i}$, the flux linkages $\boldsymbol{\psi}$ in the transformer windings are

$$\boldsymbol{\psi} = \begin{bmatrix} \psi_1 \\ \psi_2 \end{bmatrix} = \begin{bmatrix} L_1 & M \\ M & L_2 \end{bmatrix} \begin{bmatrix} i_1 \\ i_2 \end{bmatrix} = \boldsymbol{L}\boldsymbol{i}$$

where L_1 and L_2 are the self-inductances of the primary and secondary winding, respectively, and M is the mutual inductance.

Note: The above equation is an algebraic relation, that is, it is valid for any time instant t and applies to both AC and DC excitation of the transformer.

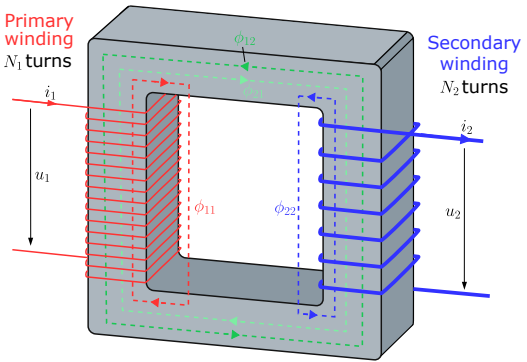

Dynamic modeling of the single-phase transformer

The dynamic transformer behavior can be represented by the ECD in Fig. 3.8, which also considers the internal resistances of the windings. Applying Faraday's law, the resulting differential equations are:

$$u_1(t) = R_1 i_1(t) + \frac{\mathrm{d}\psi_1(t)}{\mathrm{d}t}, \qquad u_2(t) = R_2 i_2(t) + \frac{\mathrm{d}\psi_2(t)}{\mathrm{d}t}. \tag{3.9}$$

Inserting (2.18) delivers:

$$u_1(t) = R_1 i_1(t) + L_1 \frac{\mathrm{d}i_1(t)}{\mathrm{d}t} + M \frac{\mathrm{d}i_2(t)}{\mathrm{d}t}, \qquad u_2(t) = R_2 i_2(t) + L_2 \frac{\mathrm{d}i_2(t)}{\mathrm{d}t} + M \frac{\mathrm{d}i_1(t)}{\mathrm{d}t}. \tag{3.10}$$

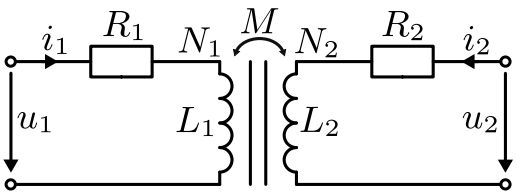

Fig. 3.8: General equivalent circuit diagram (ECD) of a transformer (note: that both ports of the transformer are denoted in the load convention reference frame which is an arbitrary representation decision).

Dynamic modeling of the single-phase transformer (cont.)

The model (3.10) can be represented by the T-type ECD in Fig. 3.9. It may be noted that $L_1 - M$ and $L_2 - M$ can have negative values due to the model representation.

By rearranging (3.10), we can also write the dynamic transformer model in vector-matrix form:

$$\begin{bmatrix} u_1(t) \\ u_2(t) \end{bmatrix} = \boldsymbol{u}(t) = \begin{bmatrix} R_1 & 0 \\ 0 & R_2 \end{bmatrix} \begin{bmatrix} i_1(t) \\ i_2(t) \end{bmatrix} + \begin{bmatrix} L_1 & M \\ M & L_2 \end{bmatrix} \frac{\mathrm{d}}{\mathrm{d}t} \begin{bmatrix} i_1(t) \\ i_2(t) \end{bmatrix} = \boldsymbol{R}\boldsymbol{i}(t) + \boldsymbol{L}\frac{\mathrm{d}}{\mathrm{d}t}\boldsymbol{i}(t). \qquad (3.11)$$

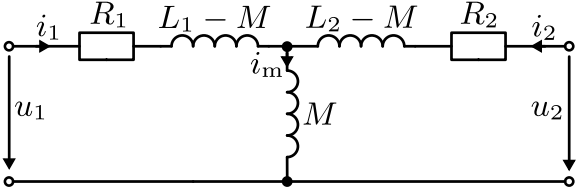

Fig. 3.9: T-type ECD of a transformer (note that the model (3.11) assumes linear time-invariant (LTI) behavior, which among other effects neglects magnetic saturation).

Dynamic modeling of the single-phase transformer (cont.)

Rearranging (3.11) gives the state-space representation of the transformer model

$$\frac{\mathrm{d}}{\mathrm{d}t}\boldsymbol{i}(t) = \boldsymbol{L}^{-1}\left(\boldsymbol{u}(t) - \boldsymbol{R}\boldsymbol{i}(t)\right) \tag{3.12}$$

with

$$\boldsymbol{L}^{-1} = \frac{1}{L_1L_2 - M^2}\begin{bmatrix} L_2 & -M \\ -M & L_1 \end{bmatrix} = \frac{1}{\sigma}\begin{bmatrix} \frac{1}{L_1} & \frac{-M}{L_1L_2} \\ \frac{-M}{L_1L_2} & \frac{1}{L_2} \end{bmatrix}.$$

Above, σ is the leakage coefficient defined as (compare also (2.21))

$$\sigma = \frac{L_1L_2 - M^2}{L_1L_2} = 1 - \frac{M^2}{L_1L_2} = 1 - k^2. \tag{3.13}$$

Finally, the state-space representation of the transformer model (with the currents as states) is

$$\frac{\mathrm{d}}{\mathrm{d}t}\boldsymbol{i}(t) = \begin{bmatrix} -\frac{R_1}{\sigma L_1} & \frac{R_2M}{\sigma L_1L_2} \\ \frac{R_1M}{\sigma L_1L_2} & -\frac{R_2}{\sigma L_2} \end{bmatrix}\boldsymbol{i}(t) + \begin{bmatrix} \frac{1}{\sigma L_1} & -\frac{M}{\sigma L_1L_2} \\ -\frac{M}{\sigma L_1L_2} & \frac{1}{\sigma L_2} \end{bmatrix}\boldsymbol{u}(t) = \boldsymbol{A}\boldsymbol{i}(t) + \boldsymbol{B}\boldsymbol{u}(t). \tag{3.14}$$

Steady-state modeling of the single-phase transformer

Assuming that the transformer operates in steady state and that all quantities are sinusoidal, the state-space model (3.14) can be simplified and represented by complex phasors:

$$x(t) = \hat{x}\cos(\omega_{\mathrm{el}}t + \varphi_{\mathrm{x}}) = \mathrm{Re}\left\{\hat{x}e^{\mathrm{j}(\omega_{\mathrm{el}}t+\varphi_{\mathrm{x}})}\right\} = \mathrm{Re}\left\{\underline{X}e^{\mathrm{j}\omega_{\mathrm{el}}t}\right\}.$$

From (3.11) we receive

$$\underline{\boldsymbol{U}} = \begin{bmatrix}\underline{U}_1\\ \underline{U}_2\end{bmatrix} = \boldsymbol{R}\underline{\boldsymbol{I}} + \mathrm{j}\omega_{\mathrm{el}}\boldsymbol{L}\underline{\boldsymbol{I}} = \underline{\boldsymbol{Z}}\,\underline{\boldsymbol{I}} = \begin{bmatrix}R_1 + \mathrm{j}\omega_{\mathrm{el}}L_1 & \mathrm{j}\omega_{\mathrm{el}}M\\ \mathrm{j}\omega_{\mathrm{el}}M & R_2 + \mathrm{j}\omega_{\mathrm{el}}L_2\end{bmatrix}\begin{bmatrix}\underline{I}_1\\ \underline{I}_2\end{bmatrix}. \tag{3.15}$$

For some given $\underline{\boldsymbol{U}}$ we can calculate the current phasor $\underline{\boldsymbol{I}}$ (i.e., the steady-state current response) by solving:

$$\underline{\boldsymbol{I}} = \underline{\boldsymbol{Z}}^{-1}\underline{\boldsymbol{U}}. \tag{3.16}$$

Alternative scenarios can be also considered, e.g., defining $\underline{U}_1$ (input voltage) and $\underline{I}_2$ (load current) as given and solving for $\underline{I}_1$ and $\underline{U}_2$ by rearranging (3.15).

Steady-state modeling of the single-phase transformer (cont.)

Assuming that the transformer is not loaded ($I_2 = 0$) and that it is lossless ($R_1 = 0$), (3.15) simplifies to

$$\begin{bmatrix} \underline{U}_1 \\ \underline{U}_2 \end{bmatrix} = \begin{bmatrix} \mathrm{j}\omega_{\mathrm{el}} L_1 \\ \mathrm{j}\omega_{\mathrm{el}} M \end{bmatrix} \underline{I}_1. \tag{3.17}$$

The voltage transformation ratio in this case results in

$$\frac{U_1}{U_2} = \frac{\mathrm{j}\omega_{\mathrm{el}} L_1 I_1}{\mathrm{j}\omega_{\mathrm{el}} M I_1} = \frac{L_1}{M}. \tag{3.18}$$

Assuming further that the transformer is leakage-free ($L_{1,\sigma} = 0$), the voltage transformation ratio simplifies to (compare also (2.20))

$$\frac{U_1}{U_2} = \frac{L_1}{M} = \frac{\Lambda_{21} N_1^2}{\Lambda_{21} N_1 N_2} = \frac{N_1}{N_2} = \ddot{u}. \tag{3.19}$$

Hence, this famous result is only valid for the abstract case of a lossless, leakage-free, and, unloaded transformer – i.e., not applicable to real-world transformers

Transformation of the secondary side variables

Sometimes it can be helpful to (mathematically) transform the secondary side variables to ease the mathematical analysis. This can be done by introducing the transformation factor α:

$$u_2' = \alpha u_2, \qquad i_2' = \frac{1}{\alpha} i_2. \tag{3.20}$$

Here, u_2' and i_2' are the transformed secondary side voltage and current, respectively. The primary voltage equation reads

$$\begin{aligned} u_1(t) &= R_1 i_1(t) + L_1 \frac{\mathrm{d}i_1(t)}{\mathrm{d}t} + M \frac{\mathrm{d}i_2(t)}{\mathrm{d}t} = R_1 i_1(t) + L_1 \frac{\mathrm{d}i_1(t)}{\mathrm{d}t} + \alpha M \frac{\mathrm{d}i_2'(t)}{\mathrm{d}t} \\ &= R_1 i_1(t) + L_1 \frac{\mathrm{d}i_1(t)}{\mathrm{d}t} + M' \frac{\mathrm{d}i_2'(t)}{\mathrm{d}t} \end{aligned} \tag{3.21}$$

with the transformed mutual inductance $M' = \alpha M$.

Transformation of the secondary side variables (cont.)

Multiplying the secondary voltage equation with α gives

$$\begin{aligned} & \alpha u_2(t) = \alpha R_2 i_2(t) + \alpha L_2 \frac{\mathrm{d}i_2(t)}{\mathrm{d}t} + \alpha M \frac{\mathrm{d}i_1(t)}{\mathrm{d}t} \\ \Leftrightarrow \quad & u_2'(t) = \alpha^2 R_2 i_2'(t) + \alpha^2 L_2 \frac{\mathrm{d}i_2'(t)}{\mathrm{d}t} + \alpha M \frac{\mathrm{d}i_1(t)}{\mathrm{d}t} \\ \Leftrightarrow \quad & u_2'(t) = R_2' i_2'(t) + L_2' \frac{\mathrm{d}i_2'(t)}{\mathrm{d}t} + M' \frac{\mathrm{d}i_1(t)}{\mathrm{d}t} \end{aligned} \tag{3.22}$$

with the transformed resistance $R_2' = \alpha^2 R_2$ and inductance $L_2' = \alpha^2 L_2$.

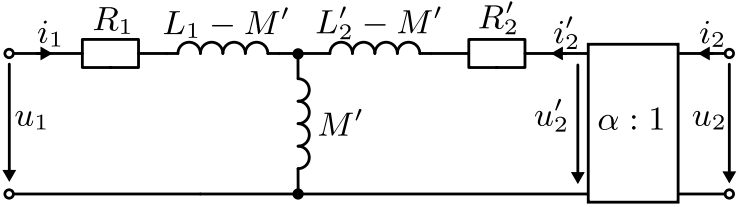

Fig. 3.10: T-type ECD of a transformer with transformed secondary side variables for some arbitrary transformation factor α (note that k and σ are transformation invariant.)

Transformation of the secondary side variables by the turn ratio

With

$$\alpha = \ddot{u} = N_1/N_2$$

being the turn ratio as the transformation factor, we receive:

$$M' = (N_1/N_2)M = L_{1,\mathrm{m}}, \qquad L_2' = (N_1^2/N_2^2)L_2 \tag{3.23}$$

with $L_{1,\mathrm{m}}$ being the primary magnetizing inductance, cf. (2.20). Moreover, we have

$$L_1 - M' = L_{1,\sigma}, \qquad L_2' - M'2 = (N_1^2/N_2^2)L_{2,\sigma} = L_{2,\sigma}' \tag{3.24}$$

with $L_{1,\sigma}$ and $L_{2,\sigma}$ being the leakage inductances of the primary and secondary winding.

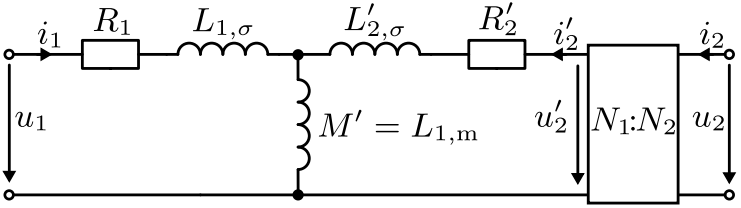

Fig. 3.11: T-type ECD of a transformer with $\alpha = N_1/N_2$ (note that all inductances within this model representation have a direct physical interpretation.)

Transformation towards a single stray inductance

With

$$\alpha = M/L_2$$

as the transformation factor, we receive:

$$L_2' - M' = \alpha^2 L_2 - \alpha M = L_{2,\sigma} = 0, \tag{3.25}$$

that is, the secondary transformed leakage inductance is vanishing. Moreover, we have

$$L_1 - M' = L_{1,\sigma}' = \sigma L_1, \qquad M' = M^2/L_2. \tag{3.26}$$

With the alternative choice $\alpha = L_1/M$, the leakage inductance gets concentrated on the secondary side (not explicitly shown).

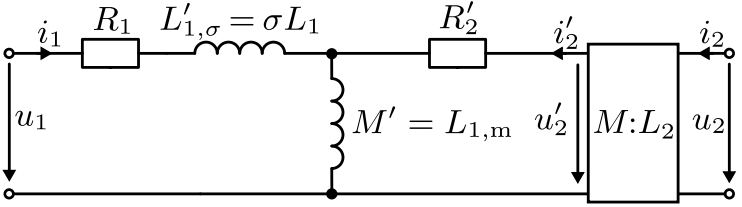

Fig. 3.12: T-type ECD of a transformer with $\alpha = M/L_2$

Typical transformer core types

- The core of a transformer typical build from laminated steel sheets (cf. Fig. 2.36). Alternatively, sintered ferrite material is also used for high-frequency applications.
- To improve the coupling between primary and secondary winding, it is beneficial to place the windings around the same leg. Hence, the middle example in Fig. 3.13 will exhibit a larger leakage.

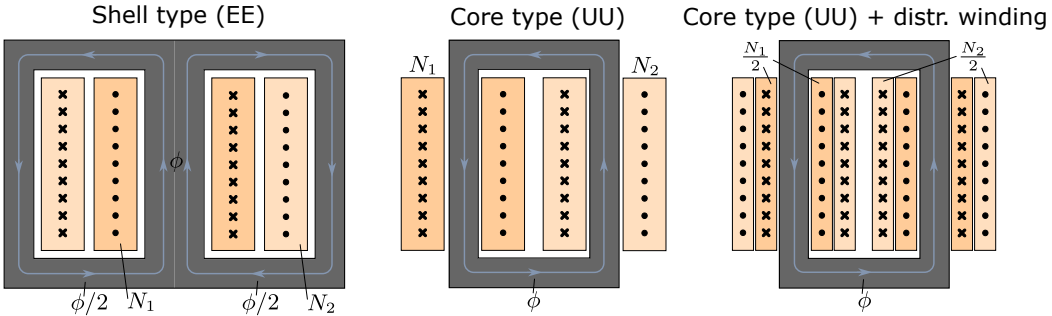

Fig. 3.13: Examples of typical transformer core types

Toroidal core

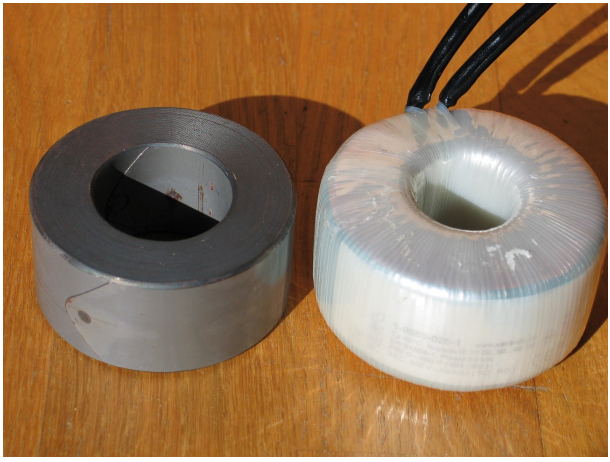

Fig. 3.14: Examples of a toroidal core and a transformer made from it – note the laminated, wound up steel sheets to form the toroid (source: Wikimedia Commons, public domain)

Typical transformer winding schemes

- The below examples show improving magnetic coupling (lower leakage) from left to right due to the reducing effective distance between the turns of the primary and secondary winding.
- Beyond these examples, various winding variations (e.g., a combination of the below schemes) are used to optimize the transformer design for specific applications.

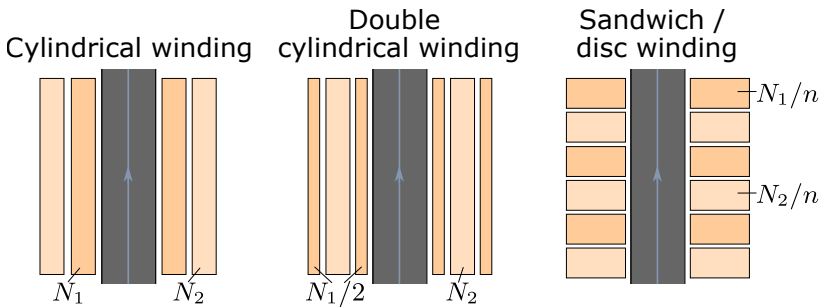

Fig. 3.15: Examples of typical transformer winding schemes

Core loss model (hysteresis and eddy current losses)

To also consider the iron losses inside the transformer core, a first-order model with the additional core loss resistance R_c can be introduced:

$$P_\mathrm{l,c} \approx R_\mathrm{c} I_\mathrm{c}^2 \approx \frac{U_1^2}{R_\mathrm{c}}. \tag{3.27}$$

Here, we consider a pure sinusoidal operation with I_c and U_1 being root-mean-square (RMS) values. Obviously, this is only a very rough model approximation (compare Fig. 2.23 and Fig. 2.36), but for many transformer designs the core losses can be significant and neglecting them completely would not be justified.

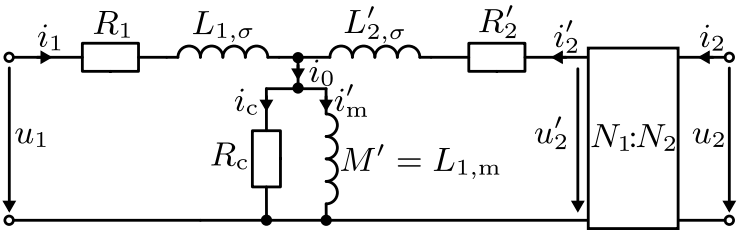

Fig. 3.16: T-type ECD of a transformer with an additional core loss resistance R_c

Transformer model parameterization via measurements – open-circuit test

Applying a sinusoidal test voltage $U_{1,\mathrm{o}}$ and several measurement devices during an open-circuit arrangement, we can determine

$$\ddot{u} \approx \frac{U_{1,\mathrm{o}}}{U_{2,\mathrm{o}}} = \frac{N_1}{N_2}, \quad S_{1,\mathrm{o}} = U_{1,\mathrm{o}} I_{1,\mathrm{o}}, \quad \cos(\varphi_{\mathrm{o}}) = \frac{P_{1,\mathrm{o}}}{U_{1,\mathrm{o}} I_{1,\mathrm{o}}} \tag{3.28}$$

with $P_{1,\mathrm{o}}$ being the active input power consumed by the transformer and $\cos(\varphi_{\mathrm{o}})$ is the power factor. With the assumptions $R_1 << R_{\mathrm{c}}$ and $L_{1,\sigma} << M'$, we can approximate

$$R_{\mathrm{c}} \approx \frac{U_{1,\mathrm{o}}^2}{P_{1,\mathrm{o}}}, \quad X_{M'} = \omega_{\mathrm{el}} M' \approx \frac{U_{1,\mathrm{o}}}{I_{1,\mathrm{o}} \sin(\varphi_{\mathrm{o}})} \tag{3.29}$$

given the angular frequency $\omega_{\mathrm{el}} = 2\pi f_{\mathrm{el}}$ and the reactance $X_{M'}$ of the mutual inductance.

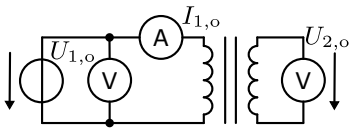

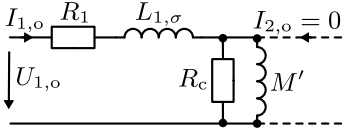

Fig. 3.17: Open-circuit (no-load) test: measuring circuit and its ECD

Transformer model parameterization via measurements – short-circuit test

Short-circuiting the secondary and applying a sinusoidal test voltage $U_{1,\mathrm{s}}$, we can determine

$$Z_\mathrm{s} = \sqrt{(R_1 + R'_2)^2 + (X_{L_{1,\sigma}} + X_{L'_{2,\sigma}})^2}, \quad \cos(\varphi_\mathrm{s}) = \frac{P_{1,\mathrm{s}}}{U_{1,\mathrm{s}} I_{1,\mathrm{s}}} \tag{3.30}$$

with Z_s being the short-circuit impedance while assuming that the impedance across M' and R_c is much larger, i.e., the short-circuit current will not flow via this branch. Hence, we have

$$R_1 + R'_2 = Z_\mathrm{s} \cos(\varphi_\mathrm{s}), \quad X_{L_{1,\sigma}} + X_{L'_{2,\sigma}} = Z_\mathrm{s} \sin(\varphi_\mathrm{s}). \tag{3.31}$$

Since we have four remaining unknown component values but only two independent equations, we additionally assume a symmetrical transformer design, leading to

$$R_1 = R'_2 = \frac{1}{2} Z_\mathrm{s} \cos(\varphi_\mathrm{s}), \quad \omega_\mathrm{el} L_{1,\sigma} = X_{L_{1,\sigma}} = \omega_\mathrm{el} L'_{2,\sigma} = X_{L'_{2,\sigma}} = \frac{1}{2} Z_\mathrm{s} \sin(\varphi_\mathrm{s}). \tag{3.32}$$

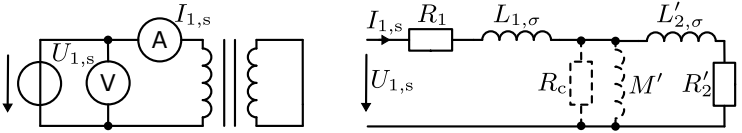

Fig. 3.18: Short-circuit test: measuring circuit and its ECD

Further short-circuit considerations

Typically the short-circuit test voltage $U_{1,\mathrm{s}}$ is limited such that the short-circuit current $I_{1,\mathrm{s}}$ is reaching its nominal value $I_{1,\mathrm{n}}$:

$$U_{1,\mathrm{s}} = u_{1,\mathrm{s}} U_{1,\mathrm{n}}, \quad I_{1,\mathrm{s}} = \frac{U_{1,\mathrm{s}}}{Z_{\mathrm{s}}} = I_{1,\mathrm{n}}. \tag{3.33}$$

Here, $u_{1,\mathrm{s}}$ is the relative short-circuit voltage w.r.t. the nominal voltage $U_{1,\mathrm{n}}$. Typical values are $u_{1,\mathrm{s}} = 3 \ldots 13\,\%$.

While the short-circuit test is conducted with a reduced primary voltage, the prospective short-circuit (PSC) current during normal operation (typical as a fault result) can be significantly higher:

$$I_{1,\mathrm{psc}} = \frac{U_{1,\mathrm{n}}}{Z_{\mathrm{s}}} = \frac{U_{1,\mathrm{s}}}{Z_{\mathrm{s}}} = \frac{I_{1,\mathrm{n}}}{u_{1,\mathrm{s}}}. \tag{3.34}$$

Hence, the transformer parameters Z_{s} and $u_{1,\mathrm{s}}$ are crucial for the short-circuit behavior and the protection coordination of the transformer. Lower bounds are typically enforced by standards to prevent catastrophic damages, in particular in the electrical energy sector.

Voltage transformer application: measuring high AC voltages

If the voltage to be measured is too high for direct measurement, a voltage transformer can be used to step down the voltage to a suitable level:

$$u_2(t) = \frac{1}{\ddot{u}} u_1(t).$$

Hence, we choose $\ddot{u} > 1$. Moreover, the voltage sensor on the secondary side comes with a high internal resistance R_i to avoid a significant current and, therefore, power flow. Neglecting the leakage inductance, we can model the voltage transformer as shown in Fig. 3.19 with

$$R_\mathrm{i}' = \ddot{u}^2 R_\mathrm{i}, \qquad R_2' = \ddot{u}^2 R_2, \qquad M' = L_{1,\mathrm{m}}.$$

The primary RL circuit represents a high-pass filter for the voltage signal, i.e., the transformer is only suitable for AC signals with $\omega_\mathrm{el} > R_1/M'$ (cutoff frequency).

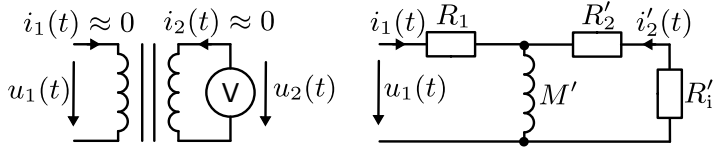

Fig. 3.19: Voltage transformer measuring circuit and its ECD (represented as transformed quantities with $\alpha = N_1/N_2$)

Current transformer application: measuring high AC currents

If the current to be measured is too high for direct measurement, a current transformer can be used to step down the current to a suitable level:

$$i_2(t) = \ddot{u} i_1(t).$$

Hence, we choose $\ddot{u} < 1$. Moreover, the current sensor on the secondary side comes with a minimal internal resistance R_i to avoid a significant ohmic power losses. Likewise, the transformer should be designed for low R_1 and R_2 (e.g., $N_1 = 1$ on the primary and sufficiently large cable cross-sections).

The secondary RL circuit represents a high-pass filter for the current signal, i.e., the transformer is only suitable for AC signals with $\omega_\mathrm{el} > (R_2' + R_\mathrm{i}')/M'$ (cutoff frequency).

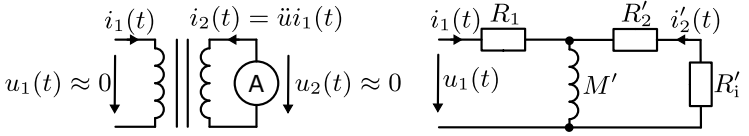

Fig. 3.20: Current transformer measuring circuit and its ECD (represented as transformed quantities with $\alpha = N_1/N_2$)

Connection nomenclature and tapped transformer

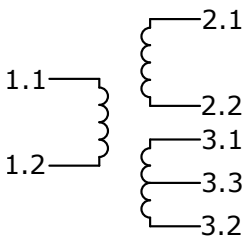

Fig. 3.21: Connection nomenclature of single-phase transformers (the lower secondary side connection represents a tapped winding)

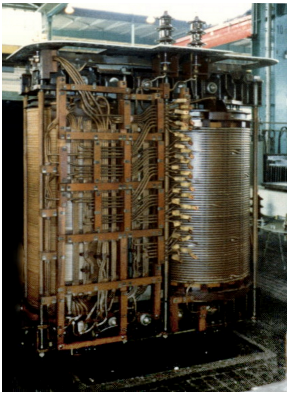

Fig. 3.22: Tapped transformer with multiple taps on the secondary side for a train drive application (source: Wikimedia Commons, Saibo, CC BY-SA 3.0)

Autotransformer

- Uses a common winding for both primary and secondary side with one or multiple taps.
- No galvanic isolation between primary and secondary side.
- The autotransformer can be used to step-up or step-down the voltage.

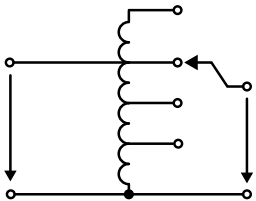

Fig. 3.23: Simplified autotransformer representation

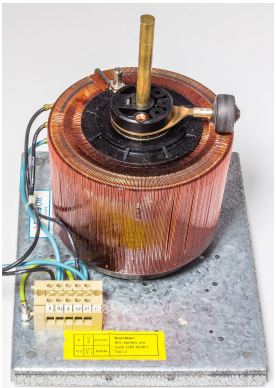

Fig. 3.24: Exemplary autotransformer (source: Wikimedia Commons, R. Spekking, CC BY-SA 4.0)

Autotransformer – step-down configuration

Assuming idealized conditions (no leakage, no losses), the apparent power of the standard transformer S and of the autotransformer S_{at} are:

$$S = U_1 I_1 = U_2 I_2, \qquad S_{\mathrm{at}} = (U_1 + U_2) I_1 = U_2 (I_2 - I_1). \tag{3.35}$$

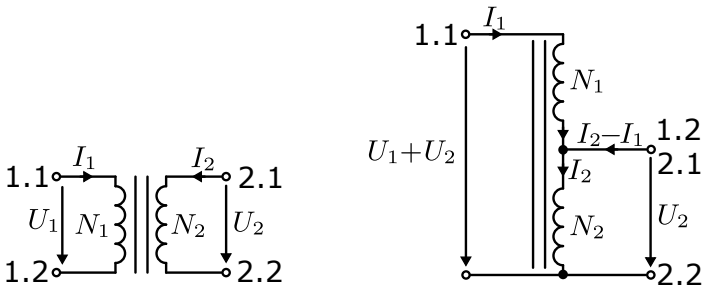

Fig. 3.25: Step-down autotransformer made from a standard two-winding transformer by connecting 1.2 from the primary to 2.1 on the secondary side

Autotransformer – step-down configuration (cont.)

From (3.35) we can express the autotransformer apparent power S_{at} in terms of the standard transformer apparent power S:

$$S_{\mathrm{at}} = (U_1 + U_2)I_1 = S + U_2 I_1 = S + U_1 I_1 \frac{U_2}{U_1} = S(1 + \frac{1}{\ddot{u}}). \tag{3.36}$$

Here, $\ddot{u}$ is the (idealized) voltage transformation ratio of the standard transformer – compare (3.19). Hence, we can express the apparent power of the autotransformer in terms of the standard transformer apparent power:

$$\frac{S_{\mathrm{at}}}{S} = 1 + \frac{1}{\ddot{u}} = 1 + \frac{N_2}{N_1}. \tag{3.37}$$

Since $N_2/N_1 > 0$ the autotransformer can transfer more apparent power than the standard transformer since the autotransformer combines two power transfer mechanisms:

- the apparent power $U_1 I_1$ is transferred via the magnetic coupling (induction) and
- the apparent power $U_2 I_1$ is transferred via the electrical conduction between primary and secondary (not available in the galvanically-isolated standard transformer).

Autotransformer – step-up configuration

The apparent power of the step-up autotransformer is

$$S_{\mathrm{at}} = U_1(I_1 - I_2) = (U_1 + U_2)I_2 = S(1 + \frac{U_1}{U_2}) = S(1 + \ddot{u}) = S(1 + \frac{N_1}{N_2}). \tag{3.38}$$

Likewise to the step-down autotransformer, the step-up autotransformer can transfer more apparent power than the standard transformer.

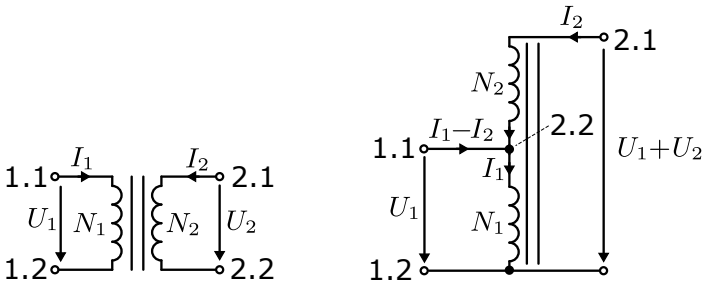

Fig. 3.26: Step-up autotransformer made from a standard two-winding transformer by connecting 1.1 from the primary to 2.2 on the secondary side

Autotransformer remarks

The previous analysis has revealed that the apparent power boost over the standard transformer is significant if

- $N_2 >> N_1$ (step-down case) or
- $N_1 >> N_2$ (step-up case),

that is, the autotransformer's input and output voltage have only a small difference. In this case, the autotransformer can be more efficient and cost-effective than the standard transformer (at the drawback of the lacking galvanic isolation).

Fig. 3.27: $750\,\text{MVA}$, $380\,\text{kV}$ / $230\,\text{kV}$ three-phase autotransformer (source: Wikimedia Commons, P. Mertens, CC BY-SA 3.0)

Autotransformer remarks (cont.)

Another challenge of the autotransformer is its short-circuit behavior. From the step-up case we know:

$$S_{\mathrm{at}} = S(1 + \frac{N_1}{N_2}).$$

Dividing both sides by U_1 delivers

$$I_{1,\mathrm{at}} = I_1(1 + \frac{N_1}{N_2}) \tag{3.39}$$

Hence, in case of a short circuit the steady-state current of the autotransformer is $1 + N_1/N_2$ times higher than the standard transformer:

$$I_{1,\mathrm{at,psc}} = I_{1,\mathrm{psc}}(1 + \frac{N_1}{N_2}). \tag{3.40}$$

The same applies to the step-down case. Therefore, the autotransformer may require additional short-circuit protection measures to prevent damages (e.g., additional choke).

Three-phase transformer

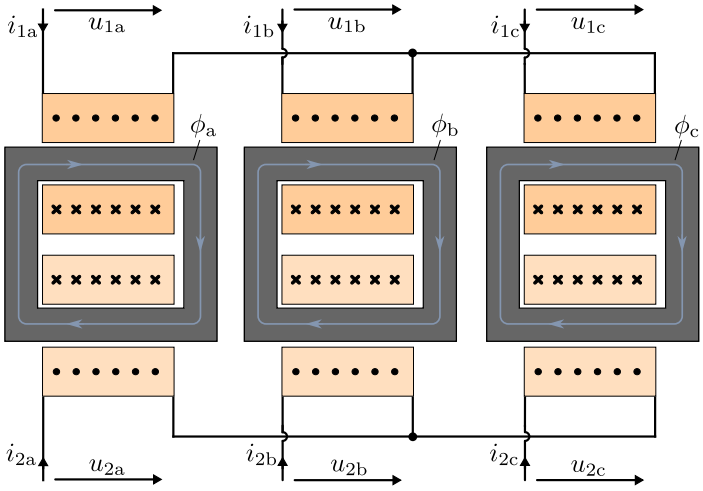

Fig. 3.28: Simple three-phase transformer with three independent single-phase transformers connected in star both on the primary and secondary side

Three-phase transformer with five legs

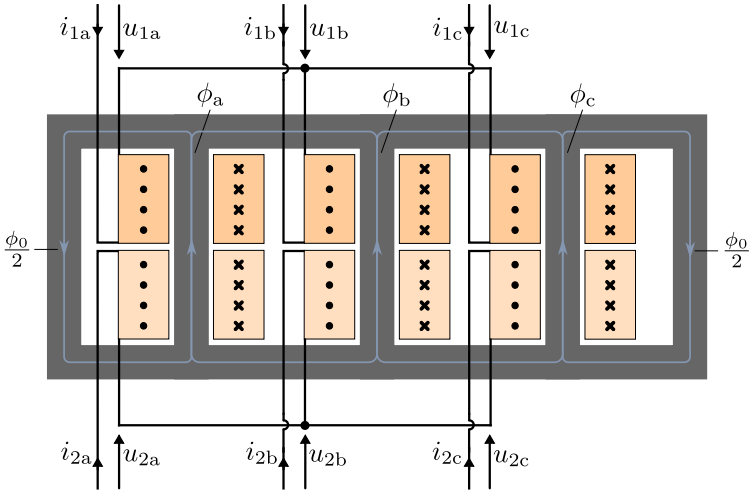

Fig. 3.29: Three-phase five-leg transformer connected in star both on the primary and secondary side

Three-phase transformer with five legs (cont.)

Obviously, the three-phase five-leg design from Fig. 3.29 can save space and material compared to the three independent single-phase transformers from Fig. 3.28. However, there might be a zero flux component

$$\phi_0(t) = \phi_\mathrm{a}(t) + \phi_\mathrm{b}(t) + \phi_\mathrm{c}(t) \tag{3.41}$$

flowing via the winding-free legs. This zero flux component can be avoided if the primary and secondary side are connected both in star configuration

$$i_{1\mathrm{a}}(t) + i_{1\mathrm{b}}(t) + i_{1\mathrm{c}}(t) = 0, \qquad i_{2\mathrm{a}}(t) + i_{2\mathrm{b}}(t) + i_{2\mathrm{c}}(t) = 0$$

and if the magnetic reluctances Λ_m of the three main legs are equal (i.e., symmetric design, no saturation):

$$\phi_0 = \phi_\mathrm{a} + \phi_\mathrm{b} + \phi_\mathrm{c} = \Lambda_\mathrm{m} N_1 \left(i_{1\mathrm{a}}(t) + i_{1\mathrm{b}}(t) + i_{1\mathrm{c}}(t)\right) + \Lambda_\mathrm{m} N_2 \left(i_{2\mathrm{a}}(t) + i_{2\mathrm{b}}(t) + i_{2\mathrm{c}}(t)\right) = 0.$$

Three-phase transformer with three legs (double star connection)

- If the flux zero component ϕ_0 can be avoided, a three-leg design as shown in Fig. 3.30 can be used.
- However, if $\phi_0 \neq 0$ due to an asymmetric design, magnetic saturation or non-ideal symmetrical operation, the zero component will act as a stray field leaving the core.
- This can lead to increased losses in auxiliary components (e.g., housing) and electromagnetic interference issues.

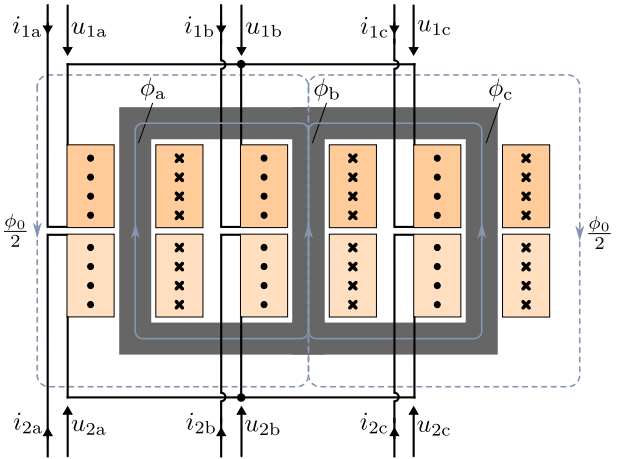

Fig. 3.30: Three-phase three-leg transformer connected in star both on the primary and secondary side

Three-phase transformer with three legs (star-delta connection)

If the primary or secondary side is connected in delta configuration, this side can carry a zero sequence current:

$$i_0 = \frac{1}{3}\left(i_\mathrm{a}(t) + i_\mathrm{b}(t) + i_\mathrm{c}(t)\right) \neq 0.$$

This zero sequence current would not be visible in the phase conductors:

$$\begin{aligned} i_\mathrm{ab} &= i_\mathrm{a} - i_\mathrm{b}, \\ i_\mathrm{bc} &= i_\mathrm{b} - i_\mathrm{c}, \\ i_\mathrm{ca} &= i_\mathrm{c} - i_\mathrm{a}. \end{aligned} \qquad (3.42)$$

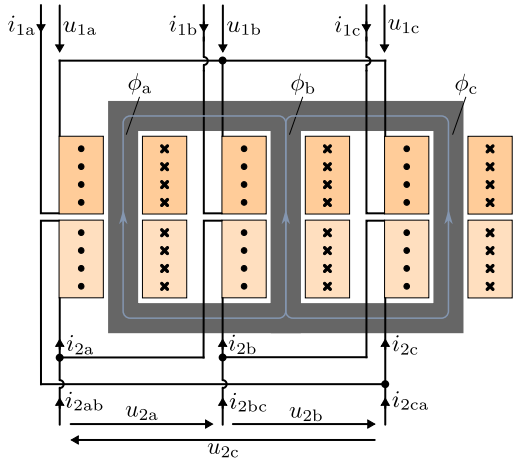

Fig. 3.31: Three-phase three-leg transformer connected in a star-delta configuration (delta on secondary is exemplary)

Zero flux and zero current components in three-phase transformers

Based on (3.42) the winding currents on the delta side becomes

$$i_{\mathrm{a}} = i_0 + \frac{1}{3}\left(i_{\mathrm{ab}} - i_{\mathrm{ca}}\right), \quad i_{\mathrm{b}} = i_0 + \frac{1}{3}\left(i_{\mathrm{bc}} - i_{\mathrm{ab}}\right), \quad i_{\mathrm{c}} = i_0 + \frac{1}{3}\left(i_{\mathrm{ca}} - i_{\mathrm{bc}}\right). \tag{3.43}$$

If the secondary side is connected in delta, the zero sequence current will result from

$$\phi_0 = \phi_{\mathrm{a}} + \phi_{\mathrm{b}} + \phi_{\mathrm{c}} = \phi(i_{1\mathrm{a}}, i_{2\mathrm{a}}, i_{20}) + \phi(i_{1\mathrm{b}}, i_{2\mathrm{b}}, i_{20}) + \phi(i_{1\mathrm{c}}, i_{2\mathrm{c}}, i_{20}) = 0 \tag{3.44}$$

where $\phi(\cdot)$ is the (potentially nonlinear) magnetic flux function (e.g., including saturation).

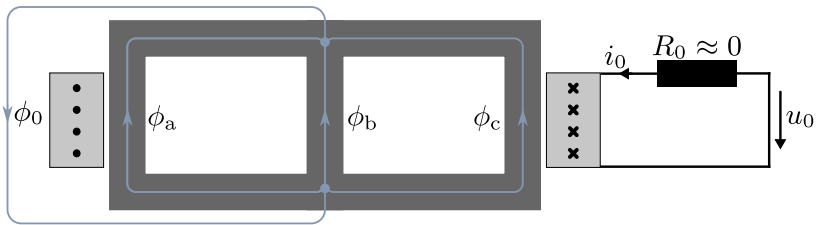

Fig. 3.32: Substitute model to represent the zero flux component

Three-phase transformer connection and winding types

Each side of a three-phase transformer can be connected in:

$$\text{Y/y: star connection,} \quad \text{D/d: delta connection,} \quad \text{Z/z: zigzag connection.}$$

The winding nomenclature is as follows:

- First upper case letter: primary side (high voltage)
- Second lower case letter: secondary side (low voltage)
- Number $(0 \ldots 11)$: phase deviation between the primary and secondary side in $^\circ 30$ steps
- Optional: N/n for neutral connection of high/low side.

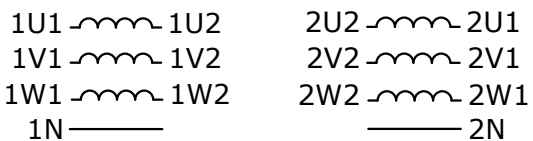

Fig. 3.33: Connection nomenclature of three-phase transformers

Three-phase transformer connection and winding types (example: Yd1)

Transformer connection Yd1 indicates

- Y: star connection on the primary side,
- d: delta connection on the secondary side,
- 1: phase deviation of $1 \cdot 30^\circ = 30^\circ$ between the primary and secondary side.

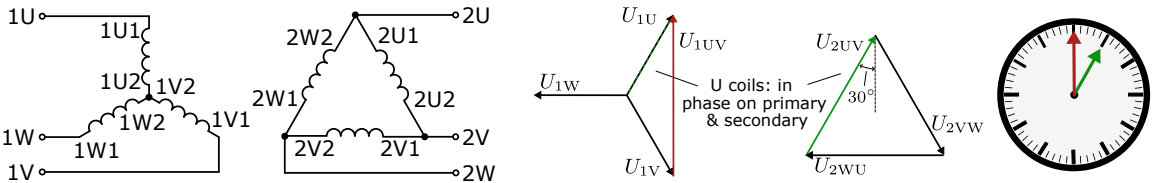

Fig. 3.34: Winding configuration and resulting phasor diagrams for Yd1 connection

Three-phase transformer connection and winding types (example: Dy11)

The transformer connection Dy11 indicates

- D: delta connection on the primary side,
- y: star connection on the secondary side,
- 11: phase deviation of $11 \cdot 30^\circ = 330^\circ$ between the primary and secondary side.

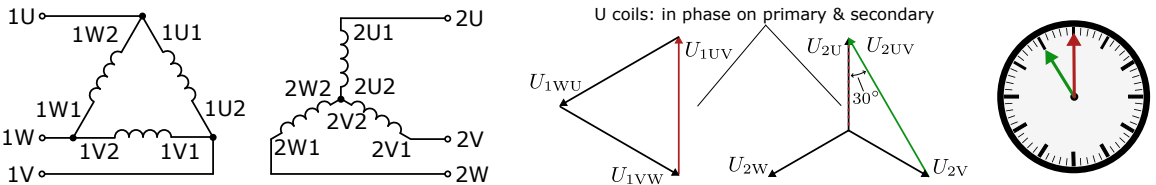

Fig. 3.35: Winding configuration and resulting phasor diagrams for Dy11 connection

Three-phase transformer connection and winding types (example: Dy5)

In this example, the primary and secondary side are still connected in a delta-star configuration, but, the polarity of the secondary side is reversed compared to the previous Dy11 connection. Consequently, the phase deviation is $5 \cdot 30° = 150°$.

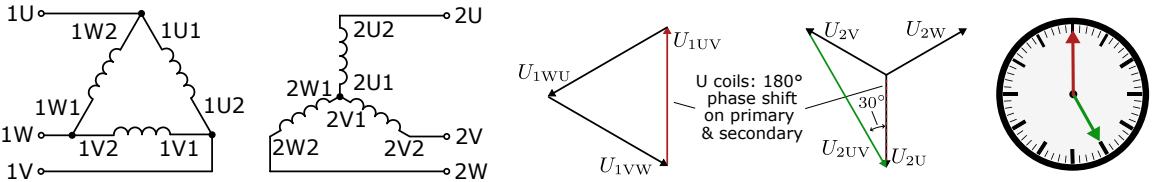

Fig. 3.36: Winding configuration and resulting phasor diagrams for Dy5 connection

Three-phase transformer connection symbols (vector groups)

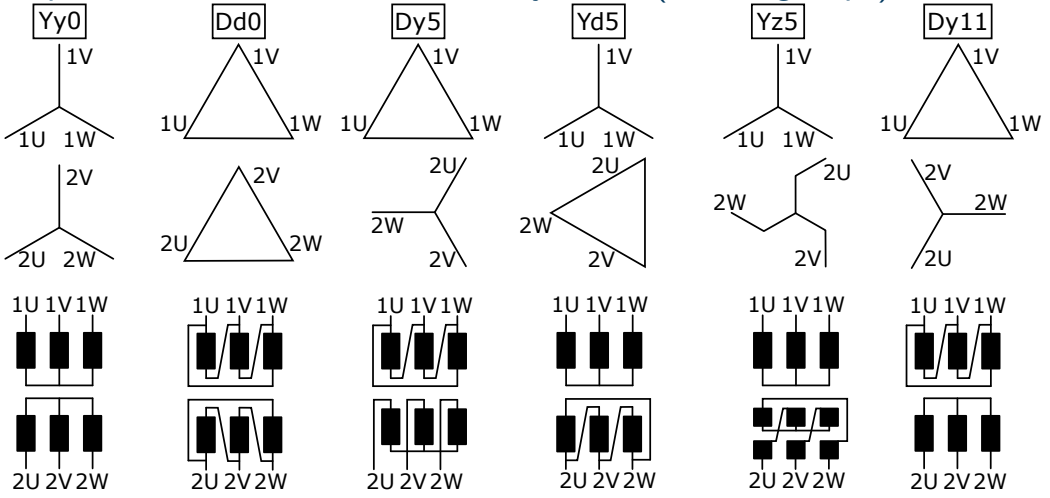

Fig. 3.37: Exemplary (simplified) connection symbols for three-phase transformers and the resulting phasor displacement representations

Three-phase transformer voltage ratio

If the three-phase connection type changes between the primary and secondary side, the voltage ratio between the primary and secondary side is affected – cf. Tab. 3.1.

primary	Y	D	Y	D	Y	D
secondary	y	y	d	d	z	z
$U_{1,\mathrm{ll}}/U_{2,\mathrm{ll}}$	1	$\sqrt{3}$	$1/\sqrt{3}$	1	$\sqrt{3}/2$	$3/2$

Tab. 3.1: Idealized voltage ratios between primary and secondary due to different connection types (assuming $N_1 = N_2$) with $U_{1,\mathrm{ll}}$ and $U_{2,\mathrm{ll}}$ being the line-to-line voltages on the primary and secondary side, respectively

Dynamic modeling of the three-phase transformer

Assuming a three-phase transformer without mutual coupling between the phases abc (as in the three independent single-phase transformers from Fig. 3.28) and without saturation, the magnetic flux linkage of the primary and secondary side can be expressed as

$$\boldsymbol{\psi}(t) = \begin{bmatrix} \psi_{1\mathrm{a}}(t) \\ \psi_{1\mathrm{b}}(t) \\ \psi_{1\mathrm{c}}(t) \\ \psi_{2\mathrm{a}}(t) \\ \psi_{2\mathrm{b}}(t) \\ \psi_{2\mathrm{c}}(t) \end{bmatrix} = \begin{bmatrix} L_{1\mathrm{a}} & 0 & 0 & M_{\mathrm{a}} & 0 & 0 \\ 0 & L_{1\mathrm{b}} & 0 & 0 & M_{\mathrm{b}} & 0 \\ 0 & 0 & L_{1\mathrm{c}} & 0 & 0 & M_{\mathrm{c}} \\ M_{\mathrm{a}} & 0 & 0 & L_{2\mathrm{a}} & 0 & 0 \\ 0 & M_{\mathrm{b}} & 0 & 0 & L_{2\mathrm{b}} & 0 \\ 0 & 0 & M_{\mathrm{c}} & 0 & 0 & L_{2\mathrm{c}} \end{bmatrix} \begin{bmatrix} i_{1\mathrm{a}}(t) \\ i_{1\mathrm{b}}(t) \\ i_{1\mathrm{c}}(t) \\ i_{2\mathrm{a}}(t) \\ i_{2\mathrm{b}}(t) \\ i_{2\mathrm{c}}(t) \end{bmatrix} = \boldsymbol{L}\boldsymbol{i}(t). \tag{3.45}$$

If the transformer's magnetic three-phase circuit is ideally symmetric, also

$$M = M_{\mathrm{a}} = M_{\mathrm{b}} = M_{\mathrm{c}}, \quad L_1 = L_{1\mathrm{a}} = L_{1\mathrm{b}} = L_{1\mathrm{c}}, \quad L_2 = L_{2\mathrm{a}} = L_{2\mathrm{b}} = L_{2\mathrm{c}}$$

holds.

Table of contents

DC machines

Bikash Sah

Universität Siegen / IAS Interconnected Automation Systems

Homopolar / unipolar machines

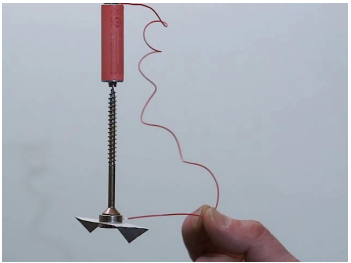

(a) Video of an operating homopolar machine (source: Wikimedia Commons, Smial, Free Art License)

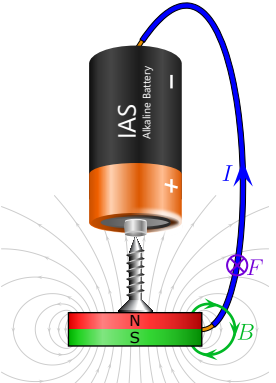

(b) Electric current, magnetic field and Lorentz force (adapted: Wikimedia Commons, M. Run, CC BY-SA)

Fig. 4.1: Working principle of homopolar machines demonstrated with a simple permanent magnet, battery and screw design

Homopolar / unipolar machines (cont.)

- Homopolar machines are the simplest form of electric machines.
- They are also true DC machines, as the current and flux paths are unidirectional.
- The general design prevents connecting multiple rotor turns in series to increase the voltage, that is, only a relatively low voltage is induced.
- Consequently, homopolar machines require high currents (in the order of kA or even MA) to reach a useful power range which limited their application.

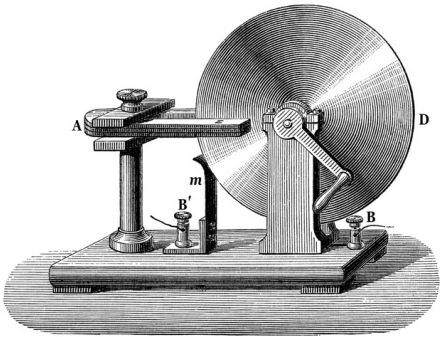

Fig. 4.2: The Faraday disk: another homopolar machine (source: Wikimedia Commons, public domain)

Working principle of usual DC machines

Let's consider Fig. 4.3 and assume that the flux density B is constant in the air gap and that the conductor loop has the axial length l_z. According to the Lorentz force we have

$$F = I_\mathrm{a} B l_\mathrm{z}. \tag{4.1}$$

The torque T on the conductor loop is given by

$$T = 2F\frac{d}{2}\cos(\varepsilon) = I_\mathrm{a} B l_\mathrm{z} d\cos(\varepsilon). \tag{4.2}$$

If the loop spins with an angular velocity ω, mechanical power $P_\mathrm{me} = T\omega$ is transferred.

Question: What is happening if the coil is outside the magnetic field?

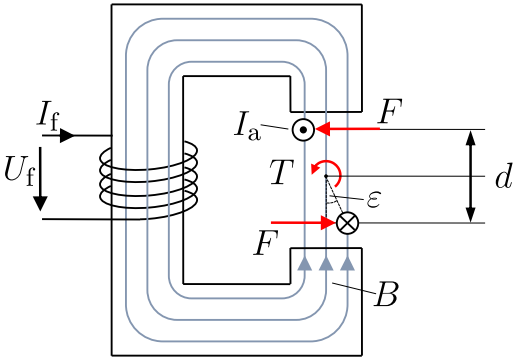

Fig. 4.3: Torque on a conductor loop (adapted from J. Böcker, *Elektrische Antriebstechnik*, Paderborn University, 2020)

DC-machine cross section

- To ensure a quasi-continuous torque, the current through the conductor loop(s) in the rotor must have a constant direction.
- This is achieved by using a commutator (brushes).
- Compared to homopolar machines, DC machines require a mechanical rectification of the current.

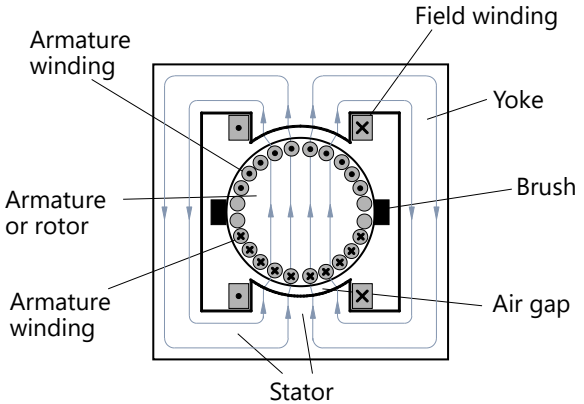

Fig. 4.4: Simplified DC machine cross section (adapted from J. Böcker, *Elektrische Antriebstechnik*, Paderborn University, 2020)

Commutation

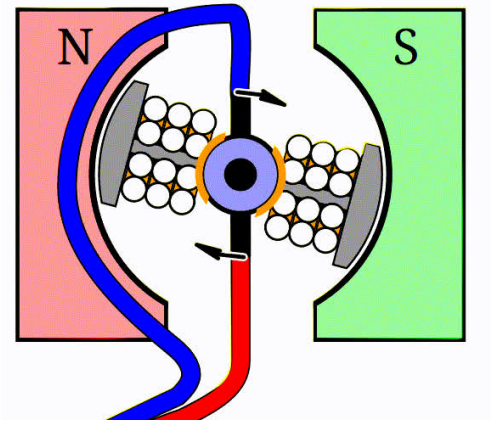

Fig. 4.5: Animation of the commutation process
(source: Wikimedia Commons, M. Frey, CC BY-SA 3.0)

Armature and commutator

(a) Commutator with brushes and springs (source: Wikimedia Commons, Marrrci, CC BY-SA 3.0)

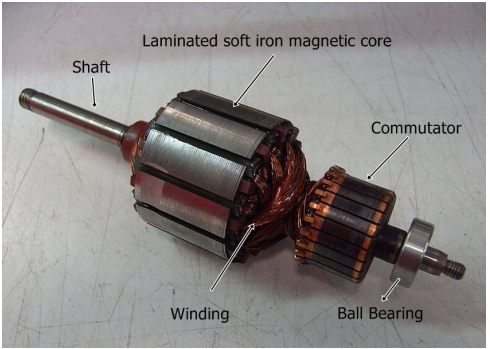

(b) DC machine armature with commutator (source: Wikimedia Commons, public domain)

Fig. 4.6: Examples of commutators and armatures

Armature and commutator (cont.)

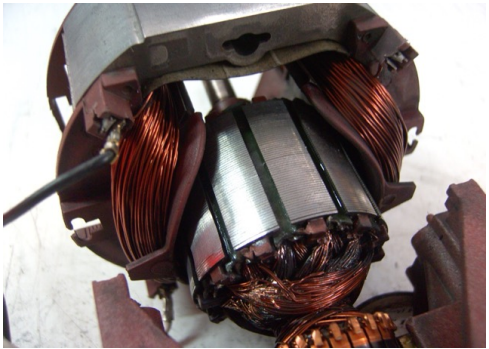

(c) Armature inside stator (source: Wikimedia Commons, Marrrci, CC BY-SA 3.0)

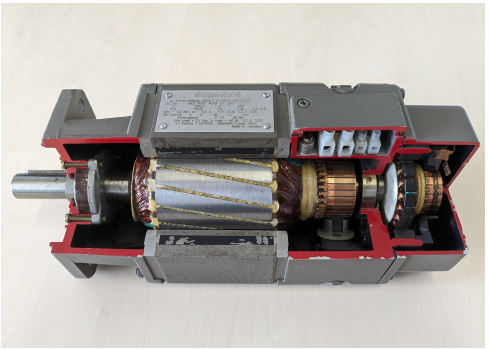

(d) DC machine with permanent magnet excitation and tacho speed sensor

Fig. 4.6: Examples of commutators and armatures (cont.)

Basic structure of the armature

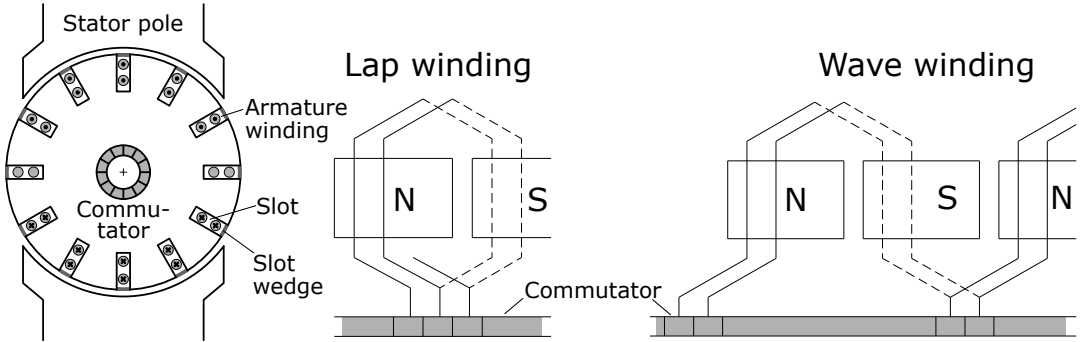

Fig. 4.7: Cross section of a drum-type armature including principle winding schemes (adapted from W. Novender, *Elektrische Maschinen*, Technische Hochschule Mittelhessen, 2023)

Types of winding conductors

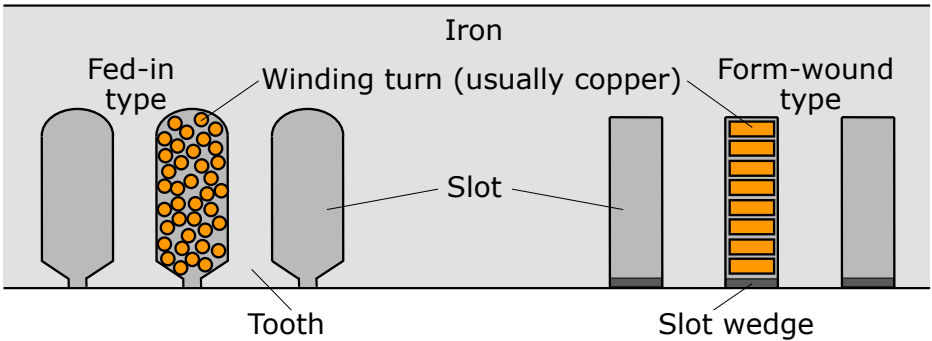

Fig. 4.8: Types of winding conductors – unwound representation along the circumference (adapted from J. Böcker, *Controlled Three-Phase Drives*, Paderborn University, 2021)

Commutation process with an armature lap winding

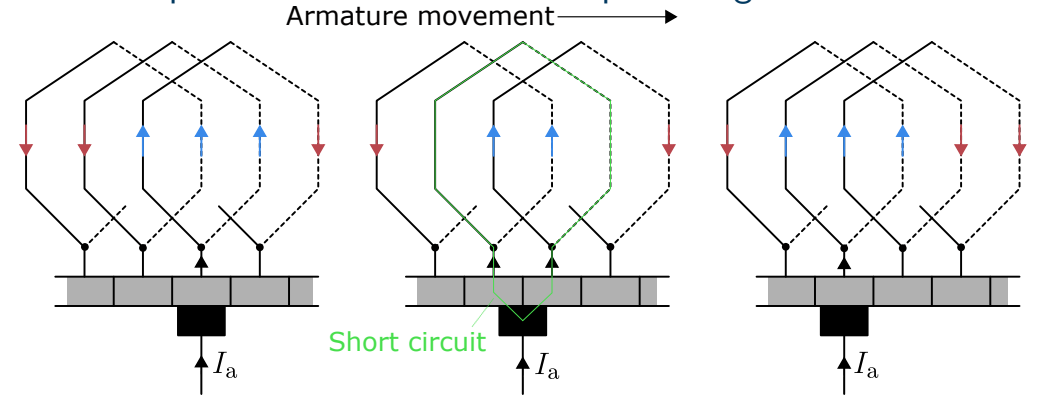

Fig. 4.9: Three still images of the commutation process with a simplified winding representation (from left to right): when the brush touches two commutator segments, the according conductor loop is short-circuited and the current is reduced to zero. The brush then moves to the next commutator segment and the current starts flowing again but in the opposite direction (adapted from W. Novender, *Elektrische Maschinen*, Technische Hochschule Mittelhessen, 2023).

DC machines with multiple pole pairs

- To reduce the effective length per armature conductor loop, the winding can form multiple pole pairs p.
- This will reduce the inductance per loop which is beneficial for the commutation process.
- The stator excitation must meet the same number of pole pairs.
- Given some inner stator diameter d_s, the resulting pole pitch is:

$$\tau_\mathrm{p} = \frac{\pi d_\mathrm{s}}{2p}, \quad \rho_\mathrm{p} = \frac{\pi}{p}. \tag{4.3}$$

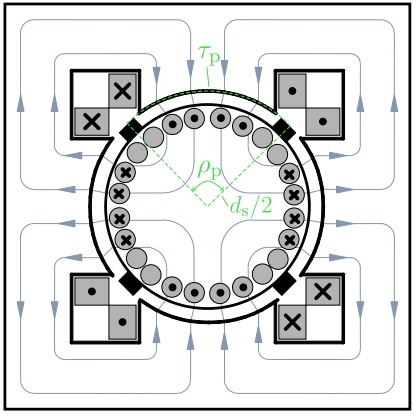

Fig. 4.10: Simplified DC machine cross section with $p = 2$ pole pairs (adapted from J. Böcker, *Elektrische Antriebstechnik*, Paderborn University, 2020)

Armature winding characteristics

For describing the armature winding layout, the following parameters are introduced:

Q : number of slots, N_c : number of conductor turns per coil,

K : number of commutator elements, $u = K/Q$: slot to commutator ratio,

$z_\mathrm{a} = 2KN_\mathrm{c}$: total number of armature conductors.

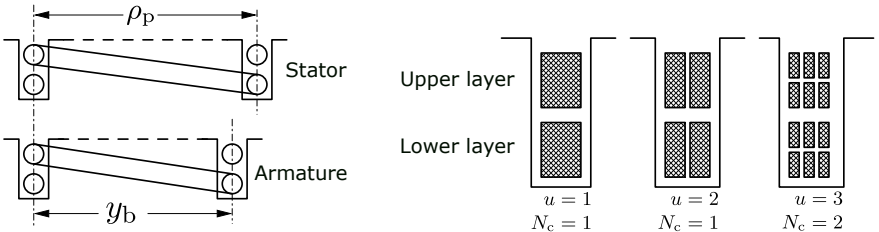

Fig. 4.11: Coil width and slot design characteristics (adapted from W. Novender, *Elektrische Maschinen*, Technische Hochschule Mittelhessen, 2023)

Double layer winding

- The forward conductor of one coil and the return conductor of another coil are placed in the same slot. This is the common winding scheme (although not limited to it).
- Enables chording of the winding ($\rho_\mathrm{p} \neq y_\mathrm{b}$), another degree of freedom for the machine design (cf. Fig. 4.11).

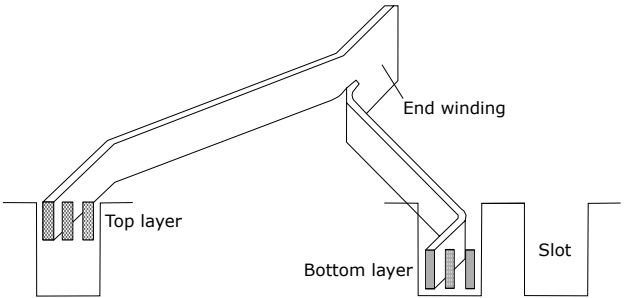

Fig. 4.12: Double layer winding with $u = 3$ with a solid conductor element (which can be pre-manufactured for cost reasons – inspired from A. Binder, *Elektrische Maschinen und Antriebe*, Vol. 2, Springer, 2017)

Lap winding characteristics

- Back pitch y_b: coil span from the back end
- Front pitch y_f: coil span from the front end
- Resultant pitch y_r: distance between two consecutive coils
- Commutator pitch y_c: distance between two consecutive commutator segments

Progressive winding

Fig. 4.13 shows a progressive winding layout with $y_\mathrm{b} > y_\mathrm{f}$, i.e., the coils do not cross themselves.

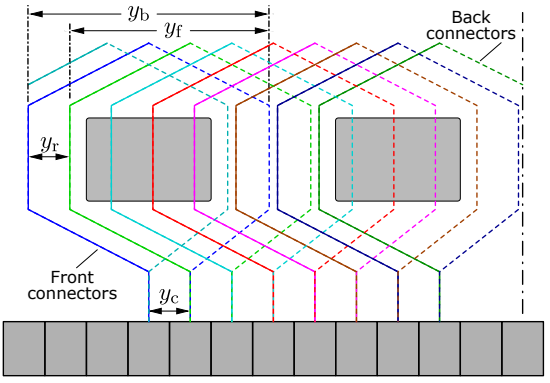

Fig. 4.13: Distance definitions of the armature lap winding (adapted from W. Novender, *Elektrische Maschinen*, Technische Hochschule Mittelhessen, 2023)

Lap winding characteristics (cont.)

Retrogressive winding

Fig. 4.14 shows a Retrogressive winding layout with $y_\mathrm{b} < y_\mathrm{f}$, i.e., each coil crosses itself.

- Retrogressive windings require more conductor material due to the crossing of the coils and, therefore, are less common.
- Technical feasibility requires $y_\mathrm{b} - y_\mathrm{f} = \pm y_\mathrm{c}$, i.e., the lap winding progresses or retrogresses by one commutator element.

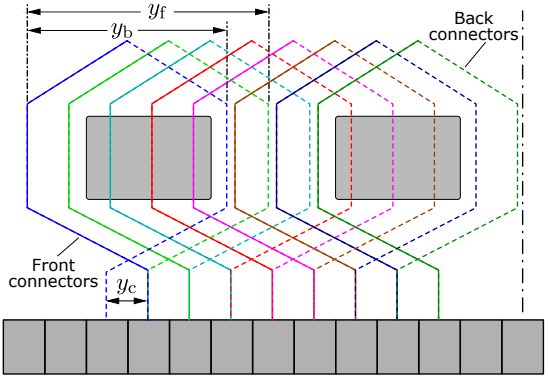

Fig. 4.14: Lap winding with a retrogressive scheme (adapted from W. Novender, *Elektrische Maschinen*, Technische Hochschule Mittelhessen, 2023)

Lap winding: final remarks and single pole pair example

- Armature turns per pole: $N_{\mathrm{p}} = \frac{KN_{\mathrm{c}}}{2p}$
- Current per armature conductor: $I_{\mathrm{c}} = \frac{I_{\mathrm{a}}}{2p}$

Parallel connection of poles

For $p > 1$ the lap winding parallels the armature coils for each pole enabling a higher current (but limited voltage) rating.

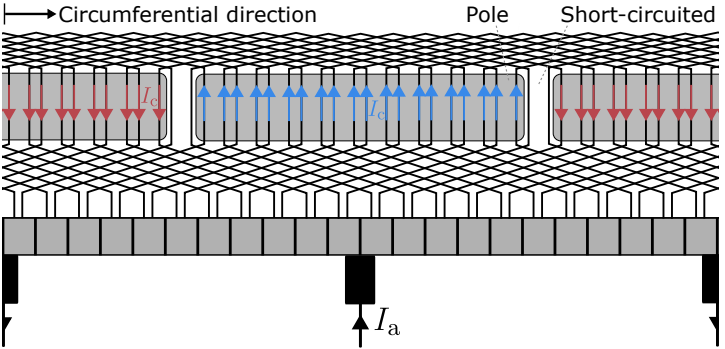

Fig. 4.15: Lap winding with commutator unrolled along the circumferential coordinate

Wave winding characteristics

- Commutator pitch (wave winding): $y_c = y_f + y_b$, i.e., each coil spans (nearly) the entire pole pitch.

Progressive winding

Fig. 4.16 shows a progressive winding layout since each new wave winding coil starts one commutator element to the right.

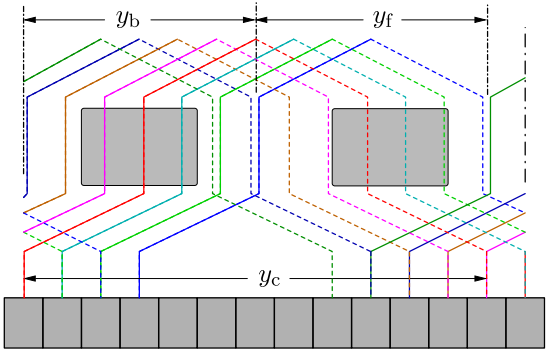

Fig. 4.16: Distance definitions of the armature wave winding (adapted from W. Novender, *Elektrische Maschinen*, Technische Hochschule Mittelhessen, 2023)

Wave winding: final remarks and single pole pair example

- Armature turns per pole: $N_{\mathrm{p}} = \frac{KN_{\mathrm{c}}}{2}$
- Current per armature conductor: $I_{\mathrm{c}} = \frac{I_{\mathrm{a}}}{2}$

Series connection of poles

For $p > 1$ the wave winding connects the armature coils for all poles in series enabling a higher voltage (but limited current) rating.

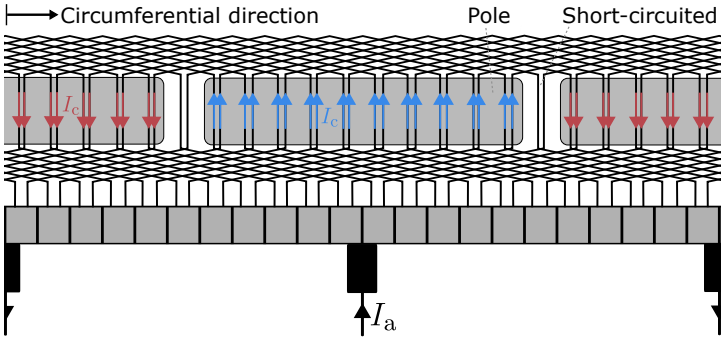

Fig. 4.17: Wave winding with commutator unrolled along the circumferential coordinate

Lap and wave winding comparison

Introducing the parameter

$$a = \text{number of parallel armature conductors} \tag{4.4}$$

we can wrap up the following summary:

$$\text{Current per conductor: } I_{\mathrm{c}} = \frac{I_{\mathrm{a}}}{2a}, \quad \text{Armature turns per pole: } N_{\mathrm{p}} = \frac{KN_{\mathrm{c}}}{2a}. \tag{4.5}$$

Comparison

- Lap winding: $a = p$ (parallel connection of poles)
- Wave winding: $a = 1$ (series connection of poles)

Commutation process

During the commutation time Δt_c the brush bridges two commutator segments and the short-circuited conductor coil current i_c is changing signs. Here, two major scenarios can be distinguished:

- The commutation is such fast that high local current densities are prevented.
- The commutation is slow and high local current densities lead to sparking effects.

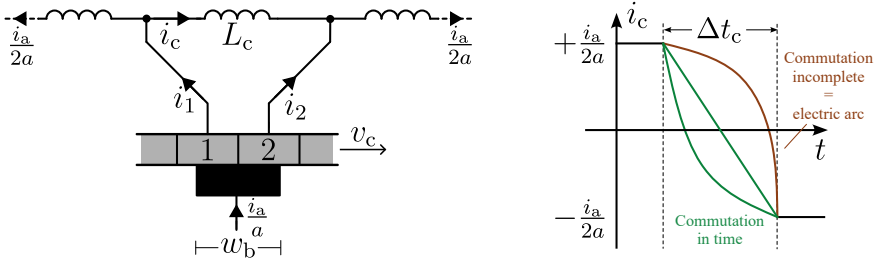

Fig. 4.18: Left: simplified equivalent circuit diagram of the short-circuited coil during commutation. Right: qualitative trajectories of the conductor current i_c

Commutation process (cont.)

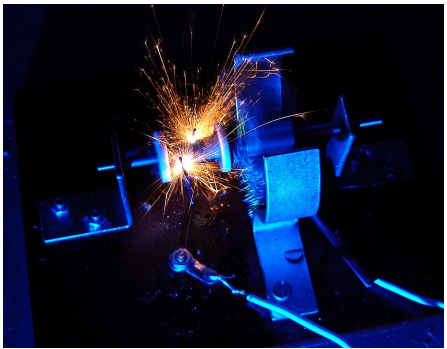

Fig. 4.19: Commutator sparking of a simple DC machine (source: Wikimedia Commons, M. Frey, CC BY-SA 4.0)

Assuming that the brush width w_b is much bigger than one commutator segment (which is usual practice), the commutation time Δt_c is given by

$$\Delta t_\mathrm{c} \approx \frac{w_\mathrm{b}}{v_\mathrm{c}}. \tag{4.6}$$

Here, v_c is the brush velocity

$$v_\mathrm{c} = \omega \frac{d_\mathrm{a}}{2} \tag{4.7}$$

with the armature angular velocity ω and the armature diameter d_a. Due to the changing current in the coil, the so-called reactane voltage u_r is induced:

$$u_\mathrm{r} = L_\mathrm{c} \frac{\mathrm{d}i_\mathrm{c}}{\mathrm{d}t} \approx L_\mathrm{c} \frac{i_\mathrm{a}}{a \Delta t_\mathrm{c}} = L_\mathrm{c} i_\mathrm{a} \frac{\omega d_\mathrm{a}}{a w_\mathrm{b} 2}. \tag{4.8}$$

Equivalent circuit diagram and summary of important equations

Field and armature voltage equations:

$$u_\mathrm{f} = R_\mathrm{f} i_\mathrm{f} + L_\mathrm{f} \frac{\mathrm{d}i_\mathrm{f}}{\mathrm{d}t}$$
$$u_\mathrm{a} = R_\mathrm{a} i_\mathrm{a} + L_\mathrm{a} \frac{\mathrm{d}i_\mathrm{a}}{\mathrm{d}t} + u_\mathrm{i} \qquad (4.9)$$

Induced voltage:

$$u_\mathrm{i} = \omega \psi'_\mathrm{f} = \omega i_\mathrm{f} L'_\mathrm{f}$$

Torque:

$$T = L'_\mathrm{f} i_\mathrm{f} i_\mathrm{a} = \psi'_\mathrm{f} i_\mathrm{a}$$

Note: we represent the machine currents with small letters to indicate that they are time-dependent (e.g., if the external voltage supplied is varying).

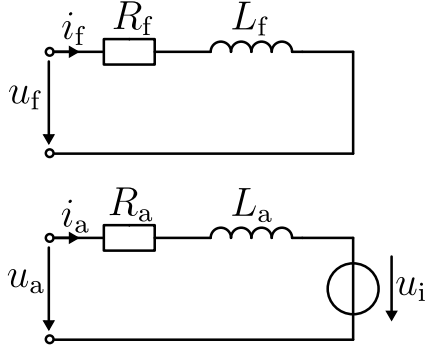

Fig. 4.20: Equivalent circuit diagram of the DC machine

Power balance and efficiency

Based on (4.20) (note the load convention), the electrical power of the DC machine is:

$$P_{\mathrm{el}} = u_{\mathrm{a}} i_{\mathrm{a}} + u_{\mathrm{f}} i_{\mathrm{f}}. \tag{4.10}$$

This power is separated into the mechanical power P_{me}, the dissipated power losses P_{l}, and the change of the stored magnetic energy $\frac{\mathrm{d}}{\mathrm{d}t} E_{\mathrm{mag}}$:

$$P_{\mathrm{el}} = P_{\mathrm{me}} + P_{\mathrm{l}} + \frac{\mathrm{d}}{\mathrm{d}t} E_{\mathrm{mag}}. \tag{4.11}$$

The power losses are (assuming dominant ohmic losses):

$$P_{\mathrm{l}} = R_{\mathrm{f}} i_{\mathrm{f}}^2 + R_{\mathrm{a}} i_{\mathrm{a}}^2. \tag{4.12}$$

The mechanical power is:

$$P_{\mathrm{me}} = T\omega = \psi'_{\mathrm{f}} i_{\mathrm{a}} \omega. \tag{4.13}$$

The magnetically stored energy is

$$E_{\mathrm{mag}} = \frac{1}{2} L_{\mathrm{f}} i_{\mathrm{f}}^2 + \frac{1}{2} L_{\mathrm{a}} i_{\mathrm{a}}^2. \tag{4.14}$$

Power balance and efficiency (cont.)

In steady state, the DC machine efficiency η is defined as

$$\eta_{\text{mot}} = \frac{P_{\text{me}}}{P_{\text{el}}} = \frac{T\omega}{u_{\text{a}}i_{\text{a}} + u_{\text{f}}i_{\text{f}}} = \frac{L'_{\text{f}}i_{\text{f}}i_{\text{a}}\omega}{R_{\text{a}}i_{\text{a}}^2 + \omega L'_{\text{f}}i_{\text{f}}i_{\text{a}} + R_{\text{f}}i_{\text{f}}^2},$$
$$\eta_{\text{gen}} = \frac{P_{\text{el}}}{P_{\text{me}}} = \frac{u_{\text{a}}i_{\text{a}} + u_{\text{f}}i_{\text{f}}}{T\omega} = \frac{R_{\text{a}}i_{\text{a}}^2 + \omega L'_{\text{f}}i_{\text{f}}i_{\text{a}} + R_{\text{f}}i_{\text{f}}^2}{L'_{\text{f}}i_{\text{f}}i_{\text{a}}\omega}. \tag{4.15}$$

It can be noted that

- The machine parameters R_{a}, R_{f}, and L'_{f} are influencing the efficiency.
- The efficiency is a function of the load torque T and the speed ω, that is, depending on the operating point.
- If i_{f} and i_{a} are independently controllable, the efficiency can be optimized as a certain torque can be produced with infinitely many combinations of i_{f} and i_{a}.

Intermediate remarks on the DC machine model

During the derivation of the DC machine model, we made several assumptions:

- The air gap magnetic field is homogenous and without any leakage.
- The air gap reluctance is dominating the magnetic circuit (neglecting the iron path reluctances including potential magnetic saturation).
- The magnetic field lines follow distinct paths through the armature winding.
- There is no mutual inductance between the stator and rotor (ideal orthogonal windings).
- The magnetic field in the air gap and in the armature is governed by the field winding current only (that is, we have neglected the armature current impact on the field).

Model accuracy

We represent the DC machine by a time-invariant, lumped-parameter model which is based on several substantial simplifications. While this model is likely sufficient for many applications, systematic deviations between the observed behavior of real machines and the model predictions are to be expected.

Armature reaction

- So far, we have neglected the impact of the armature current on the magnetic field.
- If $i_\mathrm{a} \neq 0$, the magnetic field lines in the air gap are distorted leading to a so-called armature reaction (cf. Fig. 4.21).

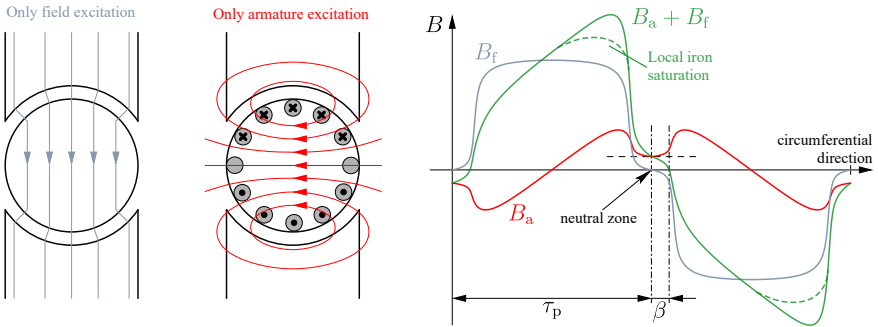

Fig. 4.21: Superposition of the field and armature magnetic excitation and the resulting air gap field normal components (adapted from W. Novender, *Elektrische Maschinen*, Technische Hochschule Mittelhessen, 2023)

Armature reaction (cont.)

Issues related to the armature reaction:

- The neutral zone (field-free commutation area) is shifted by β degrees in the circumferential direction, that is, exacerbate the commutation process (increased risk of sparking).
- High local field densities can lead to magnetic saturation which will increase the iron path reluctance and consequently decrease the machine's torque capability. Also, the iron losses will increase.
- The imbalanced magnetic field leads to an imbalanced Lorentz force distribution on the armature conductors which can cause mechanical distortions.

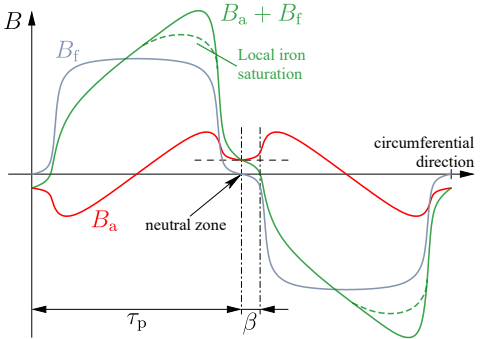

Counter measures: compensation winding and interpoles

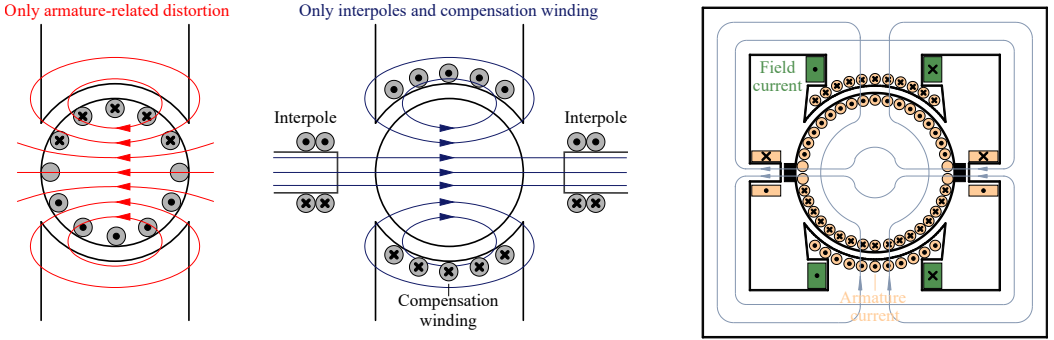

Fig. 4.22: Armature reaction counter measures utilizing compensation winding and interpoles: both are excited by the armature current with an opposite orientation to account for the load-dependent impact of the armature reaction (adapted from W. Novender, *Elektrische Maschinen*, Technische Hochschule Mittelhessen, 2023 and J. Böcker, *Elektrische Antriebstechnik*, Paderborn University, 2020)

Counter measures: compensation winding and interpoles (cont.)

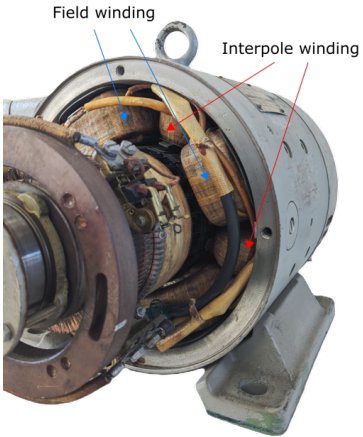

Fig. 4.23: Example of a DC machine with interpole winding (one may identify that the interpole winding is connected to the brushes and, therefore, excited by the armature current)

Counter measures: compensation winding and interpoles (cont.)

Compensation winding design: In order to compensate for the armature reaction within the air gap, the compensation winding MMF θ_{cw} must meet the armature MMF θ_{a}:

$$|\theta_{\mathrm{cw}}| = \frac{z_{\mathrm{cw}}}{2a_{\mathrm{cw}}p} I_{\mathrm{a}} \stackrel{!}{=} \alpha \frac{z_{\mathrm{a}}}{2a_{\mathrm{a}}p} I_{\mathrm{a}} = |\theta_{\mathrm{a}}|. \tag{4.16}$$

Above, the following parameters are used:

- $a_{\mathrm{cw}}/a_{\mathrm{a}}$: number of parallel conductors of the compensation and armature windings,
- $z_{\mathrm{cw}}/z_{\mathrm{a}}$: number of conductors of the compensation and armature windings.

In (4.16) α is only related to θ_{a} as we assume the armature area to be bigger (or at least the same size) as the field pole (cf. Fig. 4.22). From (4.16) we can calculate the required compensation winding conductors

$$z_{\mathrm{cw}} = \alpha z_{\mathrm{a}} \frac{a_{\mathrm{cw}}}{a_{\mathrm{a}}} = 2pQ_{\mathrm{cw}}N_{\mathrm{cw}} \tag{4.17}$$

which can be met by choosing Q_{cw} slots and N_{cw} turns per pole.

Counter measures: compensation winding and interpoles (cont.)

Interpole winding design: As discussed in (4.8), the reactane voltage $u_\mathrm{r} \approx L_\mathrm{c} i_\mathrm{a} \omega d_\mathrm{a}/(a w_\mathrm{b} 2)$ is self-induced within the short-circuited coil during commutation. To counteract this, the interpole winding is designed such that the neutral zone is (over-)compensated leading to an induced voltage u_ip which is opposite to u_r:

$$|u_\mathrm{ip}| \stackrel{!}{=} |u_\mathrm{r}|. \tag{4.18}$$

Assuming a rotational angular velocity ω and some (homogenous) $B_\mathrm{ip} \neq 0$ flux density in the interpole area, the induced voltage u_ip is

$$u_\mathrm{ip} = N_\mathrm{c} \omega d_\mathrm{a} l_\mathrm{z} B_\mathrm{ip}. \tag{4.19}$$

Here, N_c is the number of armature conductor turns per coil assuming that exatly one coil is placed in the interpole area.

Counter measures: compensation winding and interpoles (cont.)

From (4.18) and (4.19) we can calculate the required interpole flux density B_{ip}:

$$B_{\mathrm{ip}} = \frac{u_{\mathrm{r}}}{N_{\mathrm{c}}\omega d_{\mathrm{a}} l_{\mathrm{z}}} = \frac{L_{\mathrm{c}} i_{\mathrm{a}}}{2N_{\mathrm{c}} l_{\mathrm{z}} a w_{\mathrm{b}}}. \tag{4.20}$$

Applying the compensation winding design approach (4.16) results in:

$$\oint_{\partial S} \boldsymbol{H}\cdot\mathrm{d}\boldsymbol{s} = \theta_{\mathrm{ip}} + \theta_{\mathrm{cw}} - \theta_{\mathrm{a}} = \theta_{\mathrm{ip}} - \theta_{\mathrm{a}}(1-\alpha). \tag{4.21}$$

The MMFs per pole are:

$$\theta_{\mathrm{ip}} = N_{\mathrm{ip}} i_{\mathrm{a}}, \qquad \theta_{\mathrm{a}} = N_{\mathrm{a}} i_{\mathrm{a}}. \tag{4.22}$$

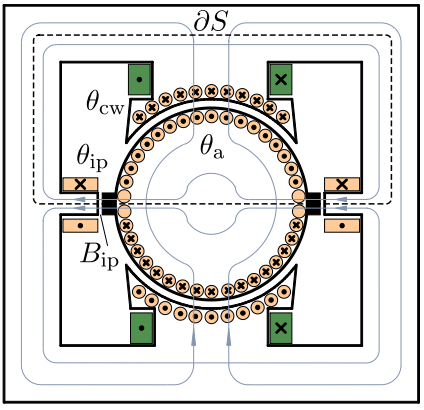

Fig. 4.24: Integration contour ∂S and related MMF components for the interpole winding design (adapted from J. Böcker, *Elektrische Antriebstechnik*, Paderborn University, 2020)

Counter measures: compensation winding and interpoles (cont.)

Assuming that the air gap reluctance is dominating the magnetic circuit, we receive

$$\oint_{\partial S} \boldsymbol{H} \cdot \mathrm{d}\boldsymbol{s} = 2\delta H_{\mathrm{ip}} = N_{\mathrm{ip}} i_{\mathrm{a}} - N_{\mathrm{a}} i_{\mathrm{a}} (1-\alpha). \quad (4.23)$$

The flux density in the interpole area is then

$$B_{\mathrm{ip}} = \mu_0 \frac{N_{\mathrm{ip}} - N_{\mathrm{a}}(1-\alpha)}{2\delta} i_{\mathrm{a}}. \quad (4.24)$$

The comparison with (4.20) reveals:

$$\mu_0 \frac{N_{\mathrm{ip}} - N_{\mathrm{a}}(1-\alpha)}{2\delta} i_{\mathrm{a}} \stackrel{!}{=} \frac{L_{\mathrm{c}}}{2 N_{\mathrm{c}} l_{\mathrm{z}} a w_{\mathrm{b}}} i_{\mathrm{a}} \quad (4.25)$$

$$\Leftrightarrow \quad N_{\mathrm{ip}} = N_{\mathrm{a}}(1-\alpha) + \frac{L_{\mathrm{c}} \delta}{\mu_0 N_{\mathrm{c}} l_{\mathrm{z}} a w_{\mathrm{b}}}.$$

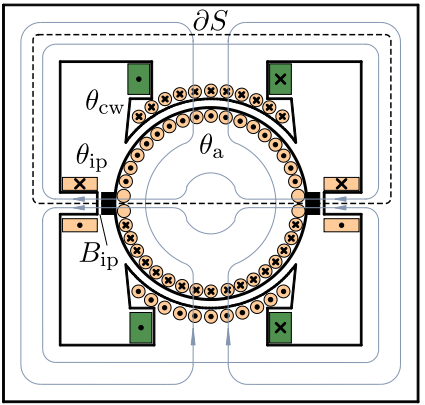

Connection types of DC machines

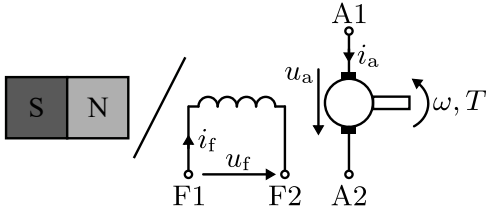

(a) Separately excited (or perm. magnet) DC machine

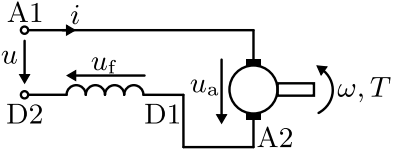

(b) Series DC machine

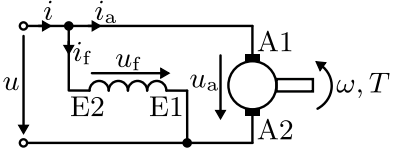

(c) Shunt DC machine

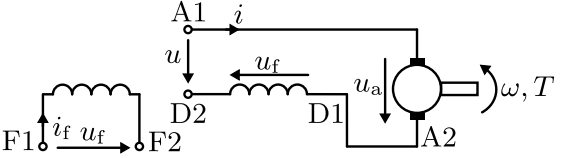

(d) Compound DC machine

Fig. 4.24: Connection types of DC machines incl. terminal block designations (note: the not shown interpole winding has the terminal block designation B1-B2 and the compensation winding C1-C2)

Steady-state behavior: separately excited DC machine

Assuming a fixed excitation ψ'_f (e.g., by a permanent magnet or constant field current), the separately excited DC machine's voltage demand for a certain speed is:

$$U_\mathrm{a} = R_\mathrm{a} I_\mathrm{a} + \omega \psi'_\mathrm{f}. \tag{4.26}$$

On the other hand, the speed-torque characteristic for a fixed armature voltage supply U_a is

$$T = \left(U_\mathrm{a} - \omega \psi'_\mathrm{f}\right) \frac{\psi'_\mathrm{f}}{R_\mathrm{a}} = U_\mathrm{a} \frac{\psi'_\mathrm{f}}{R_\mathrm{a}} - \omega \frac{\psi'^2_\mathrm{f}}{R_\mathrm{a}}. \tag{4.27}$$

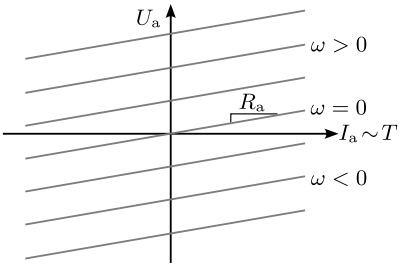

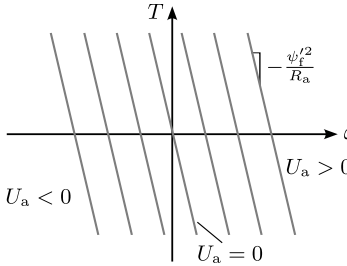

Fig. 4.25: Steady-state characteristics curves (adapted from J. Böcker, *Elektrische Antriebstechnik*, Paderborn University, 2020)

Steady-state behavior: separately excited DC machine (cont.)

For $U_\mathrm{a} = \text{const.} > 0$, the starting torque (i.e., the torque at zero speed) and the corresponding armature current are:

$$T(\omega = 0) = T_0 = U_\mathrm{a} \frac{\psi'_\mathrm{f}}{R_\mathrm{a}}, \qquad I_\mathrm{a}(\omega = 0) = I_{\mathrm{a},0} = \frac{U_\mathrm{a}}{R_\mathrm{a}}. \tag{4.28}$$

On the other hand for $T = 0$, the no-load speed ω_0 is:

$$\omega_0 = \frac{U_\mathrm{a}}{\psi'_\mathrm{f}}. \tag{4.29}$$

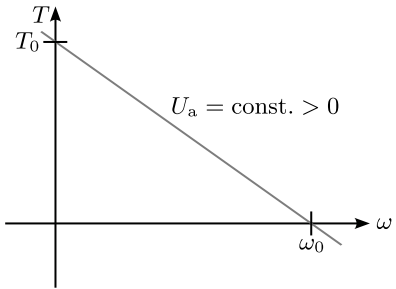

Fig. 4.26: Starting torque and no-load speed of a separately excited DC machine (adapted from J. Böcker, *Elektrische Antriebstechnik*, Paderborn University, 2020)

Steady-state behavior: separately excited DC machine (cont.)

As the start up of a DC machine with a fixed armature voltage U_a can lead to very high armature currents, which potentially cause damage, dropping resistors can be used to limit the armature current. While this approach was historically very common (e.g., in rail vehicles), its additional power losses and the necessity to carry bulky resistors are obvious drawbacks.

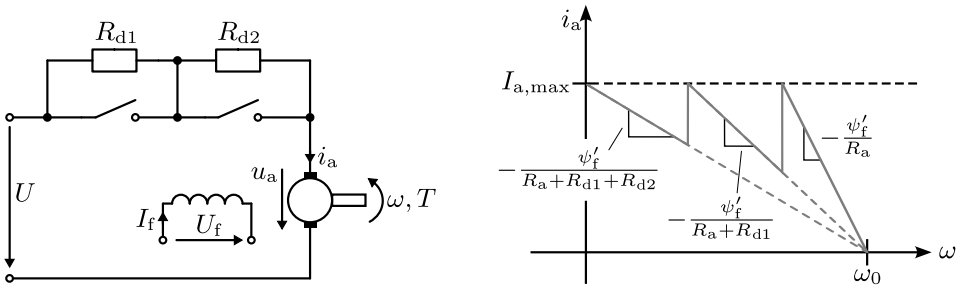

Fig. 4.27: Operation with dropping resistor during start up to limit the armature voltage (adapted from J. Böcker, *Elektrische Antriebstechnik*, Paderborn University, 2020)

Operation constraints: separately excited DC machine

Now we consider U_a being controllable (e.g., via buck converter), that is, we can also change I_a. Nevertheless, the machine is still limited by the voltage and current constraint:

$$U_\mathrm{max} \leq U_\mathrm{a} = \frac{R_\mathrm{a}}{\psi'_\mathrm{f}} T + \omega \psi'_\mathrm{f}, \qquad I_\mathrm{max} \leq I_\mathrm{a}. \tag{4.30}$$

For sake of simplicity we only consider the first quadrant (cf. Fig. 1.6), that is, positive torque and speed mode. From (4.30) $T \leq \psi'_\mathrm{f} I_\mathrm{max}$ follows. Also, the maximum speed is limited:

$$\omega \leq \frac{U_\mathrm{max}}{\psi'_\mathrm{f}} - \frac{R_\mathrm{a}}{\psi'^2_\mathrm{f}} T. \tag{4.31}$$

Hence, for a constant excitation ψ'_f, the torque must be reduced starting at ω_1 while ω_0 represents the no-load speed where no torque can be generated anymore:

$$\omega_1 = \frac{U_\mathrm{max}}{\psi'_\mathrm{f}} - \frac{R_\mathrm{a}}{\psi'_\mathrm{f}} I_\mathrm{max}, \qquad \omega_0 = \frac{U_\mathrm{max}}{\psi'_\mathrm{f}}. \tag{4.32}$$

Operation constraints: separately excited DC machine (cont.)

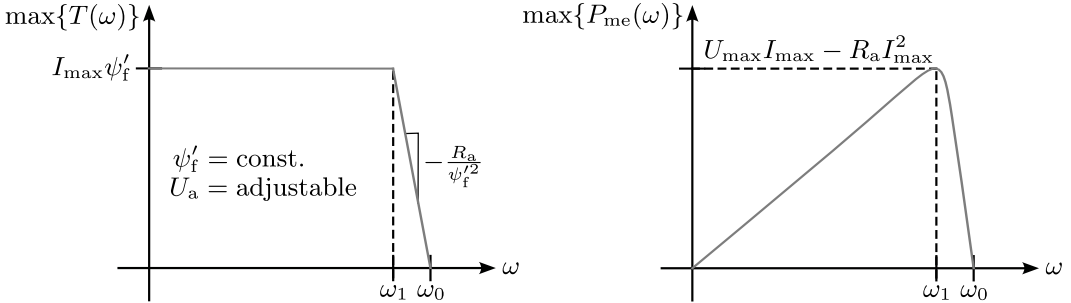

Fig. 4.28: Maximum achievable torque and mechanical power for the separately excited DC machine with a fixed excitation ψ'_f but controllable armature voltage U_a and current I_a

Field weakening of the separately excited DC machine

In the previous scenario, the no-load speed ω_0 is limited by the maximum armature voltage $U_{\max}$. However, if the field winding current I_f is also controllable, the no-load speed can be increased by decreasing the excitation ψ'_f (so-called field weakening). Consider an armature operation both at the voltage and current constraint:

$$U_{\max} = R_\mathrm{a} I_{\max} + \omega \psi'_\mathrm{f} = R_\mathrm{a} I_{\max} + \omega L'_\mathrm{f} i_\mathrm{f}. \tag{4.33}$$

For $\omega > \omega_1$ the field weakening is applied by reducing i_f to stay exactly at the armature voltage constraint:

$$i_\mathrm{f} = \frac{1}{\omega} \frac{U_{\max} - R_\mathrm{a} I_{\max}}{L'_\mathrm{f}}. \tag{4.34}$$

Hence, we need to reduce the excitation with $1/\omega$ resulting in the torque and mechanical power

$$T = \frac{1}{\omega} \left(U_{\max} I_{\max} - R_\mathrm{a} I_{\max}^2 \right), \qquad P_\mathrm{me} = U_{\max} I_{\max} - R_\mathrm{a} I_{\max}^2. \tag{4.35}$$

Field weakening of the separately excited DC machine (cont.)

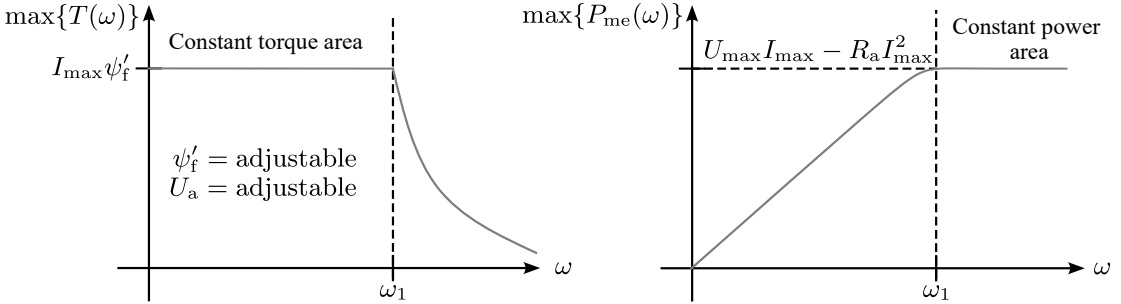

Fig. 4.29: Maximum achievable torque and mechanical power for the separately excited DC machine with a variable excitation ψ'_{f} as well as controllable armature voltage U_{a} and current I_{a}

Steady-state behavior: shunt DC machine

The shunt DC machine is characterized by:

$$U = U_\mathrm{a} = U_\mathrm{f}, \qquad I = I_\mathrm{a} + I_\mathrm{f}. \tag{4.36}$$

The steady-state currents are:

$$\begin{aligned} I_\mathrm{f} &= \frac{U_\mathrm{f}}{R_\mathrm{f}}, \\ I_\mathrm{a} &= \frac{U_\mathrm{a} - \omega L'_\mathrm{f} I_\mathrm{f}}{R_\mathrm{a}} = \frac{1 - L'_\mathrm{f}/R_\mathrm{f}\omega}{R_\mathrm{a}} U, \\ I &= I_\mathrm{a} + I_\mathrm{f} = \left(\frac{1}{R_\mathrm{a}} + \frac{1}{R_\mathrm{f}} - \frac{L'_\mathrm{f}\omega}{R_\mathrm{a} R_\mathrm{f}} \right) U. \end{aligned} \tag{4.37}$$

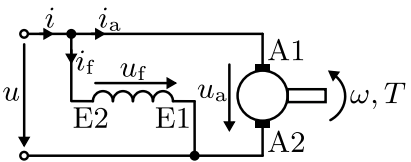

The resulting steady-state torque is:

$$T = L'_\mathrm{f} I_\mathrm{f} I_\mathrm{a} = L'_\mathrm{f} \frac{1 - L'_\mathrm{f}/R_\mathrm{f}\omega}{R_\mathrm{a} R_\mathrm{f}} U^2. \tag{4.38}$$

Steady-state behavior: series DC machine

The series DC machine is characterized by:

$$U = U_{\mathrm{a}} + U_{\mathrm{f}}, \qquad I = I_{\mathrm{a}} = I_{\mathrm{f}}. \tag{4.39}$$

We can rewrite the terminal voltage as

$$U = (R_{\mathrm{a}} + R_{\mathrm{f}})\, I + \omega L'_{\mathrm{f}} I = R'(\omega) I \tag{4.40}$$

with the effective speed-dependent resistance

$$R'(\omega) = R_{\mathrm{a}} + R_{\mathrm{f}} + \omega L'_{\mathrm{f}}. \tag{4.41}$$

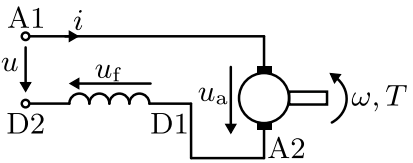

The steady-state torque is then

$$T = L'_{\mathrm{f}} I^2 = L'_{\mathrm{f}} \left(\frac{U}{R'(\omega)} \right)^2. \tag{4.42}$$

Steady-state behavior: series DC machine (cont.)

If the series DC machine is operated at the negative mechanical speed

$$\omega_\mathrm{r} = -\frac{R_\mathrm{a} + R_\mathrm{f}}{L'_\mathrm{f}}, \tag{4.43}$$

the current and the torque get (theoretically) infinite. This is due to the fact that the back EMF is exactly compensating the resistive voltage drop. Moreover, for from (4.42) we can observe that

$$T \to 0 \quad \Rightarrow \quad \omega \to \infty \tag{4.44}$$

holds for any DC voltage $U \neq 0$. This is due to inherent, load-dependent flux weakening effect of the series DC machine.

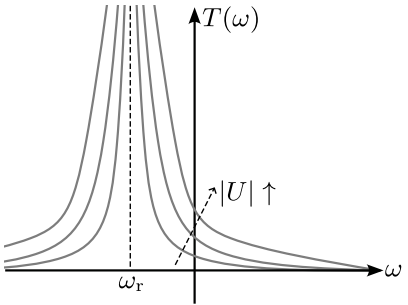

Fig. 4.30: Steady-state torque-speed characteristics for different DC voltage levels

Universal machine: series DC machine with sinusoidal excitation

From (4.42) it becomes clear that $T \sim I^2$ holds and, hence, the torque is independent of the sign of the current. Hence, the series DC machine can be also operated with an AC voltage supply (so-called universal machine).

Consider the sinusoidal excitation

$$u(t) = \hat{u}\cos(\omega_{\mathrm{el}}t + \varphi_{\mathrm{u}}) = \mathrm{Re}\left\{\hat{u}e^{\mathrm{j}(\omega_{\mathrm{el}}t+\varphi_{\mathrm{u}})}\right\}$$
$$= \mathrm{Re}\left\{\underline{U}e^{\mathrm{j}\omega_{\mathrm{el}}t}\right\},$$

which is represented by the complex phasor

$$\underline{U} = Ue^{\mathrm{j}\phi_{\mathrm{u}}} = \frac{1}{\sqrt{2}}\hat{u}e^{\mathrm{j}\varphi_{\mathrm{u}}}. \qquad (4.45)$$

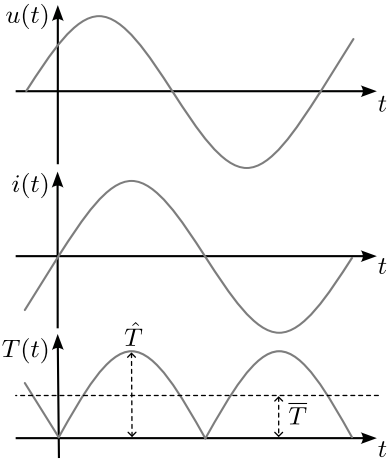

Fig. 4.31: Qualitative voltage, current and torque signals for a universal motor

Universal machine: series DC machine with sinusoidal excitation (cont.)

From (4.9) and (4.39) we can derive the complex voltage and current relations:

$$\underline{U} = R'(\omega)\underline{I} + \mathrm{j}\omega_{\mathrm{el}} L \underline{I} \tag{4.46}$$

with $L = L_{\mathrm{f}} + L_{\mathrm{a}}$. The current phasor is

$$\underline{I} = \frac{\underline{U}}{R'(\omega) + \mathrm{j}\omega_{\mathrm{el}} L} \tag{4.47}$$

resulting in the instantaneous current (setting $\varphi_{\mathrm{u}} = 0$)

$$i(t) = \mathrm{Re}\left\{\sqrt{2}\underline{I} e^{\mathrm{j}\omega_{\mathrm{el}} t}\right\} = \sqrt{2}\mathrm{Re}\left\{\frac{U\left(R'(\omega) - \mathrm{j}\omega_{\mathrm{el}} L\right)}{R'(\omega)^2 + \omega_{\mathrm{el}}^2 L^2} e^{\mathrm{j}\omega_{\mathrm{el}} t}\right\} \tag{4.48}$$

$$= \sqrt{2}\frac{U}{\sqrt{R'(\omega)^2 + \omega_{\mathrm{el}}^2 L^2}} \cos\left(\omega_{\mathrm{el}}(t - \frac{L}{R'(\omega)})\right). \tag{4.49}$$

Universal machine: series DC machine with sinusoidal excitation (cont.)

The resulting instantaneous torque is

$$
\begin{aligned}
T(t) &= L'_{\mathrm{f}} i^2(t) \\
&= 2L'_{\mathrm{f}} \frac{U^2}{R'(\omega)^2 + \omega_{\mathrm{el}}^2 L^2} \cos\left(\omega_{\mathrm{el}}(t - \frac{L}{R'(\omega)})\right)^2 \\
&= L'_{\mathrm{f}} \frac{U^2}{R'(\omega)^2 + \omega_{\mathrm{el}}^2 L^2} \left[1 + \cos\left(2\omega_{\mathrm{el}}(t - \frac{L}{R'(\omega)})\right)\right].
\end{aligned}
$$

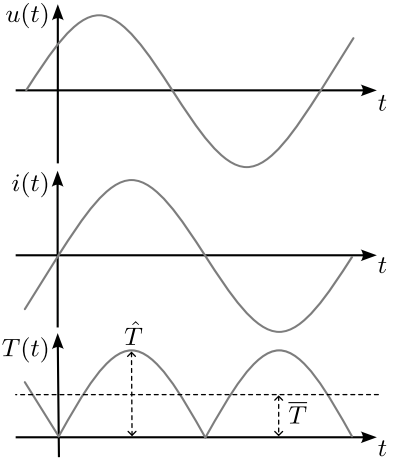

The peak and average torque are

$$
\hat{T} = 2L'_{\mathrm{f}} \frac{U^2}{R'(\omega)^2 + \omega_{\mathrm{el}}^2 L^2} = L'_{\mathrm{f}} \frac{\hat{u}^2}{R'(\omega)^2 + \omega_{\mathrm{el}}^2 L^2},
$$

$$
\overline{T} = \frac{\omega_{\mathrm{el}}}{2\pi} \int_0^{\frac{2\pi}{\omega_{\mathrm{el}}}} T(t)\mathrm{d}t = \frac{1}{2}\hat{T}. \qquad (4.50)
$$

Universal machine: series DC machine with sinusoidal excitation (cont.)

Some remarks on the universal machine:

- Only if the reactance $\omega_{\mathrm{el}} L$ impact on the voltage demand is negligible, the universal machine average torque at AC mode is identical to the series DC machine torque in DC mode applying the same effective voltage.
- Due to the AC field current, both the armature and stator should be based on a laminated iron core design to reduce iron losses.
- The peak armature and field currents are $\sqrt{2}$ times higher in the AC case than in DC operation. To prevent magnetic saturation, the iron paths must be designed larger than for an equivalent DC machine (i.e., leading to more volume and weight).

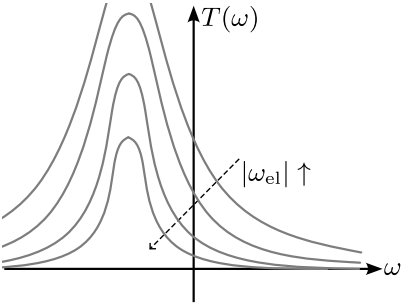

Fig. 4.32: Steady-state torque-speed characteristics for different AC voltage frequencies at a fixed voltage amplitude

Commutation of the universal machine

Assuming that the entire air gap field ϕ_δ is linked by the commutation coil, the time-varying excitation field induces an additional spark voltage u_{sp} within the commutation coil:

$$u_{\mathrm{sp}} = -N_{\mathrm{c}} \frac{p}{a} \frac{\mathrm{d}\phi_\delta}{\mathrm{d}t}. \tag{4.51}$$

Due to the time-varying excitation current, we have $\phi_\delta(t) = \hat{\phi}_\delta \cos(\omega_{\mathrm{el}} t)$ and, hence,

$$u_{\mathrm{sp}} = N_{\mathrm{c}} \frac{p}{a} \omega_{\mathrm{el}} \hat{\phi}_\delta \sin(\omega_{\mathrm{el}} t). \tag{4.52}$$

This additional induced spark voltage is shifted by (approx.) 90 degrees to the excitation field. Consequently, the interpole winding current is not in phase and does not compensate u_{sp}.

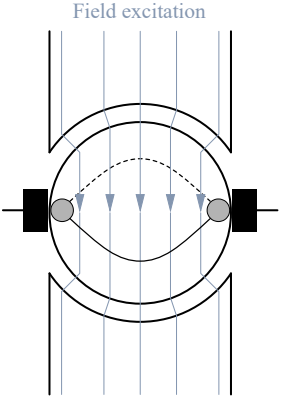

Fig. 4.33: Simplified illustration of the induced voltage within the short-circuited commutation coil by the varying excitation field

Commutation of the universal machine (cont.)

Assuming an ideal inductive behavior of the short-circuited coil, the induced spark voltage (4.52) leads to the current

$$i_{\mathrm{sp}} = -\frac{N_{\mathrm{c}}}{L_{\mathrm{c}}}\frac{p}{a}\hat{\phi}_{\delta}\cos(\omega_{\mathrm{el}}t). \tag{4.53}$$

This additional current will cause commutator sparking and, hence, the universal machine commutation process is more challenging than for a pure DC machine.

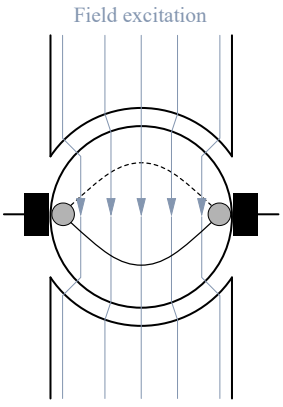

Conlusion on the universal machine

The drawbacks of the universal machine in terms of sizing and commutation sparking (leading to higher wear) are the reasons why this machine type is typical limited to low-cost applications (e.g., household appliances) nowadays.

Table of contents

Induction machines

Bikash Sah

Universität Siegen / IAS Interconnected Automation Systems

Basic induction machine (IM) representation

- Three-phase stator + three-phase rotor: "rotating three-phase transformer" (plus air gap)
- Rotor angular speed: ω_r
- Rotor angular displacement: ε_r
- Index "s" for stator, "r" for rotor quantities

Fundamental wave model

While it is known that the magnetic flux distribution in the air gap is subject to plentiful harmonics, the following model limits itself to the fundamental wave.

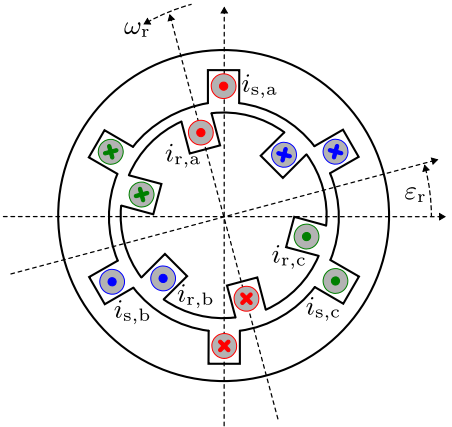

Fig. 5.1: Elementary three-phase induction machine (IM) lumped-coil representation ($p = 1$ pole pair)

Dynamical IM model

Based on Faraday's and Ohm's laws, we can write the following equations for the stator

$$\boldsymbol{u}^{\mathrm{s}}_{\mathrm{s,abc}}(t) = R_{\mathrm{s}}\boldsymbol{i}^{\mathrm{s}}_{\mathrm{s,abc}}(t) + \frac{\mathrm{d}}{\mathrm{d}t}\boldsymbol{\psi}^{\mathrm{s}}_{\mathrm{s,abc}}(t) \quad \Leftrightarrow \quad \begin{bmatrix} u^{\mathrm{s}}_{\mathrm{s,a}}(t) \\ u^{\mathrm{s}}_{\mathrm{s,b}}(t) \\ u_{\mathrm{s,c}}(t) \end{bmatrix} = R_{\mathrm{s}} \begin{bmatrix} i^{\mathrm{s}}_{\mathrm{s,a}}(t) \\ i^{\mathrm{s}}_{\mathrm{s,b}}(t) \\ i^{\mathrm{s}}_{\mathrm{s,c}}(t) \end{bmatrix} + \frac{\mathrm{d}}{\mathrm{d}t} \begin{bmatrix} \psi^{\mathrm{s}}_{\mathrm{s,a}}(t) \\ \psi^{\mathrm{s}}_{\mathrm{s,b}}(t) \\ \psi^{\mathrm{s}}_{\mathrm{s,c}}(t) \end{bmatrix} \tag{5.1}$$

and rotor

$$\boldsymbol{u}^{\mathrm{r}}_{\mathrm{r,abc}}(t) = R_{\mathrm{r}}\boldsymbol{i}^{\mathrm{r}}_{\mathrm{r,abc}}(t) + \frac{\mathrm{d}}{\mathrm{d}t}\boldsymbol{\psi}^{\mathrm{r}}_{\mathrm{r,abc}}(t) \quad \Leftrightarrow \quad \begin{bmatrix} u^{\mathrm{r}}_{\mathrm{r,a}}(t) \\ u^{\mathrm{r}}_{\mathrm{r,b}}(t) \\ u^{\mathrm{r}}_{\mathrm{r,c}}(t) \end{bmatrix} = R_{\mathrm{r}} \begin{bmatrix} i^{\mathrm{r}}_{\mathrm{r,a}}(t) \\ i^{\mathrm{r}}_{\mathrm{r,b}}(t) \\ i^{\mathrm{r}}_{\mathrm{r,c}}(t) \end{bmatrix} + \frac{\mathrm{d}}{\mathrm{d}t} \begin{bmatrix} \psi^{\mathrm{r}}_{\mathrm{r,a}}(t) \\ \psi^{\mathrm{r}}_{\mathrm{r,b}}(t) \\ \psi^{\mathrm{r}}_{\mathrm{r,c}}(t) \end{bmatrix} \tag{5.2}$$

which are generally applicable as only identical resistances per phase on the stator and rotor are assumed. Above, the lower index denotes the physical location of the quantities, while the upper index indicates the coordinate system orientation.

Flux linkage model

In contrast to the simple three-phase transformer model, the flux linkage model of the IM is more complex:

- Due to the spatial 120° phase shift between the windings of the stator and rotor, the abc phases are all mutually coupled.
- The flux paths and physical dimensions of the stator and rotor are not identical, i.e., the rotor and stator inductances are different (even if the winding turns N_s and N_r are identical).
- The coupling between the stator and rotor is rotor position-dependent (not explicitly shown on the right due to space limitations).

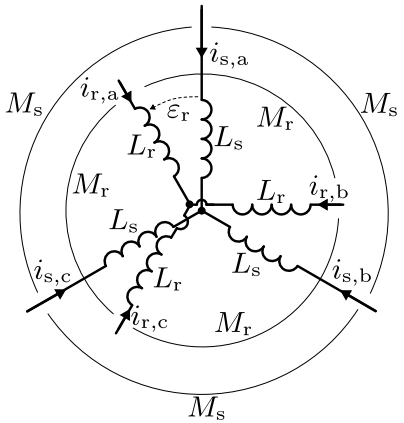

Fig. 5.2: Simplified representation of the inductive coupling between the stator/rotor phases of the IM

Flux linkages of the three-phase model

The flux linkages are given by

$$\begin{aligned}
\boldsymbol{\psi}^{\mathrm{s}}_{\mathrm{s,abc}}(t) &= \begin{bmatrix} L_{\mathrm{s}} & -\frac{M_{\mathrm{s}}}{2} & -\frac{M_{\mathrm{s}}}{2} \\ -\frac{M_{\mathrm{s}}}{2} & L_{\mathrm{s}} & -\frac{M_{\mathrm{s}}}{2} \\ -\frac{M_{\mathrm{s}}}{2} & -\frac{M_{\mathrm{s}}}{2} & L_{\mathrm{s}} \end{bmatrix} \boldsymbol{i}^{\mathrm{s}}_{\mathrm{s,abc}}(t) + M_{\mathrm{r}} \frac{N_{\mathrm{s}}}{N_{\mathrm{r}}} \boldsymbol{\mathcal{R}}_{\mathrm{abc}}(\varepsilon_{\mathrm{r,el}}(t)) \boldsymbol{i}^{\mathrm{r}}_{\mathrm{r,abc}}(t), \\
\boldsymbol{\psi}^{\mathrm{r}}_{\mathrm{r,abc}}(t) &= \begin{bmatrix} L_{\mathrm{r}} & -\frac{M_{\mathrm{r}}}{2} & -\frac{M_{\mathrm{r}}}{2} \\ -\frac{M_{\mathrm{r}}}{2} & L_{\mathrm{r}} & -\frac{M_{\mathrm{r}}}{2} \\ -\frac{M_{\mathrm{r}}}{2} & -\frac{M_{\mathrm{r}}}{2} & L_{\mathrm{r}} \end{bmatrix} \boldsymbol{i}^{\mathrm{r}}_{\mathrm{r,abc}}(t) + M_{\mathrm{s}} \frac{N_{\mathrm{r}}}{N_{\mathrm{s}}} \boldsymbol{\mathcal{R}}_{\mathrm{abc}}(\varepsilon_{\mathrm{r,el}}(t))^{\mathsf{T}} \boldsymbol{i}^{\mathrm{s}}_{\mathrm{s,abc}}(t)
\end{aligned} \tag{5.3}$$

with $\varepsilon_{\mathrm{r,el}}(t) = p\varepsilon_{\mathrm{r}}(t)$ and the transformation matrix

$$\boldsymbol{\mathcal{R}}_{\mathrm{abc}}(\varepsilon_{\mathrm{r,el}}(t)) = \begin{bmatrix} \cos(\varepsilon_{\mathrm{r,el}}(t)) & \cos(\varepsilon_{\mathrm{r,el}}(t) + \frac{2\pi}{3}) & \cos(\varepsilon_{\mathrm{r,el}}(t) - \frac{2\pi}{3}) \\ \cos(\varepsilon_{\mathrm{r,el}}(t) - \frac{2\pi}{3}) & \cos(\varepsilon_{\mathrm{r,el}}(t)) & \cos(\varepsilon_{\mathrm{r,el}}(t) + \frac{2\pi}{3}) \\ \cos(\varepsilon_{\mathrm{r,el}}(t) + \frac{2\pi}{3}) & \cos(\varepsilon_{\mathrm{r,el}}(t) - \frac{2\pi}{3}) & \cos(\varepsilon_{\mathrm{r,el}}(t)) \end{bmatrix}. \tag{5.4}$$

Inductance matrices of the three-phase model

The inductance matrices

$$\boldsymbol{L}_{\mathrm{s,abc}} = \begin{bmatrix} L_{\mathrm{s}} & -\frac{M_{\mathrm{s}}}{2} & -\frac{M_{\mathrm{s}}}{2} \\ -\frac{M_{\mathrm{s}}}{2} & L_{\mathrm{s}} & -\frac{M_{\mathrm{s}}}{2} \\ -\frac{M_{\mathrm{s}}}{2} & -\frac{M_{\mathrm{s}}}{2} & L_{\mathrm{s}} \end{bmatrix}, \qquad \boldsymbol{L}_{\mathrm{r,abc}} = \begin{bmatrix} L_{\mathrm{r}} & -\frac{M_{\mathrm{r}}}{2} & -\frac{M_{\mathrm{r}}}{2} \\ -\frac{M_{\mathrm{r}}}{2} & L_{\mathrm{r}} & -\frac{M_{\mathrm{r}}}{2} \\ -\frac{M_{\mathrm{r}}}{2} & -\frac{M_{\mathrm{r}}}{2} & L_{\mathrm{r}} \end{bmatrix}$$

are based on the following considerations.

- The self-inductances cover both the leakage and mutual coupling to other windings: $L_{\mathrm{s/r}} = L_{\mathrm{s/r},\sigma} + M_{\mathrm{s/r}}$.
- The mutual inductances on the stator/rotor $M_{\mathrm{s/r}}$ are identical, as all three phases share the same magnetic paths and have the same winding turns $N_{\mathrm{s/r}}$.
- The mutual inductances on the off diagonal represent the spatial displacement of the stator/rotor coils by $\pm 120^\circ$, which is why they are multiplied by $\cos(\pm 120^\circ) = -0.5$.
- In (5.3), the coupling term between stator and rotor is multiplied by the turn ratio to account for the different winding turns $N_{\mathrm{s/r}}$ (i.e., mapping the mutual inductances between stator/rotor).

Orthogonal representation: alpha-beta coordinates

- The three-phase IM model is obviously quite unhandy: six differential equations plus a rather complicated magnetic circuit representation.
- Remedy: transform the three-phase model into the orthogonal $\alpha\beta$ coordinates.
- Advantage: only four differential equations and a simpler magnetic circuit representation (as one will see on the next slides).

Coordinate transformations

The following transformations of the IM model into different coordinate systems are pure mathematical "tricks" to simplify the analysis. The IM remains a three-phase machine.

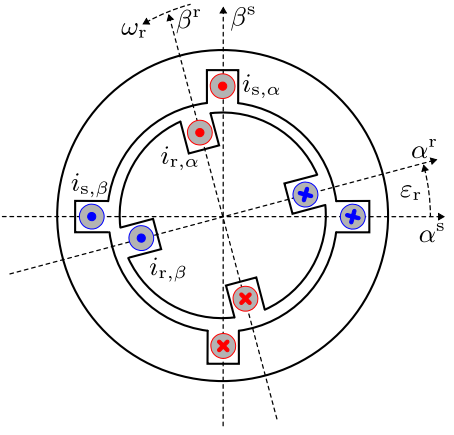

Fig. 5.3: Conceptual IM representation within the orthogonal $\alpha\beta$ coordinates ($p = 1$ pole pair)

Clarke transformation

To transform the three-phase model into the orthogonal $\alpha\beta$ coordinates, the Clarke transformation is applied. Consider any $\boldsymbol{x}_{\mathrm{abc}} \in \mathbb{R}^3$, then the Clarke transformation is given by

$$\boldsymbol{x}_{\alpha\beta 0} = \begin{bmatrix} x_\alpha \\ x_\beta \\ x_0 \end{bmatrix} = \begin{bmatrix} 2/3 & -1/3 & -1/3 \\ 0 & 1/\sqrt{3} & -1/\sqrt{3} \\ \sqrt{2}/3 & \sqrt{2}/3 & \sqrt{2}/3 \end{bmatrix} \begin{bmatrix} x_{\mathrm{a}} \\ x_{\mathrm{b}} \\ x_{\mathrm{c}} \end{bmatrix} = \boldsymbol{T}_{\mathrm{c}} \boldsymbol{x}_{\mathrm{abc}} \tag{5.5}$$

with the inverse transformation

$$\boldsymbol{x}_{\mathrm{abc}} = \begin{bmatrix} 1 & 0 & 1/\sqrt{2} \\ -1/2 & \sqrt{3}/2 & 1/\sqrt{2} \\ -1/2 & -\sqrt{3}/2 & 1/\sqrt{2} \end{bmatrix} \begin{bmatrix} x_\alpha \\ x_\beta \\ x_0 \end{bmatrix} = \boldsymbol{T}_{\mathrm{c}}^{-1} \boldsymbol{x}_{\alpha\beta 0}. \tag{5.6}$$

Above, $\boldsymbol{T}_{\mathrm{c}} \in \mathbb{R}^{3\times 3}$ is the Clarke transformation matrix and $\boldsymbol{x}_{\alpha\beta 0} \in \mathbb{R}^3$ the transformed vector.

Clarke transformation: amplitude and power scaling

The transformation (5.5) is amplitude-preserving, i.e., the amplitude of the $\alpha\beta$ vector is identical to the amplitude of the original abc vector. On the other hand, the power is not preserved, as can be seen from the inner product of the transformed vectors (which commonly occurs in power calculations):

$$\boldsymbol{x}_{\mathrm{abc}}^{\mathsf{T}}\boldsymbol{y}_{\mathrm{abc}} = \boldsymbol{x}_{\alpha\beta0}^{\mathsf{T}}\left(\boldsymbol{T}_{\mathrm{c}}^{-1}\right)^{\mathsf{T}}\boldsymbol{T}_{\mathrm{c}}^{-1}\boldsymbol{y}_{\alpha\beta0} \quad \Leftrightarrow \quad x_{\mathrm{a}}y_{\mathrm{a}} + x_{\mathrm{b}}y_{\mathrm{b}} + x_{\mathrm{c}}y_{\mathrm{c}} = \frac{3}{2}\left(x_\alpha y_\alpha + x_\beta y_\beta + x_0 y_0\right).$$

The alternative power-preserving Clarke transformation variant is given by

$$\boldsymbol{T}_{\mathrm{c}}' = \frac{\sqrt{3}}{2}\boldsymbol{T}_{\mathrm{c}} \qquad \left(\boldsymbol{T}_{\mathrm{c}}'\right)^{-1} = \left(\boldsymbol{T}_{\mathrm{c}}'\right)^{\mathsf{T}}, \tag{5.7}$$

which utilizes an orthogonal transformation matrix. However, when using $\boldsymbol{T}_{\mathrm{c}}'$ the amplitude of the transformed vector is not preserved. While being an arbitrary choice, we will stick to (5.5) as a convention for the following.

Clarke transformation: simplification for zero-component-free vectors

If the abc vector $\boldsymbol{x}_{\mathrm{abc}}$ is zero-component-free, i.e.,

$$x_{\mathrm{a}} + x_{\mathrm{b}} + x_{\mathrm{c}} = 0,$$

e.g., the phase currents of a star connected system, the Clarke transformation simplifies to

$$\boldsymbol{x}_{\alpha\beta} = \begin{bmatrix} x_\alpha \\ x_\beta \end{bmatrix} = \begin{bmatrix} 2/3 & -1/3 & -1/3 \\ 0 & 1/\sqrt{3} & -1/\sqrt{3} \end{bmatrix} \begin{bmatrix} x_{\mathrm{a}} \\ x_{\mathrm{b}} \\ x_{\mathrm{c}} \end{bmatrix} = \boldsymbol{T}_{23}\boldsymbol{x}_{\mathrm{abc}} \tag{5.8}$$

and

$$\boldsymbol{x}_{\mathrm{abc}} = \begin{bmatrix} 1 & 0 \\ -1/2 & \sqrt{3}/2 \\ -1/2 & -\sqrt{3}/2 \end{bmatrix} \begin{bmatrix} x_\alpha \\ x_\beta \end{bmatrix} = \boldsymbol{T}_{32}\boldsymbol{x}_{\alpha\beta}. \tag{5.9}$$

Clarke transformation: simplification for zero-component-free vectors

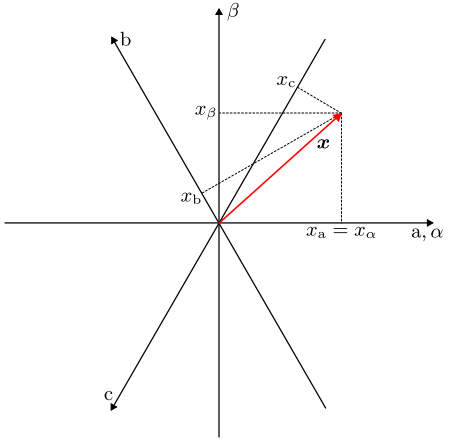

Fig. 5.4: Geometrical interpretation of the Clarke transformation without zero components: mapping $\boldsymbol{x}_{\mathrm{abc}} \in \mathbb{R}^3$ to $\boldsymbol{x}_{\alpha\beta} \in \mathbb{R}^2$ without information loss (adapted from J. Böcker, *Controlled Three-Phase Drives*, Paderborn University, 2021)

Park transformation

The Park transform rotates a vector $\boldsymbol{x}_{\alpha\beta} \in \mathbb{R}^2$ by a certain angle ε to obtain $\boldsymbol{x}_{\mathrm{dq}} \in \mathbb{R}^2$, that is,

$$\boldsymbol{x}_{\mathrm{dq}} = \begin{bmatrix} x_{\mathrm{d}} \\ x_{\mathrm{q}} \end{bmatrix} = \begin{bmatrix} \cos(\varepsilon) & \sin(\varepsilon) \\ -\sin(\varepsilon) & \cos(\varepsilon) \end{bmatrix} \begin{bmatrix} x_{\alpha} \\ x_{\beta} \end{bmatrix} = \boldsymbol{T}_{\mathrm{p}}^{-1}(\varepsilon)\boldsymbol{x}_{\alpha\beta} \tag{5.10}$$

with the counter rotation

$$\boldsymbol{x}_{\alpha\beta} = \begin{bmatrix} \cos(\varepsilon) & -\sin(\varepsilon) \\ \sin(\varepsilon) & \cos(\varepsilon) \end{bmatrix} \begin{bmatrix} x_{\mathrm{d}} \\ x_{\mathrm{q}} \end{bmatrix} = \boldsymbol{T}_{\mathrm{p}}(\varepsilon)\boldsymbol{x}_{\mathrm{dq}}. \tag{5.11}$$

Above, $\boldsymbol{T}_{\mathrm{p}} \in \mathbb{R}^{2\times 2}$ is the Park transformation matrix. It might be noted that is a (historical) convention to define that $\boldsymbol{T}_{\mathrm{p}}$ rotates into the mathematically positive direction. Depending on the application background and choice of ε, the interpretation of $\boldsymbol{x}_{\mathrm{dq}}$ can vary.

Park transformation (cont.)

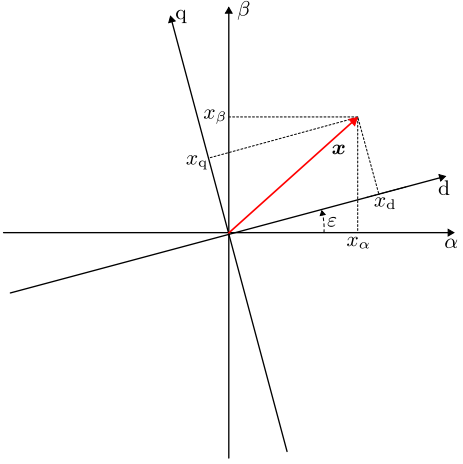

Fig. 5.5: Geometrical interpretation of the Park transformation: mapping $\boldsymbol{x}_{\alpha\beta} \in \mathbb{R}^2$ to $\boldsymbol{x}_{\mathrm{dq}} \in \mathbb{R}^2$ (adapted from J. Böcker, *Controlled Three-Phase Drives*, Paderborn University, 2021)

Park transformation: some properties

Performing the Park and inverse Park transformation sequentially, does not change the vector:

$$\boldsymbol{x}_{\alpha\beta} = \boldsymbol{T}_{\mathrm{p}}\boldsymbol{T}_{\mathrm{p}}^{-1}\boldsymbol{x}_{\alpha\beta} = \boldsymbol{T}_{\mathrm{p}}^{-1}\boldsymbol{T}_{\mathrm{p}}\boldsymbol{x}_{\alpha\beta}. \tag{5.12}$$

A frequent rotation within the electric machines and drives context is

$$\boldsymbol{T}_{\mathrm{p}}(\varepsilon = \pi/2) = \begin{bmatrix} \cos(\pi/2) & -\sin(\pi/2) \\ \sin(\pi/2) & \cos(\pi/2) \end{bmatrix} = \begin{bmatrix} 0 & -1 \\ 1 & 0 \end{bmatrix} = \boldsymbol{J} \tag{5.13}$$

leading to the definition of $\boldsymbol{J} \in \mathbb{R}^{2\times 2}$ which will be used for brevity in the following. Moreover, if ε results from some rotation, i.e., $\mathrm{d}/\mathrm{d}t\,\varepsilon(t) = \omega(t)$, we have:

$$\frac{\mathrm{d}}{\mathrm{d}t}\boldsymbol{T}_{\mathrm{p}}(\varepsilon(t)) = \begin{bmatrix} -\sin(\varepsilon(t)) & -\cos(\varepsilon(t)) \\ \cos(\varepsilon(t)) & -\sin(\varepsilon(t)) \end{bmatrix} \frac{\mathrm{d}}{\mathrm{d}t}\varepsilon(t) = \boldsymbol{T}_{\mathrm{p}}(\varepsilon(t))\boldsymbol{J}\omega(t), \tag{5.14}$$

$$\frac{\mathrm{d}}{\mathrm{d}t}\boldsymbol{T}_{\mathrm{p}}^{-1}(\varepsilon(t)) = \begin{bmatrix} -\sin(\varepsilon(t)) & \cos(\varepsilon(t)) \\ -\cos(\varepsilon(t)) & -\sin(\varepsilon(t)) \end{bmatrix} \frac{\mathrm{d}}{\mathrm{d}t}\varepsilon(t) = -\boldsymbol{T}_{\mathrm{p}}^{-1}(\varepsilon(t))\boldsymbol{J}\omega(t). \tag{5.15}$$

Visualization of different coordinate systems

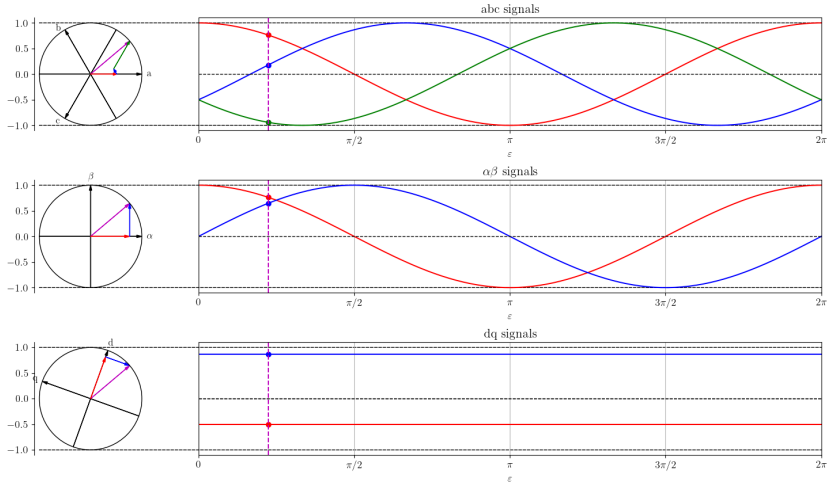

Fig. 5.6: Representation of a rotating phasor (without zero component) in different coordinate systems

IM model $\alpha\beta$ coordinates

Assuming zero-component-free three-phase quantities, multiplying the three-phase IM model (5.1) and (5.2) with $\boldsymbol{T}_{23}$ results in

$$\begin{aligned} \boldsymbol{T}_{23}\boldsymbol{u}^{\mathrm{s}}_{\mathrm{s,abc}}(t) &= R_{\mathrm{s}}\boldsymbol{T}_{23}\boldsymbol{i}^{\mathrm{s}}_{\mathrm{s,abc}}(t) + \boldsymbol{T}_{23}\frac{\mathrm{d}}{\mathrm{d}t}\boldsymbol{\psi}^{\mathrm{s}}_{\mathrm{s,abc}}(t) \\ \Leftrightarrow \quad \boldsymbol{u}^{\mathrm{s}}_{\mathrm{s},\alpha\beta}(t) &= R_{\mathrm{s}}\boldsymbol{i}^{\mathrm{s}}_{\mathrm{s},\alpha\beta}(t) + \frac{\mathrm{d}}{\mathrm{d}t}\boldsymbol{\psi}^{\mathrm{s}}_{\mathrm{s},\alpha\beta}(t) \end{aligned} \tag{5.16}$$

and

$$\begin{aligned} \boldsymbol{T}_{23}\boldsymbol{u}^{\mathrm{r}}_{\mathrm{r,abc}}(t) &= R_{\mathrm{r}}\boldsymbol{T}_{23}\boldsymbol{i}^{\mathrm{r}}_{\mathrm{r,abc}}(t) + \boldsymbol{T}_{23}\frac{\mathrm{d}}{\mathrm{d}t}\boldsymbol{\psi}^{\mathrm{r}}_{\mathrm{r,abc}}(t) \\ \Leftrightarrow \quad \boldsymbol{u}^{\mathrm{r}}_{\mathrm{r},\alpha\beta}(t) &= R_{\mathrm{r}}\boldsymbol{i}^{\mathrm{r}}_{\mathrm{r},\alpha\beta}(t) + \frac{\mathrm{d}}{\mathrm{d}t}\boldsymbol{\psi}^{\mathrm{r}}_{\mathrm{r},\alpha\beta}(t). \end{aligned} \tag{5.17}$$

Here, it must be noted that the two voltage equations are still represented in their own stator or rotor coordinate system. In particular, the rotor's $\alpha\beta$ axes are rotating (compare Fig. 5.3).

IM model $\alpha\beta$ coordinates: transformation of rotor quantities

To bring both model parts into the same coordinate system, the rotor quantities will be transformed into the stator's $\alpha\beta$ coordinates. This is done by applying the Park transformation with $\varepsilon(t) = \varepsilon_{\mathrm{r,el}}(t) = p\varepsilon_{\mathrm{r}}(t)$:

$$\begin{aligned} T_{\mathrm{p}}(\varepsilon_{\mathrm{r,el}}(t))\boldsymbol{u}^{\mathrm{r}}_{\mathrm{r},\alpha\beta}(t) &= T_{\mathrm{p}}(\varepsilon_{\mathrm{r,el}}(t))R_{\mathrm{r}}\boldsymbol{i}^{\mathrm{r}}_{\mathrm{r},\alpha\beta}(t) + T_{\mathrm{p}}(\varepsilon_{\mathrm{r,el}}(t))\frac{\mathrm{d}}{\mathrm{d}t}\boldsymbol{\psi}^{\mathrm{r}}_{\mathrm{r},\alpha\beta}(t) \\ \Leftrightarrow \quad \boldsymbol{u}^{\mathrm{s}}_{\mathrm{r},\alpha\beta}(t) &= R_{\mathrm{r}}\boldsymbol{i}^{\mathrm{s}}_{\mathrm{r},\alpha\beta}(t) + T_{\mathrm{p}}(\varepsilon_{\mathrm{r,el}}(t))\frac{\mathrm{d}}{\mathrm{d}t}\boldsymbol{\psi}^{\mathrm{r}}_{\mathrm{r},\alpha\beta}(t). \end{aligned} \tag{5.18}$$

The last term of (5.18) is rewritten as

$$\begin{aligned} T_{\mathrm{p}}(\varepsilon_{\mathrm{r,el}}(t))\frac{\mathrm{d}}{\mathrm{d}t}\boldsymbol{\psi}^{\mathrm{r}}_{\mathrm{r},\alpha\beta}(t) &= T_{\mathrm{p}}(\varepsilon_{\mathrm{r,el}}(t))\frac{\mathrm{d}}{\mathrm{d}t}\left[T_{\mathrm{p}}^{-1}(\varepsilon_{\mathrm{r,el}}(t))\boldsymbol{\psi}^{\mathrm{s}}_{\mathrm{r},\alpha\beta}(t)\right] \\ &= T_{\mathrm{p}}(\varepsilon_{\mathrm{r,el}}(t))\left[\frac{\mathrm{d}}{\mathrm{d}t}\left(T_{\mathrm{p}}^{-1}(\varepsilon_{\mathrm{r,el}}(t))\right)\boldsymbol{\psi}^{\mathrm{s}}_{\mathrm{r},\alpha\beta}(t) + T_{\mathrm{p}}^{-1}(\varepsilon_{\mathrm{r,el}}(t))\frac{\mathrm{d}}{\mathrm{d}t}\left(\boldsymbol{\psi}^{\mathrm{s}}_{\mathrm{r},\alpha\beta}(t)\right)\right] \\ &= -\omega_{\mathrm{r,el}}(t)\boldsymbol{J}\boldsymbol{\psi}^{\mathrm{s}}_{\mathrm{r},\alpha\beta}(t) + \frac{\mathrm{d}}{\mathrm{d}t}\boldsymbol{\psi}^{\mathrm{s}}_{\mathrm{r},\alpha\beta}(t). \end{aligned}$$

IM model $\alpha\beta$ coordinates: transformation of rotor quantities (cont.)

Hence, the IM model voltage equations in the stator-oriented $\alpha\beta$ coordinates are

$$\begin{aligned}\boldsymbol{u}^{\mathrm{s}}_{\mathrm{s},\alpha\beta}(t) &= R_{\mathrm{s}}\boldsymbol{i}^{\mathrm{s}}_{\mathrm{s},\alpha\beta}(t) + \frac{\mathrm{d}}{\mathrm{d}t}\boldsymbol{\psi}^{\mathrm{s}}_{\mathrm{s},\alpha\beta}(t),\\ \boldsymbol{u}^{\mathrm{s}}_{\mathrm{r},\alpha\beta}(t) &= R_{\mathrm{r}}\boldsymbol{i}^{\mathrm{s}}_{\mathrm{r},\alpha\beta}(t) - \omega_{\mathrm{r,el}}(t)\boldsymbol{J}\boldsymbol{\psi}^{\mathrm{s}}_{\mathrm{r},\alpha\beta}(t) + \frac{\mathrm{d}}{\mathrm{d}t}\boldsymbol{\psi}^{\mathrm{s}}_{\mathrm{r},\alpha\beta}(t).\end{aligned} \tag{5.19}$$

Furthermore, the flux linkages representation (5.3) should be also transformed into the stator-oriented $\alpha\beta$ coordinates. Hence, (5.3) is multiplied with $\boldsymbol{T}_{23}$:

$$\begin{aligned}\boldsymbol{\psi}^{\mathrm{s}}_{\mathrm{s},\alpha\beta}(t) &= \boldsymbol{T}_{23}\boldsymbol{\psi}^{\mathrm{s}}_{\mathrm{s,abc}}(t) = \overbrace{\boldsymbol{T}_{23}\boldsymbol{L}_{\mathrm{s,abc}}\boldsymbol{T}_{32}}^{\boldsymbol{L}_{\mathrm{s},\alpha\beta}}\boldsymbol{i}^{\mathrm{s}}_{\mathrm{s},\alpha\beta}(t) + M_{\mathrm{r}}\frac{N_{\mathrm{s}}}{N_{\mathrm{r}}}\overbrace{\boldsymbol{T}_{23}\boldsymbol{\mathcal{R}}_{\mathrm{abc}}(\varepsilon_{\mathrm{r,el}}(t))\boldsymbol{T}_{32}}^{\boldsymbol{\mathcal{R}}^{\mathrm{s}}_{\alpha\beta}(\varepsilon_{\mathrm{r,el}}(t))}\boldsymbol{i}^{\mathrm{r}}_{\mathrm{r},\alpha\beta}(t),\\ \boldsymbol{\psi}^{\mathrm{r}}_{\mathrm{r},\alpha\beta}(t) &= \boldsymbol{T}_{23}\boldsymbol{\psi}^{\mathrm{r}}_{\mathrm{r,abc}}(t) = \underbrace{\boldsymbol{T}_{23}\boldsymbol{L}_{\mathrm{r,abc}}\boldsymbol{T}_{32}}_{\boldsymbol{L}_{\mathrm{r},\alpha\beta}}\boldsymbol{i}^{\mathrm{r}}_{\mathrm{r},\alpha\beta}(t) + M_{\mathrm{s}}\frac{N_{\mathrm{r}}}{N_{\mathrm{s}}}\underbrace{\boldsymbol{T}_{23}\boldsymbol{\mathcal{R}}_{\mathrm{abc}}(\varepsilon_{\mathrm{r,el}}(t))^{\mathsf{T}}\boldsymbol{T}_{32}}_{\boldsymbol{\mathcal{R}}^{\mathrm{r}}_{\alpha\beta}(\varepsilon_{\mathrm{r,el}}(t))}\boldsymbol{i}^{\mathrm{s}}_{\mathrm{s},\alpha\beta}(t).\end{aligned} \tag{5.20}$$

IM model $\alpha\beta$ coordinates: transformation of rotor quantities (cont.)

Continuing from the previous slide, we can rewrite the newly defined inductance matrices as

$$\begin{aligned}\boldsymbol{L}_{\mathrm{s},\alpha\beta} &= \boldsymbol{T}_{23}\boldsymbol{L}_{\mathrm{s,abc}}\boldsymbol{T}_{32} = \begin{bmatrix} L_{\mathrm{s}} + {}^{M_{\mathrm{s}}}\!/_{2} & 0 \\ 0 & L_{\mathrm{s}} + {}^{M_{\mathrm{s}}}\!/_{2} \end{bmatrix} = (L_{\mathrm{s}} + {}^{M_{\mathrm{s}}}\!/_{2})\boldsymbol{I}, \\ \boldsymbol{L}_{\mathrm{r},\alpha\beta} &= \boldsymbol{T}_{23}\boldsymbol{L}_{\mathrm{r,abc}}\boldsymbol{T}_{32} = \begin{bmatrix} L_{\mathrm{r}} + {}^{M_{\mathrm{r}}}\!/_{2} & 0 \\ 0 & L_{\mathrm{r}} + {}^{M_{\mathrm{r}}}\!/_{2} \end{bmatrix} = (L_{\mathrm{r}} + {}^{M_{\mathrm{r}}}\!/_{2})\boldsymbol{I} \end{aligned} \tag{5.21}$$

and the rotation matrices as

$$\begin{aligned}\boldsymbol{\mathcal{R}}^{\mathrm{s}}_{\alpha\beta}(\varepsilon_{\mathrm{r,el}}(t)) &= \boldsymbol{T}_{23}\boldsymbol{\mathcal{R}}_{\mathrm{abc}}(\varepsilon_{\mathrm{r,el}}(t))\boldsymbol{T}_{32} \;= \frac{3}{2}\begin{bmatrix} \cos(\varepsilon_{\mathrm{r,el}}(t)) & -\sin(\varepsilon_{\mathrm{r,el}}(t)) \\ \sin(\varepsilon_{\mathrm{r,el}}(t)) & \cos(\varepsilon_{\mathrm{r,el}}(t)) \end{bmatrix} = \frac{3}{2}\boldsymbol{T}_{\mathrm{p}}(\varepsilon_{\mathrm{r,el}}(t)), \\ \boldsymbol{\mathcal{R}}^{\mathrm{r}}_{\alpha\beta}(\varepsilon_{\mathrm{r,el}}(t)) &= \boldsymbol{T}_{23}\boldsymbol{\mathcal{R}}_{\mathrm{abc}}(\varepsilon_{\mathrm{r,el}}(t))^{\mathsf{T}}\boldsymbol{T}_{32} = \frac{3}{2}\begin{bmatrix} \cos(\varepsilon_{\mathrm{r,el}}(t)) & \sin(\varepsilon_{\mathrm{r,el}}(t)) \\ -\sin(\varepsilon_{\mathrm{r,el}}(t)) & \cos(\varepsilon_{\mathrm{r,el}}(t)) \end{bmatrix} = \frac{3}{2}\boldsymbol{T}_{\mathrm{p}}^{-1}(\varepsilon_{\mathrm{r,el}}(t)). \end{aligned} \tag{5.22}$$

IM model $\alpha\beta$ coordinates: transformation of rotor quantities (cont.)

Inserting (5.21) and (5.22) into the flux linkage model (5.20) yields

$$\begin{aligned}\boldsymbol{\psi}^{\mathrm{s}}_{\mathrm{s},\alpha\beta}(t) &= (L_{\mathrm{s}} + {}^{M_{\mathrm{s}}}/_{2})\boldsymbol{i}^{\mathrm{s}}_{\mathrm{s},\alpha\beta}(t) + M_{\mathrm{r}}\frac{3}{2}\frac{N_{\mathrm{s}}}{N_{\mathrm{r}}}\boldsymbol{T}_{\mathrm{p}}(\varepsilon_{\mathrm{r,el}}(t))\boldsymbol{i}^{\mathrm{r}}_{\mathrm{r},\alpha\beta}(t),\\ \boldsymbol{\psi}^{\mathrm{r}}_{\mathrm{r},\alpha\beta}(t) &= (L_{\mathrm{r}} + {}^{M_{\mathrm{r}}}/_{2})\boldsymbol{i}^{\mathrm{r}}_{\mathrm{r},\alpha\beta}(t) + M_{\mathrm{s}}\frac{3}{2}\frac{N_{\mathrm{r}}}{N_{\mathrm{s}}}\boldsymbol{T}^{-1}_{\mathrm{p}}(\varepsilon_{\mathrm{r,el}}(t))\boldsymbol{i}^{\mathrm{s}}_{\mathrm{s},\alpha\beta}(t).\end{aligned} \tag{5.23}$$

Multiplying the second equation with $T_{\mathrm{p}}(\varepsilon_{\mathrm{r,el}}(t))$ from the left allows transforming the rotor flux linkage into the stator's $\alpha\beta$ coordinates

$$\boldsymbol{T}_{\mathrm{p}}(\varepsilon_{\mathrm{r,el}}(t))\boldsymbol{\psi}^{\mathrm{r}}_{\mathrm{r},\alpha\beta}(t) = (L_{\mathrm{r}} + {}^{M_{\mathrm{r}}}/_{2})\boldsymbol{T}_{\mathrm{p}}(\varepsilon_{\mathrm{r,el}}(t))\boldsymbol{i}^{\mathrm{r}}_{\mathrm{r},\alpha\beta}(t) + M_{\mathrm{s}}\frac{3}{2}\frac{N_{\mathrm{r}}}{N_{\mathrm{s}}}\boldsymbol{T}_{\mathrm{p}}(\varepsilon_{\mathrm{r,el}}(t))\boldsymbol{T}^{-1}_{\mathrm{p}}(\varepsilon_{\mathrm{r,el}}(t))\boldsymbol{i}^{\mathrm{s}}_{\mathrm{s},\alpha\beta}(t)$$

resulting in a mutual flux linkage model in the stator's $\alpha\beta$ coordinates:

$$\begin{aligned}\boldsymbol{\psi}^{\mathrm{s}}_{\mathrm{s},\alpha\beta}(t) &= (L_{\mathrm{s}} + {}^{M_{\mathrm{s}}}/_{2})\boldsymbol{i}^{\mathrm{s}}_{\mathrm{s},\alpha\beta}(t) + M_{\mathrm{r}}\frac{3}{2}\frac{N_{\mathrm{s}}}{N_{\mathrm{r}}}\boldsymbol{i}^{\mathrm{s}}_{\mathrm{r},\alpha\beta}(t),\\ \boldsymbol{\psi}^{\mathrm{s}}_{\mathrm{r},\alpha\beta}(t) &= (L_{\mathrm{r}} + {}^{M_{\mathrm{r}}}/_{2})\boldsymbol{i}^{\mathrm{s}}_{\mathrm{r},\alpha\beta}(t) + M_{\mathrm{s}}\frac{3}{2}\frac{N_{\mathrm{r}}}{N_{\mathrm{s}}}\boldsymbol{i}^{\mathrm{s}}_{\mathrm{s},\alpha\beta}(t).\end{aligned} \tag{5.24}$$

IM model $\alpha\beta$ coordinates: torque

To obtain the IM's torque equation, a power balance is performed w.r.t. (5.19). Dropping the time dependency for brevity, the power terms (transposed current times voltage) are

$$
\begin{aligned}
(\boldsymbol{i}^{\mathrm{s}}_{\mathrm{s},\alpha\beta})^{\mathsf{T}}\boldsymbol{u}^{\mathrm{s}}_{\mathrm{s},\alpha\beta} &= R_{\mathrm{s}}(\boldsymbol{i}^{\mathrm{s}}_{\mathrm{s},\alpha\beta})^{\mathsf{T}}\boldsymbol{i}^{\mathrm{s}}_{\mathrm{s},\alpha\beta}(t) + (\boldsymbol{i}^{\mathrm{s}}_{\mathrm{s},\alpha\beta})^{\mathsf{T}}\frac{\mathrm{d}}{\mathrm{d}t}\boldsymbol{\psi}^{\mathrm{s}}_{\mathrm{s},\alpha\beta},\\
(\boldsymbol{i}^{\mathrm{s}}_{\mathrm{r},\alpha\beta})^{\mathsf{T}}\boldsymbol{u}^{\mathrm{s}}_{\mathrm{r},\alpha\beta} &= R_{\mathrm{r}}(\boldsymbol{i}^{\mathrm{s}}_{\mathrm{r},\alpha\beta})^{\mathsf{T}}\boldsymbol{i}^{\mathrm{s}}_{\mathrm{r},\alpha\beta} - \omega_{\mathrm{r,el}}(\boldsymbol{i}^{\mathrm{s}}_{\mathrm{r},\alpha\beta})^{\mathsf{T}}\boldsymbol{J}\boldsymbol{\psi}^{\mathrm{s}}_{\mathrm{r},\alpha\beta} + (\boldsymbol{i}^{\mathrm{s}}_{\mathrm{r},\alpha\beta})^{\mathsf{T}}\frac{\mathrm{d}}{\mathrm{d}t}\boldsymbol{\psi}^{\mathrm{s}}_{\mathrm{r},\alpha\beta}.
\end{aligned}
\tag{5.25}
$$

Considering Fig. 1.5 and the Clarke transf. power mapping, one can identify the following:

$$
\begin{aligned}
&\text{Input power:} && \frac{2}{3}P_{\mathrm{el}} = (\boldsymbol{i}^{\mathrm{s}}_{\mathrm{s},\alpha\beta})^{\mathsf{T}}\boldsymbol{u}^{\mathrm{s}}_{\mathrm{s},\alpha\beta} + (\boldsymbol{i}^{\mathrm{s}}_{\mathrm{r},\alpha\beta})^{\mathsf{T}}\boldsymbol{u}^{\mathrm{s}}_{\mathrm{r},\alpha\beta},\\
&\text{Losses:} && \frac{2}{3}P_{\mathrm{l}} = R_{\mathrm{s}}(\boldsymbol{i}^{\mathrm{s}}_{\mathrm{s},\alpha\beta})^{\mathsf{T}}\boldsymbol{i}^{\mathrm{s}}_{\mathrm{s},\alpha\beta} + R_{\mathrm{r}}(\boldsymbol{i}^{\mathrm{s}}_{\mathrm{r},\alpha\beta})^{\mathsf{T}}\boldsymbol{i}^{\mathrm{s}}_{\mathrm{r},\alpha\beta},\\
&\text{Change of stored energy:} && \frac{2}{3}\frac{\mathrm{d}}{\mathrm{d}t}E_{\mathrm{i}} = (\boldsymbol{i}^{\mathrm{s}}_{\mathrm{s},\alpha\beta})^{\mathsf{T}}\frac{\mathrm{d}}{\mathrm{d}t}\boldsymbol{\psi}^{\mathrm{s}}_{\mathrm{s},\alpha\beta} + (\boldsymbol{i}^{\mathrm{s}}_{\mathrm{r},\alpha\beta})^{\mathsf{T}}\frac{\mathrm{d}}{\mathrm{d}t}\boldsymbol{\psi}^{\mathrm{s}}_{\mathrm{r},\alpha\beta},\\
&\text{Mechanical power:} && \frac{2}{3}P_{\mathrm{me}} = -\omega_{\mathrm{r,el}}(\boldsymbol{i}^{\mathrm{s}}_{\mathrm{r},\alpha\beta})^{\mathsf{T}}\boldsymbol{J}\boldsymbol{\psi}^{\mathrm{s}}_{\mathrm{r},\alpha\beta}.
\end{aligned}
\tag{5.26}
$$

IM model $\alpha\beta$ coordinates: torque (cont.)

From (5.26) one can compare the mechanical power representations

$$\frac{2}{3}P_{\mathrm{me}} = \frac{2}{3}\omega_{\mathrm{r}}T = -p\omega_{\mathrm{r}}(\boldsymbol{i}^{\mathrm{s}}_{\mathrm{r},\alpha\beta})^{\mathsf{T}}\boldsymbol{J}\boldsymbol{\psi}^{\mathrm{s}}_{\mathrm{r},\alpha\beta} \tag{5.27}$$

and find the torque expression

$$T = -\frac{3}{2}p(\boldsymbol{i}^{\mathrm{s}}_{\mathrm{r},\alpha\beta})^{\mathsf{T}}\boldsymbol{J}\boldsymbol{\psi}^{\mathrm{s}}_{\mathrm{r},\alpha\beta} = \frac{3}{2}p\left(\psi^{\mathrm{s}}_{\mathrm{r},\beta}i^{\mathrm{s}}_{\mathrm{r},\alpha} - \psi^{\mathrm{s}}_{\mathrm{r},\alpha}i^{\mathrm{s}}_{\mathrm{r},\beta}\right). \tag{5.28}$$

As all terms in (5.28) are invariant with respect to the choice of the coordinate system, the superscript labeling can be omitted:

$$T = \frac{3}{2}p\left(\psi_{\mathrm{r},\beta}i_{\mathrm{r},\alpha} - \psi_{\mathrm{r},\alpha}i_{\mathrm{r},\beta}\right). \tag{5.29}$$

If one would transform the model (5.19) into the rotor-oriented $\alpha\beta$ coordinates and redo the torque derivation, one would find the alternative torque expression

$$T = \frac{3}{2}p(\boldsymbol{i}_{\mathrm{s},\alpha\beta})^{\mathsf{T}}\boldsymbol{J}\boldsymbol{\psi}_{\mathrm{s},\alpha\beta} = \frac{3}{2}p\left(\psi_{\mathrm{s},\alpha}i_{\mathrm{s},\beta} - \psi_{\mathrm{s},\beta}i_{\mathrm{s},\alpha}\right). \tag{5.30}$$

Summary: IM model in stator-oriented $\alpha\beta$ coordinates

The most important equations of the IM model in the stator-oriented $\alpha\beta$ coordinates are:

$$\begin{aligned}
\text{Stator voltage:} \quad & \boldsymbol{u}^{\mathrm{s}}_{\mathrm{s},\alpha\beta}(t) = R_{\mathrm{s}}\boldsymbol{i}^{\mathrm{s}}_{\mathrm{s},\alpha\beta}(t) + \frac{\mathrm{d}}{\mathrm{d}t}\boldsymbol{\psi}^{\mathrm{s}}_{\mathrm{s},\alpha\beta}(t), \\
\text{Rotor voltage:} \quad & \boldsymbol{u}^{\mathrm{s}}_{\mathrm{r},\alpha\beta}(t) = R_{\mathrm{r}}\boldsymbol{i}^{\mathrm{s}}_{\mathrm{r},\alpha\beta}(t) - \omega_{\mathrm{r,el}}(t)\boldsymbol{J}\boldsymbol{\psi}^{\mathrm{s}}_{\mathrm{r},\alpha\beta}(t) + \frac{\mathrm{d}}{\mathrm{d}t}\boldsymbol{\psi}^{\mathrm{s}}_{\mathrm{r},\alpha\beta}(t), \\
\text{Stator flux linkage:} \quad & \boldsymbol{\psi}^{\mathrm{s}}_{\mathrm{s},\alpha\beta}(t) = (L_{\mathrm{s}} + {}^{M_{\mathrm{s}}}\!/_{2})\boldsymbol{i}^{\mathrm{s}}_{\mathrm{s},\alpha\beta}(t) + M_{\mathrm{r}}\frac{3}{2}\frac{N_{\mathrm{s}}}{N_{\mathrm{r}}}\boldsymbol{i}^{\mathrm{s}}_{\mathrm{r},\alpha\beta}(t), \\
\text{Rotor flux linkage:} \quad & \boldsymbol{\psi}^{\mathrm{s}}_{\mathrm{r},\alpha\beta}(t) = (L_{\mathrm{r}} + {}^{M_{\mathrm{r}}}\!/_{2})\boldsymbol{i}^{\mathrm{s}}_{\mathrm{r},\alpha\beta}(t) + M_{\mathrm{s}}\frac{3}{2}\frac{N_{\mathrm{r}}}{N_{\mathrm{s}}}\boldsymbol{i}^{\mathrm{s}}_{\mathrm{s},\alpha\beta}(t), \\
\text{Torque:} \quad & T(t) = \frac{3}{2}p(\boldsymbol{i}^{\mathrm{s}}_{\mathrm{s},\alpha\beta})^{\mathsf{T}}\boldsymbol{J}\boldsymbol{\psi}^{\mathrm{s}}_{\mathrm{s},\alpha\beta} = -\frac{3}{2}p(\boldsymbol{i}^{\mathrm{s}}_{\mathrm{r},\alpha\beta})^{\mathsf{T}}\boldsymbol{J}\boldsymbol{\psi}^{\mathrm{s}}_{\mathrm{r},\alpha\beta}.
\end{aligned}$$

It may be noted that the voltage and torque equations are independent of any linearity assumption, i.e., also apply to IMs with magnetic saturation. Only if the above flux linkage models are utilized, magnetic linearity is assumed.

Transformation of the rotor quantities based on the turn ratio

- The previous model depends on the physical parameters of the rotor: R_r, L_r, and M_r.
- Those parameters might not be accessible or known in practice (in particular when direct rotor measurements are not possible).
- Remedy: Transform the rotor quantities into the stator side based on the turn ratio $N_\mathrm{s}/N_\mathrm{r}$.
- Identical procedure to the transformer approach as from Fig. 3.11.
- Hence, stator-based measurements can be used to infer the rotor quantities (compare open-circuit test Fig. 3.17 and short-circuit test Fig. 3.18).

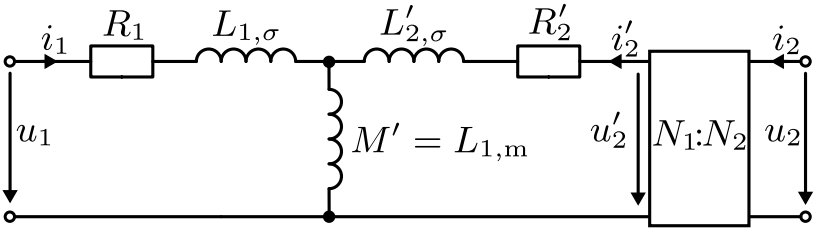

Transformation of the rotor quantities based on the turn ratio (cont.)

Applying (3.22) with $\alpha = {}^{N_\mathrm{s}}/_{N_\mathrm{r}}$ to the IM model interpreting the rotor as the secondary side results in

$$\begin{aligned} \boldsymbol{u}'_\mathrm{r} &= \frac{N_\mathrm{s}}{N_\mathrm{r}}\boldsymbol{u}_\mathrm{r}, \quad \boldsymbol{i}'_\mathrm{r} = \frac{N_\mathrm{r}}{N_\mathrm{s}}\boldsymbol{i}_\mathrm{r}, \quad \boldsymbol{\psi}'_{\mathrm{r},\alpha\beta} = \frac{N_\mathrm{s}}{N_\mathrm{r}}\boldsymbol{\psi}_{\mathrm{r},\alpha\beta}, \\ R'_\mathrm{r} &= \frac{N_\mathrm{s}^2}{N_\mathrm{r}^2}R_\mathrm{r}, \quad L'_\mathrm{r} = \frac{N_\mathrm{s}^2}{N_\mathrm{r}^2}L_\mathrm{r}, \quad M'_\mathrm{r} = \frac{N_\mathrm{s}}{N_\mathrm{r}}M_\mathrm{r}. \end{aligned} \tag{5.31}$$

Above, the indices representing the coordinate system are omitted as the transformation is independent of the chosen coordinate system.

Utilizing also $L_\mathrm{s} = L_{\sigma,\mathrm{s}} + M_\mathrm{s}$ and $L_\mathrm{r} = L_{\sigma,\mathrm{r}} + M_\mathrm{r}$, the flux linkage equations in the stator-oriented $\alpha\beta$ coordinates are then

$$\begin{aligned} \boldsymbol{\psi}^\mathrm{s}_{\mathrm{s},\alpha\beta}(t) &= (L_{\sigma,\mathrm{s}} + \frac{3}{2}M_\mathrm{s})\boldsymbol{i}^\mathrm{s}_{\mathrm{s},\alpha\beta}(t) + M'_\mathrm{r}\frac{3}{2}\boldsymbol{i}^{\mathrm{s}'}_{\mathrm{r},\alpha\beta}(t), \\ \boldsymbol{\psi}^{\mathrm{s}'}_{\mathrm{r},\alpha\beta}(t) &= (L'_{\sigma,\mathrm{r}} + \frac{3}{2}M'_\mathrm{r})\boldsymbol{i}^{\mathrm{s}'}_{\mathrm{r},\alpha\beta}(t) + M_\mathrm{s}\frac{3}{2}\boldsymbol{i}^\mathrm{s}_{\mathrm{s},\alpha\beta}(t). \end{aligned}$$

Transformation of the rotor quantities based on the turn ratio (cont.)

Analyzing the (magnetic) power balance reveals

$$\frac{3}{2}M_{\mathrm{s}} = \frac{3}{2}M'_{\mathrm{r}} = M, \tag{5.32}$$

that is, the mutual inductance is identical for both the stator and (transformed) rotor side. Hence, we can rewrite the flux linkage equations as

$$\boldsymbol{\psi}^{\mathrm{s}}_{\mathrm{s},\alpha\beta}(t) = (L_{\sigma,\mathrm{s}} + M)\boldsymbol{i}^{\mathrm{s}}_{\mathrm{s},\alpha\beta}(t) + M\boldsymbol{i}^{\mathrm{s}'}_{\mathrm{r},\alpha\beta}(t), \tag{5.33}$$

$$\boldsymbol{\psi}^{\mathrm{s}'}_{\mathrm{r},\alpha\beta}(t) = (L'_{\sigma,\mathrm{r}} + M)\boldsymbol{i}^{\mathrm{s}'}_{\mathrm{r},\alpha\beta}(t) + M\boldsymbol{i}^{\mathrm{s}}_{\mathrm{s},\alpha\beta}(t). \tag{5.34}$$

Alternatively, we can express the currents as a function of the flux linkages:

$$\boldsymbol{i}^{\mathrm{s}}_{\mathrm{s},\alpha\beta}(t) = \frac{(L_{\sigma,s} + M)\boldsymbol{\psi}^{\mathrm{s}}_{\mathrm{s},\alpha\beta}(t) - M\boldsymbol{\psi}^{\mathrm{s}'}_{\mathrm{r},\alpha\beta}(t)}{M(L_{\sigma,s} + L'_{\sigma,r}) + L_{\sigma,s}L'_{\sigma,r}}, \tag{5.35}$$

$$\boldsymbol{i}^{\mathrm{s}'}_{\mathrm{r},\alpha\beta}(t) = \frac{(L'_{\sigma,r} + M)\boldsymbol{\psi}^{\mathrm{s}'}_{\mathrm{r},\alpha\beta}(t) - M\boldsymbol{\psi}^{\mathrm{s}}_{\mathrm{s},\alpha\beta}(t)}{M(L'_{\sigma,r} + L_{\sigma,s}) + L'_{\sigma,r}L_{\sigma,s}}. \tag{5.36}$$

Transformation of the rotor quantities based on the turn ratio (cont.)

Rewriting the transformer's leakage coefficient definition (3.13) for the IM model as

$$\sigma = \frac{(L_{\sigma,s} + L'_{\sigma,r})M + L'_{\sigma,r}L_{\sigma,s}}{(M + L_{\sigma,s})(M + L'_{\sigma,r})} = 1 - \frac{M^2}{(M + L_{\sigma,s})(M + L'_{\sigma,r})} \tag{5.37}$$

allows expressing the currents as

$$\boldsymbol{i}^{\mathrm{s}}_{\mathrm{s},\alpha\beta}(t) = \frac{1}{\sigma(L_{\sigma,s} + M)} \left(\boldsymbol{\psi}^{\mathrm{s}}_{\mathrm{s},\alpha\beta}(t) - \frac{M}{M + L'_{\sigma,r}} \boldsymbol{\psi}^{\mathrm{s}'}_{\mathrm{r},\alpha\beta}(t) \right), \tag{5.38}$$

$$\boldsymbol{i}^{\mathrm{s}'}_{\mathrm{r},\alpha\beta}(t) = \frac{1}{\sigma(L'_{\sigma,r} + M)} \left(\boldsymbol{\psi}^{\mathrm{s}'}_{\mathrm{r},\alpha\beta}(t) - \frac{M}{M + L_{\sigma,s}} \boldsymbol{\psi}^{\mathrm{s}}_{\mathrm{s},\alpha\beta}(t) \right). \tag{5.39}$$

ECD of transformed IM model in general $\alpha\beta$ coordinates

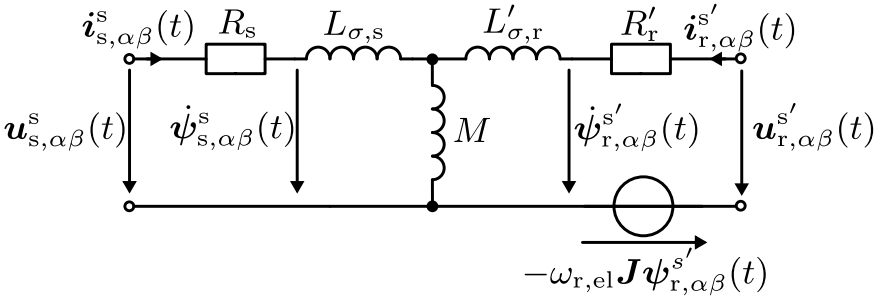

Fig. 5.7: T-type ECD of an IM in stator-oriented $\alpha\beta$ coordinates with rotor quantities transformed using $\alpha = {}^{N_{\mathrm{s}}}/_{N_{\mathrm{r}}}$

Summary: transformed IM model in stator-oriented $\alpha\beta$ coordinates

The most important equations of the IM model in the stator-oriented $\alpha\beta$ coordinates with all rotor quantities transformed to the stator side are:

$$\text{Stator voltage:} \quad \boldsymbol{u}^{\mathrm{s}}_{\mathrm{s},\alpha\beta}(t) = R_{\mathrm{s}}\boldsymbol{i}^{\mathrm{s}}_{\mathrm{s},\alpha\beta}(t) + \frac{\mathrm{d}}{\mathrm{d}t}\boldsymbol{\psi}^{\mathrm{s}}_{\mathrm{s},\alpha\beta}(t),$$

$$\text{Rotor voltage:} \quad \boldsymbol{u}^{\mathrm{s}'}_{\mathrm{r},\alpha\beta}(t) = R_{\mathrm{r}}\boldsymbol{i}^{\mathrm{s}'}_{\mathrm{r},\alpha\beta}(t) - \omega_{\mathrm{r,el}}(t)\boldsymbol{J}\boldsymbol{\psi}^{\mathrm{s}'}_{\mathrm{r},\alpha\beta}(t) + \frac{\mathrm{d}}{\mathrm{d}t}\boldsymbol{\psi}^{\mathrm{s}'}_{\mathrm{r},\alpha\beta}(t),$$

$$\text{Stator flux linkage:} \quad \boldsymbol{\psi}^{\mathrm{s}}_{\mathrm{s},\alpha\beta}(t) = (L_{\sigma,\mathrm{s}} + M)\boldsymbol{i}^{\mathrm{s}}_{\mathrm{s},\alpha\beta}(t) + M\boldsymbol{i}^{\mathrm{s}'}_{\mathrm{r},\alpha\beta}(t),$$

$$\text{Rotor flux linkage:} \quad \boldsymbol{\psi}^{\mathrm{s}'}_{\mathrm{r},\alpha\beta}(t) = (L'_{\sigma,\mathrm{r}} + M)\boldsymbol{i}^{\mathrm{s}'}_{\mathrm{r},\alpha\beta}(t) + M\boldsymbol{i}^{\mathrm{s}}_{\mathrm{s},\alpha\beta}(t),$$

$$\text{Torque:} \quad T(t) = \frac{3}{2}p(\boldsymbol{i}^{\mathrm{s}}_{\mathrm{s},\alpha\beta}(t))^{\mathsf{T}}\boldsymbol{J}\boldsymbol{\psi}^{\mathrm{s}}_{\mathrm{s},\alpha\beta}(t) = -\frac{3}{2}p(\boldsymbol{i}^{\mathrm{s}'}_{\mathrm{r},\alpha\beta}(t))^{\mathsf{T}}\boldsymbol{J}\boldsymbol{\psi}^{\mathrm{s}'}_{\mathrm{r},\alpha\beta}(t).$$

The transformed rotor quantities are $\boldsymbol{u}'_{\mathrm{r}} = \alpha\boldsymbol{u}_{\mathrm{r}}$, $\boldsymbol{i}'_{\mathrm{r}} = {}^{1}\!/\!_{\alpha}\boldsymbol{i}_{\mathrm{r}}$, $\boldsymbol{\psi}'_{\mathrm{r}} = \alpha\boldsymbol{\psi}_{\mathrm{r}}$, $R'_{\mathrm{r}} = \alpha^2 R_{\mathrm{r}}$, $L'_{\mathrm{r}} = \alpha^2 L_{\mathrm{r}}$, and $M'_{\mathrm{r}} = \alpha M_{\mathrm{r}}$ with $\alpha = {}^{N_{\mathrm{s}}}\!/\!_{N_{\mathrm{r}}}$.

General rotating coordinate system k

- In $\alpha\beta$ coordinates, all quantities have sinusoidal trajectory under regular IM operation.
- Compare rotating field theory: sinusoidal phase currents lead to sinusoidal $\alpha\beta$ currents.

K coordinate system

To simplify the machine analysis, a general rotating coordinate system k is introduced. The orientation of the d-axis of that coordinate system can be chosen freely, however, if aligned to the stator or rotor flux linkage vector all quantities become constant during steady state (cf. Fig. 5.6).

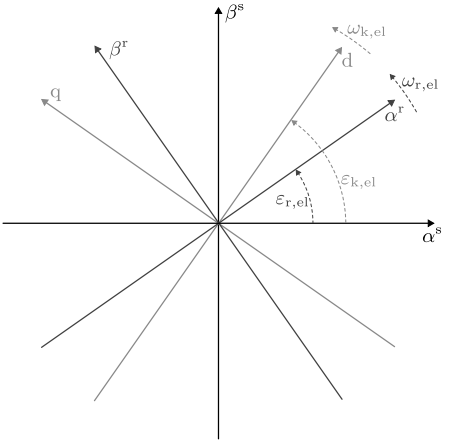

Fig. 5.8: Comparison of coordinate systems

IM model in coordinate system k

Applying the Park transformation to the IM model in the stator-oriented $\alpha\beta$ coordinates results in (dropping the time dependency for brevity):

$$\begin{aligned}
\boldsymbol{u}^{\mathrm{k}}_{\mathrm{s,dq}} &= \boldsymbol{T}^{-1}_{\mathrm{p}}(\varepsilon_{\mathrm{k,el}})\boldsymbol{u}^{\mathrm{s}}_{\mathrm{s},\alpha\beta}, \quad \boldsymbol{i}^{\mathrm{k}}_{\mathrm{s,dq}} = \boldsymbol{T}^{-1}_{\mathrm{p}}(\varepsilon_{\mathrm{k,el}})\boldsymbol{i}^{\mathrm{s}}_{\mathrm{s},\alpha\beta}, \quad \boldsymbol{\psi}^{\mathrm{k}}_{\mathrm{s,dq}} = \boldsymbol{T}^{-1}_{\mathrm{p}}(\varepsilon_{\mathrm{k,el}})\boldsymbol{\psi}^{\mathrm{s}}_{\mathrm{s},\alpha\beta}, \\
\boldsymbol{u}^{\mathrm{k}}_{\mathrm{r,dq}} &= \boldsymbol{T}^{-1}_{\mathrm{p}}(\varepsilon_{\mathrm{k,el}})\boldsymbol{u}^{\mathrm{s}}_{\mathrm{r},\alpha\beta}, \quad \boldsymbol{i}^{\mathrm{k}}_{\mathrm{r,dq}} = \boldsymbol{T}^{-1}_{\mathrm{p}}(\varepsilon_{\mathrm{k,el}})\boldsymbol{i}^{\mathrm{s}}_{\mathrm{r},\alpha\beta}, \quad \boldsymbol{\psi}^{\mathrm{k}}_{\mathrm{r,dq}} = \boldsymbol{T}^{-1}_{\mathrm{p}}(\varepsilon_{\mathrm{k,el}})\boldsymbol{\psi}^{\mathrm{s}}_{\mathrm{r},\alpha\beta}.
\end{aligned} \tag{5.40}$$

The transformed flux linkage model in the k coordinate system remains structurally unaffected by the coordinate transformation

$$\begin{aligned}
\boldsymbol{\psi}^{\mathrm{k}}_{\mathrm{s,dq}} &= (L_{\mathrm{s}} + {}^{M_{\mathrm{s}}}\!/_{2})\boldsymbol{i}^{\mathrm{k}}_{\mathrm{s,dq}} + M_{\mathrm{r}}\frac{3}{2}\frac{N_{\mathrm{s}}}{N_{\mathrm{r}}}\boldsymbol{i}^{\mathrm{k}}_{\mathrm{r,dq}}, \\
\boldsymbol{\psi}^{\mathrm{k}}_{\mathrm{r,dq}} &= (L_{\mathrm{r}} + {}^{M_{\mathrm{r}}}\!/_{2})\boldsymbol{i}^{\mathrm{k}}_{\mathrm{r,dq}} + M_{\mathrm{s}}\frac{3}{2}\frac{N_{\mathrm{r}}}{N_{\mathrm{s}}}\boldsymbol{i}^{\mathrm{k}}_{\mathrm{s,dq}}
\end{aligned} \tag{5.41}$$

since both the current and flux linkage vectors are transformed in the same way starting from (5.24).

IM model in coordinate system k (cont.)

Likewise, the torque is invariant with respect to the chosen coordinate system:

$$T = \frac{3}{2} p \left(\boldsymbol{i}_{\mathrm{s,dq}}\right)^{\mathsf{T}} \boldsymbol{J} \boldsymbol{\psi}_{\mathrm{s,dq}} = -\frac{3}{2} p \left(\boldsymbol{i}_{\mathrm{r,dq}}\right)^{\mathsf{T}} \boldsymbol{J} \boldsymbol{\psi}_{\mathrm{r,dq}}. \tag{5.42}$$

Applying the Park transformation derivative rule (5.15) to the voltage equations in the k coordinate system yields

$$\begin{aligned} \boldsymbol{u}^{\mathrm{k}}_{\mathrm{s,dq}} &= R_{\mathrm{s}} \boldsymbol{i}^{\mathrm{k}}_{\mathrm{s,dq}} + \omega_{\mathrm{k,el}} \boldsymbol{J} \boldsymbol{\psi}^{\mathrm{k}}_{\mathrm{s,dq}} + \frac{\mathrm{d}}{\mathrm{d}t} \boldsymbol{\psi}^{\mathrm{k}}_{\mathrm{s,dq}}, \\ \boldsymbol{u}^{\mathrm{k}}_{\mathrm{r,dq}} &= R_{\mathrm{r}} \boldsymbol{i}^{\mathrm{k}}_{\mathrm{r,dq}} + \left(\omega_{\mathrm{k,el}} - \omega_{\mathrm{r,el}}\right) \boldsymbol{J} \boldsymbol{\psi}^{\mathrm{k}}_{\mathrm{r,dq}} + \frac{\mathrm{d}}{\mathrm{d}t} \boldsymbol{\psi}^{\mathrm{k}}_{\mathrm{r,dq}}. \end{aligned} \tag{5.43}$$

Likewise, the transformation of the rotor quantities based on the turn ratio $\alpha = {}^{N_{\mathrm{s}}}\!/_{N_{\mathrm{r}}}$ can be applied to the k coordinate system:

$$\begin{gathered} \boldsymbol{u}^{\mathrm{k}'}_{\mathrm{r,dq}} = \alpha \boldsymbol{u}^{\mathrm{k}}_{\mathrm{r,dq}}, \quad \boldsymbol{i}^{\mathrm{k}'}_{\mathrm{r,dq}} = {}^{1}\!/_{\alpha} \boldsymbol{i}^{\mathrm{k}}_{\mathrm{r,dq}}, \quad \boldsymbol{\psi}^{\mathrm{k}'}_{\mathrm{r,dq}} = \alpha \boldsymbol{\psi}^{\mathrm{k}}_{\mathrm{r,dq}}, \\ R'_{\mathrm{r}} = \alpha^2 R_{\mathrm{r}}, \quad L'_{\mathrm{r}} = \alpha^2 L_{\mathrm{r}}, \quad M'_{\mathrm{r}} = \alpha M_{\mathrm{r}}. \end{gathered} \tag{5.44}$$

Summary: IM model in general dq coordinates

The most important equations of the IM model in the general k coordinate system with dq coordinates are:

$$\text{Stator voltage:} \quad \boldsymbol{u}^{\mathrm{k}}_{\mathrm{s,dq}}(t) = R_{\mathrm{s}}\boldsymbol{i}^{\mathrm{k}}_{\mathrm{s,dq}}(t) + \omega_{\mathrm{k,el}}(t)\boldsymbol{J}\boldsymbol{\psi}^{\mathrm{k}}_{\mathrm{s,dq}}(t) + \frac{\mathrm{d}}{\mathrm{d}t}\boldsymbol{\psi}^{\mathrm{k}}_{\mathrm{s,dq}}(t),$$

$$\text{Rotor voltage:} \quad \boldsymbol{u}^{\mathrm{k}}_{\mathrm{r,dq}}(t) = R_{\mathrm{r}}\boldsymbol{i}^{\mathrm{k}}_{\mathrm{r,dq}}(t) + \left(\omega_{\mathrm{k,el}}(t) - \omega_{\mathrm{r,el}}(t)\right)\boldsymbol{J}\boldsymbol{\psi}^{\mathrm{k}}_{\mathrm{r,dq}}(t) + \frac{\mathrm{d}}{\mathrm{d}t}\boldsymbol{\psi}^{\mathrm{k}}_{\mathrm{r,dq}}(t),$$

$$\text{Stator flux linkage:} \quad \boldsymbol{\psi}^{\mathrm{k}}_{\mathrm{s,dq}}(t) = (L_{\mathrm{s}} + {}^{M_{\mathrm{s}}}\!/_{2})\boldsymbol{i}^{\mathrm{k}}_{\mathrm{s,dq}}(t) + M_{\mathrm{r}}\frac{3}{2}\frac{N_{\mathrm{s}}}{N_{\mathrm{r}}}\boldsymbol{i}^{\mathrm{k}}_{\mathrm{r,dq}}(t),$$

$$\text{Rotor flux linkage:} \quad \boldsymbol{\psi}^{\mathrm{k}}_{\mathrm{r,dq}}(t) = (L_{\mathrm{r}} + {}^{M_{\mathrm{r}}}\!/_{2})\boldsymbol{i}^{\mathrm{k}}_{\mathrm{r,dq}}(t) + M_{\mathrm{s}}\frac{3}{2}\frac{N_{\mathrm{r}}}{N_{\mathrm{s}}}\boldsymbol{i}^{\mathrm{k}}_{\mathrm{s,dq}}(t),$$

$$\text{Torque:} \quad T(t) = \frac{3}{2}p(\boldsymbol{i}^{\mathrm{k}}_{\mathrm{s,dq}}(t))^{\mathsf{T}}\boldsymbol{J}\boldsymbol{\psi}^{\mathrm{k}}_{\mathrm{s,dq}}(t) = -\frac{3}{2}p(\boldsymbol{i}^{\mathrm{k}}_{\mathrm{r,dq}}(t))^{\mathsf{T}}\boldsymbol{J}\boldsymbol{\psi}^{\mathrm{k}}_{\mathrm{r,dq}}(t).$$

Likewise in the stator-oriented $\alpha\beta$ coordinates, one can further transform the rotor quantities based on the turn ratio $\alpha = {}^{N_{\mathrm{s}}}\!/_{N_{\mathrm{r}}}$ to infer the rotor parameters from stator-based measurements (cf. next slide).

Summary: transformed IM model in general dq coordinates

The most important equations of the IM model in the general k coordinate system with dq coordinates with all rotor quantities transformed to the stator side are:

$$\text{Stator voltage:} \quad \boldsymbol{u}^{\mathrm{k}}_{\mathrm{s,dq}}(t) = R_{\mathrm{s}}\boldsymbol{i}^{\mathrm{k}}_{\mathrm{s,dq}}(t) + \omega_{\mathrm{k,el}}(t)\boldsymbol{J}\boldsymbol{\psi}^{\mathrm{k}}_{\mathrm{s,dq}}(t) + \frac{\mathrm{d}}{\mathrm{d}t}\boldsymbol{\psi}^{\mathrm{k}}_{\mathrm{s,dq}}(t),$$

$$\text{Rotor voltage:} \quad \boldsymbol{u}^{\mathrm{k}'}_{\mathrm{r,dq}}(t) = R_{\mathrm{r}}\boldsymbol{i}^{\mathrm{k}'}_{\mathrm{r,dq}}(t) + (\omega_{\mathrm{k,el}}(t) - \omega_{\mathrm{r,el}}(t))\,\boldsymbol{J}\boldsymbol{\psi}^{\mathrm{k}'}_{\mathrm{r,dq}}(t) + \frac{\mathrm{d}}{\mathrm{d}t}\boldsymbol{\psi}^{\mathrm{k}'}_{\mathrm{r,dq}}(t),$$

$$\text{Stator flux linkage:} \quad \boldsymbol{\psi}^{\mathrm{k}}_{\mathrm{s,dq}}(t) = (L_{\sigma,\mathrm{s}} + M)\boldsymbol{i}^{\mathrm{k}}_{\mathrm{s,dq}}(t) + M\boldsymbol{i}^{\mathrm{k}'}_{\mathrm{r,dq}}(t),$$

$$\text{Rotor flux linkage:} \quad \boldsymbol{\psi}^{\mathrm{k}'}_{\mathrm{r,dq}}(t) = (L'_{\sigma,\mathrm{r}} + M)\boldsymbol{i}^{\mathrm{k}'}_{\mathrm{r,dq}}(t) + M\boldsymbol{i}^{\mathrm{k}}_{\mathrm{s,dq}}(t),$$

$$\text{Torque:} \quad T(t) = \frac{3}{2}p(\boldsymbol{i}^{\mathrm{k}}_{\mathrm{s,dq}}(t))^{\mathsf{T}}\boldsymbol{J}\boldsymbol{\psi}^{\mathrm{k}}_{\mathrm{s,dq}}(t) = -\frac{3}{2}p(\boldsymbol{i}^{\mathrm{k}'}_{\mathrm{r,dq}}(t))^{\mathsf{T}}\boldsymbol{J}\boldsymbol{\psi}^{\mathrm{k}'}_{\mathrm{r,dq}}(t).$$

The transformed rotor quantities are $\boldsymbol{u}'_{\mathrm{r}} = \alpha\boldsymbol{u}_{\mathrm{r}}$, $\boldsymbol{i}'_{\mathrm{r}} = {}^{1}/_{\alpha}\boldsymbol{i}_{\mathrm{r}}$, $\boldsymbol{\psi}'_{\mathrm{r}} = \alpha\boldsymbol{\psi}_{\mathrm{r}}$, $R'_{\mathrm{r}} = \alpha^2 R_{\mathrm{r}}$, $L'_{\mathrm{r}} = \alpha^2 L_{\mathrm{r}}$, and $M'_{\mathrm{r}} = \alpha M_{\mathrm{r}}$ with $\alpha = {}^{N_{\mathrm{s}}}/_{N_{\mathrm{r}}}$.

ECD of transformed IM model in general dq coordinates

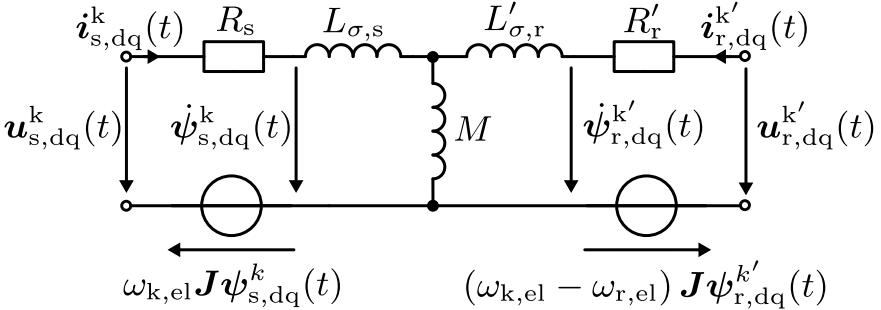

Fig. 5.9: T-type ECD of an IM in general dq coordinates with rotor quantities transformed using $\alpha = {}^{N_{\mathrm{s}}}/_{N_{\mathrm{r}}}$

Stator flux orientation in the k coordinate system

Per definition we can assign the stator flux linkage vector to the d-axis of the k coordinate system:

$$\boldsymbol{\psi}^{\mathrm{k}}_{\mathrm{s,dq}}(t) = \begin{bmatrix} \psi^{\mathrm{k}}_{\mathrm{s,d}}(t) \\ \psi^{\mathrm{k}}_{\mathrm{s,q}}(t) \end{bmatrix} = \begin{bmatrix} \psi^{\mathrm{k}}_{\mathrm{s,d}}(t) \\ 0 \end{bmatrix} = \begin{bmatrix} |\boldsymbol{\psi}^{\mathrm{k}}_{\mathrm{s,dq}}(t)| \\ 0 \end{bmatrix}. \tag{5.45}$$

In this case, the torque expression simplifies to

$$T(t) = \frac{3}{2} p (\boldsymbol{i}^{\mathrm{k}}_{\mathrm{s,dq}}(t))^{\mathsf{T}} \boldsymbol{J} \boldsymbol{\psi}^{\mathrm{k}}_{\mathrm{s,dq}}(t) = \frac{3}{2} p i^{\mathrm{k}}_{\mathrm{s,q}}(t) \psi^{\mathrm{k}}_{\mathrm{s,d}}(t). \tag{5.46}$$

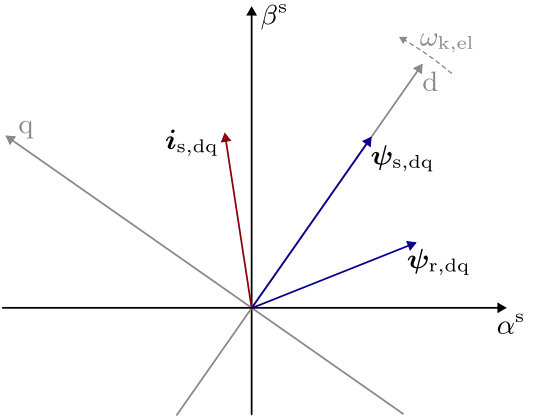

Fig. 5.10: Stator flux-oriented coordinate system

Rotor flux orientation in the k coordinate system

Per definition we can also assign the rotor flux linkage vector to the d-axis of the k coordinate system:

$$\boldsymbol{\psi}^{\mathrm{k}}_{\mathrm{r,dq}}(t) = \begin{bmatrix} \psi^{\mathrm{k}}_{\mathrm{r,d}}(t) \\ \psi^{\mathrm{k}}_{\mathrm{r,q}}(t) \end{bmatrix} = \begin{bmatrix} \psi^{\mathrm{k}}_{\mathrm{r,d}}(t) \\ 0 \end{bmatrix} = \begin{bmatrix} |\boldsymbol{\psi}^{\mathrm{k}}_{\mathrm{r,dq}}(t)| \\ 0 \end{bmatrix}. \tag{5.47}$$

In this case, the torque expression simplifies to

$$T(t) = -\frac{3}{2} p (\boldsymbol{i}^{\mathrm{k}}_{\mathrm{r,dq}}(t))^{\mathsf{T}} \boldsymbol{J} \boldsymbol{\psi}^{\mathrm{k}}_{\mathrm{r,dq}}(t) = -\frac{3}{2} p i^{\mathrm{k}}_{\mathrm{r,q}}(t) \psi^{\mathrm{k}}_{\mathrm{r,d}}(t). \tag{5.48}$$

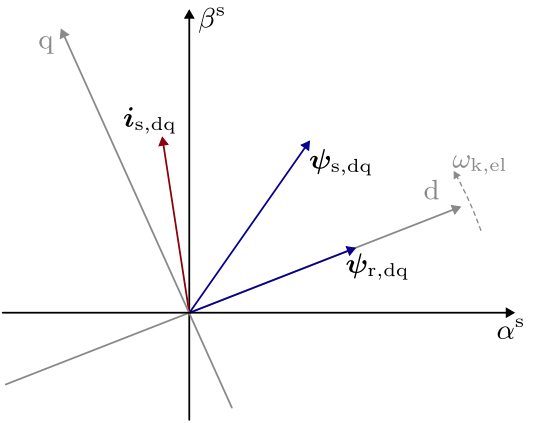

Fig. 5.11: Rotor flux-oriented coordinate system

Steady-state behavior

Starting from the general IM model voltage equations in the transformed k coordinate system (5.44), the steady-state ($\mathrm{d}x(t)/\mathrm{d}t=0$) behavior is described by

$$\begin{aligned}\boldsymbol{u}^{\mathrm{k}}_{\mathrm{s,dq}} &= R_{\mathrm{s}}\boldsymbol{i}^{\mathrm{k}}_{\mathrm{s,dq}} + \omega_{\mathrm{k,el}}\boldsymbol{J}\boldsymbol{\psi}^{\mathrm{k}}_{\mathrm{s,dq}},\\ \boldsymbol{u}^{\mathrm{k}'}_{\mathrm{r,dq}} &= R'_{\mathrm{r}}\boldsymbol{i}^{\mathrm{k}'}_{\mathrm{r,dq}} + (\omega_{\mathrm{k,el}} - \omega_{\mathrm{r,el}})\,\boldsymbol{J}\boldsymbol{\psi}^{\mathrm{k}'}_{\mathrm{r,dq}}.\end{aligned} \tag{5.49}$$

During steady state the stator is excited by a constant three-phase voltage with the stator frequency ω_{s} while the rotor is excited with the rotor or slip frequency ω_{slip}:

$$\omega_{\mathrm{k,el}} \to \omega_{\mathrm{s}}, \qquad \omega_{\mathrm{k,el}} - \omega_{\mathrm{r,el}} \to \omega_{\mathrm{slip}}. \tag{5.50}$$

Dropping the coordinate system indices, we have

$$\boldsymbol{u}_{\mathrm{s}} = R_{\mathrm{s}}\boldsymbol{i}_{\mathrm{s}} + \omega_{\mathrm{s}}\boldsymbol{J}\boldsymbol{\psi}_{\mathrm{s}}, \qquad \boldsymbol{u}'_{\mathrm{r}} = R'_{\mathrm{r}}\boldsymbol{i}'_{\mathrm{r}} + \omega_{\mathrm{slip}}\boldsymbol{J}\boldsymbol{\psi}'_{\mathrm{r}}. \tag{5.51}$$

Rewriting the vectorial quantities as complex phasors $\underline{X}_{\mathrm{dq}} = Xe^{\mathrm{j}\phi} = X_{\mathrm{d}} + \mathrm{j}X_{\mathrm{q}}$, we obtain

$$\underline{U}_{\mathrm{s}} = R_{\mathrm{s}}\underline{I}_{\mathrm{s}} + \mathrm{j}\omega_{\mathrm{s}}\underline{\Psi}_{\mathrm{s}}, \qquad \underline{U}'_{\mathrm{r}} = R'_{\mathrm{r}}\underline{I}'_{\mathrm{r}} + \mathrm{j}\omega_{\mathrm{slip}}\underline{\Psi}'_{\mathrm{r}}. \tag{5.52}$$

Steady-state behavior (cont.)

In (5.52) the complex rotor and stator fluxes rotate with different frequencies. To simplify the analysis, we introduce the slip ratio

$$s = \frac{\omega_{\mathrm{slip}}}{\omega_{\mathrm{s}}}. \tag{5.53}$$

Multiplying (5.52) with the inverse slip ratio delivers then

$$\underline{U}_{\mathrm{s}} = R_{\mathrm{s}}\underline{I}_{\mathrm{s}} + \mathrm{j}\omega_{\mathrm{s}}\underline{\Psi}_{\mathrm{s}}, \qquad \frac{1}{s}\underline{U}'_{\mathrm{r}} = \frac{1}{s}R'_{\mathrm{r}}\underline{I}'_{\mathrm{r}} + \mathrm{j}\omega_{\mathrm{s}}\underline{\Psi}'_{\mathrm{r}}. \tag{5.54}$$

Here, both the stator and rotor fluxes rotate with the same frequency ω_{s}. Additionally, we can insert the current-to-flux linkage relationships

$$\underline{\Psi}_{\mathrm{s}} = (L_{\sigma,\mathrm{s}} + M)\underline{I}_{\mathrm{s}} + M\underline{I}'_{\mathrm{r}}, \qquad \underline{\Psi}'_{\mathrm{r}} = (L'_{\sigma,\mathrm{r}} + M)\underline{I}'_{\mathrm{r}} + M\underline{I}_{\mathrm{s}} \tag{5.55}$$

leading to

$$\begin{aligned} \underline{U}_{\mathrm{s}} &= R_{\mathrm{s}}\underline{I}_{\mathrm{s}} + \mathrm{j}\omega_{\mathrm{s}}\left[(L_{\sigma,\mathrm{s}} + M)\underline{I}_{\mathrm{s}} + M\underline{I}'_{\mathrm{r}}\right], \\ \frac{1}{s}\underline{U}'_{\mathrm{r}} &= \frac{1}{s}R'_{\mathrm{r}}\underline{I}'_{\mathrm{r}} + \mathrm{j}\omega_{\mathrm{s}}\left[(L'_{\sigma,\mathrm{r}} + M)\underline{I}'_{\mathrm{r}} + M\underline{I}_{\mathrm{s}}\right]. \end{aligned} \tag{5.56}$$

Steady-state behavior: equivalent circuit diagram

The complex steady-state phasor model (5.56) can be represented by the following equivalent circuit diagram. Here, one can note the striking similarity to the T-type ECD of a transformer.

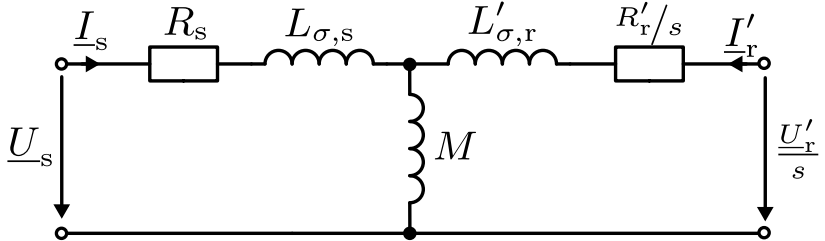

Fig. 5.12: T-type ECD of an IM in steady state represented by complex phasors

IM rotor types

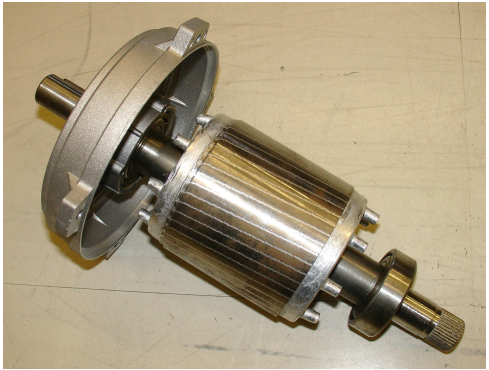

(a) Squirrel cage rotor (source: Wikimedia Commons, Zurek, CC BY-SA 3.0)

(b) Wound or slip ring rotor

Fig. 5.13: IM rotor variants

Squirrel cage IM torque-speed characteristic

Utilizing the stator flux orientation we define

$$\underline{\Psi}_{\mathrm{s}} = \Psi_{\mathrm{s,d}} + \mathrm{j}\Psi_{\mathrm{s,q}} = \Psi_{\mathrm{s,d}} = \Psi_{\mathrm{s}}.$$

Assuming that the stator ohmic voltage drop is negligible ($R_{\mathrm{s}} = 0$), we get from (5.54)

$$\underline{U}_{\mathrm{s}} = U_{\mathrm{s,d}} + \mathrm{j}U_{\mathrm{s,q}} = \mathrm{j}\omega_{\mathrm{s}}\underline{\Psi}_{\mathrm{s}} = \mathrm{j}\omega_{\mathrm{s}}\Psi_{\mathrm{d}} \tag{5.57}$$

and, therefore,

$$U_{\mathrm{s,d}} = 0, \qquad \Psi_{\mathrm{s,d}} = \frac{U_{\mathrm{s,q}}}{\omega_{\mathrm{s}}} = \frac{U_{\mathrm{s}}}{\omega_{\mathrm{s}}} = \Psi_{\mathrm{s}}. \tag{5.58}$$

Hence, the stator voltage phasor is purely imaginary and the stator flux phasor is real due to the chosen orientation. From (5.55) we can rewrite the flux-to-current relationships as

$$\begin{aligned} \underline{I}_{\mathrm{s}} &= \frac{1}{\sigma(L_{\sigma,\mathrm{s}} + M)}\underline{\Psi}_{\mathrm{s}} - \frac{M}{\sigma(L_{\sigma,\mathrm{s}} + M)(L'_{\sigma,\mathrm{r}} + M)}\underline{\Psi}'_{\mathrm{r}}, \\ \underline{I}'_{\mathrm{r}} &= \frac{1}{\sigma(L'_{\sigma,\mathrm{r}} + M)}\underline{\Psi}'_{\mathrm{r}} - \frac{M}{\sigma(L_{\sigma,\mathrm{s}} + M)(L'_{\sigma,\mathrm{r}} + M)}\underline{\Psi}_{\mathrm{s}}. \end{aligned} \tag{5.59}$$

Squirrel cage IM torque-speed characteristic (cont.)

Furthermore, the rotor voltage for the squirrel cage IM is

$$\underline{U}'_{\mathrm{r}} = 0$$

due to the short-circuited rotor winding. The rotor voltage equation (5.54) then simplifies to

$$0 = \frac{1}{s} R'_{\mathrm{r}} \underline{I}'_{\mathrm{r}} + \mathrm{j}\omega_{\mathrm{s}} \underline{\Psi}'_{\mathrm{r}} \quad \Leftrightarrow \quad \underline{\Psi}'_{\mathrm{r}} = \frac{\mathrm{j}}{\omega_{\mathrm{s}}} \frac{R'_{\mathrm{r}}}{s} \underline{I}'_{\mathrm{r}}. \tag{5.60}$$

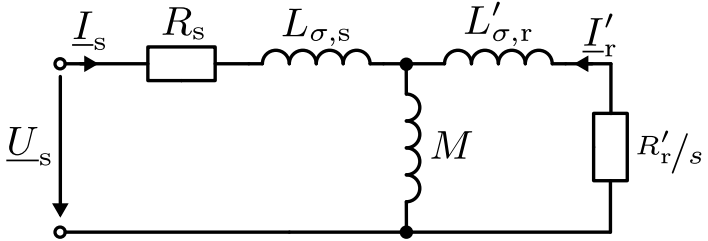

Fig. 5.14: T-type ECD of a squirrel cage IM in steady state represented by complex phasors

Squirrel cage IM torque-speed characteristic (cont.)

Combining (5.58), (5.59), and (5.60) we have a linear equation system resulting in

$$I_{\mathrm{s,d}} = \frac{U_{\mathrm{s}}}{\omega_{\mathrm{s}}} \frac{\sigma^2\omega_{\mathrm{slip}}^2(L_{\sigma,\mathrm{s}}+M)(L'_{\sigma,\mathrm{r}}+M)^3 + (L'_{\sigma,\mathrm{r}}+M)(L_{\sigma,\mathrm{s}}+M)(R'_{\mathrm{r}})^2 - M^2(R'_{\mathrm{r}})^2}{\sigma(L_{\sigma,\mathrm{s}}+M)^2(L'_{\sigma,\mathrm{r}}+M)\omega_{\mathrm{slip}}(\sigma^2\omega_{\mathrm{slip}}^2(L'_{\sigma,\mathrm{r}}+M)^2 + (R'_{\mathrm{r}})^2)}, \tag{5.61}$$

$$I_{\mathrm{s,q}} = \frac{U_{\mathrm{s}}}{\omega_{\mathrm{s}}} \frac{M^2\omega_{\mathrm{slip}}R'_{\mathrm{r}}}{(L_{\sigma,\mathrm{s}}+M)^2(\sigma^2(L'_{\sigma,\mathrm{r}}+M)^2\omega_{\mathrm{slip}}^2 + (R'_{\mathrm{r}})^2)}, \tag{5.62}$$

$$I_{\mathrm{r,d}} = -\frac{U_{\mathrm{s}}}{\omega_{\mathrm{s}}} \frac{\sigma M\omega_{\mathrm{slip}}^2(L'_{\sigma,\mathrm{r}}+M)}{(L_{\sigma,\mathrm{s}}+M)(\sigma^2(L'_{\sigma,\mathrm{r}}+M)^2\omega_{\mathrm{slip}}^2 + (R'_{\mathrm{r}})^2)}, \tag{5.63}$$

$$I_{\mathrm{r,q}} = -\frac{U_{\mathrm{s}}}{\omega_{\mathrm{s}}} \frac{MR'_{\mathrm{r}}\omega_{\mathrm{slip}}}{(L_{\sigma,\mathrm{s}}+M)(\sigma^2(L'_{\sigma,\mathrm{r}}+M)^2\omega_{\mathrm{slip}}^2 + (R'_{\mathrm{r}})^2)}, \tag{5.64}$$

$$\Psi_{\mathrm{r,d}} = \frac{U_{\mathrm{s}}}{\omega_{\mathrm{s}}} \frac{M(R'_{\mathrm{r}})^2}{(L_{\sigma,\mathrm{s}}+M)(\sigma^2(L'_{\sigma,\mathrm{r}}+M)^2\omega_{\mathrm{slip}}^2 + (R'_{\mathrm{r}})^2)}, \tag{5.65}$$

$$\Psi_{\mathrm{r,q}} = -\frac{U_{\mathrm{s}}}{\omega_{\mathrm{s}}} \frac{\sigma M(L'_{\sigma,\mathrm{r}}+M)R'_{\mathrm{r}}\omega_{\mathrm{slip}}}{(L_{\sigma,\mathrm{s}}+M)((L'_{\sigma,\mathrm{r}}+M)^2\sigma^2\omega_{\mathrm{slip}}^2 + (R'_{\mathrm{r}})^2)}. \tag{5.66}$$

Squirrel cage IM torque-speed characteristic (cont.)

With the definition of $\omega_{\max} = {R'_{\mathrm{r}}}/{\sigma(L'_{\sigma,\mathrm{r}}+M)}$ we can rewrite and receive

$$I_{\mathrm{s,d}} = \frac{U_{\mathrm{s}}}{\omega_{\mathrm{s}}} \frac{\sigma^2\omega_{\mathrm{slip}}^2(L_{\sigma,\mathrm{s}}+M)(L'_{\sigma,\mathrm{r}}+M)^3 + (L'_{\sigma,\mathrm{r}}+M)(L_{\sigma,\mathrm{s}}+M)(R'_{\mathrm{r}})^2 - M^2(R'_{\mathrm{r}})^2}{\sigma(L_{\sigma,\mathrm{s}}+M)^2(L'_{\sigma,\mathrm{r}}+M)\omega_{\mathrm{slip}}(\sigma^2\omega_{\mathrm{slip}}^2(L'_{\sigma,\mathrm{r}}+M)^2 + (R'_{\mathrm{r}})^2)}, \tag{5.67}$$

$$I_{\mathrm{s,q}} = \frac{U_{\mathrm{s}}}{\omega_{\mathrm{s}}} \frac{M^2}{\sigma(L_{\sigma,\mathrm{s}}+M)^2(L'_{\sigma,\mathrm{r}}+M)} \frac{1}{\frac{\omega_{\mathrm{slip}}}{\omega_{\max}} + \frac{\omega_{\max}}{\omega_{\mathrm{slip}}}}, \tag{5.68}$$

$$I_{\mathrm{r,d}} = -U_{\mathrm{s}} \frac{Ms}{(L_{\sigma,\mathrm{s}}+M)R'_{\mathrm{r}}} \frac{1}{\frac{\omega_{\mathrm{slip}}}{\omega_{\max}} + \frac{\omega_{\max}}{\omega_{\mathrm{slip}}}}, \tag{5.69}$$

$$I_{\mathrm{r,q}} = -\frac{U_{\mathrm{s}}}{\omega_{\mathrm{s}}} \frac{M}{\sigma(L_{\sigma,\mathrm{s}}+M)(L'_{\sigma,\mathrm{r}}+M)} \frac{1}{\frac{\omega_{\mathrm{slip}}}{\omega_{\max}} + \frac{\omega_{\max}}{\omega_{\mathrm{slip}}}}, \tag{5.70}$$

$$\Psi_{\mathrm{r,d}} = \frac{U_{\mathrm{s}}}{\omega_{\mathrm{s}}} \frac{MR'_{\mathrm{r}}}{\sigma(L_{\sigma,\mathrm{s}}+M)(L'_{\sigma,\mathrm{r}}+M)\omega_{\mathrm{slip}}} \frac{1}{\frac{\omega_{\mathrm{slip}}}{\omega_{\max}} + \frac{\omega_{\max}}{\omega_{\mathrm{slip}}}}, \tag{5.71}$$

$$\Psi_{\mathrm{r,q}} = -\frac{U_{\mathrm{s}}}{\omega_{\mathrm{s}}} \frac{M}{(L_{\sigma,\mathrm{s}}+M)} \frac{1}{\frac{\omega_{\mathrm{slip}}}{\omega_{\max}} + \frac{\omega_{\max}}{\omega_{\mathrm{slip}}}}. \tag{5.72}$$

Squirrel cage IM torque-speed characteristic (cont.)

The torque expression is then

$$T = \frac{3}{2} p \sqrt{2} \Psi_{\mathrm{s}} \sqrt{2} I_{\mathrm{s,q}} = \frac{3}{2} p \frac{U_{\mathrm{s}}^2}{\omega_{\mathrm{s}}^2} \frac{M^2}{\sigma (L_{\sigma,\mathrm{s}} + M)^2 (L'_{\sigma,\mathrm{r}} + M)} \frac{2}{\frac{\omega_{\mathrm{slip}}}{\omega_{\max}} + \frac{\omega_{\max}}{\omega_{\mathrm{slip}}}}. \tag{5.73}$$

Hence, the maximum achievable torque for a constant stator excitation is

$$T_{\max} = \frac{3}{2} p \frac{U_{\mathrm{s}}^2}{\omega_{\mathrm{s}}^2} \frac{M^2}{\sigma (L_{\sigma,\mathrm{s}} + M)^2 (L'_{\sigma,\mathrm{r}} + M)} \tag{5.74}$$

since

$$\max_{\omega_{\mathrm{slip}}} \left\{ \frac{2}{\frac{\omega_{\mathrm{slip}}}{\omega_{\max}} + \frac{\omega_{\max}}{\omega_{\mathrm{slip}}}} \right\} = 1, \qquad \arg\max_{\omega_{\mathrm{slip}}} \left\{ \frac{2}{\frac{\omega_{\mathrm{slip}}}{\omega_{\max}} + \frac{\omega_{\max}}{\omega_{\mathrm{slip}}}} \right\} = \omega_{\max} = \frac{R'_{\mathrm{r}}}{\sigma (L'_{\sigma,\mathrm{r}} + M)}$$

applies. Above, Ψ_{s} and $I_{\mathrm{s,q}}$ are RMS values according to the complex phasor definitions, which is why the factor $\sqrt{2}$ appears in the torque expression.

Squirrel cage IM torque-speed characteristic (cont.)

The torque expression

$$T = T_{\max} \frac{2}{\frac{\omega_{\text{slip}}}{\omega_{\max}} + \frac{\omega_{\max}}{\omega_{\text{slip}}}} \tag{5.75}$$

can be also alternatively expressed as a function of the slip ratio s by utilizing

$$\omega_{\text{slip}} = s\omega_{\text{s}}, \qquad s_{\max} = \frac{\omega_{\max}}{\omega_{\text{s}}} = \frac{R'_{\text{r}}}{\sigma(L'_{\sigma,\text{r}} + M)\omega_{\text{s}}}$$

leading to

$$T = T_{\max} \frac{2}{\frac{s}{s_{\max}} + \frac{s_{\max}}{s}}. \tag{5.76}$$

The torque-speed characteristic of a squirrel cage IM is also known as Kloss's formula. It should be noted that $\omega_{\max}$ and $s_{\max}$ are machine-dependent parameters (for a constant stator excitation), i.e., constants. Contrary, the slip ratio s and slip frequency ω_{slip} depend on the IM's shaft speed and vary during operation.

Kloss's formula: visual representation

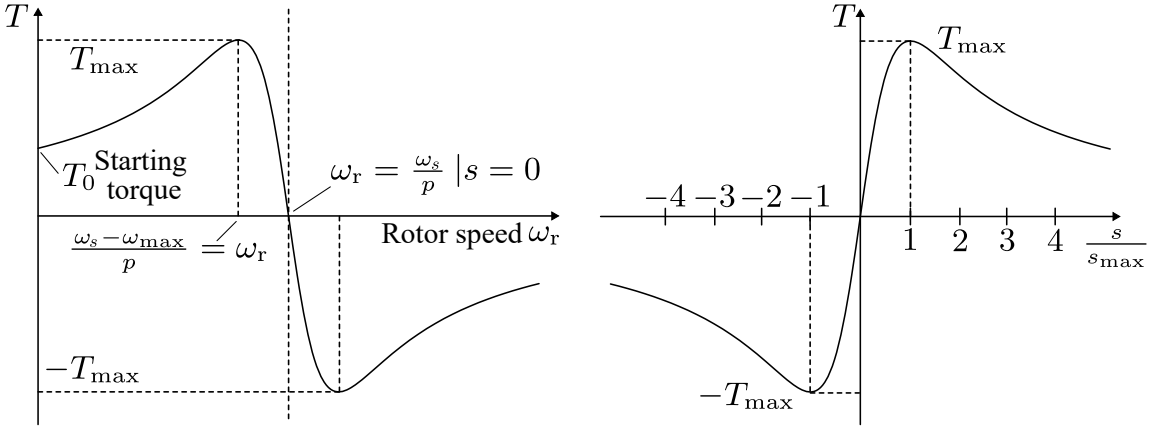

(a) Illustration based on the mechanical speed

(b) Illustration based on the slip ratio

Fig. 5.15: Steady-state torque-speed characteristic of a squirrel cage IM for a fixed stator excitation

Squirrel cage IM torque-speed characteristic: rotor resistance

The starting torque, i.e., the torque at motor standstill ($\omega_\mathrm{r} = 0$), is given by

$$T_0 = T_\mathrm{max} \frac{2 s_\mathrm{max}}{1 + s_\mathrm{max}^2} = T_\mathrm{max} \frac{2 \omega_\mathrm{max}}{1 + \omega_\mathrm{max}^2} \tag{5.77}$$

since

$$\omega_\mathrm{slip} = \omega_\mathrm{s} - p\omega_\mathrm{r} = \omega_\mathrm{s} - 0 = \omega_\mathrm{s}$$

holds. Depending on the machine design T_0 can be significantly lower than T_max, which might be a disadvantage for certain applications. Since

$$\omega_\mathrm{max} = \frac{R'_\mathrm{r}}{\sigma(L'_{\sigma,\mathrm{r}} + M)}, \qquad s_\mathrm{max} = \frac{R'_\mathrm{r}}{\sigma(L'_{\sigma,\mathrm{r}} + M)\omega_\mathrm{s}}$$

depend on the rotor resistance R'_r, the starting torque can be modified by changing the rotor resistance, e.g., via a dropping resistor or potentiometer (which would require a slip ring rotor).

Squirrel cage IM torque-speed characteristic: rotor resistance (cont.)

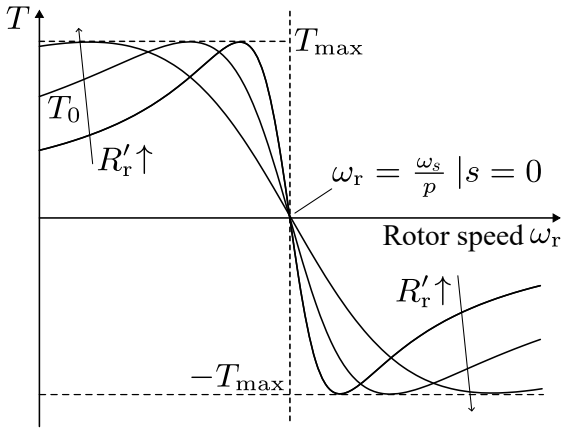

Fig. 5.16: Steady-state torque-speed characteristic of a squirrel cage IM for a fixed stator excitation with varying rotor resistance R'_{r} – note that the synchronous speed $\omega_{\mathrm{r}} = \omega_{\mathrm{s}}/p$ and the maximum torque $T_{\max}$ are independent of the rotor resistance variation

Slip frequency-dependent rotor skin effect

- If $\omega_{\text{slip}} \neq 0$, the rotor bars are exposed to a time-varying magnetic field.
- This induces eddy currents leading to an uneven current distribution within the bars.
- As a result, the effective rotor resistance increases with the slip frequency:

$$\frac{R_{\text{r}}(\omega_{\text{slip}})}{R_{\text{r,DC}}} = \delta \frac{\sinh(2\delta) + \sin(2\delta)}{\cosh(2\delta) - \cos(2\delta)} \qquad (5.78)$$

with

$$\delta = h_{\text{bar}} \sqrt{\omega_{\text{slip}} \frac{\mu_0 \kappa}{2} \frac{w_{\text{bar}}}{w_{\text{slot}}}}$$

being the skin depth. Here, μ_0 is the vacuum permeability and κ is the bar's conductivity.

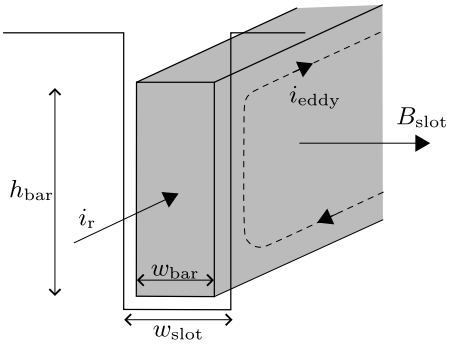

Fig. 5.17: Rotor bar with eddy currents induced by the rotating magnetic field (inspired from A. Binder, *Elektrische Maschinen und Antriebe*, Vol. 2, Springer, 2017)

Slip frequency-dependent rotor skin effect (cont.)

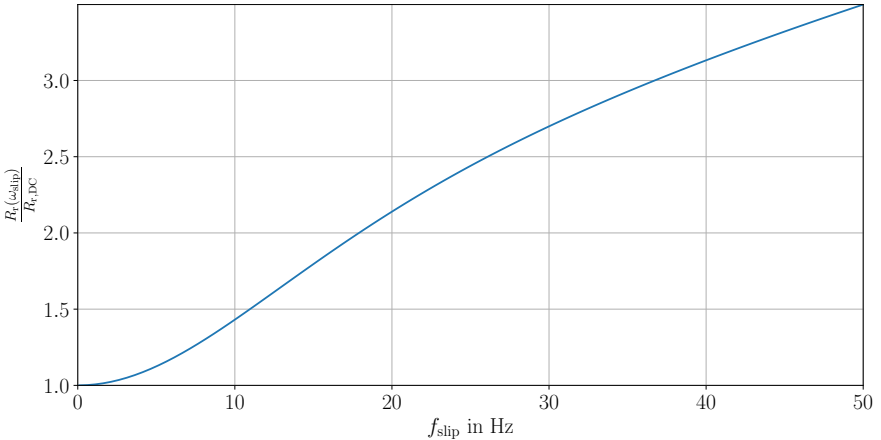

Fig. 5.18: Rotor resistance of a squirrel cage IM as a function of the slip frequency (example based on the following values: $\kappa = 3.7 \cdot 10^7 \, \frac{\mathrm{S}}{\mathrm{m}}$, $h_\mathrm{bar} = 50\,\mathrm{mm}$, $w_\mathrm{bar} = 10\,\mathrm{mm}$, $w_\mathrm{slot} = 15\,\mathrm{mm}$)

Squirrel cage IM torque-speed characteristic: varying stator frequency

- Adaption of rotor resistance might be technically tricky.
- Alternative: vary stator frequency ω_s.
- Shift of the torque-speed characteristic along the speed axis, i.e., the synchronous speed $\omega_\mathrm{r} = \omega_\mathrm{s}/p$.
- Allows utilizing T_max at different speeds (including initial starting torque).
- Requires a variable frequency source, e.g., a power electronic converter.

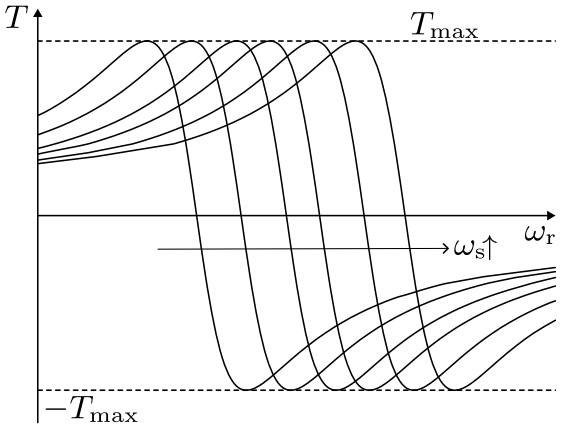

Fig. 5.19: Steady-state torque-speed characteristic of a squirrel cage IM with varying ω_s while keeping $U_\mathrm{s}/\omega_\mathrm{s} = \mathrm{const.}$

Squirrel cage IM torque-speed characteristic: flux weakening

- The previous consideration from Fig. 5.19 assumed that $U_\mathrm{s}/\omega_\mathrm{s} = \mathrm{const.}$ applies, that is, the stator voltage amplitude is adjusted according to the frequency.
- Obviously, this is only possible to a certain extent due to the voltage source limitations.
- Hence, at some point, the torque-speed characteristic is limited by the available voltage leading to a flux weakening operation mode (cf. right figure).

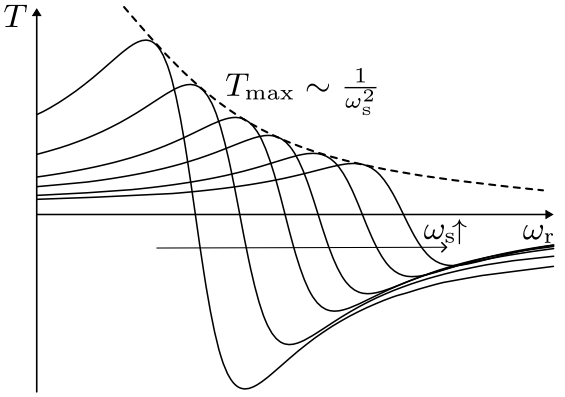

Fig. 5.20: Steady-state torque-speed characteristic of a squirrel cage IM with varying ω_s while keeping $U_\mathrm{s} = \mathrm{const.}$, i.e., field weakening operation ($\Psi_\mathrm{s} \sim 1/\omega_\mathrm{s}$)

Squirrel cage IM torque-speed characteristic: air gap harmonics

- The rotating field analysis (**??**) revealed that the air gap magnetic field contains harmonics:

$$B = \frac{6}{\pi p}\hat{B}\sum_{k}^{\infty}\frac{1}{k}\sin\left(\frac{k\pi}{2}\right)\cos(\omega t - k\vartheta_{\mathrm{el}})$$

- This induces rotor currents with the harmonic slip frequency $\omega_{\mathrm{slip}}^{(k)}$.
- Likewise the IM fundamental torque, these air gap field and rotor current harmonics lead to constant, i.e., non-harmonic, torque contributions distorting the torque-speed characteristic.

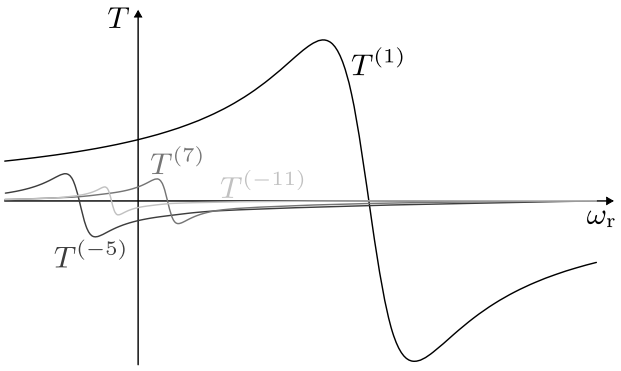

Fig. 5.21: Steady-state torque-speed characteristic of a squirrel cage IM considering torque harmonics due to stator magnetic field harmonics of order $k = 1, -5, 7, -11$

Table of contents

Synchronous machines

Bikash Sah

Universität Siegen / IAS Interconnected Automation Systems

Synchronous machine (SM) rotor types

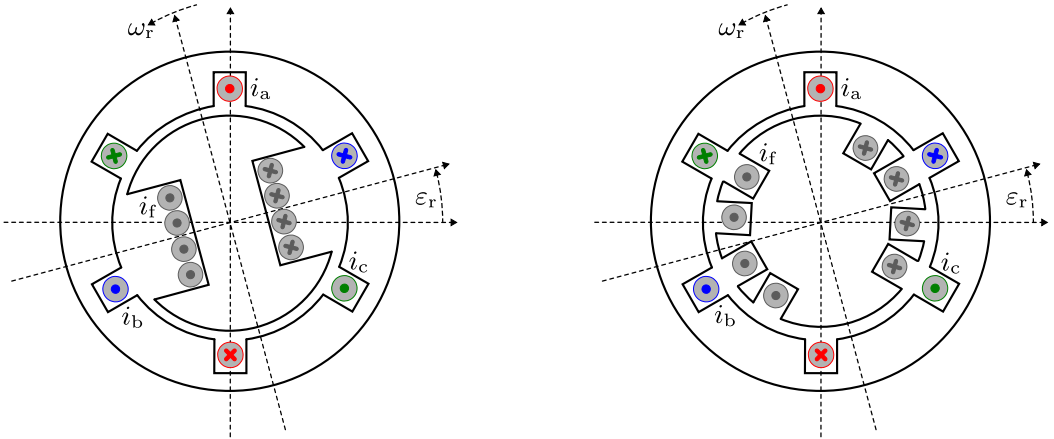

(a) Salient pole rotor

(b) Cylindrical rotor

Fig. 6.1: Major rotor types of synchronous machines (SM)

SM application examples

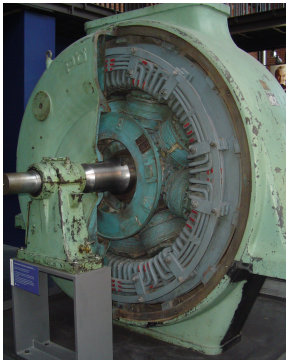

(a) 2 MVA generator from 1920 (source: Wikimedia Commons, Kolossos, CC BY-SA 3.0)

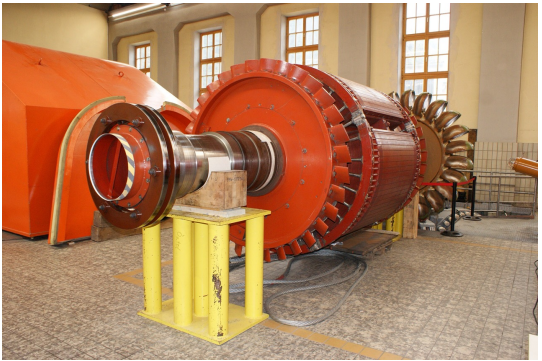

(b) 36 MVA Pelton wheel generator (source: Wikimedia Commons, Asurnipal, CC BY-SA 4.0)

Fig. 6.2: SM examples with salient pole rotor type

SM application examples (cont.)

(a) 650 MVA turbogenerator from Cernavodă nuclear power plant (source: Wikimedia Commons, R. Lavinia, CC BY-SA 4.0)

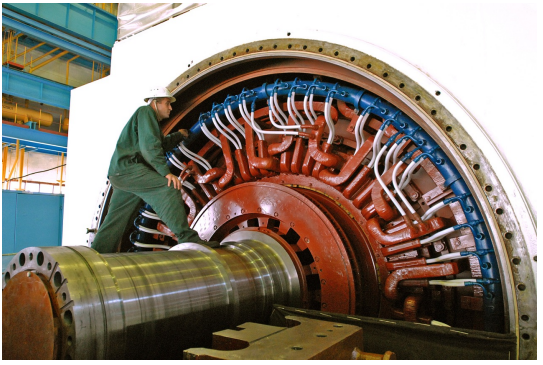

(b) 1 GVA turbogenerator SM rotor from Balakovo nuclear power plant (source: Wikimedia Commons, A. Seetenky, CC BY-SA 3.0)

Fig. 6.3: SM examples with cylindrical rotor type

Visualization of the synchronous machine operation

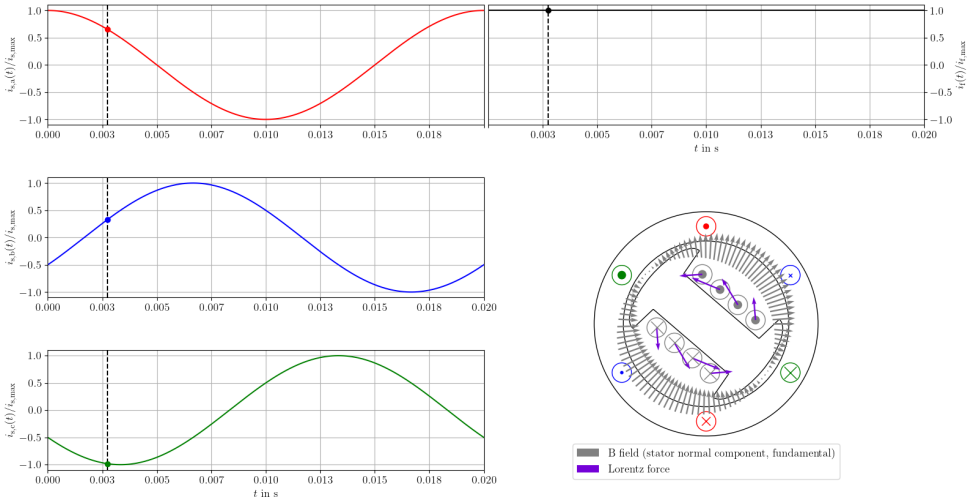

Fig. 6.4: Exemplary SM operation at $\omega = 2\pi 50\,\frac{1}{\mathrm{s}}$ in motoric operation (positive average torque)

Visualization of the synchronous machine operation (cont.)

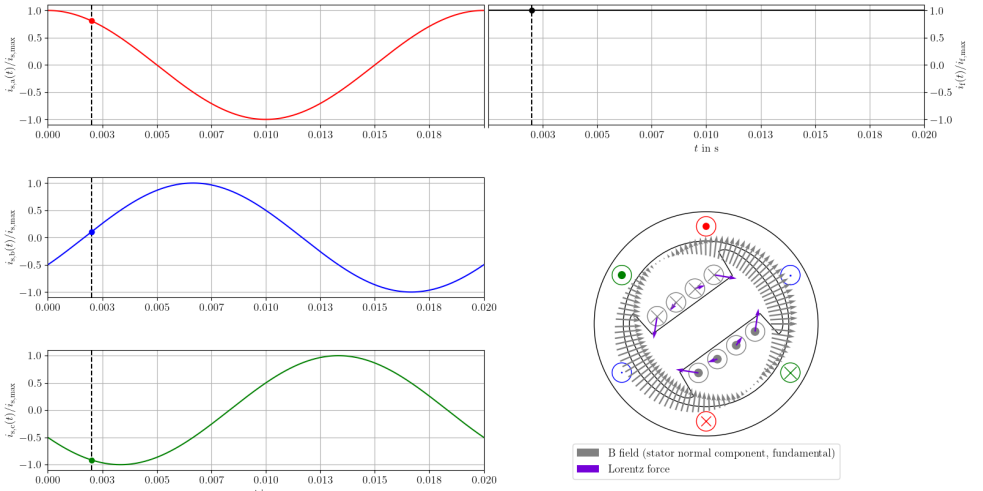

Fig. 6.5: Exemplary SM operation at $\omega = 2\pi 50\,\frac{1}{\mathrm{s}}$ in no-load operation (zero average torque)

Dynamical SM model

Based on Faraday's and Ohm's laws, we can write the following equations for the stator

$$\boldsymbol{u}^{\mathrm{s}}_{\mathrm{s,abc}}(t) = R_{\mathrm{s}}\boldsymbol{i}^{\mathrm{s}}_{\mathrm{s,abc}}(t) + \frac{\mathrm{d}}{\mathrm{d}t}\boldsymbol{\psi}^{\mathrm{s}}_{\mathrm{s,abc}}(t) \quad \Leftrightarrow \quad \begin{bmatrix} u^{\mathrm{s}}_{\mathrm{s,a}}(t) \\ u^{\mathrm{s}}_{\mathrm{s,b}}(t) \\ u_{\mathrm{s,c}}(t) \end{bmatrix} = R_{\mathrm{s}} \begin{bmatrix} i^{\mathrm{s}}_{\mathrm{s,a}}(t) \\ i^{\mathrm{s}}_{\mathrm{s,b}}(t) \\ i^{\mathrm{s}}_{\mathrm{s,c}}(t) \end{bmatrix} + \frac{\mathrm{d}}{\mathrm{d}t} \begin{bmatrix} \psi^{\mathrm{s}}_{\mathrm{s,a}}(t) \\ \psi^{\mathrm{s}}_{\mathrm{s,b}}(t) \\ \psi^{\mathrm{s}}_{\mathrm{s,c}}(t) \end{bmatrix} \tag{6.1}$$

and rotor field winding

$$u^{\mathrm{r}}_{\mathrm{f}}(t) = R_{\mathrm{f}} i^{\mathrm{r}}_{\mathrm{f}}(t) + \frac{\mathrm{d}}{\mathrm{d}t}\psi^{\mathrm{r}}_{\mathrm{f}}(t) \tag{6.2}$$

which are generally applicable as only identical resistances per phase on the stator are assumed. In contrast to the induction motor, only a single rotor field winding is present.

Flux linkage model

The SM flux linkage model is similar to the IM model:

- Assuming a cylindrical rotor, the self-induced stator flux remains identical to the IM model (derived from rotating field theory chapter).
- In contrast to the IM model Fig. 5.2, the SM's rotor field coil is a represented by a single winding.
- The coupling of the stator and rotor remains rotor position-dependent (not explicitly shown on the right due to space limitations).

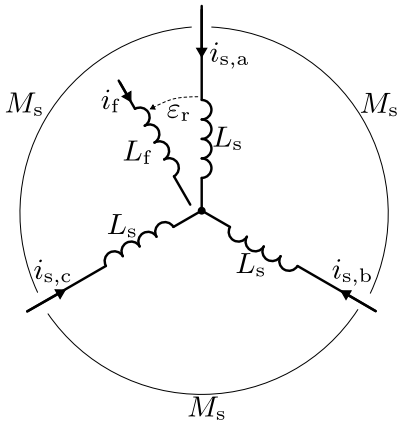

Fig. 6.6: Simplified representation of the inductive coupling between the stator/rotor phases of the cylindrical rotor SM

Flux linkages of the three-phase model

Based on the previous considerations, the flux linkages of the cylindrical SM are given by

$$\begin{aligned}\boldsymbol{\psi}^{\mathrm{s}}_{\mathrm{s,abc}}(t) &= \begin{bmatrix} L_{\mathrm{s}} & -\frac{M_{\mathrm{s}}}{2} & -\frac{M_{\mathrm{s}}}{2} \\ -\frac{M_{\mathrm{s}}}{2} & L_{\mathrm{s}} & -\frac{M_{\mathrm{s}}}{2} \\ -\frac{M_{\mathrm{s}}}{2} & -\frac{M_{\mathrm{s}}}{2} & L_{\mathrm{s}} \end{bmatrix} \boldsymbol{i}^{\mathrm{s}}_{\mathrm{s,abc}}(t) + M_{\mathrm{r}} \frac{N_{\mathrm{s}}}{N_{\mathrm{r}}} \begin{bmatrix} \cos(\varepsilon_{\mathrm{r,el}}(t)) \\ \cos(\varepsilon_{\mathrm{r,el}}(t) - \frac{2\pi}{3}) \\ \cos(\varepsilon_{\mathrm{r,el}}(t) + \frac{2\pi}{3}) \end{bmatrix} i^{\mathrm{r}}_{\mathrm{f}}(t), \\ \psi^{\mathrm{r}}_{\mathrm{f}}(t) &= L_{\mathrm{f}} i^{\mathrm{r}}_{\mathrm{f}}(t) \\ &\quad + M_{\mathrm{s}} \frac{N_{\mathrm{r}}}{N_{\mathrm{s}}} \begin{bmatrix} \cos(\varepsilon_{\mathrm{r,el}}(t)) & \cos(\varepsilon_{\mathrm{r,el}}(t) - \frac{2\pi}{3}) & \cos(\varepsilon_{\mathrm{r,el}}(t) + \frac{2\pi}{3}) \end{bmatrix} \boldsymbol{i}^{\mathrm{s}}_{\mathrm{s,abc}}(t) \end{aligned} \tag{6.3}$$

with $\varepsilon_{\mathrm{r,el}}(t) = p\varepsilon_{\mathrm{r}}(t)$. Consequently, (6.3) is a reduced representation of the IM's flux linkage model (5.3).

Cylindrical SM model in alpha-beta coordinates: voltage equations

Similar to the IM, we can represent the SM model is orthogonal $\alpha\beta$-coordinates. For the SM this only applies to the three-phase stator, as the rotor has only a single phase winding. The $\alpha\beta$-coordinates voltage equation is given by (compare to (5.16))

$$\boldsymbol{u}^{\mathrm{s}}_{\mathrm{s},\alpha\beta}(t) = R_{\mathrm{s}}\boldsymbol{i}^{\mathrm{s}}_{\mathrm{s},\alpha\beta}(t) + \frac{\mathrm{d}}{\mathrm{d}t}\boldsymbol{\psi}^{\mathrm{s}}_{\mathrm{s},\alpha\beta}(t) \tag{6.4}$$

while the rotor field winding voltage equation remains identical to (6.2):

$$u^{\mathrm{r}}_{\mathrm{f}}(t) = R_{\mathrm{f}}i^{\mathrm{r}}_{\mathrm{f}}(t) + \frac{\mathrm{d}}{\mathrm{d}t}\psi^{\mathrm{r}}_{\mathrm{f}}(t).$$

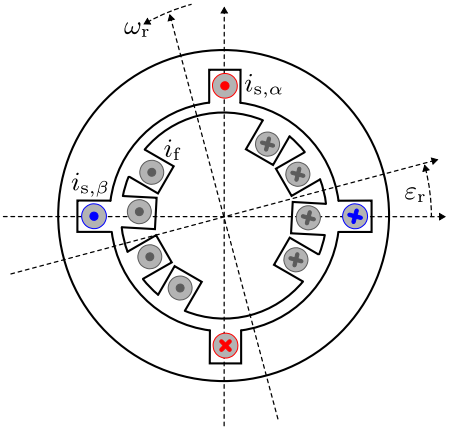

Fig. 6.7: Conceptual cylindrical SM representation within the orthogonal $\alpha\beta$ coordinates ($p = 1$ pole pair)

Cylindrical SM model in alpha-beta coordinates: flux linkage

For the flux linkage model in $\alpha\beta$-coordinates, we multiply the stator flux equations from (6.3) with $\boldsymbol{T}_{23}$ from the right

$$\begin{aligned}\boldsymbol{\psi}^{\mathrm{s}}_{\mathrm{s},\alpha\beta}(t) &= \boldsymbol{T}_{23}\boldsymbol{\psi}^{\mathrm{s}}_{\mathrm{s,abc}}(t) = \overbrace{\boldsymbol{T}_{23}\boldsymbol{L}_{\mathrm{s,abc}}\boldsymbol{T}_{32}}^{\boldsymbol{L}_{\mathrm{s},\alpha\beta}}\boldsymbol{i}^{\mathrm{s}}_{\mathrm{s},\alpha\beta}(t) + M_{\mathrm{r}}\frac{N_{\mathrm{s}}}{N_{\mathrm{r}}}\boldsymbol{T}_{23}\begin{bmatrix}\cos(\varepsilon_{\mathrm{r,el}}(t))\\ \cos(\varepsilon_{\mathrm{r,el}}(t)-\frac{2\pi}{3})\\ \cos(\varepsilon_{\mathrm{r,el}}(t)+\frac{2\pi}{3})\end{bmatrix} i^{\mathrm{r}}_{\mathrm{f}}(t)\\ &= (L_{\mathrm{s}}+{}^{M_{\mathrm{s}}}\!/_{2})\boldsymbol{i}^{\mathrm{s}}_{\mathrm{s},\alpha\beta}(t) + M_{\mathrm{r}}\frac{N_{\mathrm{s}}}{N_{\mathrm{r}}}\begin{bmatrix}\cos(\varepsilon_{\mathrm{r,el}}(t))\\ \sin(\varepsilon_{\mathrm{r,el}}(t))\end{bmatrix} i^{\mathrm{r}}_{\mathrm{f}}(t)\end{aligned} \tag{6.5}$$

and utilize $\boldsymbol{i}^{\mathrm{s}}_{\mathrm{s,abc}}(t) = \boldsymbol{T}_{32}\boldsymbol{i}^{\mathrm{s}}_{\mathrm{s},\alpha\beta}(t)$ to modify the rotor flux linkage equation accordingly:

$$\psi^{\mathrm{r}}_{\mathrm{f}}(t) = L_{\mathrm{f}}i^{\mathrm{r}}_{\mathrm{f}}(t) + M_{\mathrm{s}}\frac{N_{\mathrm{r}}}{N_{\mathrm{s}}}\begin{bmatrix}\cos(\varepsilon_{\mathrm{r,el}}(t)) & \sin(\varepsilon_{\mathrm{r,el}}(t))\end{bmatrix}\boldsymbol{i}^{\mathrm{s}}_{\mathrm{s},\alpha\beta}(t). \tag{6.6}$$

In contrast to the IM $\alpha\beta$-coordinates flux linkage model, the SM flux-to-current coupling is rotor position-dependent.

Cylindrical SM model in alpha-beta coordinates: flux linkage (cont.)

Analyzing the (magnetic) power balance reveals

$$M_{\mathrm{r}}\frac{N_{\mathrm{s}}}{N_{\mathrm{r}}} = M_{\mathrm{s}}\frac{N_{\mathrm{r}}}{N_{\mathrm{s}}} \stackrel{!}{=} M_{\mathrm{fs}}, \tag{6.7}$$

and with the shorter notation

$$L'_{\mathrm{s}} = (L_{\mathrm{s}} + {}^{M_{\mathrm{s}}}/_{2}) \tag{6.8}$$

we can rewrite the flux linkage model in $\alpha\beta$-coordinates to

$$\begin{aligned} \boldsymbol{\psi}^{\mathrm{s}}_{\mathrm{s},\alpha\beta}(t) &= L'_{\mathrm{s}}\boldsymbol{i}^{\mathrm{s}}_{\mathrm{s},\alpha\beta}(t) + M_{\mathrm{fs}}\begin{bmatrix}\cos(\varepsilon_{\mathrm{r,el}}(t))\\ \sin(\varepsilon_{\mathrm{r,el}}(t))\end{bmatrix} i^{\mathrm{r}}_{\mathrm{f}}(t), \\ \psi^{\mathrm{r}}_{\mathrm{f}}(t) &= L_{\mathrm{f}}i^{\mathrm{r}}_{\mathrm{f}}(t) \quad + M_{\mathrm{fs}}\begin{bmatrix}\cos(\varepsilon_{\mathrm{r,el}}(t))\\ \sin(\varepsilon_{\mathrm{r,el}}(t))\end{bmatrix}^{\mathsf{T}} \boldsymbol{i}^{\mathrm{s}}_{\mathrm{s},\alpha\beta}(t). \end{aligned} \tag{6.9}$$

Cylindrical SM model in alpha-beta coordinates: torque

Following the same power balance approach as from the IM, the SM's torque equation is given by

$$T(t) = \frac{3}{2} p (\boldsymbol{i}^{\mathrm{s}}_{\mathrm{s},\alpha\beta}(t))^{\mathsf{T}} \boldsymbol{J} \boldsymbol{\psi}^{\mathrm{s}}_{\mathrm{s},\alpha\beta}(t). \tag{6.10}$$

The equivalent representation with the rotor current and flux linkage as in the IM case is not applicable in the SM case, as the rotor has only a single field winding, i.e., is lacking an $\alpha\beta$ representation. Inserting the linear flux linkage model from (6.9) into the torque equation yields

$$\begin{aligned} T(t) &= \frac{3}{2} p (\boldsymbol{i}^{\mathrm{s}}_{\mathrm{s},\alpha\beta}(t))^{\mathsf{T}} \boldsymbol{J} \boldsymbol{\psi}^{\mathrm{s}}_{\mathrm{s},\alpha\beta}(t) \\ &= \frac{3}{2} p (\boldsymbol{i}^{\mathrm{s}}_{\mathrm{s},\alpha\beta}(t))^{\mathsf{T}} \boldsymbol{J} \left(L'_{\mathrm{s}} \boldsymbol{i}^{\mathrm{s}}_{\mathrm{s},\alpha\beta}(t) + M_{\mathrm{fs}} \begin{bmatrix} \cos(\varepsilon_{\mathrm{r,el}}(t)) \\ \sin(\varepsilon_{\mathrm{r,el}}(t)) \end{bmatrix} i^{\mathrm{r}}_{\mathrm{f}}(t) \right) \\ &= \frac{3}{2} p M_{\mathrm{fs}} i^{\mathrm{r}}_{\mathrm{f}} \left(\cos(\varepsilon_{\mathrm{r,el}}(t)) i^{\mathrm{s}}_{\mathrm{s},\beta}(t) - \sin(\varepsilon_{\mathrm{r,el}}(t)) i^{\mathrm{s}}_{\mathrm{s},\alpha}(t) \right). \end{aligned} \tag{6.11}$$

Cylindrical SM model in alpha-beta coordinates: torque interpretation

In (6.11) the term

$$M_{\mathrm{fs}} \begin{bmatrix} \cos(\varepsilon_{\mathrm{r,el}}(t)) \\ \sin(\varepsilon_{\mathrm{r,el}}(t)) \end{bmatrix} i_{\mathrm{f}}^{\mathrm{r}}(t) = \boldsymbol{\psi}_{\mathrm{f}}^{\mathrm{s}}(t) \qquad (6.12)$$

can be interpreted as the field winding flux linkage coupled with the stator winding. Hence, the torque expression can be rewritten as:

$$\begin{aligned} T(t) &= \frac{3}{2} p \left\| \boldsymbol{\psi}_{\mathrm{f}}^{\mathrm{s}}(t) \times \boldsymbol{i}_{\mathrm{s},\alpha\beta}^{\mathrm{s}}(t) \right\| \\ &= \frac{3}{2} p \left\| \boldsymbol{\psi}_{\mathrm{f}}^{\mathrm{s}}(t) \right\| \left\| \boldsymbol{i}_{\mathrm{s},\alpha\beta}^{\mathrm{s}}(t) \right\| \sin(\theta(t)) \end{aligned} \qquad (6.13)$$

with θ being the angle between the field winding flux linkage and the stator current vectors, also known as the load angle.

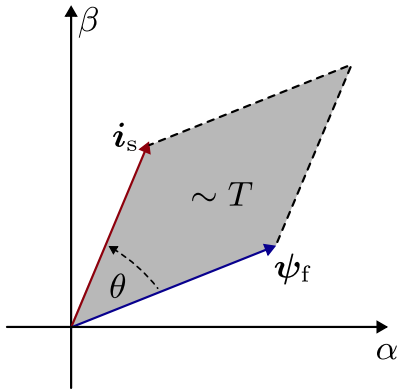

Fig. 6.8: Interpretation of the torque as the parallelogram area spannend by the vectors of the field winding flux and the stator current

Summary: cylindrical SM model in $\alpha\beta$ coordinates

The most important equations of the cylindrical SM model in the $\alpha\beta$ coordinates are:

Stator voltage:
$$\boldsymbol{u}^{\mathrm{s}}_{\mathrm{s},\alpha\beta}(t) = R_{\mathrm{s}}\boldsymbol{i}^{\mathrm{s}}_{\mathrm{s},\alpha\beta}(t) + \frac{\mathrm{d}}{\mathrm{d}t}\boldsymbol{\psi}^{\mathrm{s}}_{\mathrm{s},\alpha\beta}(t),$$

Rotor / field winding voltage:
$$u^{\mathrm{r}}_{\mathrm{f}}(t) = R_{\mathrm{f}} i^{\mathrm{r}}_{\mathrm{f}}(t) + \frac{\mathrm{d}}{\mathrm{d}t}\psi^{\mathrm{r}}_{\mathrm{f}}(t),$$

Stator flux linkage:
$$\boldsymbol{\psi}^{\mathrm{s}}_{\mathrm{s},\alpha\beta}(t) = L'_{\mathrm{s}}\boldsymbol{i}^{\mathrm{s}}_{\mathrm{s},\alpha\beta}(t) + M_{\mathrm{fs}}\begin{bmatrix}\cos(\varepsilon_{\mathrm{r,el}}(t))\\ \sin(\varepsilon_{\mathrm{r,el}}(t))\end{bmatrix} i^{\mathrm{r}}_{\mathrm{f}}(t),$$

Rotor / field winding flux linkage:
$$\psi^{\mathrm{r}}_{\mathrm{f}}(t) = L_{\mathrm{f}} i^{\mathrm{r}}_{\mathrm{f}}(t) + M_{\mathrm{fs}}\begin{bmatrix}\cos(\varepsilon_{\mathrm{r,el}}(t))\\ \sin(\varepsilon_{\mathrm{r,el}}(t))\end{bmatrix}^{\mathsf{T}} \boldsymbol{i}^{\mathrm{s}}_{\mathrm{s},\alpha\beta}(t),$$

Torque:
$$T(t) = \frac{3}{2}p(\boldsymbol{i}^{\mathrm{s}}_{\mathrm{s},\alpha\beta})^{\mathsf{T}}\boldsymbol{J}\boldsymbol{\psi}^{\mathrm{s}}_{\mathrm{s},\alpha\beta}.$$

Rotor flux orientation: the dq coordinate system

- In the SM case the rotor flux orientaton is directly related to the rotor position (cf. Fig. 6.1).
- Hence, to transfer the rotor and stator equations into a mutual coordinate system, the rotor flux orientation is typically used as a reference.
- In contrast to the $\alpha\beta$-coordinates, where the stator quantity signals are of sinusoidal shape during steady state, the rotor flux-oriented signals are constant during steady state.

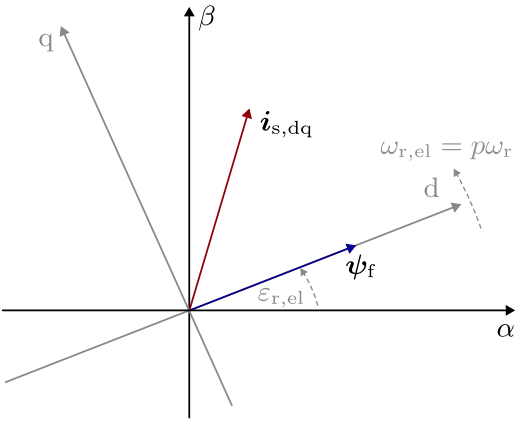

Fig. 6.9: Rotor flux-oriented coordinate system

Rotor flux orientation: the dq coordinate system (cont.)

Transferring the stator voltage equation into the dq coordinate system results in

$$\begin{aligned} & \boldsymbol{u}^{\mathrm{s}}_{\mathrm{s},\alpha\beta}(t) = R_{\mathrm{s}}\boldsymbol{i}^{\mathrm{s}}_{\mathrm{s},\alpha\beta}(t) + \frac{\mathrm{d}}{\mathrm{d}t}\boldsymbol{\psi}^{\mathrm{s}}_{\mathrm{s},\alpha\beta}(t) \\ \Leftrightarrow \quad & \boldsymbol{T}_{\mathrm{p}}^{-1}(\varepsilon_{\mathrm{r,el}})\boldsymbol{u}^{\mathrm{s}}_{\mathrm{s,dq}}(t) = R_{\mathrm{s}}\boldsymbol{T}_{\mathrm{p}}^{-1}(\varepsilon_{\mathrm{r,el}})\boldsymbol{i}^{\mathrm{s}}_{\mathrm{s,dq}}(t) + \frac{\mathrm{d}}{\mathrm{d}t}(\boldsymbol{T}_{\mathrm{p}}^{-1}(\varepsilon_{\mathrm{r,el}})\boldsymbol{\psi}^{\mathrm{s}}_{\mathrm{s,dq}}(t)) \\ \Leftrightarrow \quad & \boldsymbol{u}^{\mathrm{r}}_{\mathrm{s,dq}}(t) = R_{\mathrm{s}}\boldsymbol{i}^{\mathrm{r}}_{\mathrm{s,dq}}(t) + \omega_{\mathrm{r,el}}(t)\boldsymbol{J}\boldsymbol{\psi}^{\mathrm{r}}_{\mathrm{s,dq}}(t) + \frac{\mathrm{d}}{\mathrm{d}t}\boldsymbol{\psi}^{\mathrm{r}}_{\mathrm{s,dq}}(t). \end{aligned} \tag{6.14}$$

Since the dq coordinate system is always aligned with the rotor flux in the SM case, one can also drop the superscript r:

$$\boldsymbol{u}_{\mathrm{s,dq}}(t) = R_{\mathrm{s}}\boldsymbol{i}_{\mathrm{s,dq}}(t) + \omega_{\mathrm{r,el}}(t)\boldsymbol{J}\boldsymbol{\psi}_{\mathrm{s,dq}}(t) + \frac{\mathrm{d}}{\mathrm{d}t}\boldsymbol{\psi}_{\mathrm{s,dq}}(t).$$

Rotor flux orientation: the dq coordinate system (cont.)

The stator flux linkage model in the dq coordinate system is given by

$$\begin{aligned}
&\boldsymbol{\psi}^{\mathrm{s}}_{\mathrm{s},\alpha\beta}(t) = L'_{\mathrm{s}}\boldsymbol{i}^{\mathrm{s}}_{\mathrm{s},\alpha\beta}(t) + M_{\mathrm{fs}}\begin{bmatrix}\cos(\varepsilon_{\mathrm{r,el}}(t))\\ \sin(\varepsilon_{\mathrm{r,el}}(t))\end{bmatrix} i^{\mathrm{r}}_{\mathrm{f}}(t),\\
\Leftrightarrow\quad &\boldsymbol{T}_{\mathrm{p}}^{-1}(\varepsilon_{\mathrm{r,el}})\boldsymbol{\psi}_{\mathrm{s,dq}}(t) = L'_{\mathrm{s}}\boldsymbol{T}_{\mathrm{p}}^{-1}(\varepsilon_{\mathrm{r,el}})\boldsymbol{i}_{\mathrm{s,dq}}(t) + M_{\mathrm{fs}}\begin{bmatrix}\cos(\varepsilon_{\mathrm{r,el}}(t))\\ \sin(\varepsilon_{\mathrm{r,el}}(t))\end{bmatrix} i_{\mathrm{f}}(t)\\
\Leftrightarrow\quad &\boldsymbol{\psi}_{\mathrm{s,dq}}(t) = L'_{\mathrm{s}}\boldsymbol{i}_{\mathrm{s,dq}}(t) + \underbrace{M_{\mathrm{fs}}\begin{bmatrix}1\\0\end{bmatrix}}_{\boldsymbol{M}_{\mathrm{fs}}} i^{\mathrm{r}}_{\mathrm{f}}(t) = L'_{\mathrm{s}}\boldsymbol{i}_{\mathrm{s,dq}}(t) + \boldsymbol{M}_{\mathrm{fs}}i^{\mathrm{r}}_{\mathrm{f}}(t).
\end{aligned} \tag{6.15}$$

while the field winding flux results in

$$\begin{aligned}
&\psi^{\mathrm{r}}_{\mathrm{f}}(t) = L_{\mathrm{f}}i^{\mathrm{r}}_{\mathrm{f}}(t) + M_{\mathrm{fs}}\begin{bmatrix}\cos(\varepsilon_{\mathrm{r,el}}(t)) & \sin(\varepsilon_{\mathrm{r,el}}(t))\end{bmatrix}\boldsymbol{i}^{\mathrm{s}}_{\mathrm{s},\alpha\beta}(t)\\
\Leftrightarrow\quad &\psi^{\mathrm{r}}_{\mathrm{f}}(t) = L_{\mathrm{f}}i^{\mathrm{r}}_{\mathrm{f}}(t) + M_{\mathrm{fs}}\begin{bmatrix}\cos(\varepsilon_{\mathrm{r,el}}(t)) & \sin(\varepsilon_{\mathrm{r,el}}(t))\end{bmatrix}\boldsymbol{T}_{\mathrm{p}}^{-1}(\varepsilon_{\mathrm{r,el}})\boldsymbol{i}^{\mathrm{s}}_{\mathrm{s,dq}}(t)\\
\Leftrightarrow\quad &\psi^{\mathrm{r}}_{\mathrm{f}}(t) = L_{\mathrm{f}}i^{\mathrm{r}}_{\mathrm{f}}(t) + M_{\mathrm{fs}}\begin{bmatrix}1 & 0\end{bmatrix}\boldsymbol{i}_{\mathrm{s,dq}}(t) = L_{\mathrm{f}}i^{\mathrm{r}}_{\mathrm{f}}(t) + \boldsymbol{M}^{\mathsf{T}}_{\mathrm{fs}}\boldsymbol{i}_{\mathrm{s,dq}}(t).
\end{aligned} \tag{6.16}$$

Summary: cylindrical SM model in dq coordinates

The most important equations of the cylindrical SM model in the dq coordinates are:

$$\text{Stator voltage:} \quad \boldsymbol{u}_{\mathrm{s,dq}}(t) = R_{\mathrm{s}}\boldsymbol{i}_{\mathrm{s,dq}}(t) + \omega_{\mathrm{r,el}}(t)\boldsymbol{J}\boldsymbol{\psi}_{\mathrm{s,dq}}(t) + \frac{\mathrm{d}}{\mathrm{d}t}\boldsymbol{\psi}_{\mathrm{s,dq}}(t),$$

$$\text{Rotor / field winding voltage:} \quad u_{\mathrm{f}}(t) = R_{\mathrm{f}}i_{\mathrm{f}}(t) + \frac{\mathrm{d}}{\mathrm{d}t}\psi_{\mathrm{f}}(t),$$

$$\text{Stator flux linkage:} \quad \boldsymbol{\psi}_{\mathrm{s,dq}}(t) = L'_{\mathrm{s}}\boldsymbol{i}_{\mathrm{s,dq}}(t) + \boldsymbol{M}_{\mathrm{fs}}i_{\mathrm{f}}(t),$$

$$\text{Rotor / field winding flux linkage:} \quad \psi_{\mathrm{f}}(t) = L_{\mathrm{f}}i^{\mathrm{r}}_{\mathrm{f}}(t) + \boldsymbol{M}^{\mathsf{T}}_{\mathrm{fs}}\boldsymbol{i}_{\mathrm{s,dq}}(t),$$

$$\text{Torque:} \quad T(t) = \frac{3}{2}p(\boldsymbol{i}_{\mathrm{s,dq}})^{\mathsf{T}}\boldsymbol{J}\boldsymbol{\psi}_{\mathrm{s,dq}}.$$

Here, one can observe that the d component of the stator flux linkage is directly coupled with the field winding flux and vice versa, which was to be expected due to the rotor flux orientation of the chosen coordinate system.

ECD of cylindrical SM model in dq coordinates

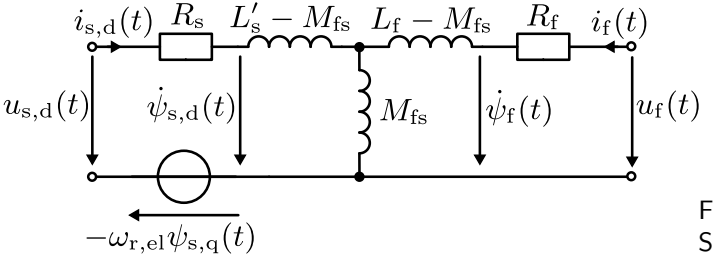

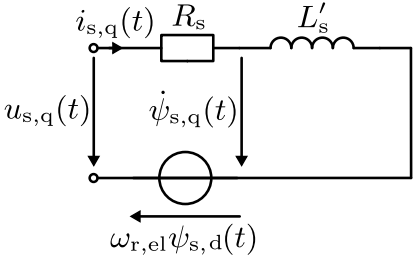

Fig. 6.10: T-type ECD of a cylindrical SM in dq coordinates (note that this ECD is represented with scalar values and not as vectors or complex numbers as in the IM case).

Salient pole SM model

- The cylindrical rotor SM model (6.15) considered an identical stator inductance L'_{s} for the d and q axis.
- In the cylindrical SM case this is a valid assumption, as the rotor is symmetrical.
- However, in the case of a salient pole SM, the rotor is not symmetrical and the flux path per axis is different (cf. Fig. 6.11).
- The q-axis reluctance is larger than the d-axis reluctance due to the larger air gap in the q-axis direction.
- Consequently, the inductance per axis is different.

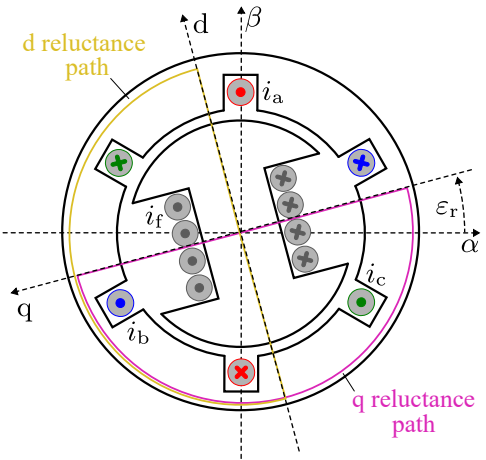

Fig. 6.11: Effective reluctance paths of the salient pole SM in the dq coordinate system

Salient pole SM model (cont.)

From Fig. 6.11 we derive the following stator flux linkage model for the salient pole SM:

$$\boldsymbol{\psi}_{\mathrm{s,dq}}(t) = \underbrace{\begin{bmatrix} L'_{\mathrm{s,d}} & 0 \\ 0 & L'_{\mathrm{s,q}} \end{bmatrix}}_{\boldsymbol{L}_{\mathrm{s,dq}}} \boldsymbol{i}_{\mathrm{s,dq}}(t) + M_{\mathrm{fs}} \begin{bmatrix} 1 \\ 0 \end{bmatrix} i_{\mathrm{f}}(t) = \boldsymbol{L}_{\mathrm{s,dq}} \boldsymbol{i}_{\mathrm{s,dq}}(t) + \boldsymbol{M}_{\mathrm{fs}} i_{\mathrm{f}}(t) \tag{6.17}$$

while the rotor field winding flux linkage remains identical to the cylindrical SM case. Inserting the stator flux linkage model into the torque equation yields

$$\begin{aligned} T(t) &= \frac{3}{2} p (\boldsymbol{i}_{\mathrm{s,dq}})^{\mathsf{T}} \boldsymbol{J} \boldsymbol{\psi}_{\mathrm{s,dq}} = \frac{3}{2} p i_{\mathrm{s,q}} \left[M_{\mathrm{fs}} i_{\mathrm{f}} + \left(L'_{\mathrm{s,d}} - L'_{\mathrm{s,q}} \right) i_{\mathrm{s,d}} \right] \\ &= \underbrace{\frac{3}{2} p M_{\mathrm{fs}} i_{\mathrm{s,q}} i_{\mathrm{f}}}_{\text{main torque}} + \underbrace{\frac{3}{2} p i_{\mathrm{s,q}} i_{\mathrm{s,d}} \left(L'_{\mathrm{s,d}} - L'_{\mathrm{s,q}} \right)}_{\text{reluctance torque}} . \end{aligned} \tag{6.18}$$

The latter part is specific to the salient pole SM since $L'_{\mathrm{s,d}} \neq L'_{\mathrm{s,q}}$ holds, while $L'_{\mathrm{s,d}} = L'_{\mathrm{s,q}} = L'_{\mathrm{s}}$ applies to the cylindrical SM, that is, the reluctance torque is zero.

Summary: salient pole SM model in dq coordinates

The most important equations of the salient pole SM model in the dq coordinates are:

Stator voltage:
$$\boldsymbol{u}_{\mathrm{s,dq}}(t) = R_{\mathrm{s}}\boldsymbol{i}_{\mathrm{s,dq}}(t) + \omega_{\mathrm{r,el}}(t)\boldsymbol{J}\boldsymbol{\psi}_{\mathrm{s,dq}}(t) + \frac{\mathrm{d}}{\mathrm{d}t}\boldsymbol{\psi}_{\mathrm{s,dq}}(t),$$

Rotor / field winding voltage:
$$u_{\mathrm{f}}(t) = R_{\mathrm{f}}i_{\mathrm{f}}(t) + \frac{\mathrm{d}}{\mathrm{d}t}\psi_{\mathrm{f}}(t),$$

Stator flux linkage:
$$\boldsymbol{\psi}_{\mathrm{s,dq}}(t) = \boldsymbol{L}_{\mathrm{s,dq}}\boldsymbol{i}_{\mathrm{s,dq}}(t) + \boldsymbol{M}_{\mathrm{fs}}i_{\mathrm{f}}(t),$$

Rotor / field winding flux linkage:
$$\psi_{\mathrm{f}}(t) = L_{\mathrm{f}}i_{\mathrm{f}}^{\mathrm{r}}(t) + \boldsymbol{M}_{\mathrm{fs}}^{\mathsf{T}}\boldsymbol{i}_{\mathrm{s,dq}}(t),$$

Torque:
$$\begin{aligned} T(t) &= \frac{3}{2}p(\boldsymbol{i}_{\mathrm{s,dq}})^{\mathsf{T}}\boldsymbol{J}\boldsymbol{\psi}_{\mathrm{s,dq}} \\ &= \frac{3}{2}pi_{\mathrm{s,q}}\left[M_{\mathrm{fs}}i_{\mathrm{f}} + \left(L'_{\mathrm{s,d}} - L'_{\mathrm{s,q}}\right)i_{\mathrm{s,d}}\right]. \end{aligned}$$

Damper winding

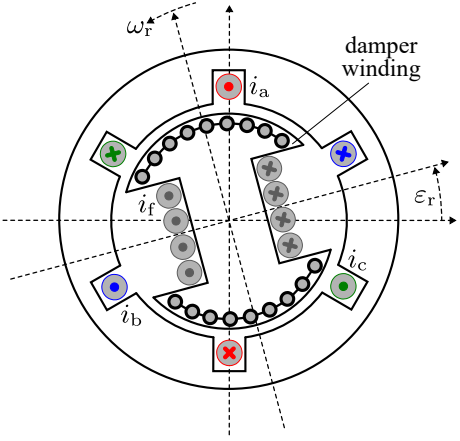

(a) Salient pole SM with damper winding

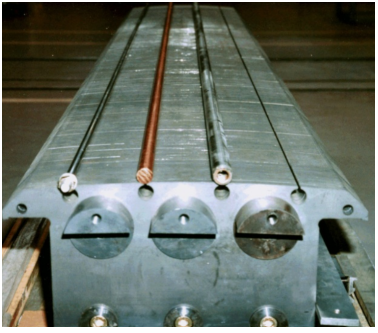

(b) Salient pole with dismantled damper winding (source: L. Frosini, *Novel Diagnostic Techniques for Rotating Electrical Machines – A Review*, Energies, 2020, CC BY 4.0)

Fig. 6.12: SM with damper winding

Damper winding (cont.)

- The damper winding is a short-circuited winding in the rotor slots of the SM.
- The damper winding is used to dampen the rotor oscillations during transients.
- This is important for synchronous generators in power systems, where the rotor oscillations can lead to instabilities.

Damper winding model

The SM damper winding can be interpreted as the IM squirrel cage, i.e., the rotor model can be extended accordingly (superposition).

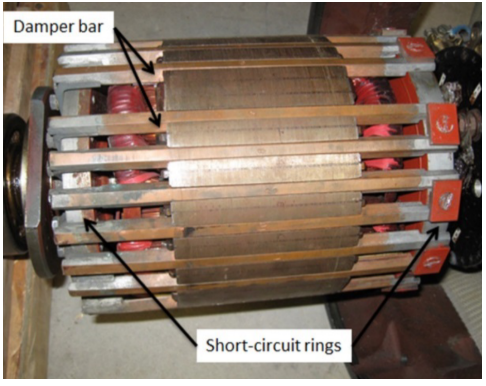

Fig. 6.13: SM rotor with solid damper bars (source: J. Cros et al., *Simulation Methods for the Transient Analysis of Synchronous Alternators*, Renewable Energy, 2016, CC BY 3.0)

SM model with damper winding

From the IM model in dq-coordinates (compare Fig. 5.9) we introduce the short-circuited damper winding voltage equation:

$$0 = \boldsymbol{R}_{\mathrm{r,DQ}} \boldsymbol{i}_{\mathrm{r,DQ}}(t) + \frac{\mathrm{d}}{\mathrm{d}t} \boldsymbol{\psi}_{\mathrm{r,DQ}}(t) = \begin{bmatrix} R_{\mathrm{r,D}} & 0 \\ 0 & R_{\mathrm{r,Q}} \end{bmatrix} \begin{bmatrix} i_{\mathrm{r,D}}(t) \\ i_{\mathrm{r,Q}}(t) \end{bmatrix} + \frac{\mathrm{d}}{\mathrm{d}t} \begin{bmatrix} \psi_{\mathrm{r,D}}(t) \\ \psi_{\mathrm{r,Q}}(t) \end{bmatrix}. \tag{6.19}$$

Here, the following applies:

- Capital indices represent the damper winding.
- $\boldsymbol{i}_{\mathrm{r,DQ}}(t)$ and $\boldsymbol{\psi}_{\mathrm{r,DQ}}(t)$ are the current as well as flux linkage in the damper winding.
- $\boldsymbol{R}_{\mathrm{r,DQ}}$ represents the resistance matrix: Since the damper winding eventually does not cover the entire rotor circumference, $R_{\mathrm{r,D}} \neq R_{\mathrm{r,Q}}$ can apply (compare Fig. 6.12).

The stator and field winding voltage equations remain unchanged:

$$\boldsymbol{u}_{\mathrm{s,dq}}(t) = R_{\mathrm{s}} \boldsymbol{i}_{\mathrm{s,dq}}(t) + \omega_{\mathrm{r,el}}(t) \boldsymbol{J} \boldsymbol{\psi}_{\mathrm{s,dq}}(t) + \frac{\mathrm{d}}{\mathrm{d}t} \boldsymbol{\psi}_{\mathrm{s,dq}}(t), \quad u_{\mathrm{f}}(t) = R_{\mathrm{f}} i_{\mathrm{f}}(t) + \frac{\mathrm{d}}{\mathrm{d}t} \psi_{\mathrm{f}}(t).$$

SM model with damper winding (cont.)

The flux linkage equations become

$$
\begin{aligned}
\boldsymbol{\psi}_{\mathrm{s,dq}}(t) &= \boldsymbol{L}_{\mathrm{s,dq}}\boldsymbol{i}_{\mathrm{s,dq}}(t) + \boldsymbol{M}_{\mathrm{fs}} i_{\mathrm{f}}(t) + \boldsymbol{M}_{\mathrm{rs}}\boldsymbol{i}_{\mathrm{r,DQ}}(t) \\
&= \begin{bmatrix} L'_{\mathrm{s,d}} & 0 \\ 0 & L'_{\mathrm{s,q}} \end{bmatrix} \begin{bmatrix} i_{\mathrm{s,d}}(t) \\ i_{\mathrm{s,q}}(t) \end{bmatrix} + M_{\mathrm{fs}} \begin{bmatrix} 1 \\ 0 \end{bmatrix} i_{\mathrm{f}}(t) + \begin{bmatrix} M_{\mathrm{dD}} & 0 \\ 0 & M_{\mathrm{qQ}} \end{bmatrix} \begin{bmatrix} i_{\mathrm{r,D}}(t) \\ i_{\mathrm{r,Q}}(t) \end{bmatrix}, \\
\psi_{\mathrm{f}}(t) &= L_{\mathrm{f}} i_{\mathrm{f}}(t) + \boldsymbol{M}_{\mathrm{fs}}^{\mathsf{T}}\boldsymbol{i}_{\mathrm{s,dq}}(t) + \boldsymbol{M}_{\mathrm{fr}}^{\mathsf{T}}\boldsymbol{i}_{\mathrm{r,DQ}}(t) \\
&= L_{\mathrm{f}} i_{\mathrm{f}}(t) + M_{\mathrm{fs}} \begin{bmatrix} 1 & 0 \end{bmatrix} \begin{bmatrix} i_{\mathrm{s,d}}(t) \\ i_{\mathrm{s,q}}(t) \end{bmatrix} + M_{\mathrm{fr}} \begin{bmatrix} 1 & 0 \end{bmatrix} \begin{bmatrix} i_{\mathrm{r,D}}(t) \\ i_{\mathrm{r,Q}}(t) \end{bmatrix}, \\
\boldsymbol{\psi}_{\mathrm{r,DQ}}(t) &= \boldsymbol{L}_{\mathrm{r,DQ}}\boldsymbol{i}_{\mathrm{r,DQ}}(t) + \boldsymbol{M}_{\mathrm{rs}}\boldsymbol{i}_{\mathrm{s,dq}}(t) + \boldsymbol{M}_{\mathrm{fr}} i_{\mathrm{f}}(t) \\
&= \begin{bmatrix} L_{\mathrm{D}} & 0 \\ 0 & L_{\mathrm{Q}} \end{bmatrix} \begin{bmatrix} i_{\mathrm{r,D}}(t) \\ i_{\mathrm{r,Q}}(t) \end{bmatrix} + \begin{bmatrix} M_{\mathrm{dD}} & 0 \\ 0 & M_{\mathrm{qQ}} \end{bmatrix} \begin{bmatrix} i_{\mathrm{s,d}}(t) \\ i_{\mathrm{s,q}}(t) \end{bmatrix} + M_{\mathrm{fr}} \begin{bmatrix} 1 \\ 0 \end{bmatrix} i_{\mathrm{f}}(t).
\end{aligned}
\tag{6.20}
$$

SM model with damper winding (cont.)

The torque equation results in

$$\begin{aligned} T(t) &= \frac{3}{2} p (\boldsymbol{i}_{\mathrm{s,dq}})^{\mathsf{T}} \boldsymbol{J} \boldsymbol{\psi}_{\mathrm{s,dq}} \\ &= \frac{3}{2} p \left[M_{\mathrm{fs}} i_{\mathrm{f}} i_{\mathrm{s,q}} + \left(L'_{\mathrm{s,d}} - L'_{\mathrm{s,q}} \right) i_{\mathrm{s,d}} i_{\mathrm{s,q}} + M_{\mathrm{dD}} i_{\mathrm{s,q}} i_{\mathrm{r,D}} - M_{\mathrm{qQ}} i_{\mathrm{s,d}} i_{\mathrm{r,Q}} \right]. \end{aligned} \tag{6.21}$$

Here, the last two terms represent the torque contribution of the damper winding:

- In steady state, that is, the stator field rotates synchronously with the rotor, the damper winding current is zero, cf. (6.19). Consequently, the damper torque is zero.
- Only during transients, when a changing flux linkage induces a voltage within the damper winding, non-zero damper currents occur.
- The resulting damper torque will oppose the transient and, e.g., dampen mechanical rotor oscillations in generator applications.

Permanent magnet synchronous machine (PMSM)

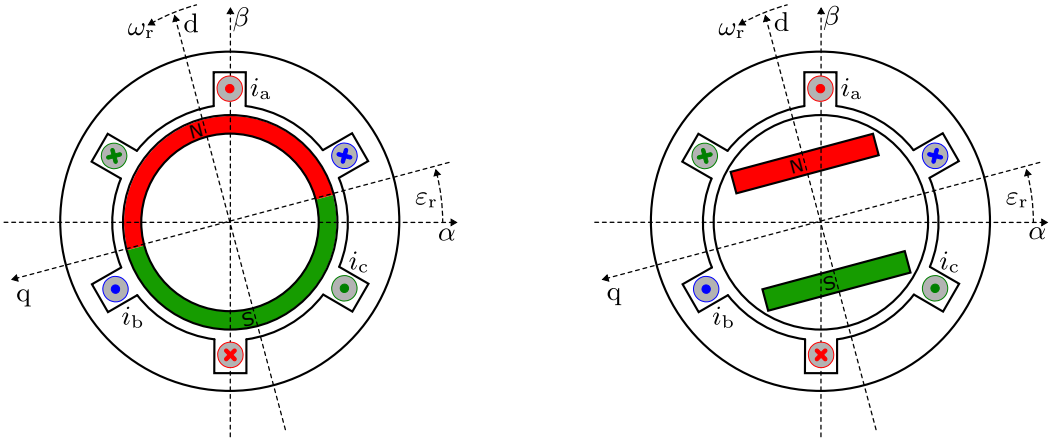

(a) Surface-mounted PMSM (SPMSM)

(b) Interior PMSM (IPMSM)

Fig. 6.14: SM with permanent magnet excitation

PMSM characteristics

- Field winding is replaced by permanent magnets (PMs) in the rotor.
- Typically increases efficiency and power density, since no field winding losses occur.
- However, PMs are often more expensive than field windings and the machine is less flexible in terms of field weakening.

PMSM applications

Due to weight and size advantages, PMSMs are often used in automotive applications (e.g., electric vehicles) and in highly dynamic industrial applications (e.g., servo drives).

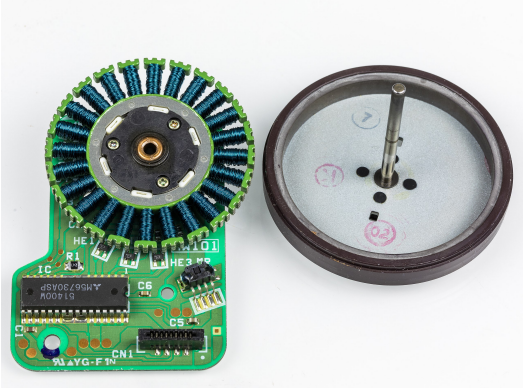

Fig. 6.15: PMSM with external rotor (source: Wikimedia Commons, R. Spekking, CC BY-SA 4.0)

PMSM model

Due to the absence of a field winding, the PMSM model simplifies: The general stator voltage equation in the dq coordinate system remains identical to the SM model

$$\boldsymbol{u}_{\mathrm{s,dq}}(t) = R_{\mathrm{s}}\boldsymbol{i}_{\mathrm{s,dq}}(t) + \omega_{\mathrm{r,el}}(t)\boldsymbol{J}\boldsymbol{\psi}_{\mathrm{s,dq}}(t) + \frac{\mathrm{d}}{\mathrm{d}t}\boldsymbol{\psi}_{\mathrm{s,dq}}(t)$$

while the field winding voltage equation is omitted. The stator flux linkage model becomes

$$\boldsymbol{\psi}_{\mathrm{s,dq}}(t) = \boldsymbol{L}_{\mathrm{s,dq}}\boldsymbol{i}_{\mathrm{s,dq}}(t) + \boldsymbol{\psi}_{\mathrm{pm}} = \begin{bmatrix} L'_{\mathrm{s,d}} & 0 \\ 0 & L'_{\mathrm{s,q}} \end{bmatrix} \begin{bmatrix} i_{\mathrm{s,d}}(t) \\ i_{\mathrm{s,q}}(t) \end{bmatrix} + \begin{bmatrix} \psi_{\mathrm{pm}} \\ 0 \end{bmatrix}. \tag{6.22}$$

Here, $\boldsymbol{\psi}_{\mathrm{pm}}$ represents the (constant) permanent magnet flux linkage. By definition of the dq coordinate system, the permanent magnet flux linkage is directed exclusively along the d-axis (cf. Fig. 6.14). The rotor flux linkage model is omitted, since no field winding is present. Also, a damper winding is very uncommon for PMSMs. Hence, torque equation results in

$$T(t) = \frac{3}{2}p(\boldsymbol{i}_{\mathrm{s,dq}})^{\mathsf{T}}\boldsymbol{J}\boldsymbol{\psi}_{\mathrm{s,dq}} = \frac{3}{2}p i_{\mathrm{s,q}}\left[\boldsymbol{\psi}_{\mathrm{pm}} + \left(L'_{\mathrm{s,d}} - L'_{\mathrm{s,q}}\right) i_{\mathrm{s,d}}\right]. \tag{6.23}$$

Isotropic vs. anisotropic PMSM

From (2.26) we know that the relative permeability of the PM material is nearly as that of air, i.e.,

$$\mu_{\mathrm{r,PM}} \approx 1$$

applies. Consequently, the PM flux path can be considered as an (additional) air gap. Against this background, the two types for PMSM rotors as in Fig. 6.14 show different characteristics:

- SPMSM: The PMs are distributed over the entire rotor circumference.
  - The PM flux path is isotropic, i.e., the same in all directions.
  - Consequently, the relucance paths in the d and q axis are identical.
  - $L'_{\mathrm{s,d}} = L'_{\mathrm{s,q}} = L'_{\mathrm{s}}$ applies.
- IPMSM: The PMs are concentrated inside the rotor core.
  - The PM flux path is anisotropic, i.e., different in the d and q axis.
  - Consequently, the effective reluctance along the d axis is much higher than along the q axis.
  - $L'_{\mathrm{s,d}} < L'_{\mathrm{s,q}}$ applies.

Synchronous reluctance machine (SynRM)

- SynRM: utilizes only the reluctance torque.
- No field winding or PMs are present.
- The rotor is designed such that the reluctance difference in the d and q axis is maximized.
- PMSM model equations can be used, but the PM flux linkage is zero.

$$\begin{aligned} \boldsymbol{\psi}_{\mathrm{s,dq}}(t) &= \boldsymbol{L}_{\mathrm{s,dq}} \boldsymbol{i}_{\mathrm{s,dq}}(t), \\ T(t) &= \frac{3}{2} p (\boldsymbol{i}_{\mathrm{s,dq}})^{\mathsf{T}} \boldsymbol{J} \boldsymbol{\psi}_{\mathrm{s,dq}} \\ &= \frac{3}{2} p i_{\mathrm{s,q}} \left(L'_{\mathrm{s,d}} - L'_{\mathrm{s,q}} \right) i_{\mathrm{s,d}}. \end{aligned} \tag{6.24}$$

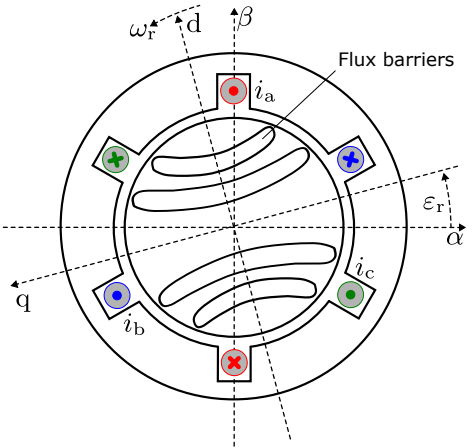

Fig. 6.16: Example of a SynRM with rotor flux barriers (no PMs or field winding present)

Steady-state behavior

We limit the following discussion to the isotropic case

$$L'_{\mathrm{s,d}} = L'_{\mathrm{s,q}} = L'_{\mathrm{s}}$$

which covers the SPMSM and the cylindrical SM. In steady state ($\mathrm{d}x/\mathrm{d}t = 0$), the flux linked with possibly present damper windings is constant, i.e., no voltage is induced within the damper windings and

$$\boldsymbol{I}_{\mathrm{r,DQ}} = 0$$

applies. Hence, the damper winding can be neglected in steady state. Furthermore, in steady state the field winding current is constant:

$$I_{\mathrm{f}} = \frac{\mathrm{U_f}}{\mathrm{R_f}} = \mathrm{const.}$$

Consequently, the stator flux linkage share resulting from the field winding $\boldsymbol{M}_{\mathrm{fs}} I_{\mathrm{f}}$ is constant and can be interpreted as an equivalent permanent magnet flux linkage. Hence, we will focus on the steady-state behavior of the cylindrical SM in the following, which implicitly covers the SPMSM case as well. The steady-state characteristics of the other SM types are not covered.

Steady-state behavior (cont.)

In steady state, the flux linkage equation remains

$$\boldsymbol{\psi}_{\mathrm{s,dq}} = L'_{\mathrm{s}} \boldsymbol{I}_{\mathrm{s,dq}} + \boldsymbol{M}_{\mathrm{fs}} I_{\mathrm{f}} \quad \Leftrightarrow \quad \begin{bmatrix} \psi_{\mathrm{s,d}} \\ \psi_{\mathrm{s,q}} \end{bmatrix} = \left(L_{\mathrm{s}} + \frac{M_{\mathrm{s}}}{2} \right) \begin{bmatrix} I_{\mathrm{s,d}} \\ I_{\mathrm{s,q}} \end{bmatrix} + M_{\mathrm{fs}} \begin{bmatrix} I_{\mathrm{f}} \\ 0 \end{bmatrix}.$$

With the decomposition of L_{s} into its leakage part $L_{\sigma,\mathrm{s}}$ and the mutual part M_{s},

$$L_{\mathrm{s}} = L_{\sigma,\mathrm{s}} + M_{\mathrm{s}}, \tag{6.25}$$

we obtain

$$\begin{bmatrix} \psi_{\mathrm{s,d}} \\ \psi_{\mathrm{s,q}} \end{bmatrix} = \left(L_{\sigma,\mathrm{s}} + \frac{3}{2} M_{\mathrm{s}} \right) \begin{bmatrix} I_{\mathrm{s,d}} \\ I_{\mathrm{s,q}} \end{bmatrix} + M_{\mathrm{fs}} \begin{bmatrix} I_{\mathrm{f}} \\ 0 \end{bmatrix}. \tag{6.26}$$

In the context of simplified modeling, the assumption is (often) made that the (scaled) mutual inductances are equal, i.e.,

$$M_{\mathrm{fs}} = {}^{3}\!/_{2} M_{\mathrm{s}} = M$$

leading to

$$\psi_{\mathrm{s,d}} = (L_{\sigma,\mathrm{s}} + M)\, I_{\mathrm{s,d}} + M I_{\mathrm{f}}, \qquad \psi_{\mathrm{s,q}} = (L_{\sigma,\mathrm{s}} + M)\, I_{\mathrm{s,q}}. \tag{6.27}$$

Steady-state behavior (cont.)

The steady-state voltage equation is

$$\boldsymbol{U}_{\mathrm{s,dq}} = R_{\mathrm{s}}\boldsymbol{I}_{\mathrm{s,dq}} + \omega_{\mathrm{r,el}}\boldsymbol{J}\boldsymbol{\psi}_{\mathrm{s,dq}} \quad \Leftrightarrow \quad \begin{bmatrix} U_{\mathrm{s,d}} \\ U_{\mathrm{s,q}} \end{bmatrix} = R_{\mathrm{s}} \begin{bmatrix} I_{\mathrm{s,d}} \\ I_{\mathrm{s,q}} \end{bmatrix} + \omega_{\mathrm{r,el}} \begin{bmatrix} -\psi_{\mathrm{s,q}} \\ \psi_{\mathrm{s,d}} \end{bmatrix}. \tag{6.28}$$

Inserting the (simplified) flux linkage equation (6.27) yields

$$\begin{bmatrix} U_{\mathrm{s,d}} \\ U_{\mathrm{s,q}} \end{bmatrix} = R_{\mathrm{s}} \begin{bmatrix} I_{\mathrm{s,d}} \\ I_{\mathrm{s,q}} \end{bmatrix} + \omega_{\mathrm{r,el}} \begin{bmatrix} -\left(L_{\sigma,\mathrm{s}} + M\right) I_{\mathrm{s,q}} \\ \left(L_{\sigma,\mathrm{s}} + M\right) I_{\mathrm{s,d}} + M I_{\mathrm{f}} \end{bmatrix}. \tag{6.29}$$

Rewriting the vectorial quantities as complex phasors $\underline{X}_{\mathrm{dq}} = X e^{\mathrm{j}\phi} = X_{\mathrm{d}} + \mathrm{j}X_{\mathrm{q}}$ rotating with the angular frequency $\omega_{\mathrm{r,el}} \rightarrow \omega_{\mathrm{s}}$, we obtain

$$\underline{U}_{\mathrm{s}} = R_{\mathrm{s}}\underline{I}_{\mathrm{s}} + \mathrm{j}\omega_{\mathrm{s}}\left[\left(L_{\sigma,\mathrm{s}} + M\right)\underline{I}_{\mathrm{s}} + M I_{\mathrm{f}}\right] = R_{\mathrm{s}}\underline{I}_{\mathrm{s}} + \mathrm{j}\underbrace{\omega_{\mathrm{s}}\left(L_{\sigma,\mathrm{s}} + M\right)}_{X_{\mathrm{s}}}\underline{I}_{\mathrm{s}} + \underbrace{\mathrm{j}\omega_{\mathrm{s}} M I_{\mathrm{f}}}_{\underline{U}_{\mathrm{i}}} \tag{6.30}$$

with $\underline{U}_{\mathrm{i}}$ being the internal voltage, i.e., the induced voltage due to the field winding excitation and X_{s} being the synchronous reactance (which can be empirically identified using open-circuit and short-circuit tests, cf. after next slide).

Steady-state behavior (cont.)

The ECD of the cylindrical SM is sown in Fig. 6.17. Here, the following can be noted:

- The internal voltage $\underline{U}_\mathrm{i}$ is purely imaginary as the field winding current is a DC current and defined as real (convention).
- If $\underline{U}_\mathrm{s}$ is fixed, e.g., by a stiff grid voltage, the stator current $\underline{I}_\mathrm{s}$ is determined by the voltage difference $\Delta\underline{U} = \underline{U}_\mathrm{s} - \underline{U}_\mathrm{i}$.
- Hence, in grid operation the field winding current I_f is adjusted to reach a certain operation point, that is, the field excitation is controlled.

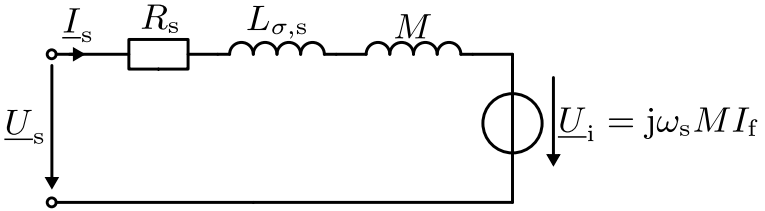

Fig. 6.17: ECD of a (simplified) cylindrical SM in steady state represented by complex phasors

Short-circuit and open-circuit tests

From Fig. 6.17 the open-circuit voltage is

$$\underline{U}_{\mathrm{s,oc}} = \underline{U}_{\mathrm{i}} = \mathrm{j}\omega_{\mathrm{s}} M I_{\mathrm{f}}. \tag{6.31}$$

Here, the stator current is zero. On the other hand, the short-circuit current is given by

$$\underline{I}_{\mathrm{s,sc}} = -\frac{\underline{U}_{\mathrm{i}}}{\mathrm{j}X_{\mathrm{s}}} = -\frac{\omega_{\mathrm{s}} M I_{\mathrm{f}}}{\mathrm{j}\omega_{\mathrm{s}}\left(L_{\sigma,\mathrm{s}} + M\right)} = \frac{\mathrm{j}M}{\left(L_{\sigma,\mathrm{s}} + M\right)} I_{\mathrm{f}}. \tag{6.32}$$

Here, the stator voltage is zero and one can observe that the short-circuit current $\underline{I}_{\mathrm{s,sc}}$ can be interpreted as the excitation current I_{f} converted via the inductance ratio. Finally, the synchronous reactance can be calculated by the ratio of the open-circuit voltage and the short-circuit current:

$$X_{\mathrm{s}} = \frac{\underline{U}_{\mathrm{s,oc}}}{\underline{I}_{\mathrm{s,sc}}}. \tag{6.33}$$

Steady-state torque

The steady-state torque of the cylindrical SM is given by

$$T = \frac{3}{2} p \sqrt{2} I_{\mathrm{s,q}} M I_{\mathrm{f}} = \frac{3}{\sqrt{2}} p I_{\mathrm{s,q}} M I_{\mathrm{f}}.$$

Here, the factor $\sqrt{2}$ results from the RMS value representation of the AC stator current in the complex phasor component $I_{\mathrm{s,q}}$. Note that I_{f} is a DC quantity, i.e., its RMS value is equal to the DC value in the time domain. From (6.30) we obtain the stator current as

$$\underline{I}_{\mathrm{s}} = \frac{\underline{U}_{\mathrm{s}} - \underline{U}_{\mathrm{i}}}{R_{\mathrm{s}} + \mathrm{j}\omega_{\mathrm{s}} \left(L_{\sigma,\mathrm{s}} + M \right)}. \tag{6.34}$$

Assuming that the ohmic voltage drop is negligible ($R_{\mathrm{s}} \approx 0$), which typically applies to high power machines, the stator current simplifies to

$$\underline{I}_{\mathrm{s}} = \mathrm{j} \frac{\underline{U}_{\mathrm{i}} - \underline{U}_{\mathrm{s}}}{\omega_{\mathrm{s}} \left(L_{\sigma,\mathrm{s}} + M \right)}. \tag{6.35}$$

Steady-state torque (cont.)

The q part from $\underline{I}_\mathrm{s} = I_\mathrm{s,d} + \mathrm{j}I_\mathrm{s,q}$ is

$$I_\mathrm{s,q} = \frac{|\underline{U}_\mathrm{i} - \underline{U}_\mathrm{s}|}{\omega_\mathrm{s}\left(L_{\sigma,\mathrm{s}} + M\right)}. \tag{6.36}$$

From Fig. 6.18 we identify

$$\sin(\theta) = \frac{|\underline{U}_\mathrm{i} - \underline{U}_\mathrm{s}|}{|\underline{U}_\mathrm{s}|}$$

and can rewrite $I_\mathrm{s,q}$ as

$$I_\mathrm{s,q} = \frac{|\underline{U}_\mathrm{s}|}{\omega_\mathrm{s}\left(L_{\sigma,\mathrm{s}} + M\right)} \sin(\theta). \tag{6.37}$$

Here, θ is the load angle counted from $\underline{U}_\mathrm{i}$ to $\underline{U}_\mathrm{s}$.

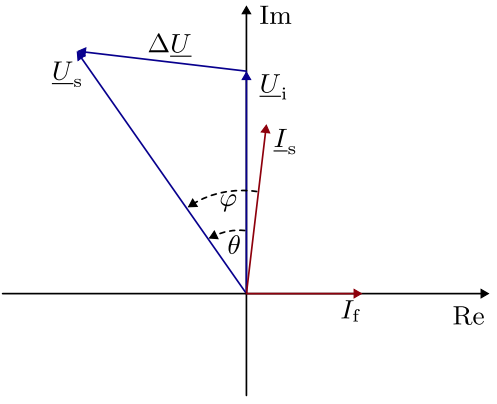

Fig. 6.18: Exemplary phasor diagram of the cylindrical SM

Steady-state torque (cont.)

Moreover, from (6.30) we can express the field winding current (amplitude, DC quantity) as

$$I_{\mathrm{f}} = \sqrt{2}\frac{|\underline{U}_{\mathrm{i}}|}{\omega_{\mathrm{s}} M}. \tag{6.38}$$

Inserting the expressions for $I_{\mathrm{s,q}}$ and I_{f} into the torque equation yields

$$T = 3p\frac{|\underline{U}_{\mathrm{s}}|\,|\underline{U}_{\mathrm{i}}|}{\omega_{\mathrm{s}}^2\,(L_{\sigma,\mathrm{s}} + M)}\sin(\theta) = 3p\frac{U_{\mathrm{s}} U_{\mathrm{i}}}{\omega_{\mathrm{s}}^2\,(L_{\sigma,\mathrm{s}} + M)}\sin(\theta). \tag{6.39}$$

Hence, the load angle θ determines the torque of the cylindrical SM:

- For $\theta < 0°$, the torque is negative (generator mode, if $\omega_{\mathrm{r}} > 0$).
- For $\theta = 0°$, the torque is zero.
- For $\theta > 0°$, the torque is positive (motor mode, if $\omega_{\mathrm{r}} > 0$).
- For $\theta = \pm 90°$, the absolute torque is maximal.

Stable steady-state operation (with fixed stator excitation)

- From (6.39) we see that the torque depends on $\sin(\theta)$.
- Beyond $\theta = \pm 90°$, the absolute torque decreases again.
- If the SM is operated with a fixed stator excitation, e.g., by a stiff grid voltage, the load angle θ is determined by the mechanical load.
- If the absolute mechanical load is increased such that $|\theta| > 90°$ applies, the SM will lose synchronicity and stall.
- Hence, the stable operation range is limited to $|\theta| \leq 90°$ (while in practice an additional safety margin is considered).

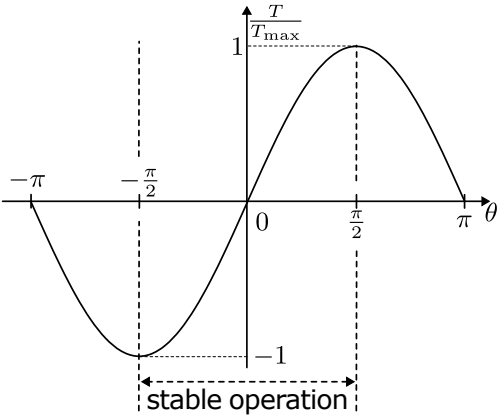

Fig. 6.19: Torque vs. load angle for the cylindrical SM

Power balance

The SM's complex power is given by

$$\underline{S} = 3\underline{U}_\mathrm{s}\overline{\underline{I}}_\mathrm{s} = 3(P + \mathrm{j}Q) = 3Se^{\mathrm{j}\varphi} \tag{6.40}$$

with $\overline{X}$ being the complex conjugate and the factor 3 results from the representation of the three-phase machine in an orthogonal coordinate system (cf. Clarke transf.) plus the RMS phasor representation of currents and voltages. Above, S is the apparent power, P and Q are the active and reactive power, respectively. The active power is

$$P = 3\mathrm{Re}\left\{\underline{U}_\mathrm{s}\overline{\underline{I}}_\mathrm{s}\right\} = 3U_\mathrm{s}I_\mathrm{s}\cos(\varphi) \tag{6.41}$$

and the reactive power is

$$Q = 3\mathrm{Im}\left\{\underline{U}_\mathrm{s}\overline{\underline{I}}_\mathrm{s}\right\} = 3U_\mathrm{s}I_\mathrm{s}\sin(\varphi). \tag{6.42}$$

Here, φ is the power factor angle, that is, the phase change between stator voltage and current (compare Fig. 6.18).

Power balance (cont.)

From (6.39) we receive the active power as

$$P = T\omega_\mathrm{r} = T\frac{\omega_\mathrm{s}}{p} = 3\frac{U_\mathrm{s}U_\mathrm{i}}{\omega_\mathrm{s}\left(L_{\sigma,\mathrm{s}} + M\right)}\sin(\theta). \tag{6.43}$$

For the reactive power we insert (6.35) in (6.42) and obtain (after some rewritting)

$$Q = 3\frac{U_\mathrm{s}}{\omega_\mathrm{s}\left(L_{\sigma,\mathrm{s}} + M\right)}\left(U_\mathrm{s} - U_\mathrm{i}\cos(\theta)\right). \tag{6.44}$$

Four quadrant operation

Due to a combination of θ and U_i, which are adjustable via the field winding current I_f, the (cylindrical) SM can cover all four quadrants of operation (i.e., combine positive / negative signs of both the active and reactive power). This is why the externally-excited SM is often used in generator / power plant applications.

Phasor diagrams for the cylindrical SM in all four quadrants

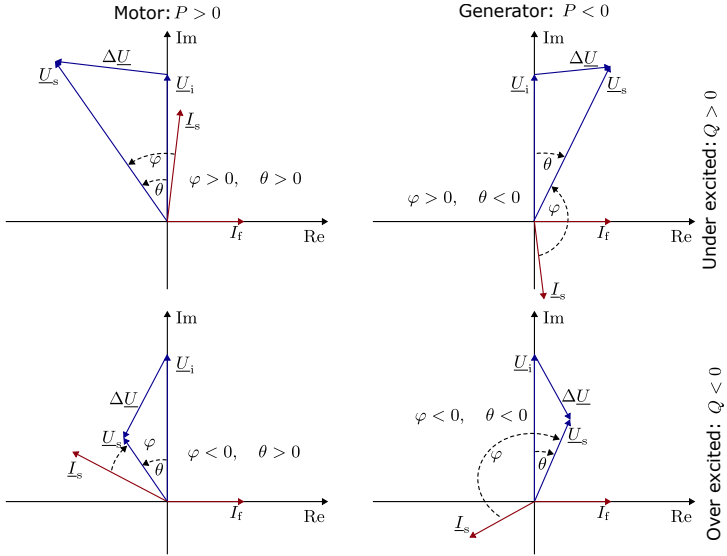

Power Electronics

Bikash Sah

Universität Siegen / IAS Interconnected Automation Systems

Table of contents

What are power electronics?

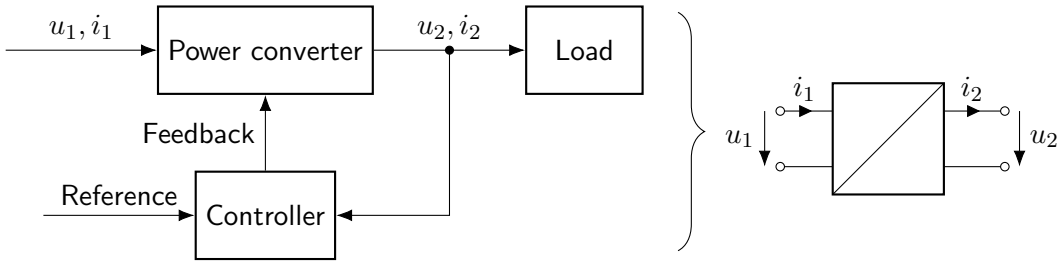

Fig. 7.1: High-level block diagram of a power electronic system

Power electronics – a definition

Power electronics is a multidisciplinary branch of electrical engineering. It focuses on processing, controlling, and converting electric power. Power electronics manipulate voltages and currents to deliver a defined power to electrical equipment and devices.

Power electronics vs. microelectronics

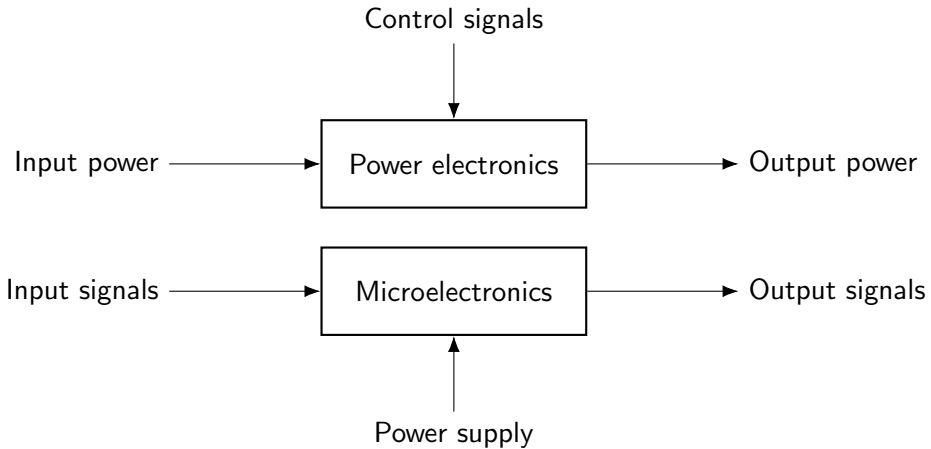

Fig. 7.2: Power electronics vs. microelectronics

Typical voltage and current manipulation tasks of power electronics

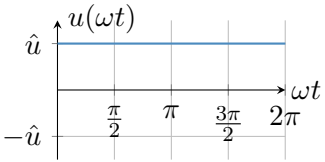

rectifier ↑ ↓ inverter

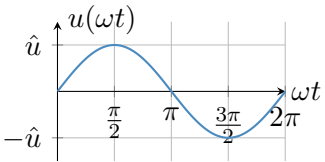

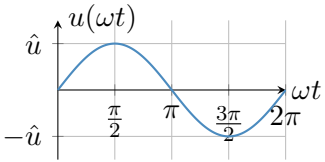

frequency ↕ amplitude
phase

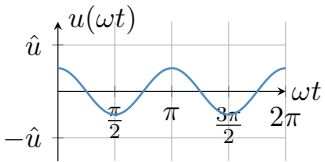

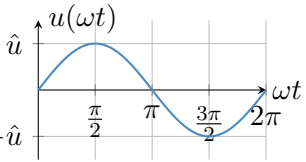

number of ↕
phases

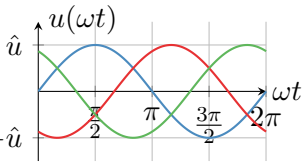

Power electronic application examples: residential

(a) Home appliances (source: pxhere, CC0 1.0)

(b) Smartphone charger (source: rawpixel, CC0 1.0)

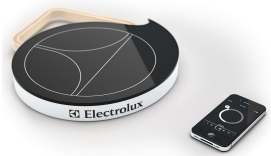

(c) Induction plate (source: flickr, Electrolux, CC BY-SA-NC 2.0)

(d) LED rectifier (source: Wikimedia Commons, D. Tribble, CC BY-SA 4.0)

Power electronic application examples: industrial

(a) Uninterruptible power supply (source: Wikimedia Commons, Stevebwallace, CC BY-SA 4.0)

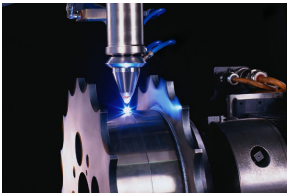

(b) Welding power supply (source: Wikimedia Commons, Trumpf GmbH, CC BY-SA 3.0)

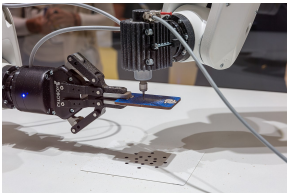

(c) Industrial drives / automation (source: Wikimedia Commons, M. Blume, CC BY-SA 4.0)

(d) Conveyor belt drive (source: Wikimedia Commons, K. Hannessen, CC BY-SA 4.0)

Power electronic application examples: energy system

(a) Wind power plants (source: pxhere, CC0 1.0)

(b) PV power plants (source: pxhere, CC0 1.0)

(c) Battery storage systems (source: flickr, Portland General Electric, CC BY-ND 2.0)

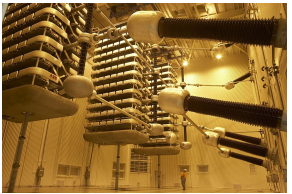

(d) High voltage DC transmission (source: Wikimedia Commons, Marshelec, CC BY-SA 3.0)

Power electronic application examples: transportation

(a) Train drive (source: Wikimedia Commons, T. Wolf, CC0 1.0)

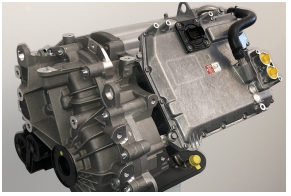

(b) Electric vehicle drive (source: Wikimedia Commons, Caprolactam123, CC BY-SA 4.0)

(c) Electric scooter (source: Wikimedia Commons, Raju, CC BY-SA 4.0)

(d) Electic ship (source: Wikimedia Commons, Wikimalte, CC BY-SA 4.0)

A broad range of nominal power ratings

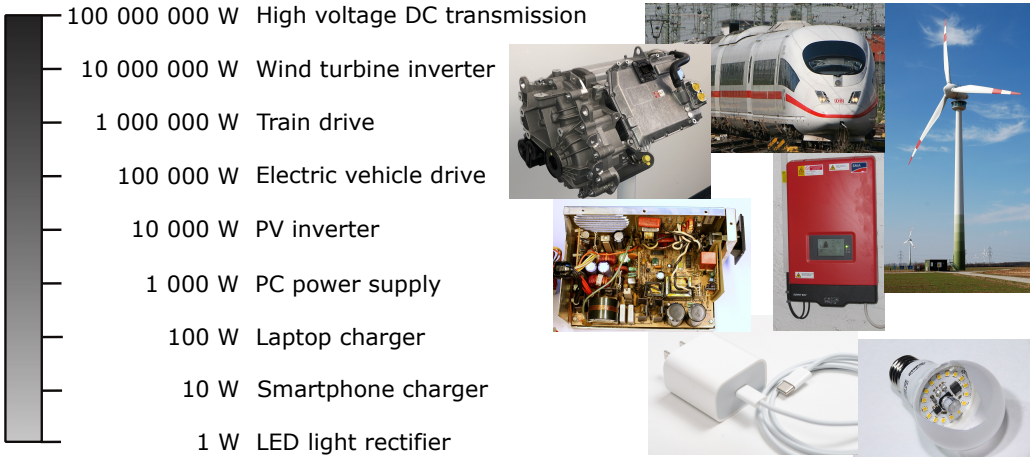

Fig. 7.7: Power range overview (figure sources: T. Wolf, KoeppiK, Caprolactam123, D. Hawgood, Mister rf, D. Tribble and rawpixel under varying CC licenses)

Typical power electronic objectives

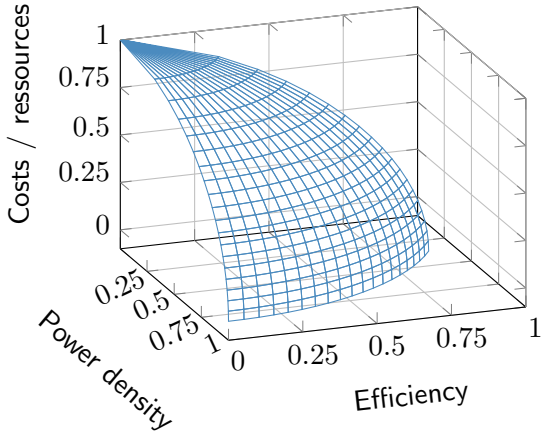

Fig. 7.8: Illustration of typical, conflicting power electronic (normalized) objectives via a Pareto front

Table of contents

Terminology: work vs. energy

Work

Work is the integral of the power over a time integral (or force over distance) and is a measure of the energy transfer.

Energy

Energy is the capacity to do work, that is, a quantity depending on the state of a system at a given point of time.

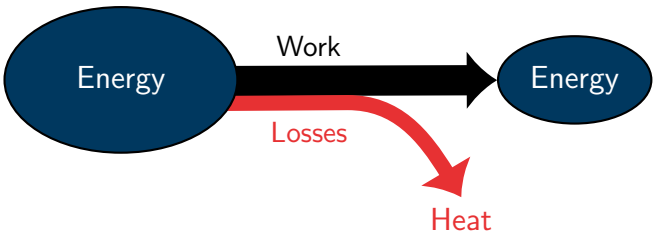

Fig. 7.9: Illustration addressing the work vs. energy terminology (simplified Sankey diagram)

Power balance of an electrical energy conversion system

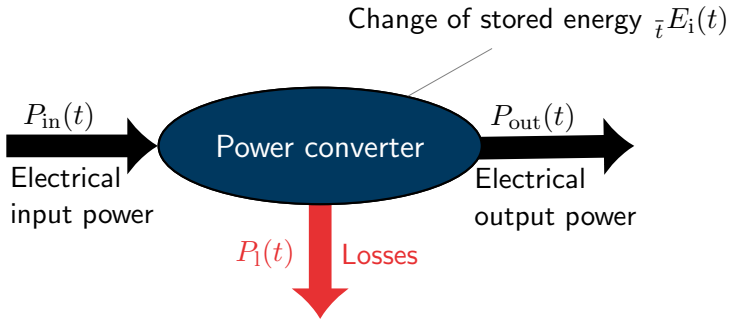

Fig. 7.10: Power balance of an energy conversion system

The power balance

$$P_{\mathrm{in}}(t) = P_{\mathrm{l}}(t) + \frac{}{t}E_{\mathrm{i}}(t) + P_{\mathrm{out}}(t) \tag{7.1}$$

must hold for any point in time as energy is conserved, that is, not created or destroyed.

Efficiency

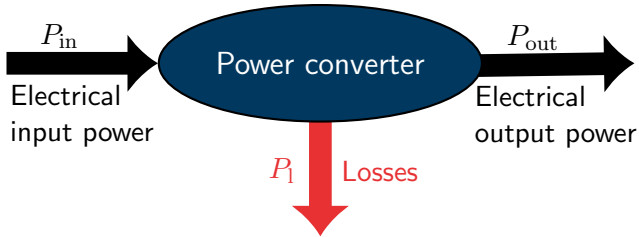

Fig. 7.11: Power balance of an energy conversion system in steady state

The power balance in steady state $\left({\mathrm{d}x(t)}/{\mathrm{d}t} = 0\right)$ is

$$P_{\text{in}} = P_{\text{out}} + P_{\text{l}} \tag{7.2}$$

and leads to the definition of the efficiency

$$\eta = \frac{P_{\text{out}}}{P_{\text{in}}} = \frac{P_{\text{out}}}{P_{\text{out}} + P_{\text{l}}}. \tag{7.3}$$

Four quadrants of operation

Depending on the current and voltage signs, the power P can be positive or negative. This leads to four quadrants of operation:

- Quadrants I & III: $P \geq 0$,
  (Power transfer from input to output)
- Quadrants II & IV: $P \leq 0$.
  (Power transfer from output to input)

How many quadrants a power converter can operate in depends on the topology and control strategy, i.e., is an important design criterion.

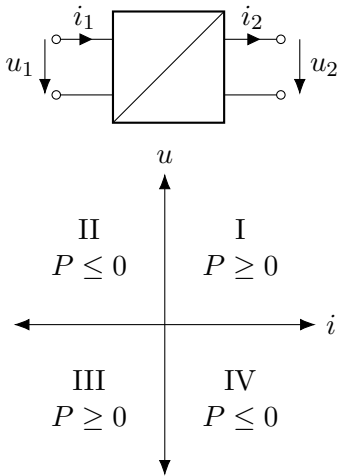

Fig. 7.12: Four quadrants of energy conversion

Why efficiency matters: a computer supply example

	Power supply A 80 PLUS Gold	Power supply B 80 PLUS Titanium
Input power	$250\,\mathrm{W}$	
Efficiency	$89\,\%$	$94\,\%$
Power loss	$27.5\,\mathrm{W}$	$15\,\mathrm{W}$
Operating hours per year	$8\,\mathrm{h} \times 220 = 1760\,\mathrm{h}$	
Cumulated loss work per year	$48.4\,\mathrm{kWh}$	$26.4\,\mathrm{kWh}$
Electricity cost for yearly losses	$14.52\,€$	$7.92\,€$
Cumulated loss work in Germany	$1.936\,\mathrm{TWh}$	$1.056\,\mathrm{TWh}$
Electricity cost for yearly losses in Germany	$580.8\,\mathrm{M€}$	$316.8\,\mathrm{M€}$

Tab. 7.1: Comparison of two computer power supplies (further assumptions: effective nominal power calculation, electricity price $0.3\,€/\mathrm{kWh}$, $40 \cdot 10^6$ computers in Germany)

Why efficiency matters: a wind power plant example

	Wind power plant A	Wind power plant B
Input power	5 MW	
Efficiency	97 %	97.1 %
Power loss	150 kW	145 kW
Nominal power operating hours per year	3000 h	
Cumulated loss work per year	450 MWh	435 MWh
Cumulated loss work (lifetime)	9.0 GWh	8.7 GWh
Lost sales proceeds due to losses per year	22.5 k€	21.75 k€
Lost sales proceeds due to losses (lifetime)	450 k€	435 k€
Cumulated loss work (lifetime, Germany)	9.0 TWh	8.7 TWh
Lost sales proceeds (lifetime, Germany)	450 M€	435 M€

Tab. 7.2: Comparison of two wind power plants (further assumptions: electricity sales price $0.05\,€/\mathrm{kWh}$, 20 years of life time, 1000 newly constructed wind power plants per year in Germany)

Table of contents

Linear power conversion

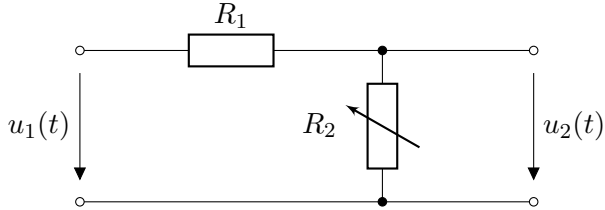

Fig. 7.13: Adjustable resistive voltage divider as step-down converter

With Kirchhoff's voltage law, the output voltage $u_2(t)$ is

$$u_2(t) = u_1(t)\frac{R_2}{R_1 + R_2}. \tag{7.4}$$

By adjusting the resistance R_2, the output voltage can be controlled. However, this method is inefficient as the power loss is independent of the output power and given by

$$P_l(t) = \frac{u_1^2(t)}{R_1 + R_2}. \tag{7.5}$$

Linear power conversion (cont.)

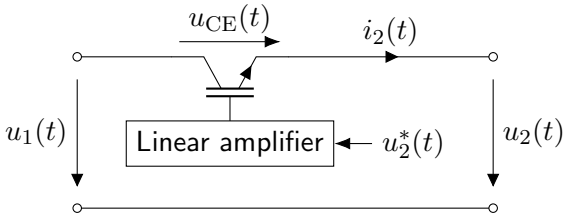

Fig. 7.14: Transistor-based step-down converter

For a transistor-based step-down converter, the output voltage is $u_2(t) = u_1(t) - u_{\mathrm{CE}}(t)$ leading to the power losses

$$P_{\mathrm{l}}(t) = u_{\mathrm{CE}}(t) i_2(t). \qquad (7.6)$$

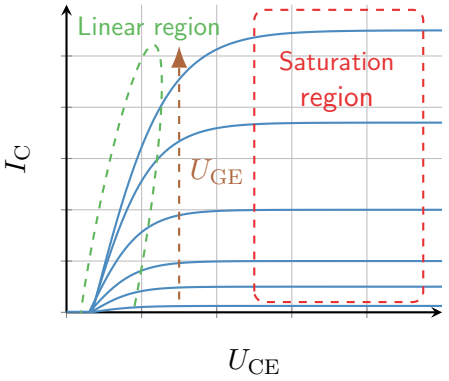

Fig. 7.15: Output characteristics of an insulated-gate bipolar transistor (IGBT)

Switching power conversion

Alternative idea: switch either fully on or off. The average output voltage $\overline{u}_2$ is controlled by the duty cycle (assuming that $u_1(t) = \overline{u}_1$ is constant)

$$D = \frac{T_{\text{on}}}{T_{\text{s}}}, \qquad \overline{u}_2 = \frac{1}{T_{\text{s}}} \int_0^{T_{\text{s}}} u_2(t)t = D\overline{u}_1. \tag{7.7}$$

As the switching losses are typically small, the overall efficiency is (much) higher compared to linear power conversion.

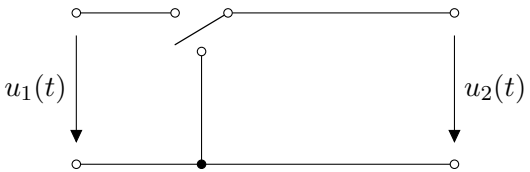

Fig. 7.16: Ideal switch-based step-down converter

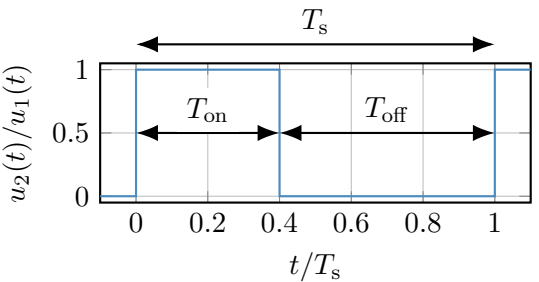

Fig. 7.17: Switching output voltage from Fig. 7.16

Switching power conversion: switching losses

Switching process is not free of power loss:

$$\overline{P}_{\mathrm{l}} = \frac{1}{T_{\mathrm{s}}} \int_0^{T_{\mathrm{s}}} u_{\mathrm{s}}(t) i_{\mathrm{s}}(t) t.$$

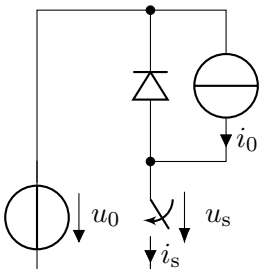

Fig. 7.18: Idealized switching loss model

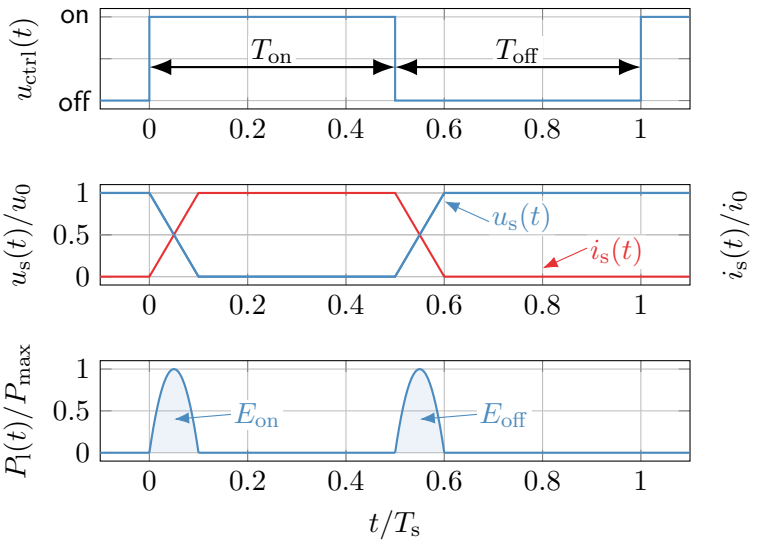

Switching power conversion: soft switching

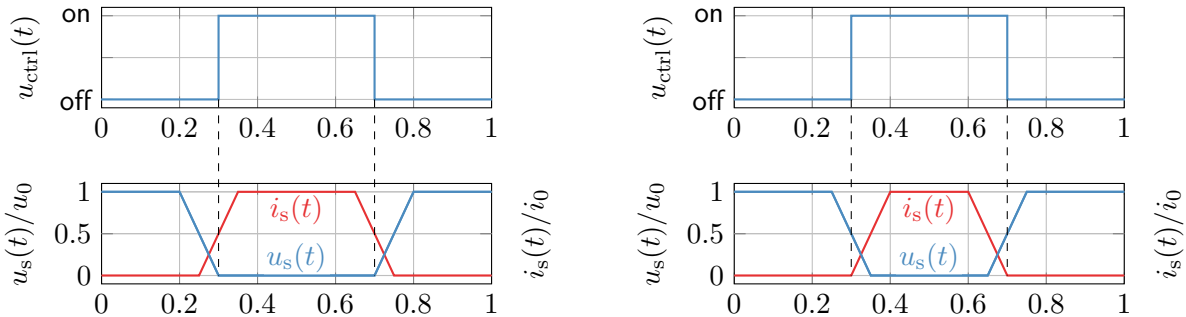

(a) Zero-voltage switching (ZVS)

(b) Zero-current switching (ZCS)

Fig. 7.19: Soft switching: reducing switching losses by turning on or off the switch when it does not transfer any power (note: above's voltage and current shapes are heavily idealized and require an appropriate circuit design besides the actual switch to enable soft switching)

Switching power conversion: passive components as filters / energy buffers

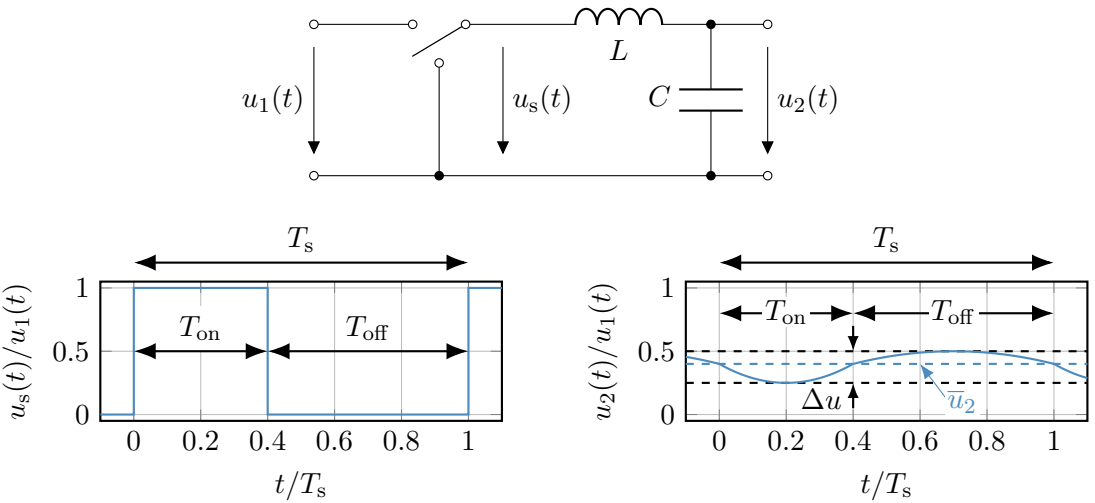

Fig. 7.20: Exemplary voltage signals for a switched power conversion system with output filter

Feasible and infeasible filter topologies

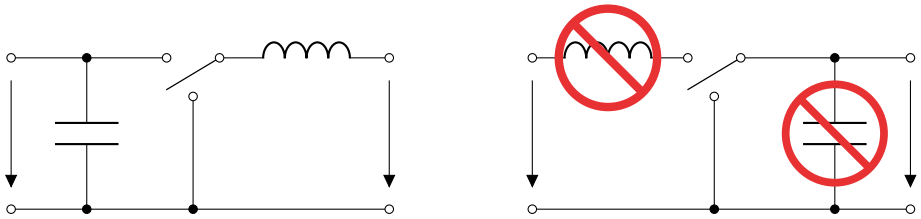

(a) Feasible filter topology

(b) Infeasible filter topology

Fig. 7.21: Basic filter topologies for switched power conversion

Short and open circuit situations

Prevent the following situations as they can lead to sparkover and damage:

- Short circuit of capacitor: current peak,
- Open circuit of inductor: voltage peak.

Important power electronic devices and idealized characteristics

Diode

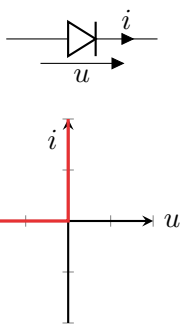

Thyristor

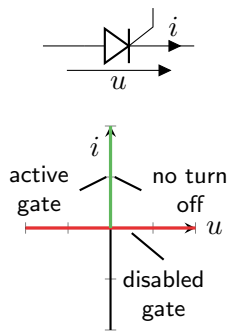

TRIAC (triode for alternating current)

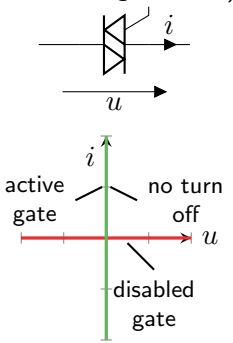

GTO (gate turn-off thyristor)

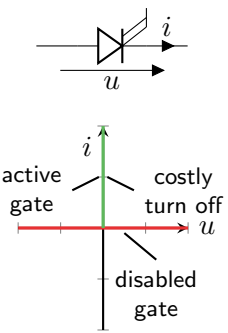

Important power electronic devices and idealized characteristics (cont.)

Bipolar junction transistor

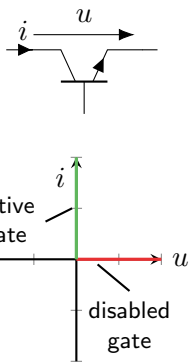

MOSFET [1] (with body diode)

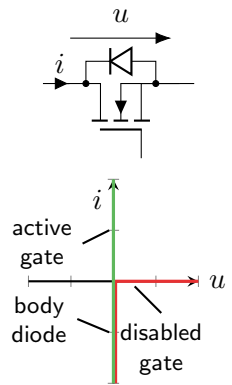

IGBT

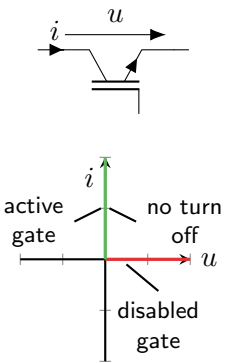

IGBT (with series diode)

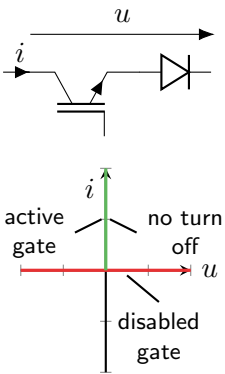

[1] metal-oxide-semiconductor field-effect transistor

Important power electronic devices and idealized characteristics (cont.)

4Q switch

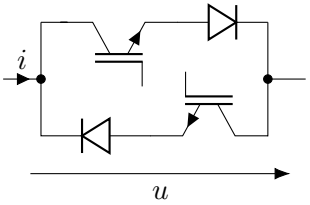

Capacitor

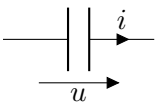

Inductor

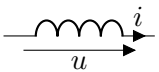

Transformer

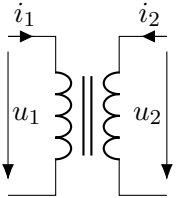

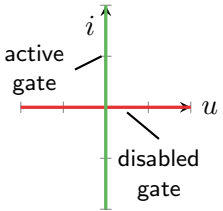

$$i(t) = C\frac{\mathrm{d}}{\mathrm{d}t}u(t) \qquad u(t) = L\frac{\mathrm{d}}{\mathrm{d}t}i(t) \qquad \boldsymbol{u}(t) = \boldsymbol{L}\frac{\mathrm{d}}{\mathrm{d}t}\boldsymbol{i}(t)$$

Important power electronic devices and idealized characteristics (cont.)

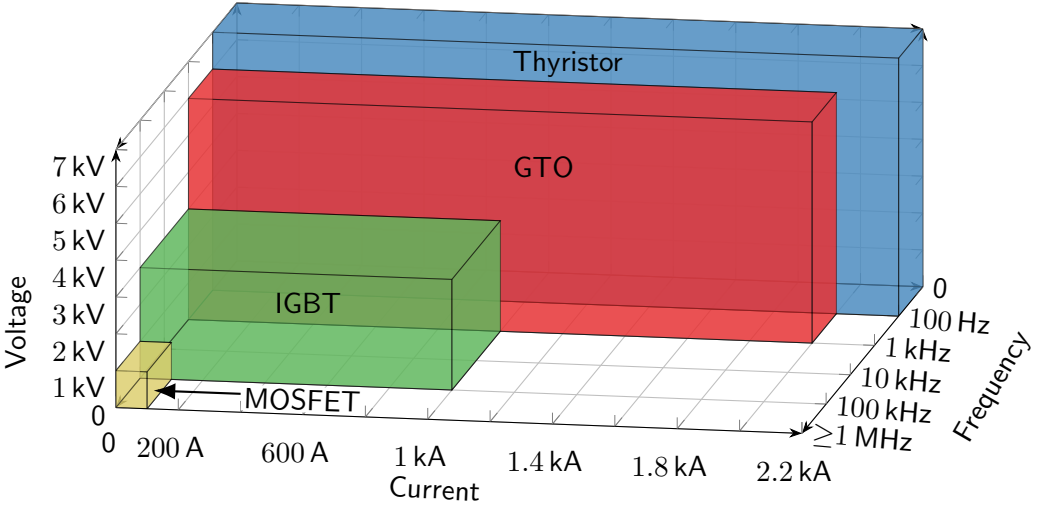

Fig. 7.22: Power electronic devices and their typical operating ranges

Internal device resistance

Besides the switching losses, power electronic devices have an internal resistance R_i that causes conduction losses. Designing such components for a low resistance is crucial, however, there is typically a conflict with weight and volume constraints.

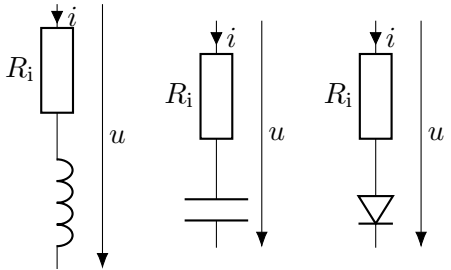

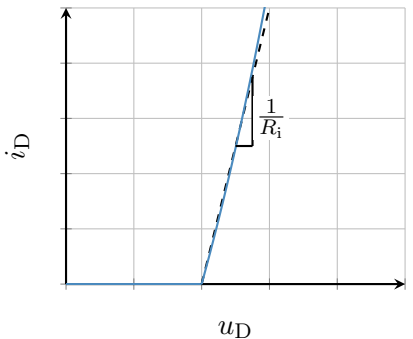

Fig. 7.23: Qualitative diode characteristic in the forward direction

Why is knowledge about power electronics important?

Power electronics are an essential pillar of the modern society

Power electronics are the key technology for the efficient conversion of electrical energy. They are used in a wide range of applications, such as renewable energy systems, electric vehicles, industrial automation, computing and communication systems as well as a wide range of consumer electronics. Hence, power electronics are an essential pillar of the modern society.

Energy efficiency and sustainability is key

Electricity as a share of primary energy is current at $20\,\%$ and is expected to further increase (source: Ember and Energy Institute). Power electronics convert a major share of the worldwide electrical energy as they are used on the generation, transmission, storage and load side. Increasing the conversion and resource efficiency of power electronics direct reduces the primary energy consumption and the environmental impact of the energy system.

Table of contents

Learning objectives

- Understand the electrical energy conversion principles of power electronics.
- Differentiate the main converter application types:
  - DC-DC converters.
  - DC-AC inverters.
  - AC-DC rectifiers.
  - AC-AC converters.
  - And their plentiful realization variants ...
- Analyze the operation of power electronics:
  - in steady state and
  - in transient conditions.
- Understand modulation techniques for switching actuators.
- Have fun learning about power electronics.

Necessary prior knowledge for this course

You should have a basic understanding of the following topics:

- Linear differential equations (modeling, solution techniques),
- Linear algebra basics (e.g., vector and matrix operations),
- Basic signal theory knowledge (e.g., signal properties like root mean square),
- Basic knowledge of electrical circuit theory,
- Basic knowledge of semiconductor physics.

What we will not cover, that is, you do not need to know (covered in separate courses):

- Control engineering (design converter controllers),
- Specific load characteristics (e.g., electric drives or batteries).

Recommended reading

- R. Erickson and D. Maksimovic, Fundamentals of Power Electronics, Vol. 3, Springer, 2020, https://doi.org/10.1007/978-3-030-43881-4
- J. Kassakian et al, Principles of Power Electronics, Vol. 2, Cambridge University Press, 2023, https://doi.org/10.1017/9781009023894
- J. Specovius, Grundkurs Leistungselektronik (in German), Vol. 10, Springer, 2020, https://doi.org/10.1007/978-3-658-21169-1
- F. Zach, Leistungselektronik (in German), Vol. 6, Springer, 2022, https://doi.org/10.1007/978-3-658-31436-1
- D. Schröder and R. Marquardt, Leistungselektronische Schaltungen (in German), Vol. 4, Springer, 2019, https://doi.org/10.1007/978-3-662-55325-1

Table of contents

Step-down converter: overview and assumptions

We consider the following assumptions:

- The switch is ideal, that is, infinitely fast.
- The input voltage is constant: $u_1(t) = U_1$.
- The output voltage is constant: $u_2(t) = U_2$.
- The input voltage is greater than the output voltage: $U_1 > U_2$.

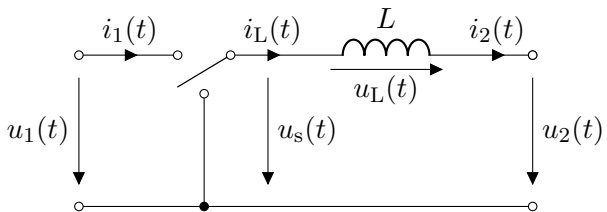

Fig. 8.1: Step-down converter (aka buck converter, ideal switch representation)

Step-down converter: switch states

The voltage at the switch is given by

$$u_{\mathrm{s}}(t) = \begin{cases} U_1, & t \in [kT_{\mathrm{s}}, kT_{\mathrm{s}} + T_{\mathrm{on}}], \\ 0, & t \in [kT_{\mathrm{s}} + T_{\mathrm{on}}, (k+1)T_{\mathrm{s}}] \end{cases} \tag{8.1}$$

with $k \in \mathbb{N}$ being the k-th switching period, T_{s} the switching period time interval, and T_{on} the switch-on time.

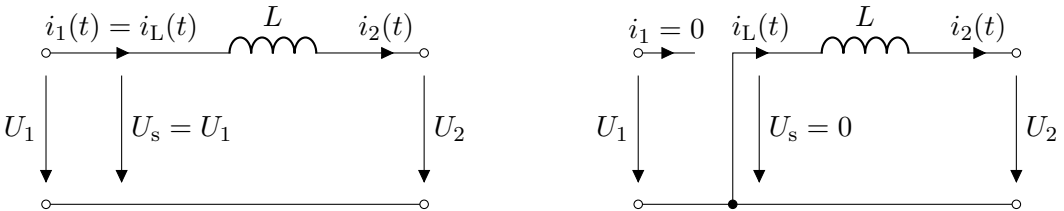

(a) Switch-on time

(b) Switch-off time

Fig. 8.2: Switch states of the step-down converter

Basic terms and definitions

T_{on}	Switch-on time	T_{off}	Switch-off time
$T_{\text{s}} = T_{\text{on}} + T_{\text{off}}$	Switching period	$f_{\text{s}} = 1/T_{\text{s}}$	Switching frequency
$D = T_{\text{on}}/T_{\text{s}}$	Duty cycle		

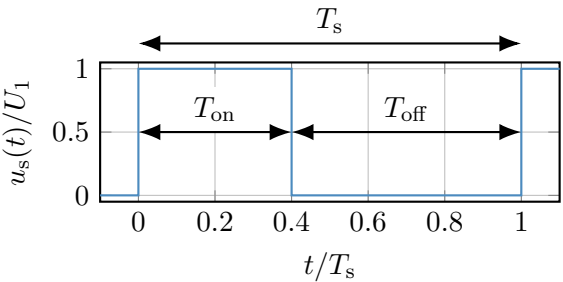

Steady-state analysis

The inductor current from Fig. 8.1 is represented by the differential equation

$$L\frac{\mathrm{d}i_{\mathrm{L}}(t)}{\mathrm{d}t} = u_{\mathrm{L}}(t) = u_{\mathrm{s}}(t) - U_2. \tag{8.2}$$

During the switch-on period we have

$$\begin{aligned} i_{\mathrm{L}}(t) &= i_{\mathrm{L}}(kT_{\mathrm{s}}) + \frac{1}{L}\int_{kT_{\mathrm{s}}}^{t} u_{\mathrm{L}}(\tau)\mathrm{d}\tau \\ &= i_{\mathrm{L}}(kT_{\mathrm{s}}) + \frac{U_1 - U_2}{L}(t - kT_{\mathrm{s}}), \quad t \in [kT_{\mathrm{s}}, kT_{\mathrm{s}} + T_{\mathrm{on}}] \end{aligned} \tag{8.3}$$

and during the switch-off period we receive

$$\begin{aligned} i_{\mathrm{L}}(t) &= i_{\mathrm{L}}(kT_{\mathrm{s}} + T_{\mathrm{on}}) + \frac{1}{L}\int_{kT_{\mathrm{s}}+T_{\mathrm{on}}}^{t} u_{\mathrm{L}}(\tau)\mathrm{d}\tau = i_{\mathrm{L}}(kT_{\mathrm{s}} + T_{\mathrm{on}}) - \frac{U_2}{L}(t - kT_{\mathrm{s}} - T_{\mathrm{on}}) \\ &= i_{\mathrm{L}}(kT_{\mathrm{s}}) + \frac{U_1 - U_2}{L}T_{\mathrm{on}} - \frac{U_2}{L}(t - kT_{\mathrm{s}} - T_{\mathrm{on}}), \quad t \in [kT_{\mathrm{s}} + T_{\mathrm{on}}, (k+1)T_{\mathrm{s}}]. \end{aligned} \tag{8.4}$$

Steady-state analysis (cont.)

In steady state the inductor current is periodic with period T_s, that is,

$$i_\mathrm{L}(t) = i_\mathrm{L}(t + T_\mathrm{s}).$$

From (8.4) we obtain for $t = kT_\mathrm{s}$

$$\begin{aligned} \overbrace{i_\mathrm{L}(kT_\mathrm{s})}^{\text{Start of period}} &= \overbrace{i_\mathrm{L}(kT_\mathrm{s}) + \frac{U_1 - U_2}{L} T_\mathrm{on} - \frac{U_2}{L}(T_\mathrm{s} - T_\mathrm{on})}^{\text{End of period}} \\ \Leftrightarrow \quad 0 &= \frac{U_1 - U_2}{L} T_\mathrm{on} - \frac{U_2}{L}(T_\mathrm{s} - T_\mathrm{on}) \\ \Leftrightarrow \quad 0 &= U_1 T_\mathrm{on} - U_2 T_\mathrm{s}. \end{aligned} \tag{8.5}$$

Rewriting delivers the output voltage as

$$U_2 = \frac{T_\mathrm{on}}{T_\mathrm{s}} U_1 = D U_1. \tag{8.6}$$

Step-down converter: steady-state time-domain behavior

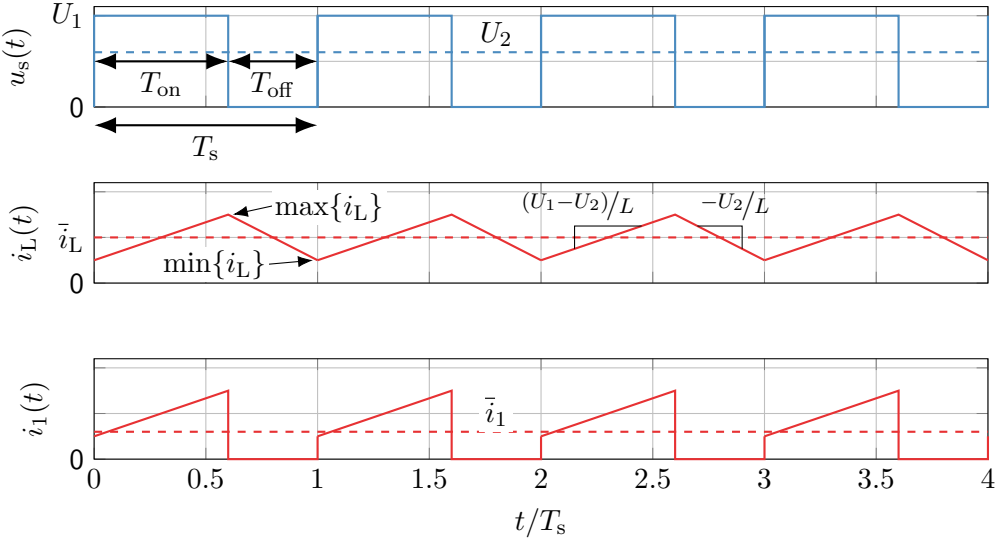

Current ripple

Due to the switching operation of the step-down converter, the inductor current exhibits an inherent ripple. The peak-to-peak current ripple is given by

$$\begin{aligned}\Delta i_{\mathrm{L}} &= \max\{i_{\mathrm{L}}(t)\} - \min\{i_{\mathrm{L}}(t)\} = i_{\mathrm{L}}(t = T_{\mathrm{on}}) - i_{\mathrm{L}}(t = T_{\mathrm{s}}) \\ &= \frac{U_1 - U_2}{L} T_{\mathrm{on}} = \frac{U_2}{L} T_{\mathrm{off}} \\ &= \frac{D(1-D)T_{\mathrm{s}}}{L} U_1.\end{aligned} \tag{8.7}$$

The current ripple has two main implications:

- The output power is not constant but varies with the current ripple.
- The root mean square (RMS) current is higher than the average current.

The latter point should be investigated in more detail as it influences the design and loss characteristics of the converter.

Current ripple (cont.)

We define

$$\Delta I_{\mathrm{L}} = \sqrt{\frac{1}{T_{\mathrm{s}}} \int_0^{T_{\mathrm{s}}} \left(i_{\mathrm{L}}(t) - \bar{i}_{\mathrm{L}} \right)^2 \mathrm{d}t} \tag{8.8}$$

as the RMS deviation of the inductor current from its average value. As the average-corrected inductor current has a triangular shape (cf. Fig. 8.3) we can calculate the RMS current as

$$\Delta I_{\mathrm{L}} = \frac{1}{\sqrt{3}} \frac{\Delta i_{\mathrm{L}}}{2} = \frac{D(1-D) T_{\mathrm{s}} U_1}{2\sqrt{3} L}. \tag{8.9}$$

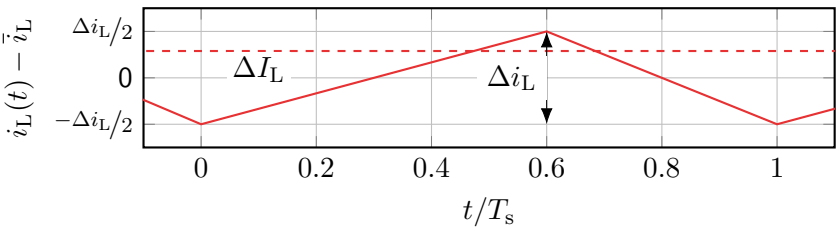

Fig. 8.3: Inductor current ripple

Current ripple (cont.)

The (total) RMS value of the inductor current (triangular signal with offset) is given by

$$I_{\mathrm{L}} = \sqrt{\bar{i}_{\mathrm{L}}^2 + \Delta I_{\mathrm{L}}^2}. \tag{8.10}$$

Considering the internal resistance R_{i} of the inductor, the ohmic power loss in the inductor is

$$P_{\mathrm{L}} = R_{\mathrm{i}} I_{\mathrm{L}}^2 = R_{\mathrm{i}} \left(\bar{i}_{\mathrm{L}}^2 + \Delta I_{\mathrm{L}}^2 \right). \tag{8.11}$$

The power loss in the inductor is thus composed of a constant part $\overline{P}_{\mathrm{L}} = R_{\mathrm{i}} \bar{i}_{\mathrm{L}}^2$, which is related to the power transfer from input to output, and a ripple part $\Delta P_{\mathrm{L}} = R_{\mathrm{i}} \Delta I_{\mathrm{L}}^2$.

Current ripple and power losses

The current ripple produces additional losses in the inductor. From (8.9) it seems tempting to increase the switching frequency f_{s} to reduce the ripple, but this will increase switching losses (compare Fig. 7.18). Hence, there is a trade-off decision between switching and conduction losses.

Current ripple and duty cycle

Rewriting the current ripple expression

$$\Delta i_{\mathrm{L}} = \frac{D(1-D)T_{\mathrm{s}}}{L} U_1 = (D - D^2)\frac{T_{\mathrm{s}} U_1}{L}$$

and calculating the derivative with respect to the duty cycle D delivers

$$\frac{\mathrm{d}\Delta i_{\mathrm{L}}}{\mathrm{d}D} = \frac{T_{\mathrm{s}} U_1}{L} - 2D\frac{T_{\mathrm{s}} U_1}{L}. \tag{8.12}$$

Setting the derivative to zero, we find the duty cycle $D_{\max}$ as

$$\frac{\mathrm{d}\Delta i_{\mathrm{L}}}{\mathrm{d}D} = 0 \quad \Leftrightarrow \quad D_{\max} = \frac{1}{2} \tag{8.13}$$

which is associated with the maximum current ripple since the second derivative

$$\frac{\mathrm{d}^2\Delta i_{\mathrm{L}}}{\mathrm{d}D^2} = -\frac{2T_{\mathrm{s}} U_{\mathrm{on}}}{L} \tag{8.14}$$

is negative.

Current ripple and duty cycle (cont.)

From (8.13) we can conclude that the maximum current ripple is given by

$$\Delta i_{\mathrm{L,max}} = \frac{1}{4}\frac{T_{\mathrm{s}} U_1}{L} \quad \Rightarrow \quad \Delta i_{\mathrm{L}} = 4D(1-D)\Delta i_{\mathrm{L,max}}. \tag{8.15}$$

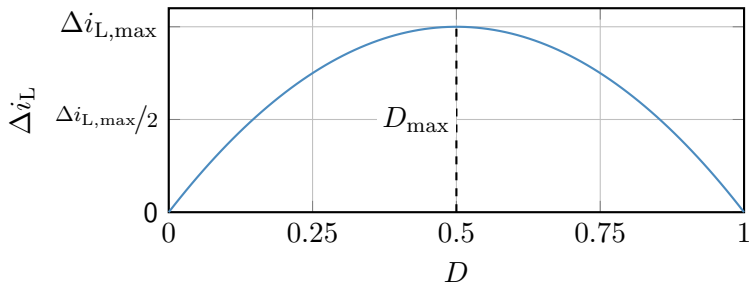

Fig. 8.4: Inductor current ripple as a function of the duty cycle

Table of contents

Step-down converter with output capacitor: overview and assumption

We consider the following assumptions:

- The switch is ideal, that is, infinitely fast.
- The input voltage is constant: $u_1(t) = U_1$.
- The output current is constant: $i_2(t) = I_2$.
- The input voltage is greater than the output voltage: $U_1 > u_2(t)$.

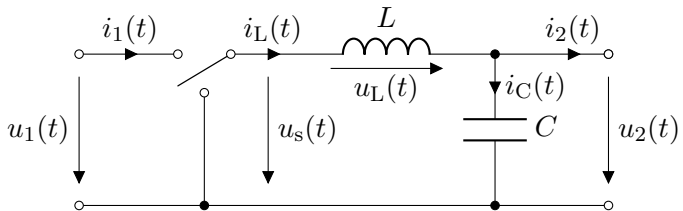

Fig. 8.5: Step-down converter (ideal switch representation) with output capacitor

Steady-state analysis

From (8.3) we know that the inductor current during the switch-on period is given by

$$i_{\mathrm{L}}(t) = i_{\mathrm{L}}(kT_{\mathrm{s}}) + \frac{U_1 - u_{\mathrm{C}}(t)}{L}(t - kT_{\mathrm{s}}), \quad t \in [kT_{\mathrm{s}}, kT_{\mathrm{s}} + T_{\mathrm{on}}].$$

Note that the inductor current is now dependent on $u_{\mathrm{C}}(t)$:

- Formally, we need to consider the impact of the varying output capacitor voltage.
- This would lead to a second-order differential equation which is more complex to solve.
- We will simplify the analysis by assuming that the impact of the output capacitor voltage variation on the inductor current is negligible: $u_{\mathrm{C}}(t) \approx U_2 = \overline{u}_{\mathrm{c}}$.

Simplification comment

The above assumption is valid for sufficiently large output capacitors with only small voltage ripples. Otherwise, the output voltage ripple and the inductor current ripple will be significantly coupled and require a more thoughtful analysis.

Steady-state analysis (cont.)

The capacitor's voltage differential equation is given by

$$C\frac{\mathrm{d}u_{\mathrm{C}}(t)}{\mathrm{d}t} = i_{\mathrm{C}}(t) = i_{\mathrm{L}}(t) - I_2. \tag{8.16}$$

While I_2 is considered a known constant, we first need to determine the inductor current $i_{\mathrm{L}}(t)$. Combining (8.3) and (8.7) we obtain

$$i_{\mathrm{L}}(kT_{\mathrm{s}}) = I_2 - \frac{\Delta i_{\mathrm{L}}}{2} = I_2 - \frac{U_1 - U_2}{L}\frac{T_{\mathrm{on}}}{2} \tag{8.17}$$

and

$$i_{\mathrm{L}}(kT_{\mathrm{s}} + T_{\mathrm{on}}) = I_2 + \frac{\Delta i_{\mathrm{L}}}{2} = I_2 + \frac{U_1 - U_2}{L}\frac{T_{\mathrm{on}}}{2} \tag{8.18}$$

as the initial conditions for the inductor current in steady state.

Steady-state analysis (cont.)

The capacitor's current during the switch-on period is given by

$$\begin{aligned} i_{\mathrm{C}}(t) &= i_{\mathrm{L}}(t) - I_2 = \frac{U_1 - U_2}{L}\left(t - \frac{T_{\mathrm{on}}}{2} - kT_{\mathrm{s}}\right) \\ &= -\frac{\Delta i_{\mathrm{L}}}{2} + \frac{U_1 - U_2}{L}(t - kT_{\mathrm{s}}), \quad t \in [kT_{\mathrm{s}}, kT_{\mathrm{s}} + T_{\mathrm{on}}] \end{aligned} \tag{8.19}$$

and during the switch-off period we receive

$$\begin{aligned} i_{\mathrm{C}}(t) &= i_{\mathrm{L}}(t) - I_2 = \frac{U_1 - U_2}{L}\frac{T_{\mathrm{on}}}{2} - \frac{U_2}{L}(t - kT_{\mathrm{s}} - T_{\mathrm{on}}) \\ &= \frac{\Delta i_{\mathrm{L}}}{2} - \frac{U_2}{L}(t - kT_{\mathrm{s}} - T_{\mathrm{on}}), \quad t \in [kT_{\mathrm{s}} + T_{\mathrm{on}}, (k+1)T_{\mathrm{s}}]. \end{aligned} \tag{8.20}$$

Steady-state analysis (cont.)

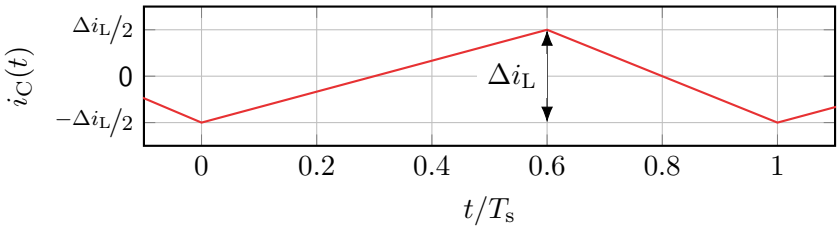

Current ripples through the capacitor and inductor

Based on the made assumptions, the capacitor's current is raising and falling linearly during the switch-on and switch-off periods, that is, it corresponds to the previously considered inductor current ripple.

Output voltage ripple: via charge balance

If one is not interested in the specific signal shape $u_{\mathrm{C}}(t)$, the output voltage ripple can be derived from the charge balance over half a period (cf. Fig. 8.6):

$$\Delta Q = \frac{1}{2}\frac{\Delta i_{\mathrm{L}}}{2}\frac{T_{\mathrm{s}}}{2}. \qquad (8.21)$$

From

$$\frac{1}{C}\int i_{\mathrm{C}}(t)\mathrm{d}t = u_{\mathrm{C}}(t) + u_{\mathrm{C}}(0)$$

we receive

$$\Delta u_{\mathrm{C}} = \frac{\Delta Q}{C} = \frac{\Delta i_{\mathrm{L}} T_{\mathrm{s}}}{8C}. \qquad (8.22)$$

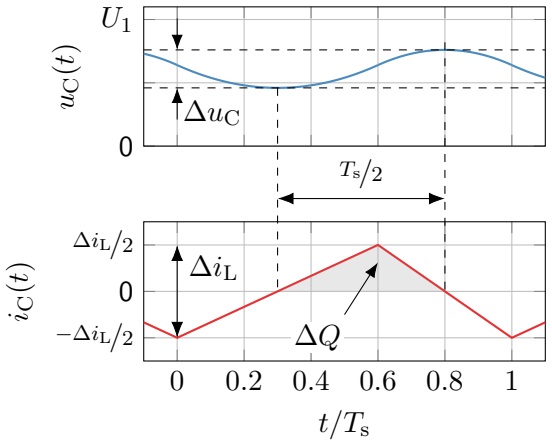

Fig. 8.6: Voltage ripple derivation via charge balance

Average and initial capacitor voltage

The initial voltage $u_\mathrm{C}(kT_\mathrm{s})$ at the beginning of a period is still unknown. We can derive it from the capacitor's average voltage over one period. For simplicity, we consider $k = 0$:

$$\overline{u}_\mathrm{c} = \frac{1}{T_\mathrm{s}} \int_0^{T_\mathrm{s}} u_\mathrm{C}(t)\mathrm{d}t = \frac{1}{T_\mathrm{s}} \left(\int_0^{T_\mathrm{on}} u_\mathrm{C}(t)\mathrm{d}t + \int_{T_\mathrm{on}}^{T_\mathrm{s}} u_\mathrm{C}(t)\mathrm{d}t \right) \stackrel{!}{=} DU_1. \tag{8.23}$$

Inserting (**??**) we receive for the first part

$$\begin{aligned} \int_0^{T_\mathrm{on}} u_\mathrm{C}(t)\mathrm{d}t &= \left[u_\mathrm{C}(0)t + \frac{\Delta i_\mathrm{L}}{2C}\frac{t^2}{2} + \frac{U_1 - U_2}{LC}\frac{t^3}{6} \right]_0^{T_\mathrm{on}} = \dots \\ &= u_\mathrm{C}(0)T_\mathrm{on} - \frac{\Delta i_\mathrm{L}}{C}\frac{T_\mathrm{on}^2}{12}. \end{aligned} \tag{8.24}$$

Average and initial capacitor voltage (cont.)

Inserting (**??**) into the second part of (8.23) delivers

$$\int_{T_{\mathrm{on}}}^{T_{\mathrm{s}}} u_{\mathrm{C}}(t)\mathrm{d}t = \left[u_{\mathrm{C}}(0)t + \frac{\Delta i_{\mathrm{L}}}{2C}(\frac{t^2}{2} - T_{\mathrm{on}}t) - \frac{U_2}{LC}(\frac{t^3}{6} - T_{\mathrm{on}}\frac{t^2}{2} + \frac{T_{\mathrm{on}}^2}{2}t)\right]_{T_{\mathrm{on}}}^{T_{\mathrm{s}}} = \ldots$$
$$= u_{\mathrm{C}}(0)T_{\mathrm{off}} + \frac{\Delta i_{\mathrm{L}}}{C}\frac{T_{\mathrm{off}}^2}{12}. \tag{8.25}$$

Combining both parts results in

$$\overline{u}_{\mathrm{c}} = \frac{1}{T_{\mathrm{s}}}\left(u_{\mathrm{C}}(0)T_{\mathrm{s}} + \frac{\Delta i_{\mathrm{L}}}{C}\frac{T_{\mathrm{off}}^2 - T_{\mathrm{on}}^2}{12}\right)$$
$$= u_{\mathrm{C}}(0) + \frac{\Delta i_{\mathrm{L}}}{12C}T_{\mathrm{s}}(1-2D) \stackrel{!}{=} DU_1. \tag{8.26}$$

Solving for $u_{\mathrm{C}}(0)$ we receive the initial capacitor voltage as

$$u_{\mathrm{C}}(0) = DU_1 - \frac{\Delta i_{\mathrm{L}}}{12C}T_{\mathrm{s}}(1-2D). \tag{8.27}$$

Table of contents

Circuit realization

- The ideal (mechanical) switch cannot be operated with high frequency in practice.
- It must be replaced with semiconductor devices to allow for a practical realization.
- In Fig. 8.7 the simplest realization is shown utilizing one transistor and one diode.
- However, this configuration can only provide positive voltages and currents.
- Hence, the converter can operate in the first quadrant only.

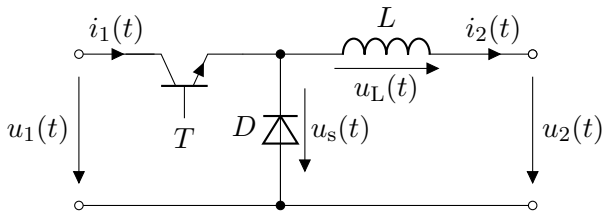

Fig. 8.7: Step-down converter with real components (single quadrant type)

Discontinous conduction mode (DCM)

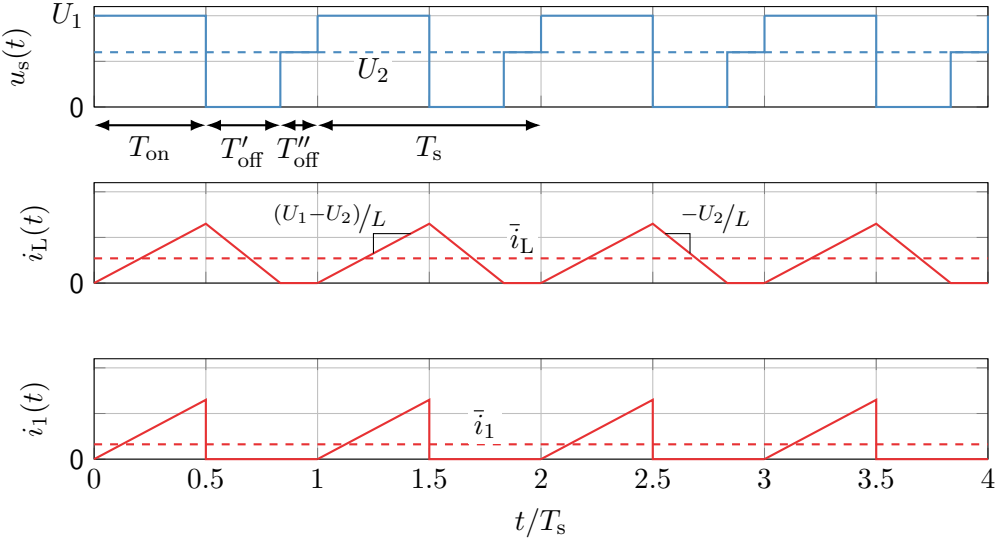

Switch states DCM

In contrast to the previous continuous conduction mode (CCM), the converter traverses three states in the discontinuous conduction mode (DCM):

- Transistor on-time: $T_{\mathrm{on}} = DT_{\mathrm{s}}$,
- Transistor off-time (conducting diode): $T'_{\mathrm{off}} = D'T_{\mathrm{s}}$,
- Transistor off-time (no conduction): $T''_{\mathrm{off}} = T_{\mathrm{s}} - T_{\mathrm{on}} - T'_{\mathrm{off}}$.

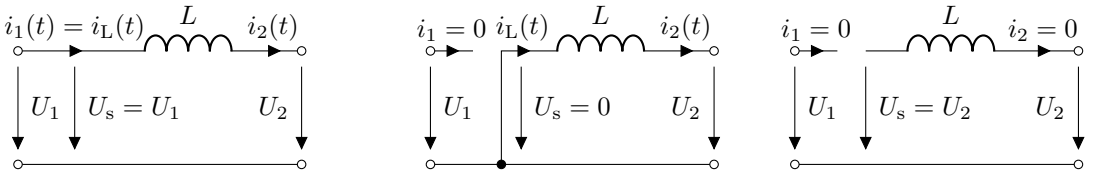

(a) Switch-on time T_{on} (b) Switch-off time T'_{off} (c) Switch-off time T''_{off}

Fig. 8.8: Switch states of the step-down converter including DCM

DCM operation characteristics

The operation in CCM and DCM can be distinguished by the inductor current ripple

$$\bar{i}_{\mathrm{L}} = \bar{i}_2 \begin{cases} \geq \frac{\Delta i_{\mathrm{L}}}{2} = 2D(1-D)\Delta i_{\mathrm{L,max}}: & \text{CCM}, \\ < \frac{\Delta i_{\mathrm{L}}}{2} = 2D(1-D)\Delta i_{\mathrm{L,max}}: & \text{DCM} \end{cases} \tag{8.28}$$

with

$$\Delta i_{\mathrm{L,max}} = \frac{U_1 T_{\mathrm{s}}}{4L}.$$

Hence, the operation mode directly depends on the duty cycle D and average load current $\bar{i}_2$, that is, it can change during runtime. While we have already discussed the operation in CCM, we will now focus on the operation in DCM. Here, it must be noted that

$$U_2 \neq U_1 D \quad \text{(DCM operation)}$$

applies due to the non-conducting diode during T''_{off}.

DCM operation characteristics (cont.)

To find the input-to-output voltage ratio in DCM, we can utilize the current ripple balance:

$$\begin{aligned} \Delta i_{\mathrm{L}} &= \frac{U_1 - U_2}{L} T_{\mathrm{on}} = i_{\mathrm{L}} = \frac{U_1 - U_2}{L} D T_{\mathrm{s}} \quad \text{(rising edge)}, \\ \Delta i_{\mathrm{L}} &= \frac{U_2}{L} T'_{\mathrm{off}} = \frac{U_2}{L} D' T_{\mathrm{s}} \qquad\qquad\quad \text{(falling edge)}. \end{aligned} \tag{8.29}$$

Solving for D' results in

$$D' = \frac{L \Delta i_{\mathrm{L}}}{U_2 T_{\mathrm{s}}} = \frac{U_1 - U_2}{U_2} D = \left(\frac{U_1}{U_2} - 1 \right) D. \tag{8.30}$$

The average load current is

$$\bar{i}_2 = \bar{i}_{\mathrm{L}} = \frac{1}{2} \Delta i_{\mathrm{L}} \frac{T_{\mathrm{on}} + T'_{\mathrm{off}}}{T_{\mathrm{s}}} = \frac{1}{2} \Delta i_{\mathrm{L}} (D + D') \tag{8.31}$$

which is derived from the area under the triangular-shaped current during T_{on} and T'_{off}.

DCM operation characteristics (cont.)

Inserting (8.30) into (8.31) yields

$$\begin{aligned}\bar{i}_2 &= \frac{1}{2}\Delta i_\mathrm{L} D \frac{U_1}{U_2} = \frac{U_1 - U_2}{2L} D T_\mathrm{s} D \frac{U_1}{U_2} \\ &= 2D^2 \left(\frac{U_1}{U_2} - 1 \right) \Delta i_{\mathrm{L,max}}.\end{aligned} \tag{8.32}$$

Solving for the DCM input-to-output voltage ratio results in

$$\frac{U_2}{U_1} = \frac{1}{1 + \frac{\bar{i}_2}{2\Delta i_{\mathrm{L,max}} D^2}}. \tag{8.33}$$

Since $\Delta i_{\mathrm{L,max}}$ also depends on U_1, cf. (8.15), the relation (8.33) only holds for a given U_1. Alternatively, we can utilize (8.32) and solve for U_2 to receive

$$U_2 = \frac{D^2 T_\mathrm{s} U_1^2}{D^2 T_\mathrm{s} U_1 + 2L\bar{i}_2}. \tag{8.34}$$

Step-down converter load curves

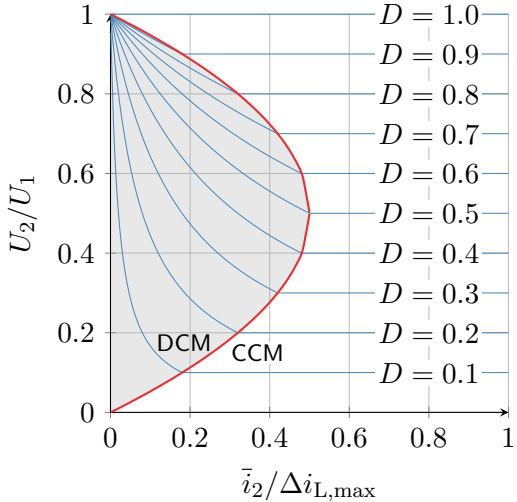

Fig. 8.9: Step-down converter load curves for CCM and DCM

Boundary conduction mode (BCM)

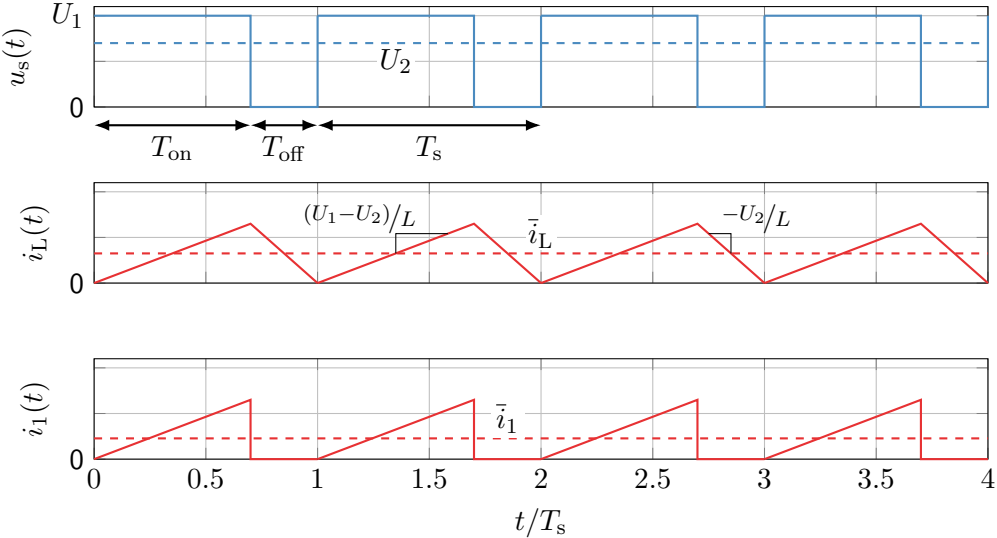

BCM operation characteristics

In the boundary conduction mode (BCM), the average inductor current load is exactly half of the current ripple, that is,

$$\bar{i}_{\mathrm{L}} = \bar{i}_2 = \frac{\Delta i_{\mathrm{L}}}{2} = 2D(1-D)\Delta i_{\mathrm{L,max}}. \tag{8.35}$$

- Diode current becomes zero and then the transistor turns on again.
  - The diode is not hard turned-off but its current naturally decays to zero.
  - Also known as zero current switching (ZCS) or generally soft switching.
- Requires adaptive switching frequency control if load changes. From (8.7) and (8.35) the BCM switching frequency results in

$$f_{\mathrm{s}} = \frac{1}{T_{\mathrm{s}}} = \frac{D(1-2)U_1}{L\Delta i_{\mathrm{L}}} = \frac{D(1-2)U_1}{2L\bar{i}_2}. \tag{8.36}$$

Motivation for BCM: diode reverse recovery

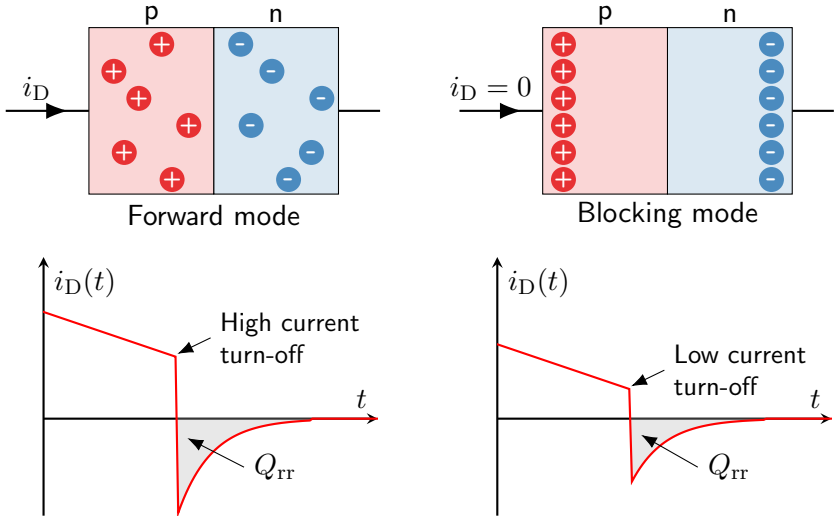

Fig. 8.10: Qualitative and simplified representation of the reverse recovery effect

BCM operation characteristics: comments

Advantages of BCM:

- Reduces the reverse recovery effect, that is, ZCS of the diode during turn on.
- Also allows ZCS transistor turn on.

Limitations of BCM:

- Transistor turn off and diode turn on cannot be soft switched due to topology constraints.
- Ripple current increases with load current: $\Delta i_{\mathrm{L}} = 2\bar{i}_2$.
  - May negatively affects load.
  - Increases conduction losses due to higher RMS current – compare (8.11).
  - High switching frequency required at low loads (switching losses).

Table of contents

Step-up converter: overview and assumptions

We consider the following assumptions:

- The switch is ideal, that is, infinitely fast.
- The input voltage is constant: $u_1(t) = U_1$.
- The output voltage is constant: $u_2(t) = U_2$.
- The input voltage is lower than the output voltage: $U_1 < U_2$.

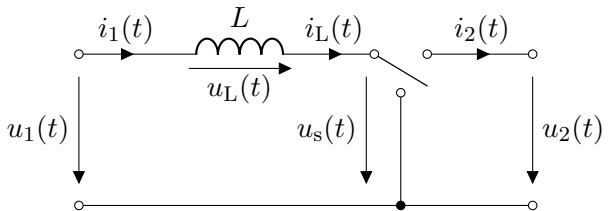

Fig. 8.11: Step-up converter (aka boost converter, ideal switch representation)

Step-up converter: switch states

The voltage at the switch is given by

$$u_{\mathrm{s}}(t) = \begin{cases} 0, & t \in [kT_{\mathrm{s}}, kT_{\mathrm{s}} + T_{\mathrm{on}}], \\ U_2, & t \in [kT_{\mathrm{s}} + T_{\mathrm{on}}, (k+1)T_{\mathrm{s}}]. \end{cases} \tag{8.37}$$

Note: switch on/off definition is reversed compared to the step-down converter.

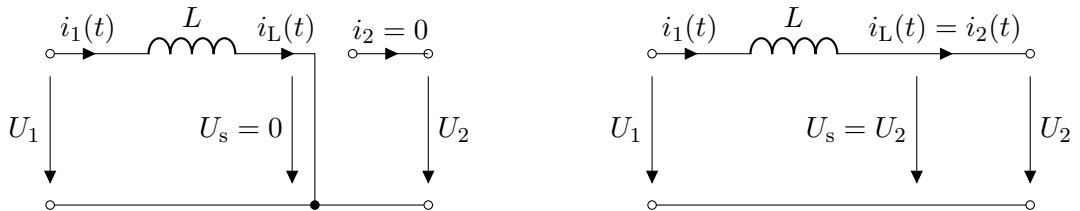

(a) Switch-on time (b) Switch-off time

Fig. 8.12: Switch states of the step-up converter

Step-up converter: steady-state time-domain behavior

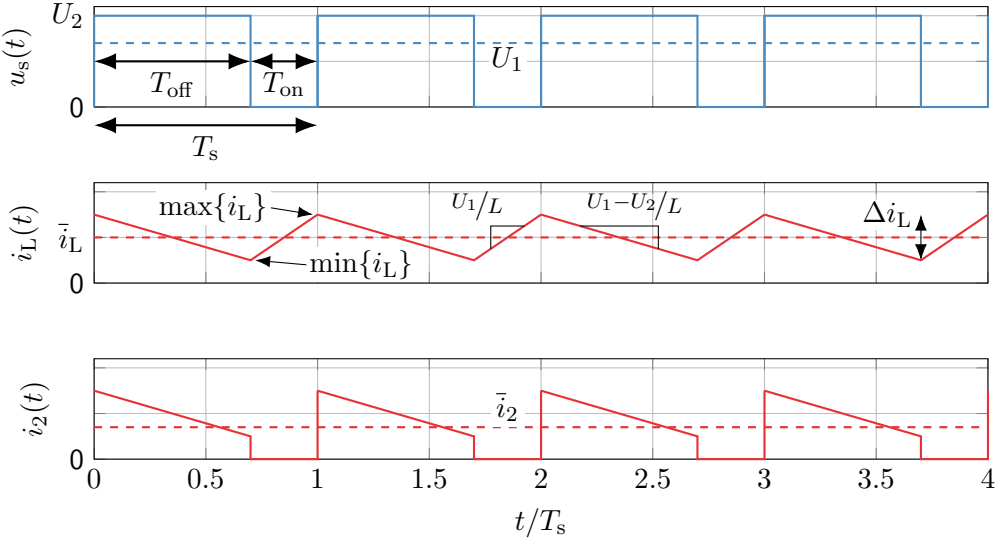

Step-up converter: voltage and current transfer ratios during steady state

In steady state, the absolute voltage-time integral over the inductor must be identical for the switch-on and switch-off interval, that is,

$$\int_0^{T_{\text{off}}} |u_{\text{L}}(t)|\,\mathrm{d}t \stackrel{!}{=} \int_{T_{\text{off}}}^{T_{\text{off}}+T_{\text{on}}} |u_{\text{L}}(t)|\,\mathrm{d}t \tag{8.38}$$

resulting in

$$(U_2 - U_1)T_{\text{off}} = U_1 T_{\text{on}} \quad \Leftrightarrow \quad (U_2 - U_1)(1-D)T_{\text{s}} = U_1 D T_{\text{s}} \tag{8.39}$$

and finally delivering the voltage transfer ratio

$$\frac{U_2}{U_1} = \frac{1}{1-D}. \tag{8.40}$$

Assuming a lossless converter ($P_{\text{in}} = P_{\text{out}}$), the current transfer ratio is

$$\frac{\bar{i}_1}{\bar{i}_2} = \frac{1}{1-D}. \tag{8.41}$$

Step-up converter: current ripple

The inductor current ripple can be found considering the positive slope during T_{on} with

$$\Delta i_{\mathrm{L}} = \frac{U_1}{L} T_{\mathrm{on}} = \frac{U_1}{L} D T_{\mathrm{s}} \tag{8.42}$$

or alternatively evaluating the negative slope during T_{off} with

$$\Delta i_{\mathrm{L}} = \frac{U_2 - U_1}{L} T_{\mathrm{off}} = \frac{U_2 - U_1}{L} (1 - D) T_{\mathrm{s}} = \frac{D(1 - D) T_{\mathrm{s}}}{L} U_2. \tag{8.43}$$

In addition, one can find that the output current and power is changing step-like within the step-up converter, while this is the case for the input side in the step-down converter:

$$\text{step-down:} \quad i_1(t) = \begin{cases} i_{\mathrm{L}}(t), & \text{switch on,} \\ 0, & \text{switch off,} \end{cases} \qquad \text{step-up:} \quad i_1(t) = \begin{cases} i_{\mathrm{L}}(t), & \text{switch on,} \\ i_{\mathrm{L}}(t), & \text{switch off,} \end{cases}$$

$$\text{step-down:} \quad i_2(t) = \begin{cases} i_{\mathrm{L}}(t), & \text{switch on,} \\ i_{\mathrm{L}}(t), & \text{switch off,} \end{cases} \qquad \text{step-up:} \quad i_2(t) = \begin{cases} 0, & \text{switch on,} \\ i_{\mathrm{L}}(t), & \text{switch off.} \end{cases}$$

Step-up converter: current ripple (cont.)

In contrast to the step-down converter, cf. (8.13), the worst-case current ripple of the step-up converter occurs for

$$\Delta i_{\mathrm{L}} = \frac{U_1}{L} D T_{\mathrm{s}} \quad \Rightarrow \quad D_{\max} \to 1. \tag{8.44}$$

This corresponds to the case of an infinitely large output voltage U_2:

$$\lim_{D \to 1} U_2 = \lim_{D \to 1} \frac{1}{1 - D} U_1 = \infty. \tag{8.45}$$

The maximum current ripple is then

$$\Delta i_{\mathrm{L,max}} = \frac{1}{L} U_1 T_{\mathrm{s}}. \tag{8.46}$$

Consequently, we can express the current ripple as:

$$\Delta i_{\mathrm{L}} = D \Delta i_{\mathrm{L,max}}. \tag{8.47}$$

Step-up converter with output capacitor: overview and assumptions

We consider the following assumptions:

- The switch is ideal, that is, infinitely fast.
- The input voltage is constant: $u_1(t) = U_1$.
- The output current is constant: $i_2(t) = I_2$.
- The inductor current $i_\mathrm{L}(t)$ is unaffected by the output voltage ripple (remains triangular).
- The output voltage is greater than the output voltage: $u_2(t) > U_1$.

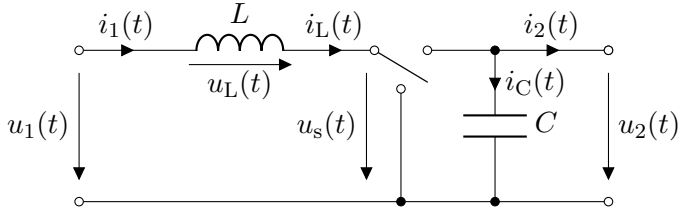

Fig. 8.13: Step-up converter (ideal switch representation) with output capacitor

Step-up converter: capacitor voltage analysis

In contrast to the step-down converter, the capacitor current is changing step-like during the switching event:

$$i_{\mathrm{C}}(t) = \begin{cases} i_{\mathrm{L}}(t) - I_2, & t \in [kT_{\mathrm{s}}, kT_{\mathrm{s}} + T_{\mathrm{off}}], \\ -I_2, & t \in [kT_{\mathrm{s}} + T_{\mathrm{off}}, (k+1)T_{\mathrm{s}}]. \end{cases} \tag{8.48}$$

The steady-state inductor current during the switch-off interval is

$$\begin{aligned} i_{\mathrm{L}}(t) &= \bar{i}_{\mathrm{L}} + \frac{\Delta i_{\mathrm{L}}}{2} - \frac{\Delta i_{\mathrm{L}}}{T_{\mathrm{off}}}(t - kT_{\mathrm{s}}) \\ &= \frac{1}{1-D} I_2 + \Delta i_{\mathrm{L}} \frac{T_{\mathrm{off}} - 2(t - kT_{\mathrm{s}})}{2T_{\mathrm{off}}}, \quad t \in [kT_{\mathrm{s}}, kT_{\mathrm{s}} + T_{\mathrm{off}}]. \end{aligned} \tag{8.49}$$

which follows from the triangular signal shape. Inserting into (8.48) yields

$$i_{\mathrm{C}}(t) = \begin{cases} \frac{D}{1-D} I_2 + \Delta i_{\mathrm{L}} \frac{T_{\mathrm{off}} - 2(t - kT_{\mathrm{s}})}{2T_{\mathrm{off}}}, & t \in [kT_{\mathrm{s}}, kT_{\mathrm{s}} + T_{\mathrm{off}}], \\ -I_2, & t \in [kT_{\mathrm{s}} + T_{\mathrm{off}}, (k+1)T_{\mathrm{s}}]. \end{cases} \tag{8.50}$$

Step-up converter: capacitor voltage analysis (cont.)

The capacitor voltage during the switch-off period is then

$$\begin{aligned} u_{\mathrm{C}}(t) &= u_{\mathrm{C}}(kT_{\mathrm{s}}) + \frac{1}{C}\int_{kT_{\mathrm{s}}}^{t} i_{\mathrm{C}}(\tau)\mathrm{d}\tau, \quad t \in [kT_{\mathrm{s}}, kT_{\mathrm{s}} + T_{\mathrm{off}}] \\ &= u_{\mathrm{C}}(kT_{\mathrm{s}}) + \frac{1}{C}\left(\int_{kT_{\mathrm{s}}}^{t} \frac{D}{1-D} I_2 + \Delta i_{\mathrm{L}} \frac{T_{\mathrm{off}} - 2(\tau - kT_{\mathrm{s}})}{2T_{\mathrm{off}}}\mathrm{d}\tau\right) \\ &= u_{\mathrm{C}}(kT_{\mathrm{s}}) + \left[\frac{D\tau}{(1-D)C} I_2 + \frac{\Delta i_{\mathrm{L}}}{2T_{\mathrm{off}}C}\left(T_{\mathrm{off}}\tau - \tau^2 + 2\tau kT_{\mathrm{s}}\right)\right]_{kT_{\mathrm{s}}}^{t} \\ &= u_{\mathrm{C}}(kT_{\mathrm{s}}) + \frac{D(t - kT_{\mathrm{s}})}{(1-D)C} I_2 + \frac{\Delta i_{\mathrm{L}}}{2T_{\mathrm{off}}C}\left(T_{\mathrm{off}}(t - kT_{\mathrm{s}}) - t(t - 2kT_{\mathrm{s}}) - (kT_{\mathrm{s}})^2\right). \end{aligned} \tag{8.51}$$

The capacitor voltage at the end of the switch-off period is

$$u_{\mathrm{C}}(kT_{\mathrm{s}} + T_{\mathrm{off}}) = u_{\mathrm{C}}(kT_{\mathrm{s}}) + \frac{DI_2}{(1-D)C} T_{\mathrm{off}}. \tag{8.52}$$

Step-up converter: capacitor voltage analysis (cont.)

The capacitor voltage during the switch-on period is then

$$
\begin{aligned}
u_{\mathrm{C}}(t) &= u_{\mathrm{C}}(kT_{\mathrm{s}}+T_{\mathrm{off}}) + \frac{1}{C}\int_{kT_{\mathrm{s}}+T_{\mathrm{off}}}^{t} i_{\mathrm{C}}(\tau)\mathrm{d}\tau, \quad t \in [kT_{\mathrm{s}}+T_{\mathrm{off}}, (k+1)T_{\mathrm{s}}] \\
&= u_{\mathrm{C}}(kT_{\mathrm{s}}+T_{\mathrm{off}}) + \frac{1}{C}\int_{kT_{\mathrm{s}}+T_{\mathrm{off}}}^{t} -I_2\mathrm{d}\tau \\
&= u_{\mathrm{C}}(kT_{\mathrm{s}}+T_{\mathrm{off}}) - \frac{I_2}{C}(t-kT_{\mathrm{s}}-T_{\mathrm{off}}) \\
&= \underbrace{u_{\mathrm{C}}(kT_{\mathrm{s}}) + \frac{DI_2}{(1-D)C}T_{\mathrm{off}}}_{=u_{\mathrm{C}}(kT_{\mathrm{s}}+T_{\mathrm{off}})} - \frac{I_2}{C}(t-kT_{\mathrm{s}}-T_{\mathrm{off}}).
\end{aligned}
\tag{8.53}
$$

Here, $u_{\mathrm{C}}(kT_{\mathrm{s}})$ is the (yet unknown) initial capacitor voltage at the beginning of a period, which will be derived later.

Step-up converter: capacitor voltage analysis (cont.)

In steady state, the capacitor voltage at the end of the switch-on period is identical to the voltage at the beginning of the switch-off period, that is,

$$u_{\mathrm{C}}(kT_{\mathrm{s}}) = u_{\mathrm{C}}((k+1)T_{\mathrm{s}}).$$

Hence, we can identify the voltage ripple from (8.53) as

$$\begin{aligned}\Delta u_{\mathrm{C}} &= \frac{I_2}{C}T_{\mathrm{on}} = \frac{DI_2}{(1-D)C}T_{\mathrm{off}} \\ &= \frac{I_2}{C}DT_{\mathrm{s}} = \frac{\Delta Q}{C}\end{aligned} \tag{8.54}$$

with the charge ripple $\Delta Q = DI_2T_{\mathrm{s}}$.

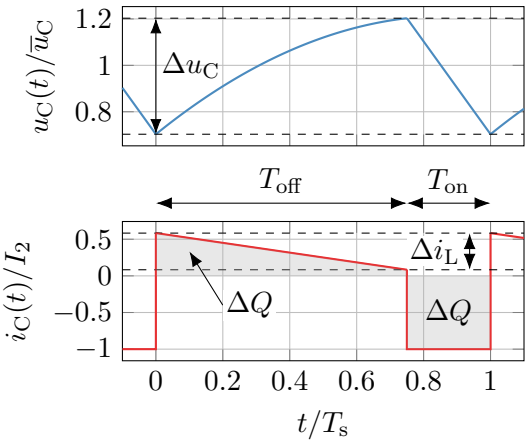

Fig. 8.14: Step-up converter voltage ripple

Step-up converter: capacitor voltage analysis (cont.)

To calculate the initial capacitor voltage $u_{\mathrm{C}}(kT_{\mathrm{s}})$, we can utilize

$$\overline{u}_{\mathrm{c}} = \frac{1}{T_{\mathrm{s}}} \int_0^{T_{\mathrm{s}}} u_{\mathrm{C}}(t)\mathrm{d}t \stackrel{!}{=} \overline{u}_2 = \frac{U_1}{1-D} \tag{8.55}$$

since the average capacitor voltage must be equal to the average output voltage. This yields

$$\begin{aligned} \overline{u}_{\mathrm{c}} &= \frac{1}{T_{\mathrm{s}}} \left(\int_0^{T_{\mathrm{off}}} u_{\mathrm{C}}(t)\mathrm{d}t + \int_{T_{\mathrm{off}}}^{T_{\mathrm{s}}} u_{\mathrm{C}}(t)\mathrm{d}t \right) \\ &= \dots \\ &= u_{\mathrm{C}}(kT_{\mathrm{s}}) + \frac{\Delta u_{\mathrm{C}}}{2} + \frac{\Delta i_{\mathrm{L}} T_{\mathrm{s}}}{12C}(1-D)^2 \end{aligned} \tag{8.56}$$

and finally delivers

$$\begin{aligned} u_{\mathrm{C}}(kT_{\mathrm{s}}) &= \frac{U_1}{1-D} - \frac{\Delta u_{\mathrm{C}}}{2} - \frac{\Delta i_{\mathrm{L}} T_{\mathrm{s}}}{12C}(1-D)^2 \\ &= \frac{U_1}{1-D} - \frac{I_2}{2C} D T_{\mathrm{s}} - \frac{U_1 T_{\mathrm{s}}^2}{12LC} D(1-D)^2. \end{aligned} \tag{8.57}$$

Circuit realization

- In Fig. 8.15 the simplest realization is shown utilizing one transistor and one diode.
- This configuration can only provide positive voltages and currents (first quadrant).
- The previously made step-up converter's switch-on definition (cf. Fig. 8.12) results from the transistor position in the circuit – difference to the step-down converter.

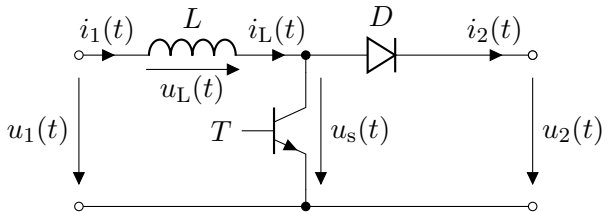

Fig. 8.15: Step-up converter with real components (single quadrant type)

Step-up converter: DCM

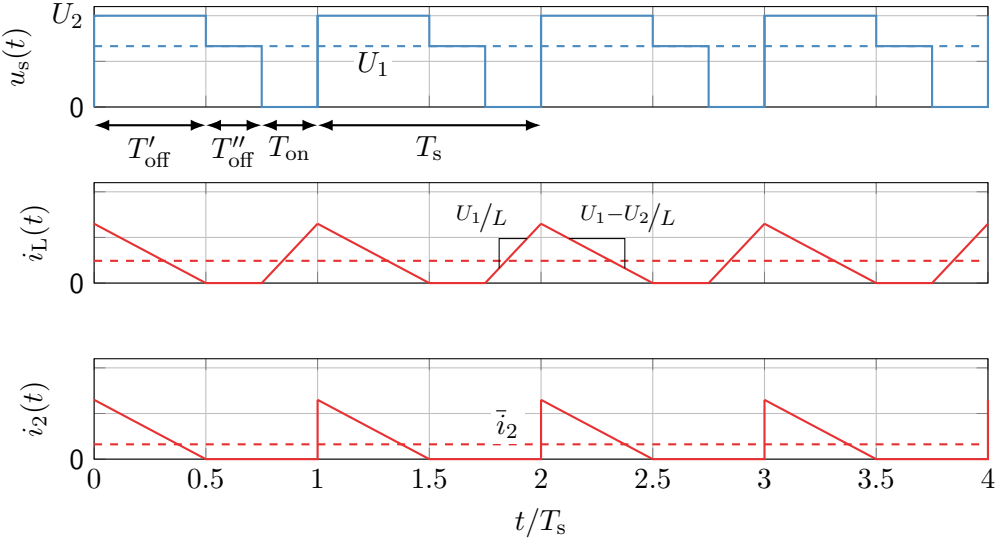

Step-up converter: switch states in DCM

The step-up converter in DCM has three different switch states:

- Transistor on-time: $T_{\mathrm{on}} = DT_{\mathrm{s}}$,
- Transistor off-time (conducting diode): $T'_{\mathrm{off}} = D'T_{\mathrm{s}}$,
- Transistor off-time (no conduction): $T''_{\mathrm{off}} = T_{\mathrm{s}} - T_{\mathrm{on}} - T'_{\mathrm{off}}$.

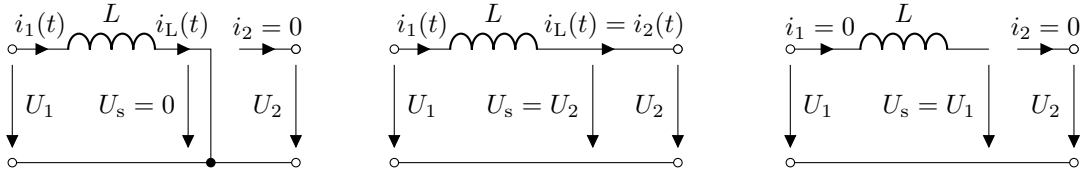

(a) Switch-on time T_{on} (b) Switch-off time T'_{off} (c) Switch-off time T''_{off}

Fig. 8.16: Switch states of the step-up converter including DCM

Step-up converter: DCM operation characteristics

In DCM operation

$$\bar{i}_{\mathrm{L}} = \bar{i}_1 < \frac{\Delta i_{\mathrm{L}}}{2} \quad \Rightarrow \quad U_2 \neq U_1 \frac{1}{1-D}$$

applies due to the non-conducting diode during T''_{off}. To find the input-to-output voltage ratio in DCM, we again utilize the current ripple balance:

$$\begin{aligned} \Delta i_{\mathrm{L}} &= \frac{U_1}{L} T_{\mathrm{on}} = \frac{U_1}{L} D T_{\mathrm{s}} && \text{(rising edge)}, \\ \Delta i_{\mathrm{L}} &= \frac{U_2 - U_1}{L} T'_{\mathrm{off}} = \frac{U_2 - U_1}{L} D' T_{\mathrm{s}} && \text{(falling edge)}. \end{aligned} \tag{8.58}$$

Solving for D' yields

$$D' = \frac{U_1}{U_2 - U_1} D. \tag{8.59}$$

The average load current is

$$\bar{i}_2 = \frac{\Delta i_{\mathrm{L}}}{2} \frac{T'_{\mathrm{off}}}{T_{\mathrm{s}}} = \frac{\Delta i_{\mathrm{L,max}} D}{2} D' = \frac{\Delta i_{\mathrm{L,max}}}{2} \frac{U_1}{U_2 - U_1} D^2. \tag{8.60}$$

Step-up converter: DCM operation characteristics (cont.)

Solving (8.60) delivers the step-up converter voltage gain in DCM as

$$\frac{U_2}{U_1} = 1 + \frac{D^2}{2}\frac{\Delta i_{\mathrm{L,max}}}{\bar{i}_2}. \tag{8.61}$$

Since $\Delta i_{\mathrm{L,max}}$ also depends on U_1, cf. (8.46), the relation (8.61) only holds for a given U_1. Hence, we can insert (8.46) in (8.61) and solve for U_2 to receive

$$U_2 = U_1 + \frac{D^2}{2}\frac{T_{\mathrm{s}}}{L\bar{i}_2}. \tag{8.62}$$

Finally, the step-up converter operates in BCM if

$$\bar{i}_{\mathrm{L}} = \bar{i}_1 = \frac{\Delta i_{\mathrm{L}}}{2} \quad \Leftrightarrow \quad \bar{i}_2 = (1-D)\frac{\Delta i_{\mathrm{L}}}{2}. \tag{8.63}$$

Step-up converter load curves

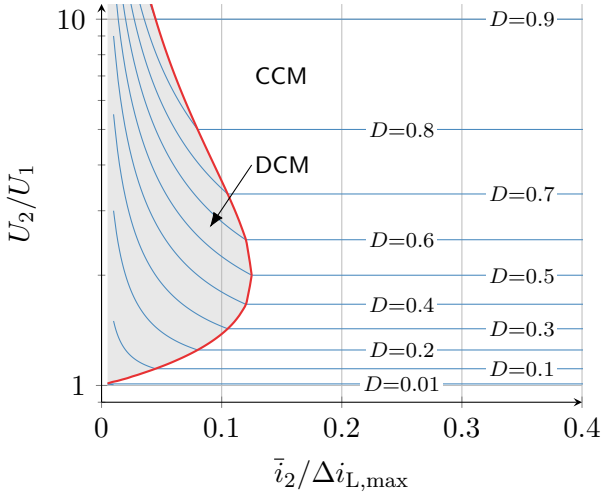

Fig. 8.17: Step-up converter load curves for CCM and DCM (note: logarithmic ordinate)

Table of contents

Buck-boost converter: combining step-up and step-down stages

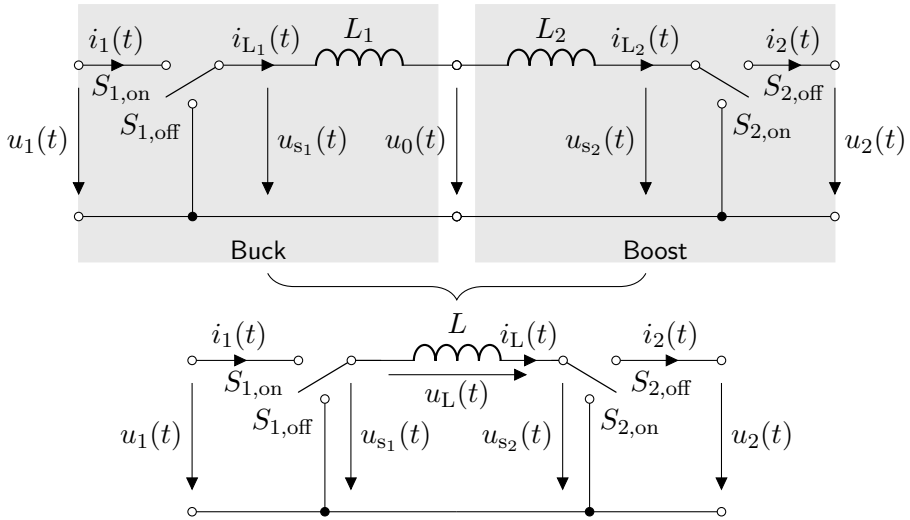

Fig. 8.18: Buck-boost converter (ideal switch representation)

Buck-boost converter: switching states

The buck-boost converter switches are operated synchronously, that is, S_1 and S_2 are either on or off at the same time. Thus, the converter has only two switch states:

$$\begin{aligned} \{S_{1,\text{on}}, S_{2,\text{on}}\} \quad &\rightarrow \quad u_{\text{s}_1}(t) = U_1, u_{\text{s}_2}(t) = 0, \\ \{S_{1,\text{off}}, S_{2,\text{off}}\} \quad &\rightarrow \quad u_{\text{s}_1}(t) = 0, \quad u_{\text{s}_2}(t) = U_2. \end{aligned} \tag{8.64}$$

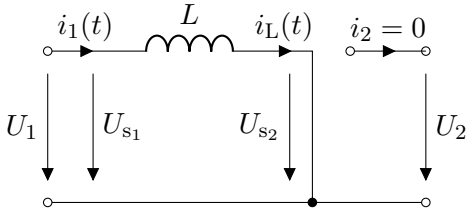

(a) Switch-on time

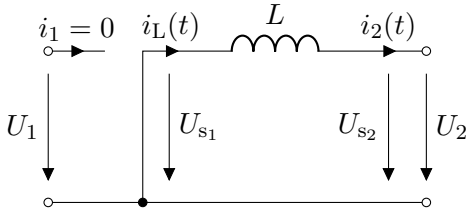

(b) Switch-off time

Fig. 8.19: Switch states of the (synchronous) buck-boost converter

Buck-boost converter: CCM voltage transfer ratio

In CCM, we can derive the voltage transfer ratio directly by the serial connection of the buck and boost stages from Fig. 8.18

$$\frac{U_0}{U_1} = D, \qquad \frac{U_2}{U_0} = \frac{1}{1-D}, \tag{8.65}$$

leading to

$$\frac{U_2}{U_1} = \frac{D}{1-D}. \tag{8.66}$$

Alternatively, we can derive this result from the voltage balance of the inductor L:

$$u_{\mathrm{L}}(t) = \begin{cases} U_1, & t \in [kT_{\mathrm{s}}, kT_{\mathrm{s}} + T_{\mathrm{on}}], \\ -U_2 & t \in [kT_{\mathrm{s}} + T_{\mathrm{on}}, (k+1)T_{\mathrm{s}}]. \end{cases} \tag{8.67}$$

In steady state, the average inductor voltage per period must be zero, yielding

$$U_1 T_{\mathrm{on}} = U_2 T_{\mathrm{off}} \quad \Leftrightarrow \quad U_1 D T_{\mathrm{s}} = U_2 (1-D) T_{\mathrm{s}} \quad \Leftrightarrow \quad \frac{U_2}{U_1} = \frac{D}{1-D}. \tag{8.68}$$

Buck-boost converter: steady-state time-domain behavior

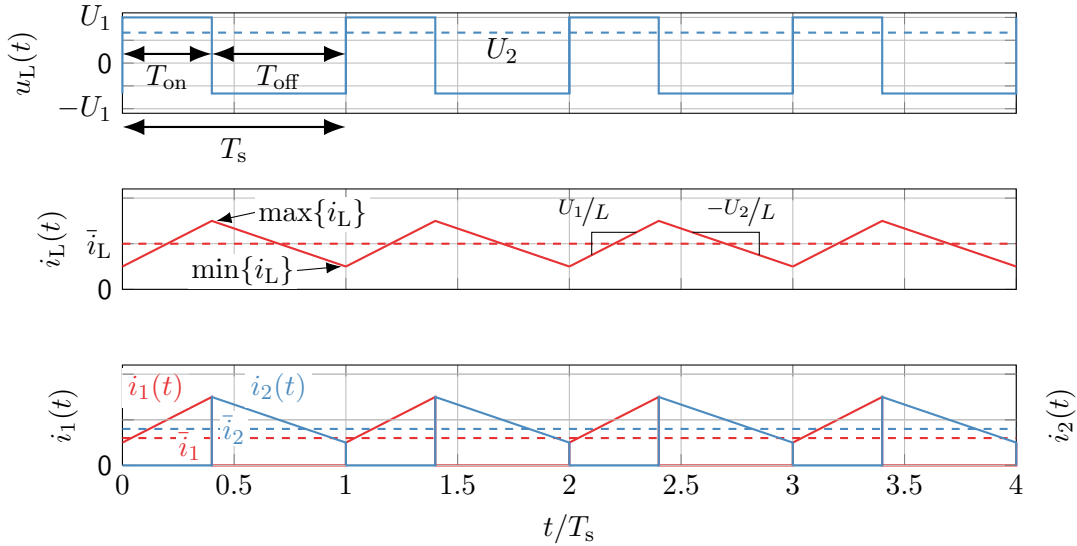

Buck-boost converter: current ripple

The peak-to-peak current ripple of the buck-boost converter is given by

$$\begin{aligned}\Delta i_{\mathrm{L}} &= \max\{i_{\mathrm{L}}(t)\} - \min\{i_{\mathrm{L}}(t)\} = i_{\mathrm{L}}(t = T_{\mathrm{on}}) - i_{\mathrm{L}}(t = T_{\mathrm{s}}) \\ &= \frac{U_1}{L} T_{\mathrm{on}} = \frac{U_2}{L} T_{\mathrm{off}} \\ &= D \frac{T_{\mathrm{s}}}{L} U_1 = D \Delta i_{\mathrm{L,max}}.\end{aligned} \tag{8.69}$$

The buck-boost converter current ripple characteristic matches the previous boost converter behavior – compare (8.44):

- Its minimal for $D \to 0$ since the output voltage becomes zero and the inductor is connected to the output voltage over the entire switching period.
- Its maximal for $D \to 1$ since the inductor is connected to the (non-zero) input voltage over the entire switching period.

Buck-boost converter: output capacitor and voltage ripple

With the usual simplifying assumptions (cf. Fig. 8.13), in particular, a constant output current $i_2(t) = I_2$, the capacitor's current during the switch-on time is given by

$$i_{\mathrm{C}}(t) = -i_2(t) = -I_2, \quad t \in [kT_{\mathrm{s}}, kT_{\mathrm{s}} + T_{\mathrm{off}}].$$

This is identical to the step-up converter, leading to the same voltage ripple

$$\Delta u_{\mathrm{C}} = \frac{I_2}{C} T_{\mathrm{on}} = \frac{I_2}{C} D T_{\mathrm{s}}.$$

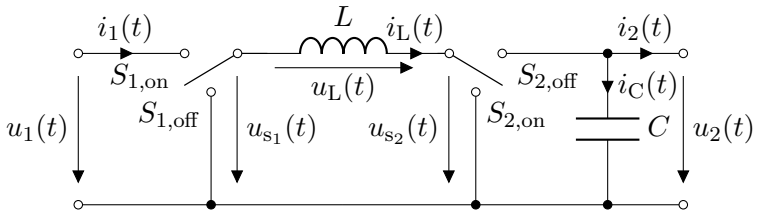

Fig. 8.20: Buck-boost converter with output capacitor

Buck-boost converter: circuit realization

- In Fig. 8.21 the buck-boost converter realization is a direct series circuit combination of Fig. 8.7 and Fig. 8.15.
- This configuration can only provide positive voltages and currents (first quadrant).
- It should be noted that this circuit requires two diodes and two transistors.

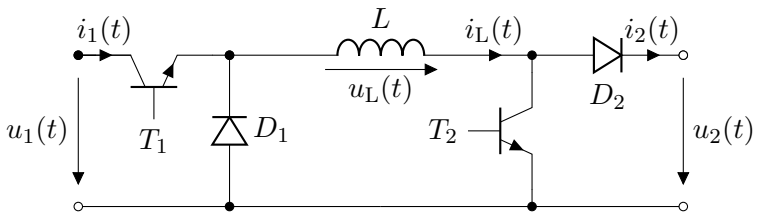

Fig. 8.21: Buck-boost converter with real components (single quadrant type)

Buck-boost converter: switch states in DCM

The buck-boost converter in DCM has three different switch states:

- Transistor on-time: $T_{\mathrm{on}} = DT_{\mathrm{s}}$,
- Transistor off-time (conducting diode): $T'_{\mathrm{off}} = D'T_{\mathrm{s}}$,
- Transistor off-time (no conduction): $T''_{\mathrm{off}} = T_{\mathrm{s}} - T_{\mathrm{on}} - T'_{\mathrm{off}}$.

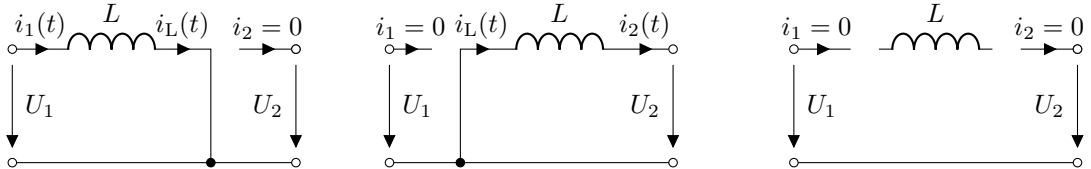

(a) Switch-on time T_{on} (b) Switch-off time T'_{off} (c) Switch-off time T''_{off}

Fig. 8.22: Switch states of the (synchronous) buck-boost converter including DCM

Buck-boost converter: DCM operation characteristics

In DCM operation

$$\bar{i}_{\mathrm{L}} < \frac{\Delta i_{\mathrm{L}}}{2} \quad \Rightarrow \quad U_2 \neq U_1 \frac{D}{1-D}$$

applies due to the non-conducting diode during T''_{off}. To find the input-to-output voltage ratio in DCM, we again utilize the current ripple balance:

$$\begin{aligned} \Delta i_{\mathrm{L}} &= \frac{U_1}{L} T_{\mathrm{on}} = \frac{U_1}{L} D T_{\mathrm{s}} \quad \text{(rising edge)}, \\ \Delta i_{\mathrm{L}} &= \frac{U_2}{L} T'_{\mathrm{off}} = \frac{U_2}{L} D' T_{\mathrm{s}} \quad \text{(falling edge)}. \end{aligned} \tag{8.70}$$

Solving for D' yields

$$D' = \frac{U_1}{U_2} D. \tag{8.71}$$

The average load current is

$$\bar{i}_2 = \frac{\Delta i_{\mathrm{L}}}{2} \frac{T'_{\mathrm{off}}}{T_{\mathrm{s}}} = \frac{\Delta i_{\mathrm{L,max}} D}{2} D' = \frac{\Delta i_{\mathrm{L,max}}}{2} \frac{U_1}{U_2} D^2. \tag{8.72}$$

Buck-boost converter: DCM operation characteristics (cont.)

Solving (8.72) delivers the buck-boost converter voltage gain in DCM as

$$\frac{U_2}{U_1} = \frac{D^2}{2} \frac{\Delta i_{\mathrm{L,max}}}{\bar{i}_2}. \tag{8.73}$$

Since $\Delta i_{\mathrm{L,max}}$ also depends on U_1, the relation (8.73) only holds for a given U_1. Hence, we can insert (8.69) in (8.73) and solve for U_2 to receive

$$U_2 = U_1^2 \frac{D^2}{2} \frac{T_{\mathrm{s}}}{L \bar{i}_2}. \tag{8.74}$$

Finally, the buck-boost converter operates in BCM if

$$\bar{i}_{\mathrm{L}} = \frac{\Delta i_{\mathrm{L}}}{2} \quad \Leftrightarrow \quad \bar{i}_2 = \Delta i_{\mathrm{L,max}} \frac{1}{2} \frac{D}{1-D}. \tag{8.75}$$

Buck-boost converter load curves

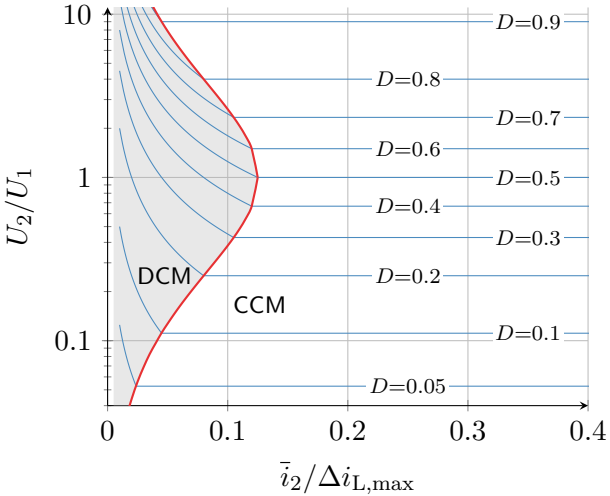

Fig. 8.23: Buck-boost converter load curves for CCM and DCM (note: logarithmic ordinate)

Table of contents

Recap: buck-boost converter switching states

Key characteristic of (synchronous) buck-boost converter

The switching scheme of the (synchronous) buck-boost converter from Fig. 8.19 is realized by two switches and characterized by:

- During switch-on: inductor is connected to $u_1(t)$,
- During switch-off: inductor is connected to $u_2(t)$.

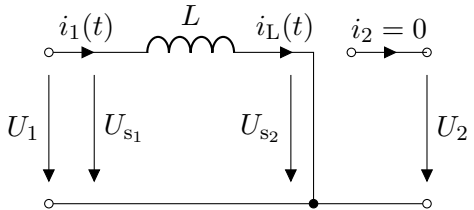

(a) Switch-on time

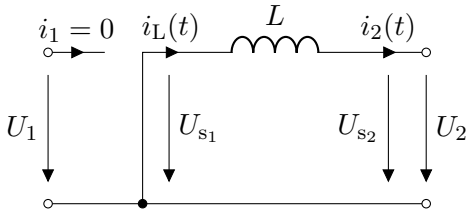

(b) Switch-off time

Inverting buck-boost converter: overview

- Voltage change at the inductor can be also achieved by a single switch which input is connected to the inductor.
- Assuming an ideal, infinitely fast switch, the inductor current $i_{\mathrm{L}}(t)$ remains well-defined (no open switch at inductor).

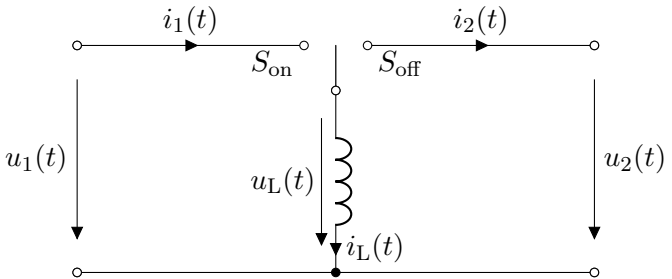

Fig. 8.25: Inverting buck-boost converter (ideal switch representation)

Polarity change of inverting buck-boost converter

- One side of the inductor remains connected to the common connection rail between input and output side.
- The other inductor side switches between the upper input and output rail.
- Consequence: voltage and current directions are inverted between the two switch states.

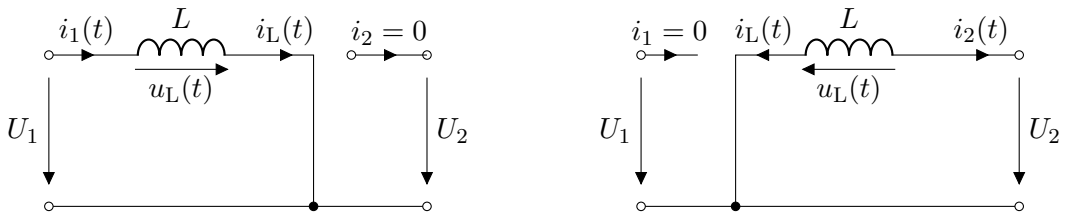

(a) Switch-on time

(b) Switch-off time

Fig. 8.26: Voltage and current definitions of the inverting buck-boost converter

Inverting buck-boost converter: voltage transfer ratios

In CCM, the voltage balance of the inductor L delivers:

$$u_{\mathrm{L}}(t) = \begin{cases} U_1, & t \in [kT_{\mathrm{s}}, kT_{\mathrm{s}} + T_{\mathrm{on}}], \\ U_2 & t \in [kT_{\mathrm{s}} + T_{\mathrm{on}}, (k+1)T_{\mathrm{s}}]. \end{cases} \tag{8.76}$$

In steady state, the average inductor voltage per period must be zero, yielding

$$U_1 T_{\mathrm{on}} = -U_2 T_{\mathrm{off}} \quad \Leftrightarrow \quad U_1 D T_{\mathrm{s}} = -U_2 (1-D) T_{\mathrm{s}} \quad \Leftrightarrow \quad \frac{U_2}{U_1} = -\frac{D}{1-D}. \tag{8.77}$$

Likewise, the analysis of the DCM mode reveals

$$\frac{U_2}{U_1} = -\frac{D^2}{2} \frac{\Delta i_{\mathrm{L,max}}}{\bar{i}_2} \quad \Leftrightarrow \quad U_2 = -U_1^2 \frac{D^2}{2} \frac{T_{\mathrm{s}}}{L \bar{i}_2}. \tag{8.78}$$

Hence, the inverting buck-boost converter has a negative voltage transfer ratio in CCM and DCM, but the same absolute voltage gain as the synchronous buck-boost converter.

Inverting buck-boost converter: circuit realization

- Energy transfer takes place solely indirect by intermediate storage within inductor.
- Further characteristics (current and voltage ripple, operation modes) are analogous to the synchronous buck-boost converter.
- Transistor needs to block up to $|u_1(t)| + |u_2(t)|$, in contrast to step-down/up converter where only the input or output voltage is blocked by the transistor.

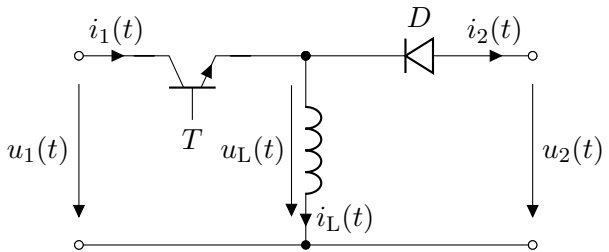

Fig. 8.27: Inverting buck-boost converter with real components (single quadrant type)

Table of contents

Semiconductor utilization

We define the semiconductor utilization as the ratio of the average output power to the transistor (peak) power:

$$\frac{P_2}{P_\mathrm{T}} = \frac{U_2 I_2}{\max\{u_\mathrm{T}\} \cdot \max\{i_\mathrm{T}\}}. \tag{8.79}$$

Background and interpretation:

- Transistor needs to withstand the peak voltage and current (rating requirement).
- The lower the semiconductor utilization, the more costly / bulky the transistor for a given converter power (key parameter for the selection of the power stage).

Assumptions for following calculations:

- Lossless operation in CCM,
- Current and voltage ripple are marginal and can be neglected,
- Given a constant P_2, the duty cycle D is adjusted to achieve the desired output power.

Semiconductor utilization: step-down converter

The step-down converter's transistor peak voltage and current are (cf. Fig. 8.2)

$$\begin{aligned} \max\{u_\mathrm{T}\} &= U_1, \\ \max\{i_\mathrm{T}\} &= \frac{\bar{i}_1}{D} = \frac{I_1}{D}. \end{aligned} \tag{8.80}$$

The transistor must block the (constant) input voltage U_1 and step-like changing current $i_1(t) = i_\mathrm{T}(t)$. The semiconductor utilization is

$$\begin{aligned} \frac{P_2}{P_\mathrm{T}} &= \frac{U_2 I_2}{U_1 \frac{\bar{i}_1}{D}} = \frac{U_1 I_1}{U_1 \frac{I_1}{D}} \\ &= D. \end{aligned} \tag{8.81}$$

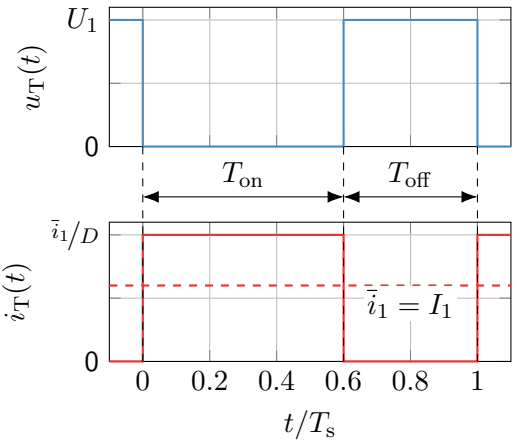

Fig. 8.28: Voltage and current at the step-down converter transistor (w/o current ripple)

Semiconductor utilization: step-up converter

The step-up converter's transistor peak voltage and current are (cf. Fig. 8.12)

$$\begin{aligned} \max\{u_\mathrm{T}\} &= U_2, \\ \max\{i_\mathrm{T}\} &= \max\{i_\mathrm{L}\} = I_1. \end{aligned} \tag{8.82}$$

The transistor must block the (constant) output voltage U_2 and (constant) input current $i_1(t) = i_\mathrm{T}(t)$, which is filtered by the inductor. The semiconductor utilization is

$$\begin{aligned} \frac{P_2}{P_\mathrm{T}} = \frac{U_2 I_2}{U_2 I_1} = \frac{I_2}{I_1} \\ = 1 - D. \end{aligned} \tag{8.83}$$

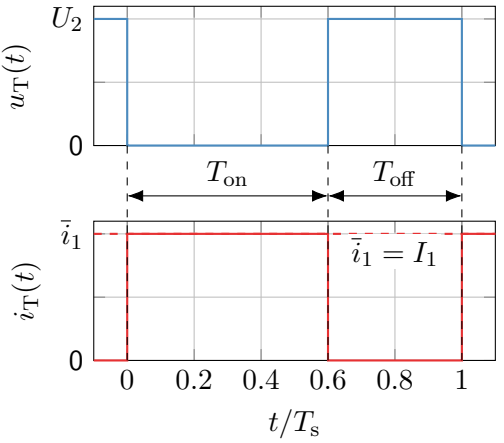

Fig. 8.29: Voltage and current at the step-up converter transistor (w/o current ripple)

Semiconductor utilization: inverting buck-boost converter

The inv. buck-boost converter's transistor peak voltage and current are (cf. Fig. 8.26)

$$\begin{aligned} \max\{u_\mathrm{T}\} &= U_1 - U_2, \\ \max\{i_\mathrm{T}\} &= \frac{\bar{i}_1}{D} = \frac{I_1}{D}. \end{aligned} \tag{8.84}$$

The transistor must block the (combined) input and output voltage and step-like changing current $i_1(t) = i_\mathrm{T}(t)$. The semiconductor utilization is

$$\begin{aligned} \frac{P_2}{P_\mathrm{T}} &= \frac{U_2 I_2}{(U_1 - U_2)\frac{\bar{i}_1}{D}} = \frac{U_1 I_1}{U_1 \frac{1}{1-D}\frac{I_1}{D}} \\ &= (1-D)D. \end{aligned} \tag{8.85}$$

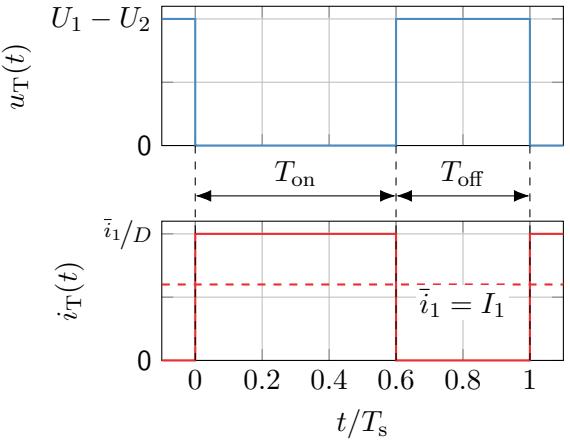

Fig. 8.30: Voltage and current at the inv. buck-boost converter transistor (w/o current ripple)

Semiconductor utilization: summary

- The converters' semiconductor utilization is generally the highest if the input and output voltages are similar:
  - Step-down: $D \to 1$,
  - Step-up: $D \to 0$,
  - Inv. buck-boost: $D \to 0.5$.
- Inverting buck-boost has generally a lower utilization.
- Finding indicates that the inv. buck-boost should be only considered if an application truly requires both step-up and step-down operation.

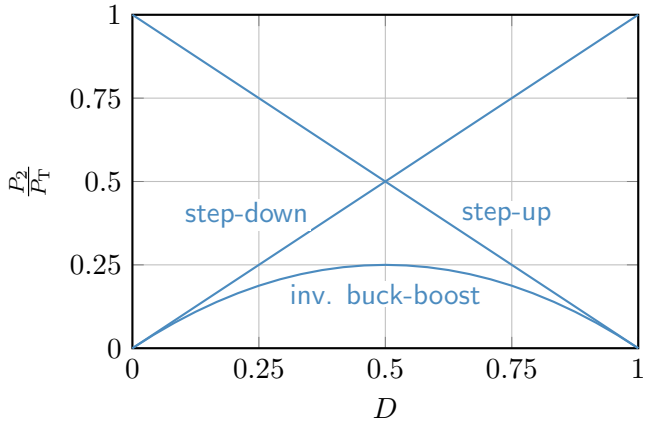

Fig. 8.31: Comparison of the semiconductor utilization for the step-down, step-up, and inv. buck-boost converter

Filter component requirements: step-down converter

Open question regarding filter dimensioning:

- How large do the filter components need to be sized to ensure sufficiently smooth input and output signals?

To answer this, we consider the following assumptions:

- The input and output current are constant: $i_1(t) = I_1$, $i_2(t) = I_2$.
- Additional input capacitor necessary to buffer the pulsating input current.
- Voltage and current ripples do not influence each other (simplified superposition).

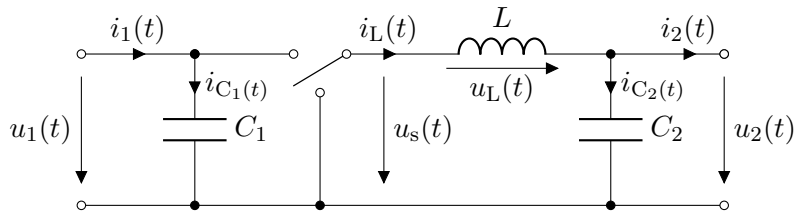

Fig. 8.32: Step-down converter with filter components

Filter component requirements: step-down converter (cont.)

The input voltage ripple is

$$\Delta u_{\mathrm{C}_1} = \frac{I_1(1-D)T_\mathrm{s}}{C_1} \tag{8.86}$$

assuming that the input capacitor is loaded with the input current I_1 during the off-time $T_\mathrm{off} = (1-D)T_\mathrm{s}$. Assuming that there is an input voltage ripple requirement on Δu_{C_1}, that is, an upper limit ripple, the minimum input capacitance is

$$C_1 \geq \frac{I_1(1-D)T_\mathrm{s}}{\Delta u_{\mathrm{C}_1}} = C_{1,\mathrm{min}}. \tag{8.87}$$

The stored input capacitor energy yields

$$E_{\mathrm{C}_1} = \frac{1}{2}C_{1,\mathrm{min}}\left(U_1 + \frac{1}{2}\Delta u_{\mathrm{C}_1}\right)^2 = \frac{1}{2}(1-D)\frac{P_2}{f_\mathrm{s}}\frac{\left(1+\frac{\varepsilon_{u_{\mathrm{C}_1}}}{2}\right)^2}{\varepsilon_{u_{\mathrm{C}_1}}} \tag{8.88}$$

with the normalized ripple factor $\varepsilon_{u_{\mathrm{C}_1}} = {}^{\Delta u_{\mathrm{C}_1}}/_{U_1}$.

Filter component requirements: step-down converter (cont.)

We already know from (8.7) the inductor current ripple being

$$\Delta i_{\mathrm{L}} = \frac{(1-D)U_2 T_{\mathrm{s}}}{L}.$$

Assuming that there is an inductor current ripple requirement on Δi_{L}, that is, an upper limit ripple, the minimum inductance is

$$L \geq \frac{(1-D)U_2 T_{\mathrm{s}}}{\Delta i_{\mathrm{L}}} = L_{\min}. \tag{8.89}$$

The stored inductor energy is

$$E_{\mathrm{L}} = \frac{1}{2} L_{\min} \left(I_2 + \frac{1}{2}\Delta i_{\mathrm{L}} \right)^2 = \frac{1}{2}(1-D)\frac{P_2}{f_{\mathrm{s}}} \frac{\left(1 + \frac{\varepsilon_{i_{\mathrm{L}}}}{2}\right)^2}{\varepsilon_{i_{\mathrm{L}}}} \tag{8.90}$$

with the normalized ripple factor $\varepsilon_{i_{\mathrm{L}}} = {}^{\Delta i_{\mathrm{L}}}/_{I_2}$.

Filter component requirements: step-down converter (cont.)

We already know from (**??**) the output capacitor voltage ripple being

$$\Delta u_{\mathrm{C}_2} = \frac{D(1-D)T_{\mathrm{s}}^2 U_1}{8LC_2} = \frac{(1-D)}{8LC_2}\frac{U_2}{f_{\mathrm{s}}^2}.$$

Inserting the inductor sizing (8.89) delivers

$$\Delta u_{\mathrm{C}_2} = \frac{1}{8C_2}\frac{\Delta i_{\mathrm{L}}}{f_{\mathrm{s}}} = \frac{\varepsilon_{i_{\mathrm{L}}}}{8C_2}\frac{I_2}{f_{\mathrm{s}}}. \tag{8.91}$$

Assuming that there is an output voltage ripple requirement on Δu_{C_2}, that is, an upper limit ripple, the minimum output capacitance is

$$C_2 \geq \frac{\varepsilon_{i_{\mathrm{L}}} I_2}{8 f_{\mathrm{s}} \Delta u_{\mathrm{C}_2}} = C_{2,\mathrm{min}}. \tag{8.92}$$

The stored output capacitor energy yields

$$E_{\mathrm{C}_2} = \frac{1}{2}C_{2,\mathrm{min}}\left(U_2 + \frac{1}{2}\Delta u_{\mathrm{C}_2}\right)^2 = \frac{1}{16}\varepsilon_{i_{\mathrm{L}}}\frac{P_2}{f_{\mathrm{s}}}\frac{\left(1+\frac{\varepsilon_{u_{\mathrm{C}_2}}}{2}\right)^2}{\varepsilon_{u_{\mathrm{C}_2}}}. \tag{8.93}$$

Filter component requirements: step-down converter interpretation

The stored energy in the filter components is a good proxy for the filter size and weight. All three step-down converter filter components share the following characteristics:

- The stored energy is proportional to the output power P_2.
- The stored energy is inversely proportional to the switching frequency f_s.
- The stored energy is minimal at $\varepsilon_{u_{\mathrm{C}_1}} = \varepsilon_{i_\mathrm{L}} = \varepsilon_{u_{\mathrm{C}_2}} = 1/2$ (i.e., large signal ripples).
  - $\varepsilon_{i_\mathrm{L}} = 1/2$ refers to BCM mode.
  - Increased input voltage ripple and inductor current ripple also increases the transistor requirements, see (8.80).

In addition, E_L and E_{C_1} also scale with

$$(1 - D),$$

that is, are small if the converter's input and output voltage are similar. In the following, we do not analyze the step-up converter in detail, since the findings are analogous.

Filter component requirements: inverting buck-boost converter

Again, we assume the following:

- The input and output current are constant: $i_1(t) = I_1$, $i_2(t) = I_2$.
- Additional capacitors necessary to buffer the pulsating input / output currents.
- Voltage and current ripples do not influence each other (simplified superposition).

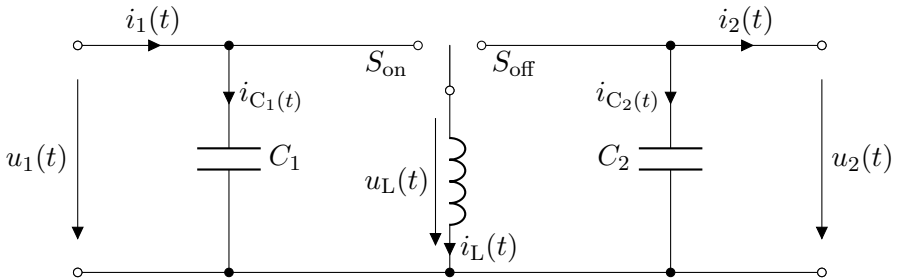

Fig. 8.33: Inverting buck-boost converter with filter components

Filter component requirements: inverting buck-boost converter (cont.)

We further assume an identical normalized input and output voltage ripple requirement

$$\varepsilon_{u_{\mathrm{C}_1}} = \frac{\Delta u_{\mathrm{C}_1}}{U_1} = \varepsilon_{u_{\mathrm{C}_2}} = \frac{\Delta u_{\mathrm{C}_2}}{U_2} = \varepsilon_{u_{\mathrm{C}}}.$$

Following the same derivation as for the step-down converter, the stored filter energies are

$$E_{\mathrm{C}} = E_{\mathrm{C}_1} + E_{\mathrm{C}_2} = \frac{1}{2}\frac{P_2}{f_{\mathrm{s}}}\frac{\left(1+\frac{\varepsilon_{u_{\mathrm{C}}}}{2}\right)^2}{\varepsilon_{u_{\mathrm{C}}}}, \qquad E_{\mathrm{L}} = \frac{1}{2}\frac{P_2}{f_{\mathrm{s}}}\frac{\left(1+\frac{\varepsilon_{i_{\mathrm{L}}}}{2}\right)^2}{\varepsilon_{i_{\mathrm{L}}}}. \tag{8.94}$$

Compared to the step-down converter we can find:

- Same dependence on P_2, f_{s}, and $\varepsilon_{u_{\mathrm{C}}}$ or $\varepsilon_{i_{\mathrm{L}}}$.
- Missing $(1-D)$ scaling factor.
- Result: The inverting buck-boost converter's passive components are generally larger due to the pulsating input and output current which needs to be filtered.

Table of contents

Recap: (inverting) buck-boost converter switching states

Key characteristic drawback of (inverting) buck-boost converter

The switching scheme of the (inverting) buck-boost converter utilizes an indirect inductive energy transfer resulting in pulsating input and output currents which need to be filtered. This leads to larger filter components.

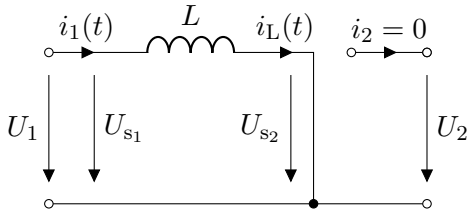

(a) Switch-on time

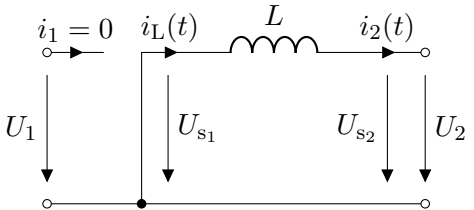

(b) Switch-off time

Ćuk converter: the boost-buck converter with capacative energy transfer

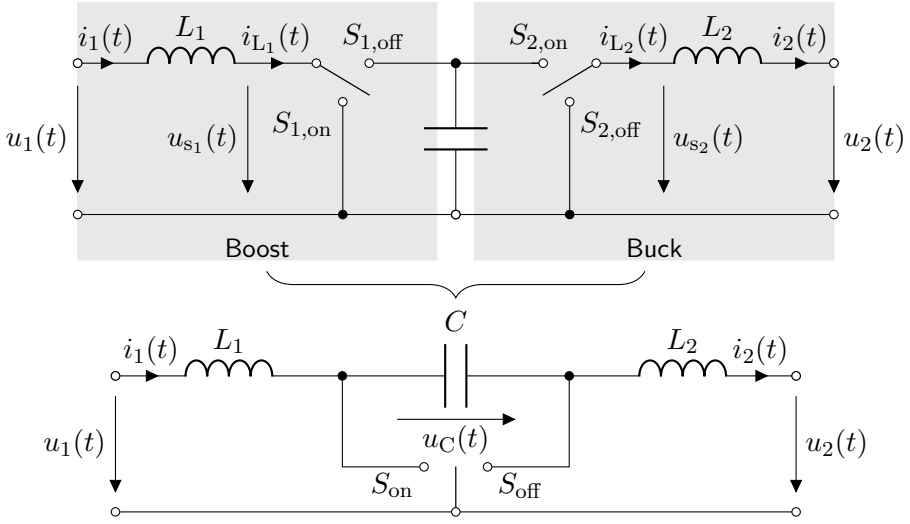

Fig. 8.35: Ćuk converter (ideal switch representation)

Ćuk converter: switching states

- The Ćuk converter uses the capacitor C to transfer energy between the input and output.
- The polarity of C is changed between the two switch states (inverting voltage gain).
- In contrast to the previous topologies, there is no pulsating output or input current thanks to the outer two inductors.

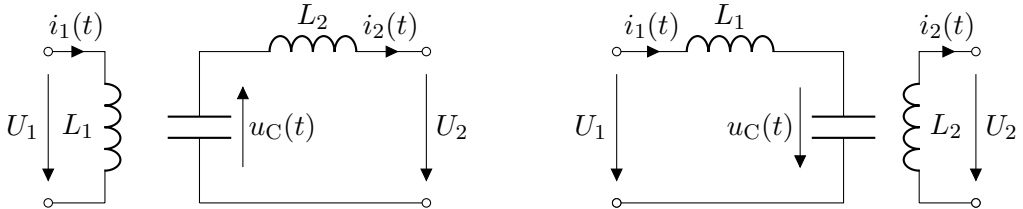

(a) Switch-on time (b) Switch-off time

Fig. 8.36: Switch states of the Ćuk converter

Ćuk converter: voltage gain

In periodic steady-state operation, the voltage balance during a switching period of the two inductors must be fulfilled:

$$L_1: \quad DU_1 + (1-D)(U_1 - U_\mathrm{C}) = 0, \qquad L_2: \quad D(U_2 + U_\mathrm{C}) + (1-D)U_2 = 0. \tag{8.95}$$

Above, U_1, U_2, and U_C are considered constant.From those we can derive:

$$L_1: \quad U_\mathrm{C} = \frac{U_1}{1-D}, \qquad L_2: \quad U_\mathrm{C} = -\frac{U_2}{D}. \tag{8.96}$$

Combining both equations delivers the voltage gain of the Ćuk converter:

$$\frac{U_2}{U_1} = -\frac{D}{1-D}. \tag{8.97}$$

This is the same finding as for the inverting buck-boost converter, which seems quite obvious, as the Ćuk converter just flips the order of the buck and boost parts.

Ćuk converter: circuit realization

- Like the inverting buck-boost, the Ćuk converter only requires one diode and transistor.
- Transistor T needs to block $u_{\mathrm{C}}(t)$ during the off-time, while it covers both the input and output current during the on-time: semiconductor utilization is also $P_2/P_{\mathrm{T}} = (1-D)D$ as for the inverting buck-boost (cf. Fig. 8.31).

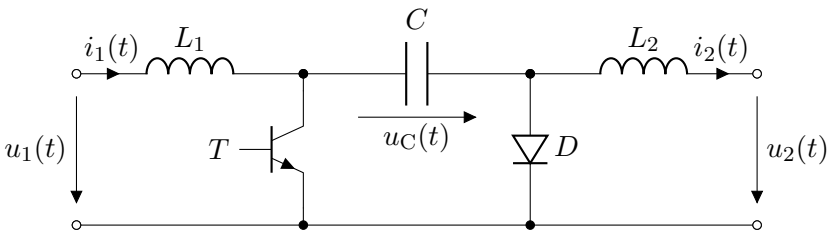

Fig. 8.37: Ćuk converter with real components (single quadrant type)

Single ended primary inductance converter (SEPIC)

- Output inductor and diode change places compared to the Ćuk converter.
- Output current becomes pulsating (compared to Ćuk).
- Input to output gain becomes non-inverting (cf. next slides).

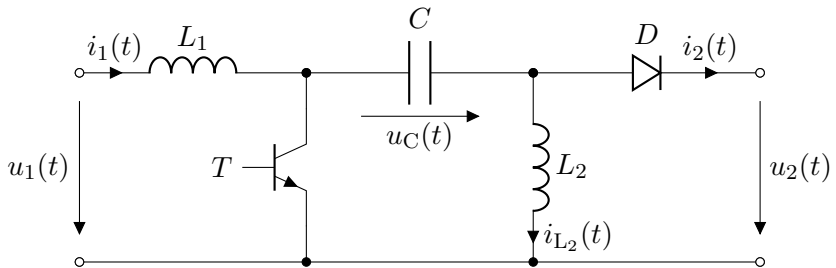

Fig. 8.38: SEPIC with real components (single quadrant type)

SEPIC: switching states

- During switch on-time, the transistor is conducting and the diode is blocking (causing the output current pulsation).
- During switch off-time, the diode is conducting and the transistor is blocking.

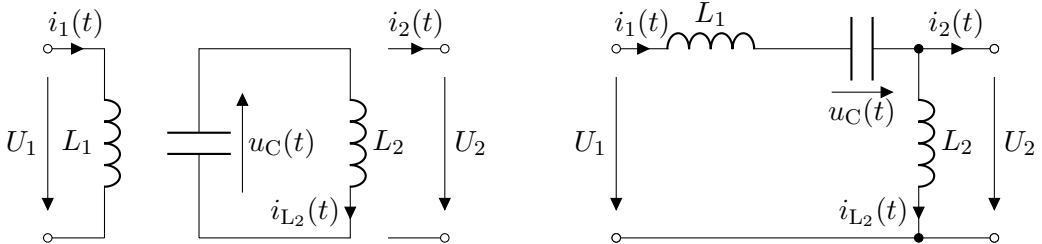

(a) Switch-on time

(b) Switch-off time

Fig. 8.39: Switch states of the SEPIC

SEPIC: voltage gain

In periodic steady-state operation, the voltage balance during a switching period of the two inductors must be fulfilled:

$$L_1: \quad DU_1 + (1-D)(U_1 - U_2 - U_\mathrm{C}) = 0, \qquad L_2: \quad -DU_\mathrm{C} + (1-D)U_2 = 0. \tag{8.98}$$

Above, U_1, U_2, and U_C are considered constant.From those we can derive:

$$L_1: \quad U_\mathrm{C} = \frac{U_1}{1-D} - U_2, \qquad L_2: \quad U_\mathrm{C} = \left(\frac{1}{D} - 1\right) U_2. \tag{8.99}$$

Combining both equations delivers the voltage gain of the SEPIC:

$$\frac{U_2}{U_1} = \frac{D}{1-D}. \tag{8.100}$$

Similar to the synchronous buck-boost, the SEPIC comes with a positive voltage gain, but with the advantages of a single transistor and diode as well as non-pulsating input currents (at the cost of more filter components).

Buck/boost converter for both current polarities

- Previous buck/boost realizations allowed only unidirectional current flow (cf. Fig. 8.7 and Fig. 8.15).
- Right realization with two transistors and body diodes enables both current polarities (two quadrant type).
- No discontinuous current flow (no DCM mode).
- Transistors must be switched complementary to prevent a DC-link short-circuit:
  - T_1: on, T_2: off,
  - T_1: off, T_2: on.

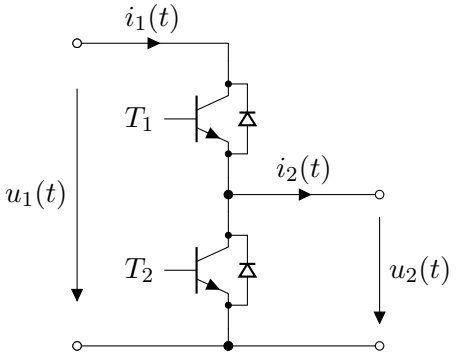

Fig. 8.40: DC-DC converter realization for both current polarities (w/o filter components, aka half-bridge)

Buck/boost converter for both voltage polarities

- Required constraints are:
  - $u_1 > 0$: otherwise DC link short-circuit,
  - $i_2 > 0$: to meet semiconductor capabilities.
- Possible switching states:

T_1	T_2	u_2	i_1
on	off	$+u_1$	$+i_2$
off	on	$-u_1$	$-i_2$
on	on	0	0
off	off	0	0

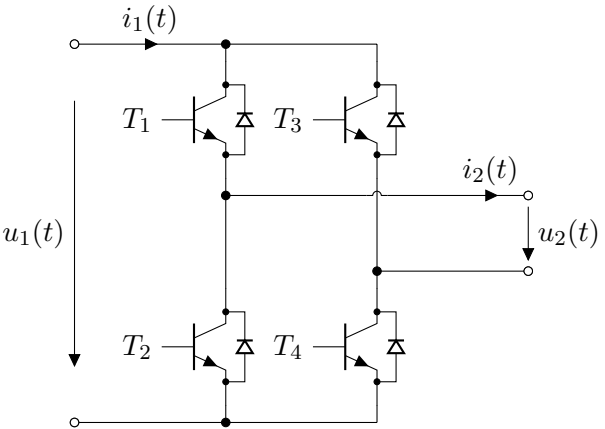

Fig. 8.41: DC-DC converter realization for both voltage polarities (w/o filter components, aka asymmetrical half-bridge)

Buck/boost converter for both current and voltage polarities

- For achieving full four quadrant operation (4Q), we combine the previous half-bridge variants.
- Also requires complementary switching of $\{T_1, T_2\}$ and $\{T_3, T_4\}$ to prevent a DC-link short-circuit.
- Possible (allowed) switching states:

T_1	T_2	T_3	T_4	u_2	i_1
on	off	off	on	$+u_1$	$+i_2$
off	on	on	off	$-u_1$	$-i_2$
on	off	on	off	0	0
off	on	off	on	0	0

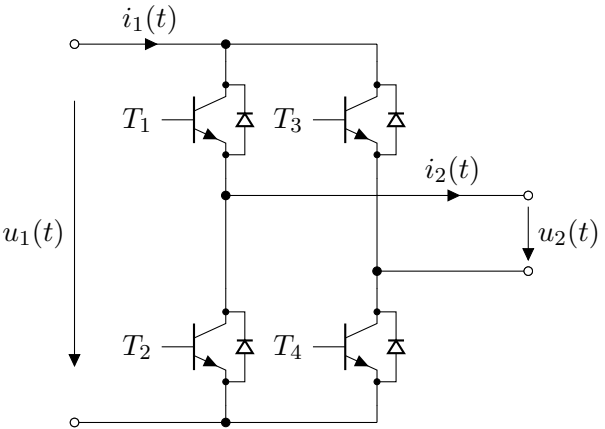

Fig. 8.42: DC-DC converter realization for both current and voltage polarities (w/o filter components, aka full-bridge)

Buck/boost converter for both current and voltage polarities (cont.)

Define duty cycle as relative on-times

$$D = \frac{T_{\text{on}}}{T_{\text{s}}}, \quad \text{for } T_1, T_4,$$

and conversely

$$D' = \frac{T_{\text{on}}}{T_{\text{s}}} = (1 - D), \quad \text{for } T_2, T_3.$$

This leads to the average output voltage of

$$U_2 = (2D - 1)U_1. \tag{8.101}$$

- Also holds 2Q converter from Fig. 8.41.
- Boost mode follows analogously.

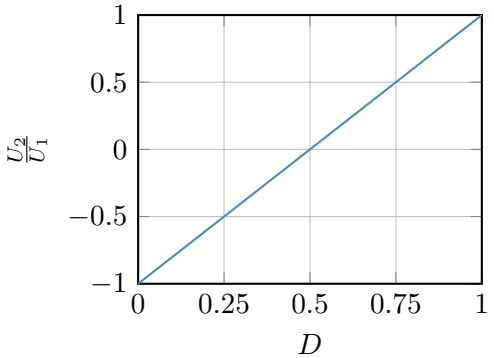

Fig. 8.43: Voltage gain for a buck converter with two voltage polarities

Section summary

This section introduced non-isolated DC-DC converters. The key takeaways are:

- **Buck converter:** step-down voltage conversion, voltage gain $0 \leq D \leq 1$,
- **Boost converter:** step-up voltage conversion, voltage gain $1 \leq \frac{1}{(1-D)}$.

From those basic topologies, we could derive all others:

- **(Inverting) buck-boost converter:** voltage gain $(-)\frac{D}{(1-D)}$,
- **(Inverting) boost-buck / Ćuk converter and SEPIC:** voltage gain $(-)\frac{D}{(1-D)}$.

Finally, we discussed the realization of converters for both current and voltage polarities by using bridge-type switch realizations. Also, we have emphasized the trade-off decisions between

- semiconductor utilization
- filter requirements / sizing,
- applied voltage gain as well as voltage and current signal quality.

Table of contents

Galvanic isolation

A definition

Galvanic isolation is a principle of decoupling functional sections of electrical circuits to prevent a direct current flow from input to output, that is, enabling different ground potentials for the circuit sections.

Typical reasons for requiring galvanic isolation are:

- Safety (prevention of electric shock),
- Noise reduction,
- contact corrosion reduction.

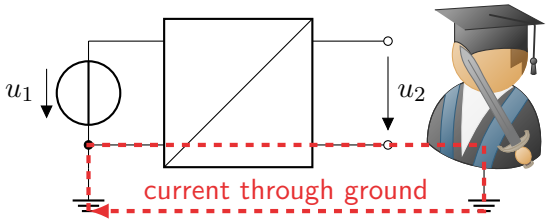

(a) Lack of galvanic isolation

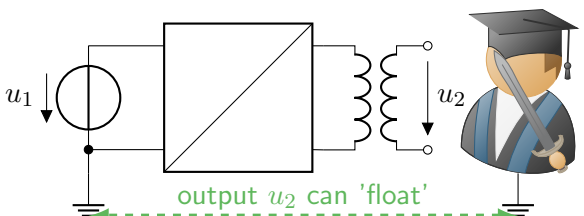

(b) Galvanic isolation via inductive separation

Fig. 9.1: Why galvanic isolation can be useful

Galvanic isolation: technical realization

Capacative

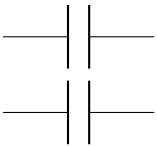

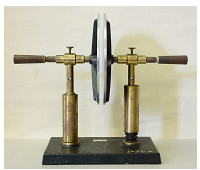

source: Wikimedia Commons, H. Grobe, CC BY 3.0

Optical

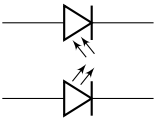

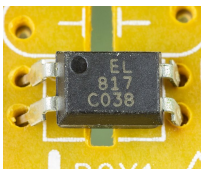

source: Wikimedia Commons, R. Spekking, CC BY-SA 4.0

Inductive

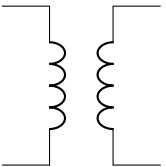

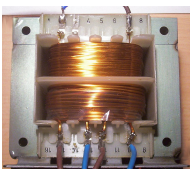

source: Wikimedia Commons, S. Riepl, public domain

Galvanic isolation via transformer

- In power electronics, transformers are mostly used to provide galvanic isolation.
- Reason: the power density per volume and weight is typically higher than for capacitive or optical isolation.
- Assumptions for the following model:
  - Ideal coupling (no leakage flux),
  - no losses,
  - no saturation.

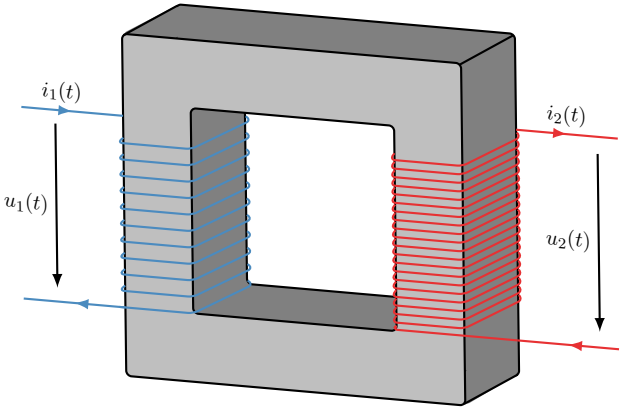

Fig. 9.2: Simple transformer with primary and secondary winding

Simplistic transformer model

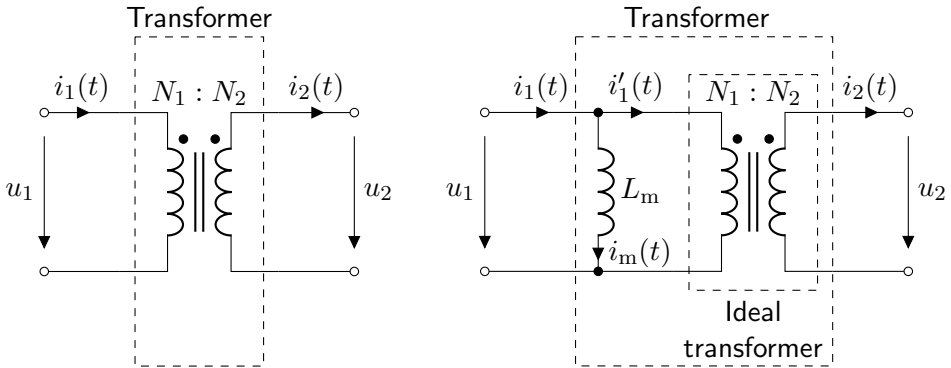

(a) Schematic symbol representation

(b) Equivalent circuit model

Fig. 9.3: Transformer model

Simplistic transformer model (cont.)

Based on Fig. 9.3 we consider the transformer as a combination of an ideal transformer with the conversion ratios

$$\frac{u_1(t)}{u_2(t)} = \frac{N_1}{N_2} \quad \text{and} \quad \frac{i_1'(t)}{i_2(t)} = \frac{N_2}{N_1} \tag{9.1}$$

and an inductor with the magnetizing inductance L_m:

$$u_1(t) = L_\mathrm{m}\frac{\mathrm{d}i_\mathrm{m}(t)}{\mathrm{d}t} \quad \text{and} \quad i_1(t) = i_1'(t) + i_\mathrm{m}(t). \tag{9.2}$$

- L_m models the magnetic energy stored in the transformer.
- Above model is a significant simplification (very first principle approach).
- More details on the transformer model can be found in the Electrical Machines and Drives course material.

Table of contents

Topology derivation based on the inverting buck-boost converter

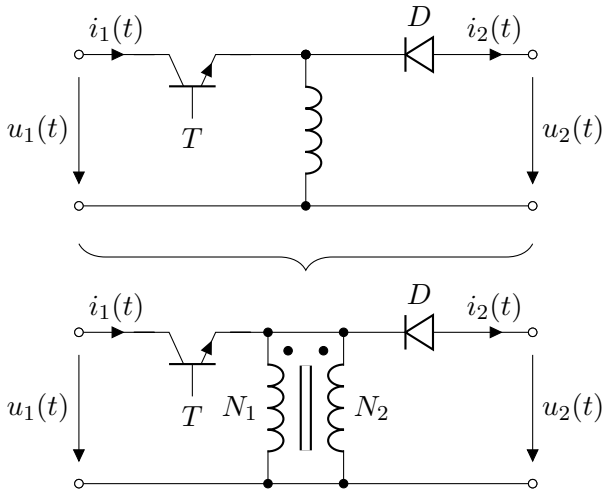

Topology derivation based on the inverting buck-boost converter (cont.)

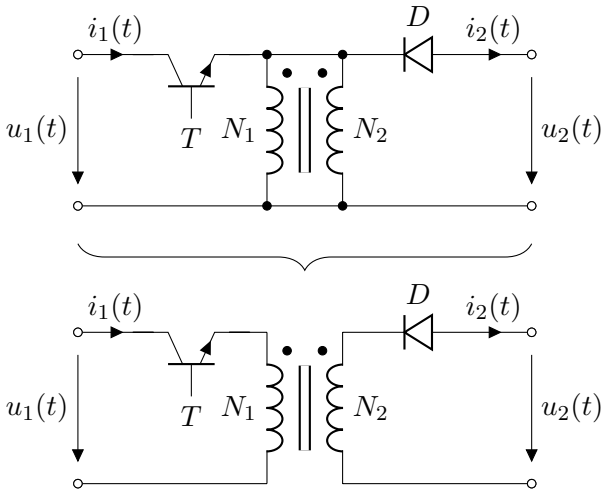

Flyback converter: topology

- Flyback converter = non-inverting, galvanically isolated buck-boost converter.
- Polarity change of primary and secondary transformer windings compensate for the inverting buck-boost characteristic.
- Transistor T is placed below the transformer to enable a fixed emitter / source potential (beneficial for driver).
- Transformer's magnetizing inductance serves as the converter's energy buffer.

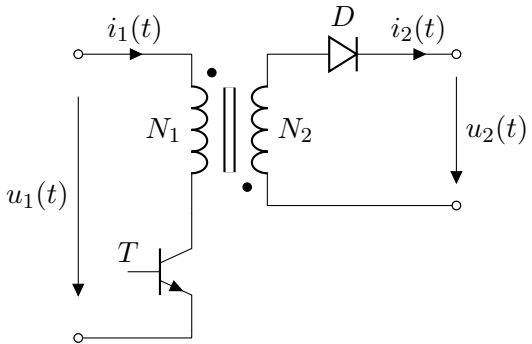

Fig. 9.4: Flyback converter topology

Flyback converter: switching states in CCM

- Switch-on time: rising primary current induces a negative voltage at the transformer's secondary winding leading to blocking diode. Energy is stored in L_{m}.
- Switch-off time: primary current is blocked by transistor and an equivalent current is induced in the secondary winding. Energy is taken from L_{m}.

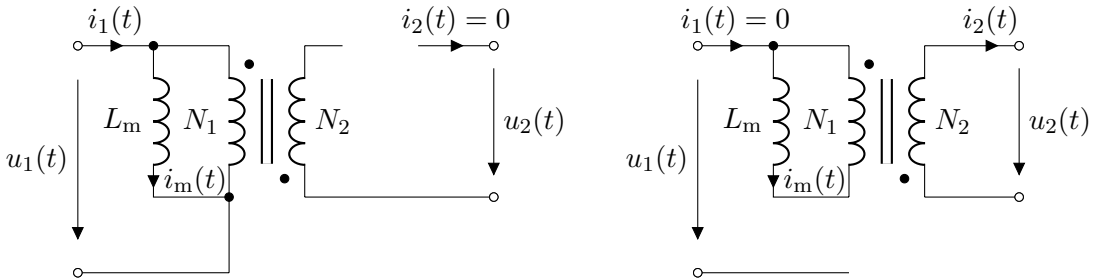

(a) Switch-on time

(b) Switch-off time

Fig. 9.5: Switch states of the flyback converter

Flyback converter: steady-state time-domain behavior in CCM

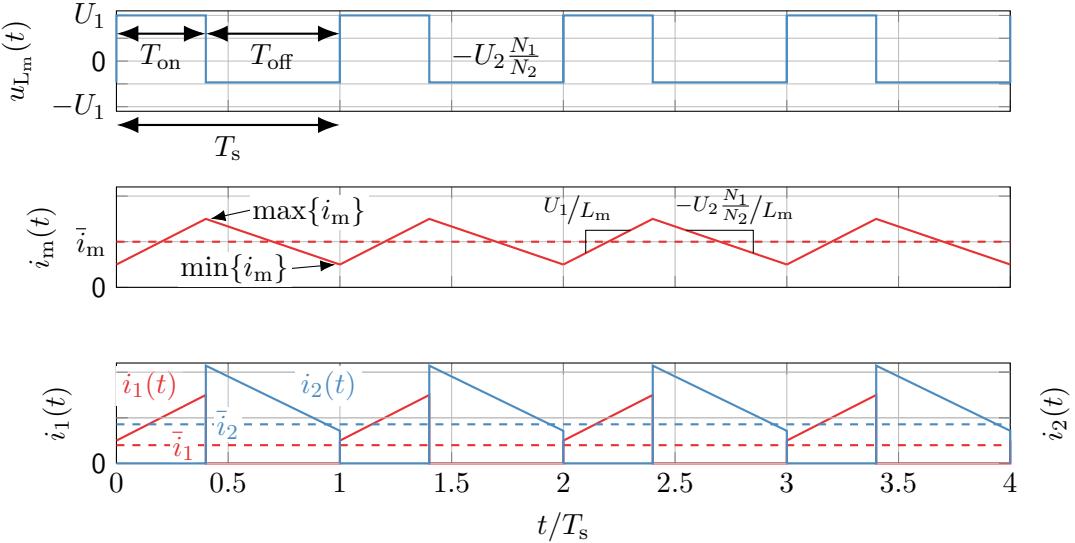

Flyback converter: impact of the transformer turns ratio

The transformer scales the peak input and output current according to the turns ratio N_2/N_1 (with ε being a small time period)

$$i_2(t = T_{\text{on}} + \varepsilon) = \frac{N_1}{N_2} i_1(t = T_{\text{on}} - \varepsilon),$$

i.e., the output side may carry significantly different peak currents than the input. Also, when the transistor blocks it must withstand the voltage

$$u_{\text{T}}(t) = u_1(t) + \frac{N_1}{N_2} u_2(t), \quad t \in [T_{\text{on}}, T_{\text{s}}].$$

Hence, the turn ratio has a significant impact on components' stress factors.

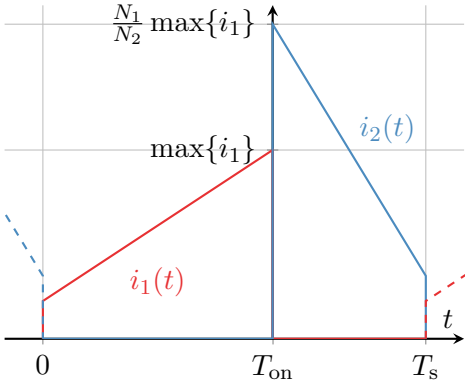

Fig. 9.6: Example of the ratio of the input and output current for $N_2/N_1 = 0.6$

Flyback converter: voltage transfer ratio in CCM

In CCM, the voltage balance of the magnetizing inductor L_m delivers:

$$u_{\mathrm{L_m}}(t) = \begin{cases} U_1, & t \in [kT_\mathrm{s}, kT_\mathrm{s} + T_\mathrm{on}], \\ -\frac{N_1}{N_2} U_2 & t \in [kT_\mathrm{s} + T_\mathrm{on}, (k+1)T_\mathrm{s}]. \end{cases} \tag{9.3}$$

In steady state, the average inductor voltage per period must be zero, yielding

$$U_1 T_\mathrm{on} = \frac{N_1}{N_2} U_2 T_\mathrm{off} \quad \Leftrightarrow \quad U_1 D T_\mathrm{s} = \frac{N_1}{N_2} U_2 (1-D) T_\mathrm{s} \quad \Leftrightarrow \quad \frac{U_2}{U_1} = \frac{N_2}{N_1} \frac{D}{1-D}. \tag{9.4}$$

- Structurally similar result to the (inverting/synchronous) buck-boost converter.
- The voltage transfer ratio is additionally scaled by the turns ratio N_2/N_1.
- The flyback's tranformer enables additional degrees of freedom to achieve a certain voltage transfer ratio via D and N_2/N_1.

Flyback converter: switch states in DCM

The flyback converter in DCM has three different switch states:

- Transistor on-time: $T_{\mathrm{on}} = DT_{\mathrm{s}}$,
- Transistor off-time (conducting diode): $T'_{\mathrm{off}} = D'T_{\mathrm{s}}$,
- Transistor off-time (no conduction): $T''_{\mathrm{off}} = T_{\mathrm{s}} - T_{\mathrm{on}} - T'_{\mathrm{off}}$.

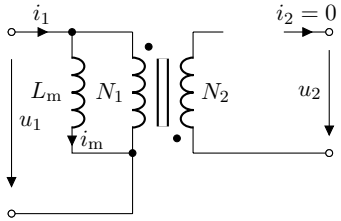

(a) Switch-on time T_{on}

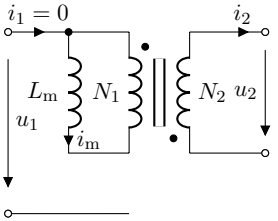

(b) Switch-off time T'_{off}

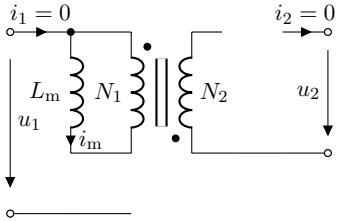

(c) Switch-off time T''_{off}

Fig. 9.7: Switch states of the flyback converter including DCM

Flyback converter: steady-state time-domain behavior in DCM

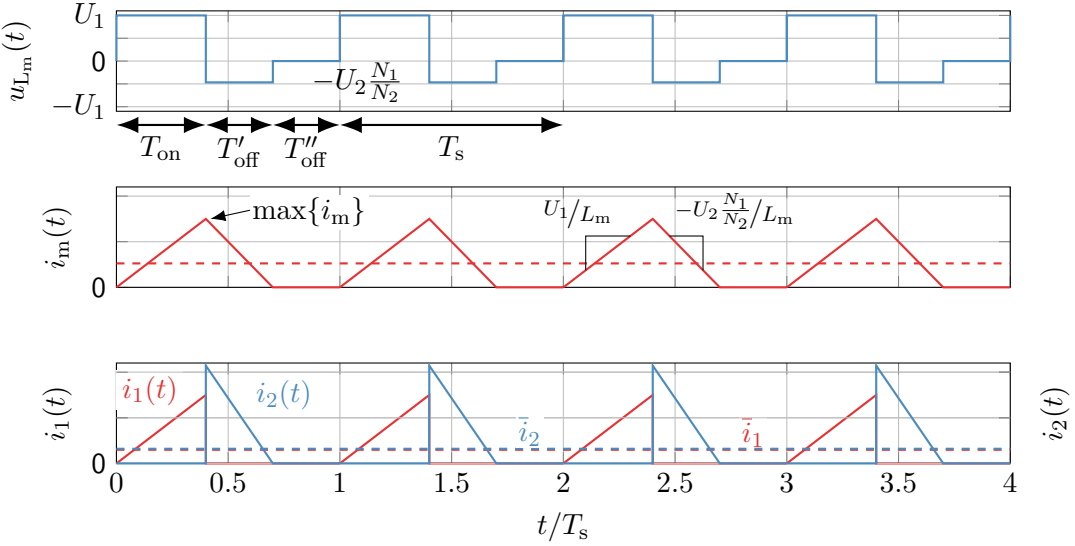

Flyback converter: DCM operation characteristics

In DCM operation

$$\bar{i}_{\mathrm{m}} < \frac{\Delta i_{\mathrm{m}}}{2} \quad \Rightarrow \quad U_2 \neq U_1 \frac{N_2}{N_1} \frac{D}{1-D}$$

applies due to the non-conducting diode during T''_{off}. To find the input-to-output voltage ratio in DCM, we again utilize the current ripple balance:

$$\begin{aligned} \Delta i_{\mathrm{m}} &= \frac{U_1}{L_{\mathrm{m}}} T_{\mathrm{on}} = \frac{U_1}{L_{\mathrm{m}}} D T_{\mathrm{s}} && \text{(rising edge)}, \\ \Delta i_{\mathrm{m}} &= \frac{N_1}{N_2} \frac{U_2}{L_{\mathrm{m}}} T'_{\mathrm{off}} = \frac{N_1}{N_2} \frac{U_2}{L_{\mathrm{m}}} D' T_{\mathrm{s}} && \text{(falling edge)}. \end{aligned} \tag{9.5}$$

Solving for D' yields

$$D' = \frac{N_2}{N_1} \frac{U_1}{U_2} D. \tag{9.6}$$

The average load current is

$$\bar{i}_2 = \frac{N_1}{N_2} \frac{\Delta i_{\mathrm{m}}}{2} \frac{T'_{\mathrm{off}}}{T_{\mathrm{s}}} = \frac{N_1}{N_2} \frac{\Delta i_{\mathrm{m,max}} D}{2} D' = \frac{N_1}{N_2} \frac{\Delta i_{\mathrm{m,max}}}{2} \frac{U_1}{U_2} D^2 \frac{N_2}{N_1} = \frac{\Delta i_{\mathrm{m,max}}}{2} \frac{U_1}{U_2} D^2. \tag{9.7}$$

Flyback converter: DCM operation characteristics (cont.)

Solving (9.7) delivers the flyback converter voltage gain in DCM as

$$\frac{U_2}{U_1} = \frac{D^2}{2} \frac{\Delta i_{\mathrm{m,max}}}{\bar{i}_2}. \tag{9.8}$$

Since $\Delta i_{\mathrm{m,max}}$ also depends on U_1, the relation (9.8) only holds for a given U_1. Hence, we can insert $\Delta i_{\mathrm{m,max}} = {}^{T_\mathrm{s} \cdot U_1}/_{L}$ in (9.7) and solve for U_2 to receive

$$U_2 = U_1^2 \frac{D^2}{2} \frac{T_\mathrm{s}}{L_\mathrm{m} \bar{i}_2}. \tag{9.9}$$

- Interestingly, the voltage gain in DCM seems independent of the turns ratio ${}^{N_2}/_{N_1}$.
- Reason: output voltage U_2 depends on the (average) output current $\bar{i}_2$ which is inversely scaled by the turns ratio – cf. cancelation of ${}^{N_2}/_{N_1}$ in (9.7).
- However, the transformer's magnetizing inductance is actually a function of the turns ratio $L_\mathrm{m}(N_1, N_2)$ (compare Electrical Machines and Drives course material).

Outlook: multi-port (flyback) converter

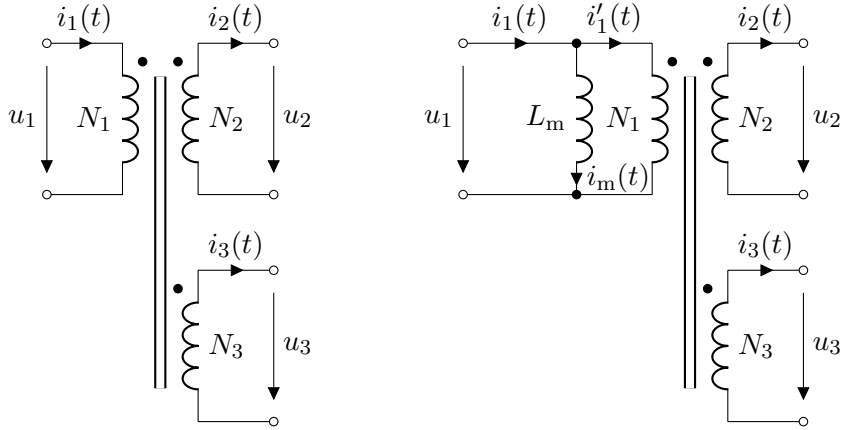

(a) Schematic symbol representation

(b) Equivalent circuit model

Fig. 9.8: Multi-port (flyback) transformer: add multiple secondary windings to a common core to enable different input-to-output voltage ratios

Table of contents

Topology derivation based on the buck converter

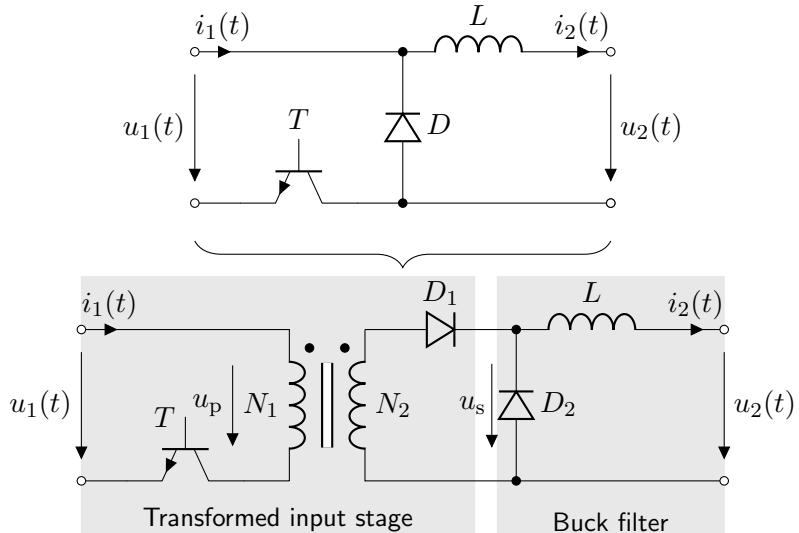

Forward converter: topology

- Forward converter = galvanically isolated buck converter.
- Main energy buffer: inductor L.
- Transformer: galvanic isolation plus voltage scaling:

$$u_{\mathrm{s}}(t) = \frac{N_2}{N_1} u_{\mathrm{p}}(t)$$

with $u_{\mathrm{p}}(t) = u_1(t), t \in [0, T_{\mathrm{on}}]$.

- Different to flyback, where the transformer's purpose is to provide both energy storage and galvanic isolation.

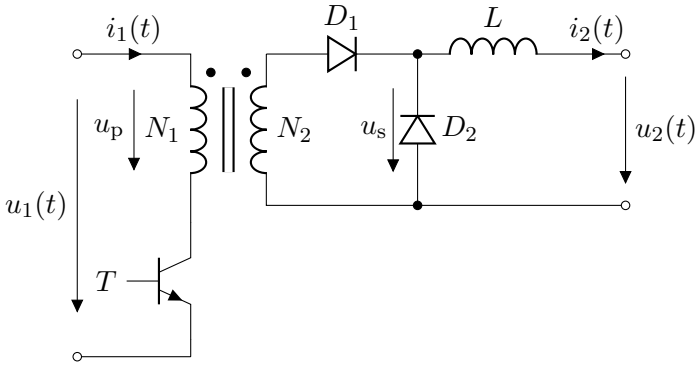

Fig. 9.9: Forward converter topology

Forward converter: steady-state time-domain behavior (ideal transformer)

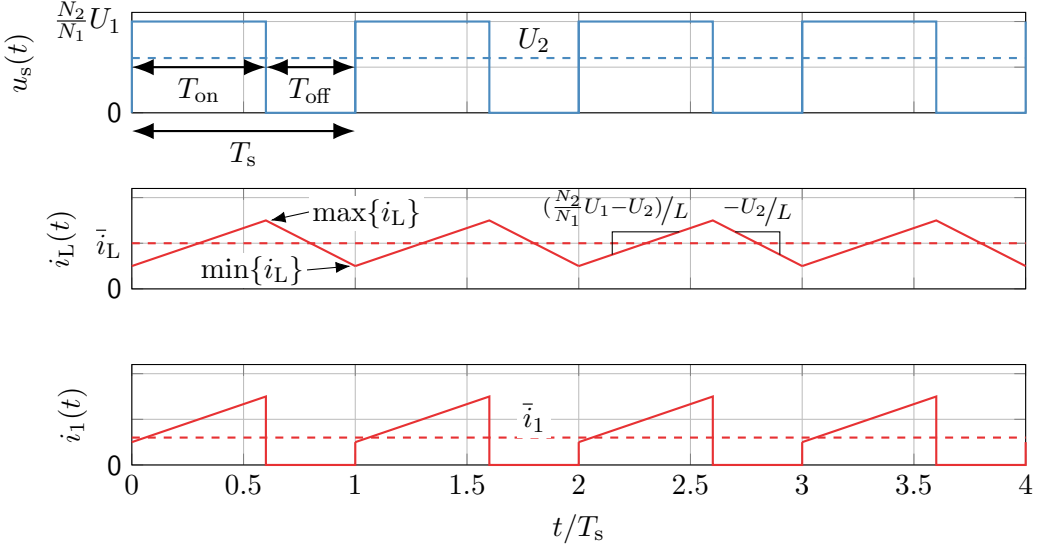

Forward converter: idealized steady-state operation

Assumption:

- The transformer is ideal and does not exhibit a magnetizing inductance.

Consequence:

- The transformer's secondary output voltage $u_\mathrm{s}(t)$ is a N_2/N_1 scaled version of the standard buck converter's switch voltage (compare Fig. 8.7).
- The (idealized) forward converter characteristics are analogous to the buck converter.

Hence, the voltage input-to-output voltage ratios for the (idealized) forward converter are:

$$\text{CCM:}\quad \frac{U_2}{U_1} = \frac{N_2}{N_1} D, \qquad \text{DCM:}\quad U_2 = \frac{N_2^2}{N_1^2} \frac{D^2 T_\mathrm{s} U_1^2}{D^2 T_\mathrm{s} \frac{N_2}{N_1} U_1 + 2L\bar{i}_2}. \tag{9.10}$$

Forward converter: magnetizing inductance issue

Magnetizing inductance

With every switching cycle the primary magnetizing current $i_\mathrm{m}(t)$ increases (i.e., transformer saturates and takes damage).

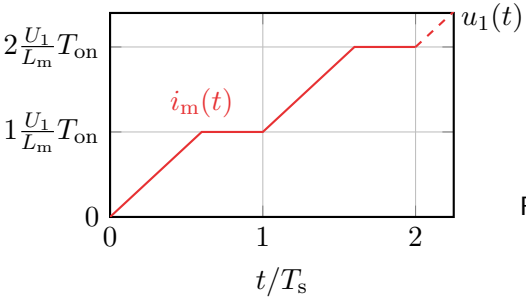

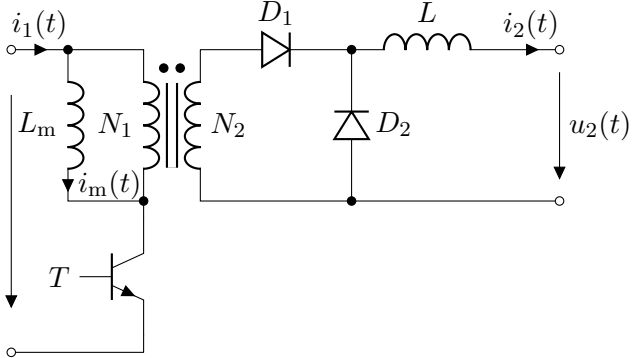

Fig. 9.10: Forward converter topology with primary magnetizing inductance

Forward converter: demagnetization via negative input voltage

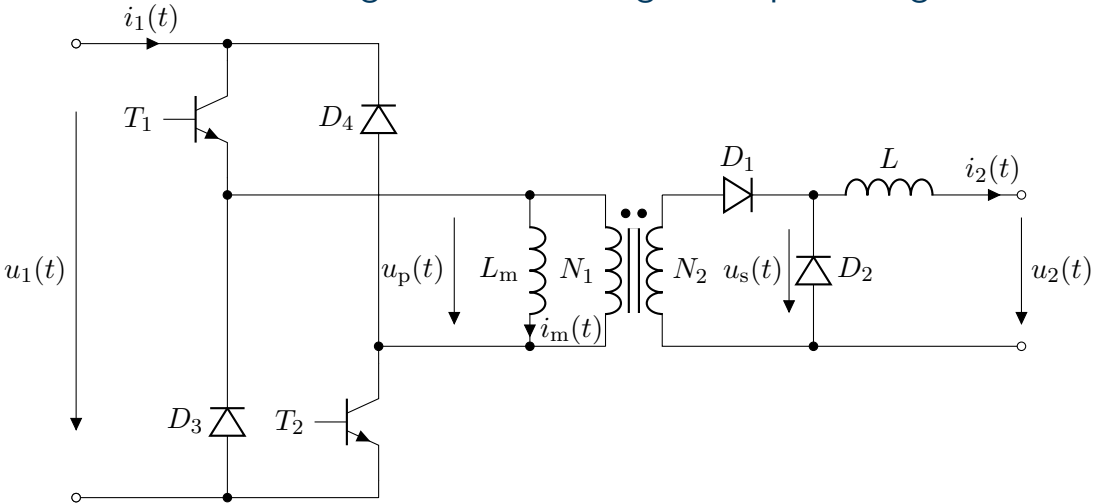

Fig. 9.11: Forward converter topology with an asymmetrical half-bridge

Forward converter: steady-state time-domain behavior (asym. half-bridge)

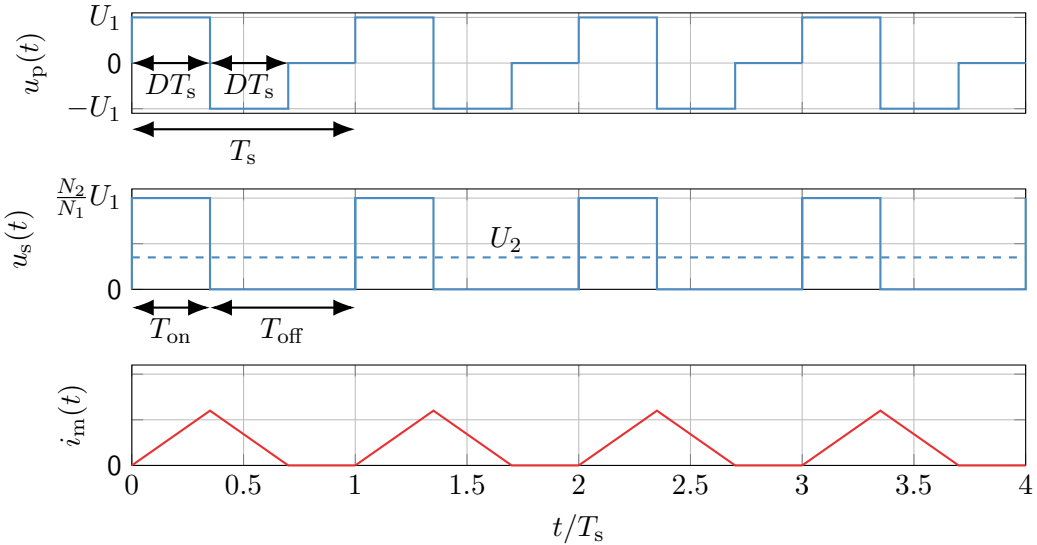

Forward converter with asym. half-bridge input stage

To demagnetize the transformer, the input voltage $u_{\mathrm{p}}(t)$ is modulated as follows:

$$u_{\mathrm{p}}(t) = \begin{cases} U_1, & t \in [kT_{\mathrm{s}}, kT_{\mathrm{s}} + DT_{\mathrm{s}}], \quad T_1 = T_2 = \mathrm{on}, \\ -U_1, & t \in [kT_{\mathrm{s}} + DT_{\mathrm{s}}, kT_{\mathrm{s}} + 2DT_{\mathrm{s}}], \quad T_1 = T_2 = \mathrm{off}, \\ 0, & t \in [kT_{\mathrm{s}} + 2DT_{\mathrm{s}}, kT_{\mathrm{s}} + T_{\mathrm{s}}], \quad T_1 = \mathrm{on},\ T_2 = \mathrm{off}. \end{cases} \tag{9.11}$$

Consequently, we have

$$\overline{u}_{\mathrm{L_m}} = \frac{1}{T_{\mathrm{s}}} \int_0^{T_{\mathrm{s}}} u_{\mathrm{p}}(t) \mathrm{d}t = 0 \tag{9.12}$$

and, therefore, the transformer's magnetizing current $i_{\mathrm{m}}(t)$ does not increase during a pulse period.However, this also limits the applicable duty cycle to

$$D \leq \frac{1}{2}$$

since otherwise (9.12) cannot be fulfilled.

Forward converter: demagnetization via negative input voltage (cont.)

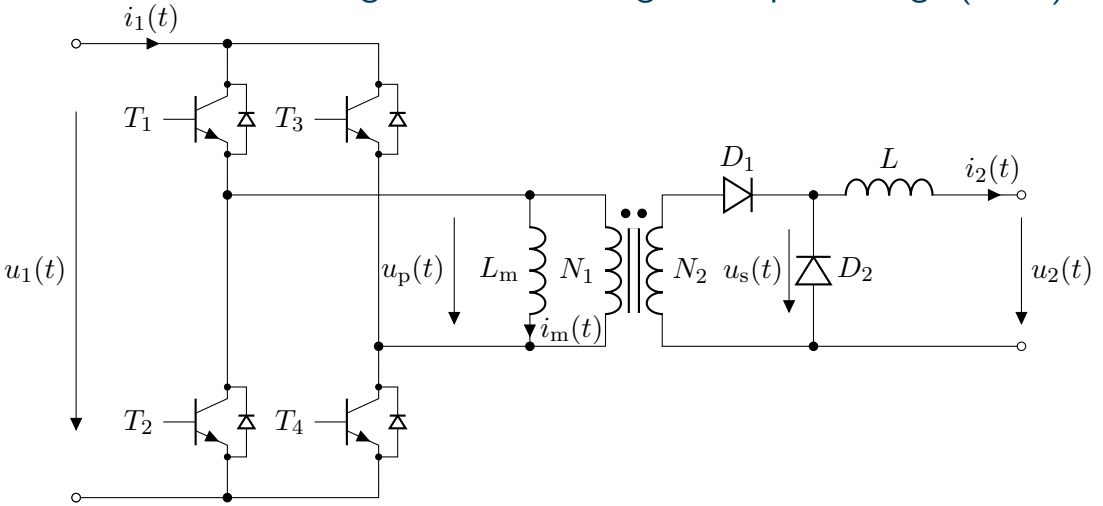

Fig. 9.12: Forward converter topology with a full-bridge

Forward converter: steady-state time-domain behavior (full-bridge)

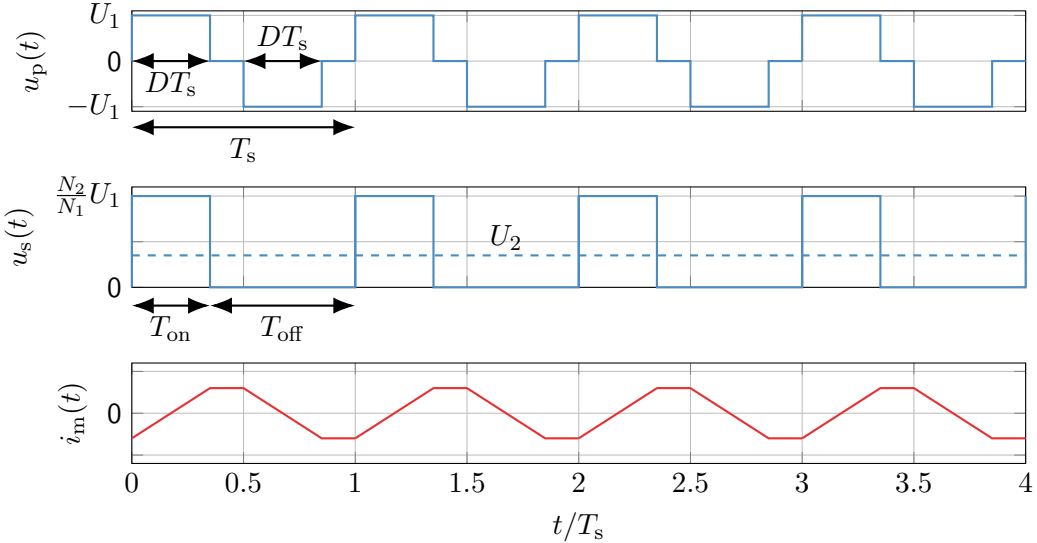

Forward converter: hysteresis curves of the transformer

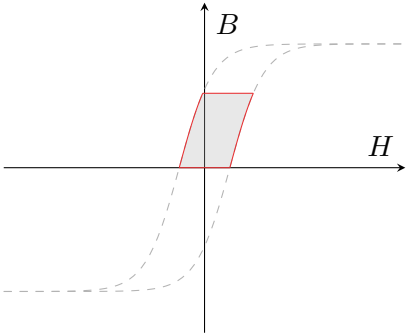

(a) Asym. half-bridge: utilizes only the upper half of the hysteresis curve due to non-negative magnetizing currents

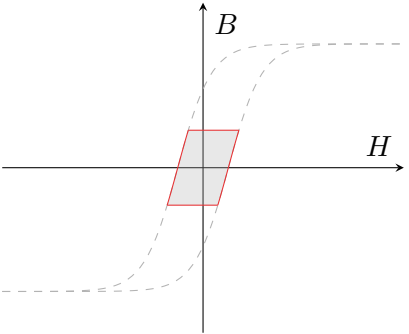

(b) Full-bridge: utilizes both positive and negative hysteresis curve parts due the four-quadrant input stage

Fig. 9.13: Hysteresis curves of the forward converter's transformer with different input stages (qualitative and simplified representation)

Forward converter with full-bridge input stage

The average input voltage $\overline{u}_\mathrm{p}$ of the full-bridge forward converter is conceptually identical to the asym. half-bridge variant and with the constraint

$$\overline{u}_{\mathrm{L_m}} = \frac{1}{T_\mathrm{s}} \int_0^{T_\mathrm{s}} u_\mathrm{p}(t)\mathrm{d}t = 0$$

the duty cycle also remains limited to

$$D \leq \frac{1}{2}.$$

However, the full-bridge realization comes with distinct differences compared to the asym. half-bridge:

- Utilizes magnetic core more efficiently, i.e., core can be made smaller or less winding turns are required.
- Effective switching frequency is doubled allowing for smaller filter components.
- Obvious disadvantage: more complex input stage (costs).

Forward converter with additional demagnetization winding

Alternative: transfer the idea of the flyback converter and add another winding N_3 to the transformer with reversed polarity. When T blocks, the energy stored in the transformer's magnetic field is inherited by N_3 and transferred back to the input.

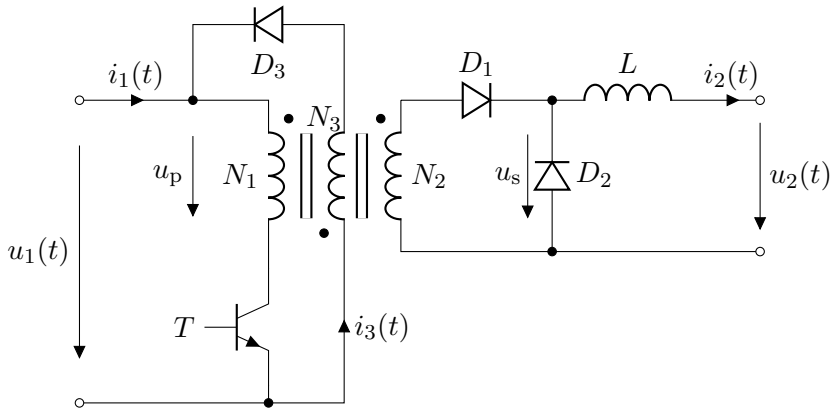

Fig. 9.14: Forward converter with demagnetization winding (aka single-ended forward converter)

Forward converter: steady-state time-domain behavior (demag. winding)

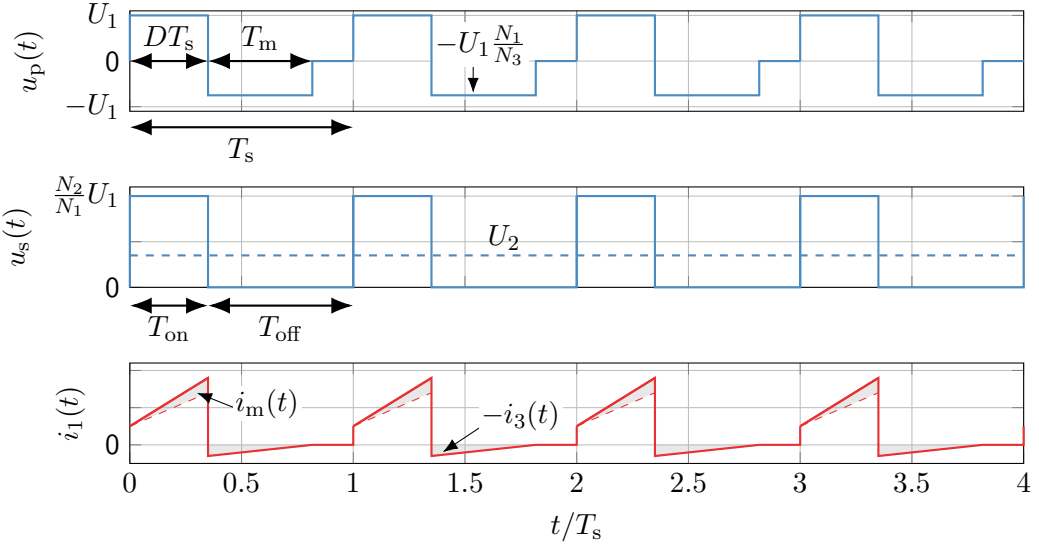

Forward converter with additional demagnetization winding (cont.)

The maximum magnetizing current is

$$\max\{i_{\mathrm{m}}(t)\} = i_{\mathrm{m}}(t = (k+D)T_{\mathrm{s}}) = \frac{U_1}{L_{\mathrm{m}}} D T_{\mathrm{s}} \tag{9.13}$$

which is reached at the end of the turn-on time T_{on}.After switching off the transistor, the winding N_3 takes over the magnetizing current leading to

$$\max\{|i_3(t)|\} = |i_3(t = (k+D)T_{\mathrm{s}})| = \frac{N_1}{N_3} \max\{i_{\mathrm{m}}(t)\} = \frac{N_1}{N_3} \frac{U_1}{L_{\mathrm{m}}} D T_{\mathrm{s}}. \tag{9.14}$$

To ensure that $i_{\mathrm{m}}(t = kT_{\mathrm{s}}) = 0$ holds at the next switch-on event, the voltage balance regarding the magnetizing inductance must be zero:

$$\overline{u}_{\mathrm{L_m}} = \frac{1}{T_{\mathrm{s}}} \int_0^{T_{\mathrm{s}}} u_{\mathrm{p}}(t)\mathrm{d}t = U_1 D T_{\mathrm{s}} - \frac{N_1}{N_3} U_1 T_{\mathrm{m}} = 0. \tag{9.15}$$

Here, T_{m} denotes the demagnetization time interval which results in

$$T_{\mathrm{m}} = \frac{N_3}{N_1} D T_{\mathrm{s}}. \tag{9.16}$$

Forward converter with additional demagnetization winding (cont.)

Since the transistor switch-on time already covers DT_s, the demagnetization time interval T_m is limited to

$$T_\mathrm{m} \leq (1-D)T_\mathrm{s}. \tag{9.17}$$

Combining (9.16) and (9.17) yields

$$\frac{N_3}{N_1} \leq \frac{1-D}{D} \quad \Leftrightarrow \quad D \leq \frac{N_1}{N_1+N_3} \tag{9.18}$$

as a threshold for the turns ratio to enable certain switch-on times.Also, it should be noted that the turns ratio directly influences the maximum blocking voltage of the transistor:

$$\max\{u_\mathrm{T}(t)\} = U_1 + U_1\frac{N_1}{N_3} = U_1\left(1+\frac{N_1}{N_3}\right). \tag{9.19}$$

Hence, to allow relatively high duty cycles by a high N_1 to N_3 ratio, cf. (9.18), the blocking voltage of the transistor increases.

Section summary

This section provided a (very) limited introduction to isolated DC-DC converters with the forward and flyback converters as examples.The key takeaways are:

- The forward converter is a buck-derived topology while the flyback converter is a buck-boost-derived topology.
- A transformer is used to provide galvanic isolation between input and output.
- Limiting the magnetiziation of the transformer is a key aspect in the operation of these converters to prevent saturation (nonlinear behavior, extra losses).

In addition, there are many other isolated topologies that are used in practice, e.g.,

- Push-pull converter,
- Isolated Ćuk / SEPIC variants,
- Boost-derived topologies with full-/half bridge input stages,
- ...

Table of contents

High-level view of the rectification task

Assuming that the input voltage is an ideal sinusoidal signal

$$u_1(t) = \hat{u}_1 \sin(\omega t)$$

with the angular frequency $\omega = 2\pi f$ and the amplitude $\hat{u}_1$, the task of a rectifier is to convert this input into a unidirectional, ideally constant, voltage $u_2(t) \approx u_2$, as shown in Figure 10.1. A typical application is the grid voltage rectification in power supplies.

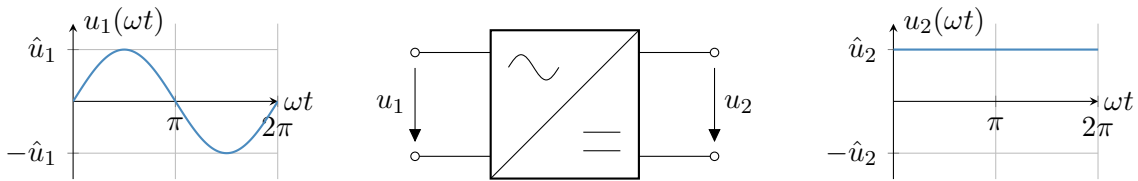

Fig. 10.1: Simplified representation of a single-phase rectifier

Frequency analysis: Fourier series

Often the rectification introduces non-fundamental frequency components, e.g., due to the output voltage rectification or by a load current feedback towards the input side. To analyze the frequency spectrum of a periodic signal $x(t)$, the Fourier series is used:

$$x(t) = \frac{a^{(0)}}{2} + \sum_{k=1}^{\infty} \left(a^{(k)} \cos(k\omega t) + b^{(k)} \sin(k\omega t) \right), \quad k \in \mathbb{N}, \tag{10.1}$$

$$a^{(k)} = \frac{1}{\pi} \int_0^{2\pi} u(t) \cos(k\omega t) \mathrm{d}\omega t, \; k \geq 0, \qquad b^{(k)} = \frac{1}{\pi} \int_0^{2\pi} u(t) \sin(k\omega t) \mathrm{d}\omega t, \; k \geq 1.$$

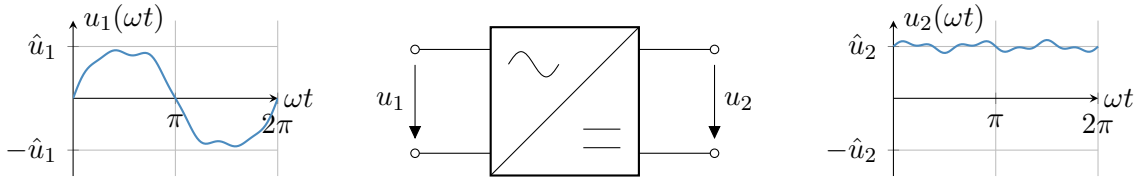

Fig. 10.2: Rectification under distorted conditions

Frequency analysis: Fourier series (cont.)

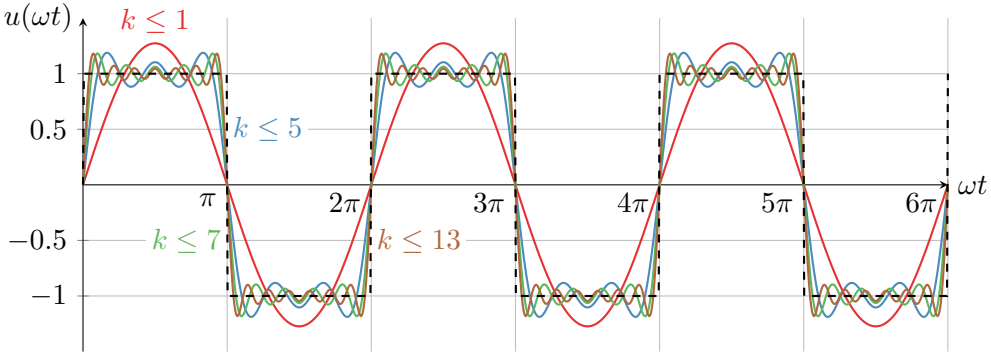

Fig. 10.3: Fourier series example: representation of a square wave signal

M1U uncontrolled rectifier circuit

Based on Fig. 10.4, the output voltage $u_2(t)$ of the M1U rectifier is

$$u_2(t) = \begin{cases} u_1(t) = \hat{u}_1 \sin(\omega t), & 0 \leq \omega t < \pi, \\ 0, & \pi \leq \omega t < 2\pi. \end{cases} \tag{10.2}$$

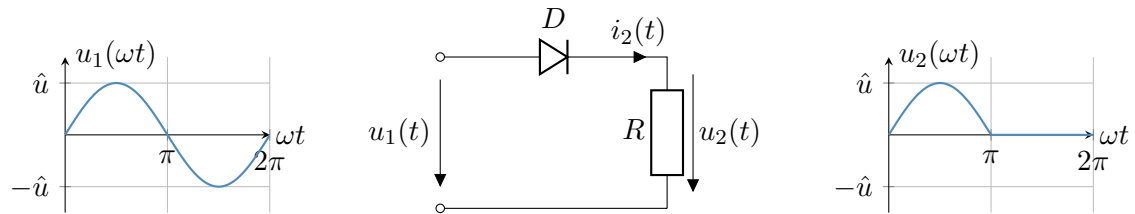

Fig. 10.4: M1U topology (aka single-pulse rectifier) with typical input and output voltage signals feeding a resistive load

M1U uncontrolled rectifier circuit (cont.)

From (10.2), the average output voltage of the M1U rectifier is

$$\begin{aligned}\overline{u}_2 &= \frac{1}{T}\int_0^T u_2(t)\mathrm{d}t = \frac{1}{2\pi}\int_0^{2\pi} u_2(\omega t)\mathrm{d}\omega t = \frac{1}{2\pi}\int_0^{\pi} \hat{u}_1 \sin(\omega t)\mathrm{d}\omega t \\ &= \frac{\hat{u}_1}{2\pi}\left[-\cos(\omega t)\right]_0^{\pi} = \frac{\hat{u}_1}{2\pi}\left(1+1\right) = \frac{\hat{u}_1}{\pi} = \frac{\sqrt{2}U_1}{\pi}\end{aligned} \tag{10.3}$$

with U_1 being the RMS value of the input voltage $u_1(t)$. The RMS value of the output voltage $u_2(t)$ results in

$$\begin{aligned}U_2 &= \sqrt{\frac{1}{2\pi}\int_0^{\pi} \hat{u}_1^2 \sin^2(\omega t)\mathrm{d}\omega t} = \hat{u}_1\sqrt{\frac{1}{2\pi}\left[\frac{1}{2}\omega t - \frac{\sin(2\omega t)}{4}\right]_0^{\pi}} \\ &= \frac{\hat{u}_1}{2} = \frac{U_1}{\sqrt{2}}.\end{aligned} \tag{10.4}$$

M1U uncontrolled rectifier circuit (cont.)

The Fourier coefficients of the output voltage $u_2(t)$ from (10.2) are

$$
\begin{aligned}
a^{(0)} &= \frac{1}{\pi}\int_0^{2\pi} u_2(t)\mathrm{d}\omega t = 2\overline{u}_2 = 2\frac{\hat{u}_1}{\pi}, \\
a^{(k)} &= \frac{1}{\pi}\int_0^{2\pi} u_2(t)\cos(k\omega t)\mathrm{d}\omega t = \frac{1}{\pi}\int_0^{\pi} \hat{u}_1\sin(\omega t)\cos(k\omega t)\mathrm{d}\omega t \\
&= \frac{\hat{u}_1}{2\pi}\int_0^{\pi} \sin(\omega t(1-k)) + \sin(\omega t(1+k))\mathrm{d}\omega t = \ldots = \begin{cases} \frac{\hat{u}_1}{\pi}\frac{2}{1-k^2}, & k = 2,4,6,\ldots \\ 0, & \text{otherwise.} \end{cases} \qquad (10.5) \\
b^{(k)} &= \frac{1}{\pi}\int_0^{2\pi} u_2(t)\sin(k\omega t)\mathrm{d}\omega t = \frac{1}{\pi}\int_0^{\pi} \hat{u}_1\sin(\omega t)\sin(k\omega t)\mathrm{d}\omega t \\
&= \frac{\hat{u}_1}{2\pi}\int_0^{\pi} \cos(\omega t(1-k)) - \cos(\omega t(k+1))\mathrm{d}\omega t = \ldots = \begin{cases} \frac{\hat{u}_1}{2}, & k = 1, \\ 0, & k \geq 2. \end{cases}
\end{aligned}
$$

Above, $a^{(0)}$ represents a DC component, while the $a^{(k)} \neq 0$ coefficients indicate harmonics.

M1U uncontrolled rectifier circuit (cont.)

From (10.5) the Fourier series of $u_2(t)$ results in

$$u_2(t) = \hat{u}_1 \left(\frac{1}{\pi} + \frac{1}{2} \sin(\omega t) + \sum_{k=2,4,6,\ldots} \frac{2}{\pi(1-k^2)} \cos(k\omega t) \right). \tag{10.6}$$

For a resistive load, the output current has the same harmonic spectrum:

$$i_2(t) = \frac{\hat{u}_1}{R} \left(\frac{1}{\pi} + \frac{1}{2} \sin(\omega t) + \sum_{k=2,4,6,\ldots} \frac{2}{\pi(1-k^2)} \cos(k\omega t) \right). \tag{10.7}$$

Resulting observations are:

- Non-fundamental current frequency components can distort the input side.
- Higher frequency harmonics decrease with $\sim 1/(1-k^2)$.

Transformer input filtering

To reduce the input side distortion, a transformer can be used to filter out the harmonics:

- Impedance of magnetizing inductance L_m is zero for DC components, i.e., the transformer blocks the DC current from the input (cf. dotted red line for $\bar{i}_2$ below).
- With higher frequency harmonics, the impedance of L_m increases, i.e., filtering out the harmonics less effectively.

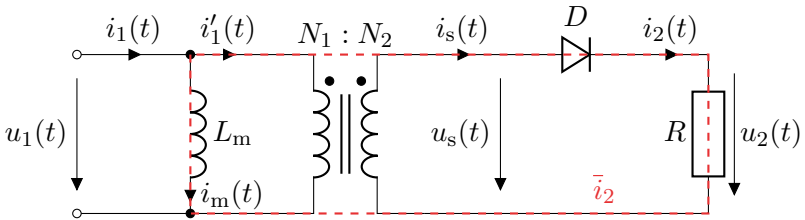

Fig. 10.5: M1U topology with input transformer and DC current path (red dotted line)

Transformer input filtering (cont.)

While the transformer can help out filter unwanted harmonics, the output DC current also introduces an offset magnetization to the transformer's core. Issues related with this are:

- **Core utilization:** To prevent core saturation, the transformer must be oversized.
- **Core losses:** The magnetization offset can increase the core losses.

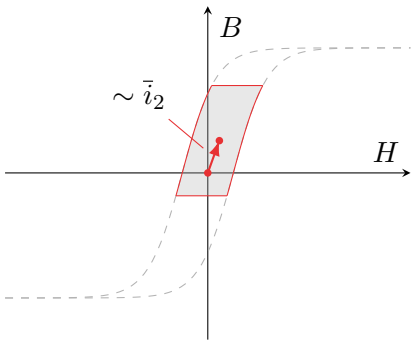

Fig. 10.6: Shift of the hysteresis curve due to the DC magnetization

Capacitive output filtering

To smooth the output voltage $u_2(t)$, a capacitor C is added. The initial charging voltage is

$$u_2(t) = \begin{cases} u_1(t) = \hat{u}_1 \sin(\omega t), & 0 \le \omega t < \pi/2, \\ \hat{u}_1, & \omega t > \pi/2 \end{cases} \tag{10.8}$$

with the capacitor current $i_2(t)$ being

$$i_2(t) = \begin{cases} C\mathrm{d}u_2(t)/\mathrm{d}t = \hat{i}_2 \cos(\omega t) = C\omega\hat{u}_1 \cos(\omega t), & 0 \le \omega t < \pi/2, \\ 0, & \omega t > \pi/2. \end{cases} \tag{10.9}$$

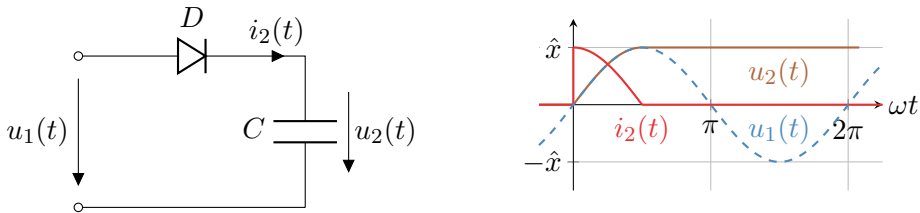

Fig. 10.7: M1U topology with output capacitor (unloaded and idealized charging curve)

Capacitive output filtering (cont.)

If the rectified output is loaded, the capacitor voltage ripples:

- If $u_2(t) \leq u_1(t)$: diode conducts, capacitor charges (follows input voltage).
- If $u_2(t) > u_1(t)$: diode blocks, capacitor discharges via I_0.

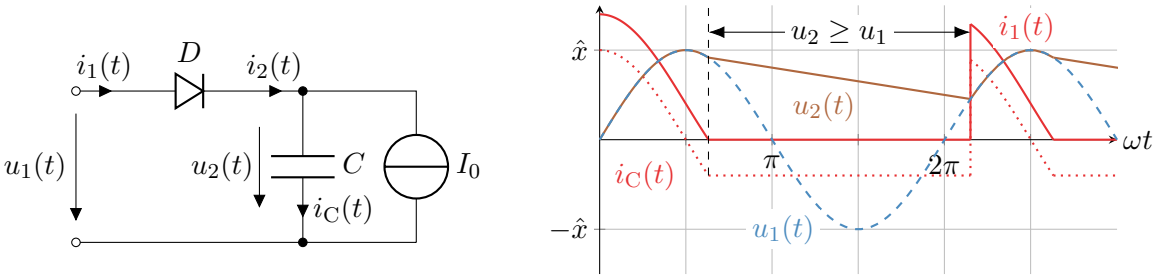

Fig. 10.8: M1U topology with output capacitor and constant load current

Table of contents

M2U uncontrolled rectifier circuit

The previous M1U topology only rectified half of a cycle resulting in a reduced output voltage utilization and increased voltage ripple. By adding another diode and utilizing a center-tapped transformer, the circuit can be extended towards a full-cycle rectifier.

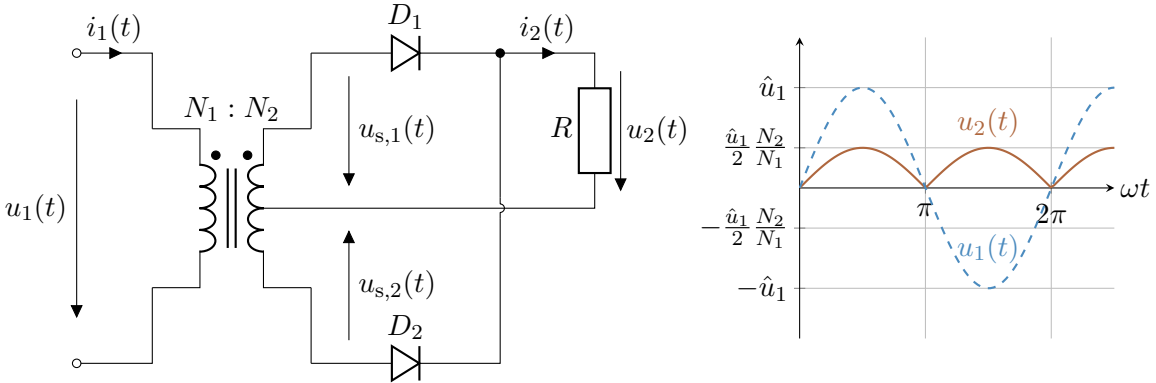

Fig. 10.9: M2U topology (aka two-pulse mid-point rectifier) with center-tapped transformer

M2U uncontrolled rectifier circuit (cont.)

From Fig. 10.9 we can conclude the following:

- During the positive half-cycle of $u_1(t)$: D_1 conducts, D_2 blocks, and $u_2(t) = u_{\mathrm{s},1}(t)$.
- During the negative half-cycle of $u_1(t)$: D_2 conducts, D_1 blocks, and $u_2(t) = u_{\mathrm{s},2}(t)$.

The output voltages of the center-tapped transformer are

$$u_{\mathrm{s},1}(t) = \frac{1}{2}\frac{N_2}{N_1}\hat{u}_1 \sin(\omega t) \quad \text{and} \quad u_{\mathrm{s},2}(t) = -\frac{1}{2}\frac{N_2}{N_1}\hat{u}_1 \sin(\omega t). \tag{10.10}$$

Here, it should be noted that both $u_{\mathrm{s},1}(t)$ and $u_{\mathrm{s},2}(t)$ are utilizing only half of the secondary winding turns due to the central tapping.The output voltage results in

$$u_2(t) = \frac{1}{2}\frac{N_2}{N_1}\left|u_1(t)\right| = \frac{1}{2}\frac{N_2}{N_1}\hat{u}_1 \left|\sin(\omega t)\right|. \tag{10.11}$$

M2U uncontrolled rectifier circuit (cont.)

From (10.11), the average output voltage of the M2U rectifier is

$$\begin{aligned}\overline{u}_2 &= \frac{1}{T}\int_0^T u_2(t)\mathrm{d}t = \frac{1}{2\pi}\int_0^{2\pi}\frac{1}{2}\frac{N_2}{N_1}\hat{u}_1\left|\sin(\omega t)\right|\mathrm{d}\omega t = \frac{1}{\pi}\int_0^{\pi}\frac{1}{2}\frac{N_2}{N_1}\hat{u}_1\sin(\omega t)\mathrm{d}\omega t \\ &= \frac{1}{2\pi}\frac{N_2}{N_1}\hat{u}_1\left[-\cos(\omega t)\right]_0^{\pi} = \frac{1}{2\pi}\frac{N_2}{N_1}\hat{u}_1\left(1+1\right) = \frac{1}{\pi}\frac{N_2}{N_1}\hat{u}_1.\end{aligned} \tag{10.12}$$

Not considering the transformer conversion via N_2/N_1, this is twice as much as in the M1U case, compare (10.3). The RMS value of the output voltage $u_2(t)$ results in

$$\begin{aligned}U_2 &= \sqrt{\frac{1}{2\pi}\frac{1}{2^2}\frac{N_2^2}{N_1^2}\hat{u}_1^2\int_0^{2\pi}\sin^2(\omega t)\mathrm{d}\omega t} = \frac{1}{2}\frac{N_2}{N_1}\hat{u}_1\sqrt{\frac{1}{\pi}\int_0^{\pi}\sin^2(\omega t)\mathrm{d}\omega t} \\ &= \frac{1}{2}\frac{N_2}{N_1}\hat{u}_1\sqrt{\frac{1}{2\pi}\left[\frac{1}{2}\omega t - \frac{\sin(2\omega t)}{4}\right]_0^{\pi}} = \frac{N_2}{N_1}\frac{\hat{u}_1}{\sqrt{2}} = \frac{N_2}{N_1}U_1.\end{aligned} \tag{10.13}$$

M2U uncontrolled rectifier circuit (cont.)

The Fourier coefficients of the output voltage $u_2(t)$ from (10.11) are

$$
\begin{aligned}
a^{(0)} &= \frac{1}{\pi}\int_0^{2\pi} u_2(t)\mathrm{d}\omega t = 2\overline{u}_2 = \frac{2}{\pi}\frac{N_2}{N_1}\hat{u}_1, \\
a^{(k)} &= \frac{1}{\pi}\int_0^{2\pi} u_2(t)\cos(k\omega t)\mathrm{d}\omega t = \frac{1}{2\pi}\frac{N_2}{N_1}\left(\int_0^{\pi} \hat{u}_1\sin(\omega t)\cos(k\omega t)\mathrm{d}\omega t\right. \\
&\quad \left. + \int_{\pi}^{2\pi}(-1)\hat{u}_1\sin(\omega t)\cos(k\omega t)\mathrm{d}\omega t\right) = \ldots = \begin{cases} \frac{\hat{u}_1}{\pi}\frac{N_2}{N_1}\frac{2}{1-k^2}, & k = 2,4,6,\ldots \\ 0, & \text{otherwise.} \end{cases} \qquad (10.14) \\
b^{(k)} &= \frac{1}{\pi}\int_0^{2\pi} u_2(t)\sin(k\omega t)\mathrm{d}\omega t = \frac{1}{2\pi}\frac{N_2}{N_1}\left(\int_0^{\pi} \hat{u}_1\sin(\omega t)\sin(k\omega t)\mathrm{d}\omega t\right. \\
&\quad \left. + \int_{\pi}^{2\pi}(-1)\hat{u}_1\sin(\omega t)\sin(k\omega t)\mathrm{d}\omega t\right) = \ldots = 0.
\end{aligned}
$$

These coefficients also indicate significant harmonics, which are in particular scaled by the transformer turns ratio.

Table of contents

B2U uncontrolled rectifier circuit

The B2U circuit also allows full-cycle rectification but without the need for a center-tapped transformer, that is, fully utilizes the input voltage without halving it on the output side.

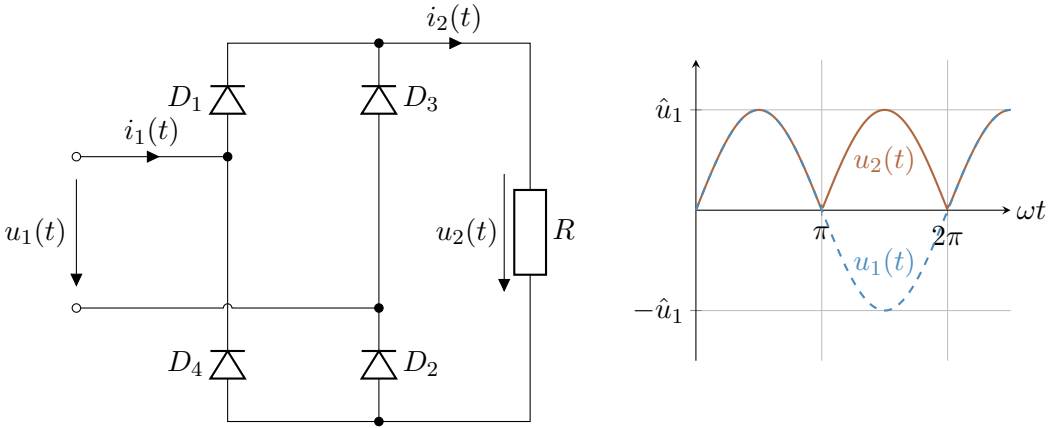

Fig. 10.10: B2U topology (aka two-pulse bridge rectifier) with resistive load

B2U uncontrolled rectifier circuit (cont.)

For a purely resistive load as in Fig. 10.10 the output voltage $u_2(t)$ is

$$u_2(t) = |u_1(t)| = \hat{u}_1 \left|\sin(\omega t)\right| . \tag{10.15}$$

Here, following diodes are conducting:

- Positive half-cycle: D_1 and D_2,
- Negative half-cycle: D_3 and D_4.

The average output voltage $\overline{u}_2$ is

$$\overline{u}_2 = \frac{1}{T}\int_0^T u_2(t)\mathrm{d}t = \frac{1}{2\pi}\int_0^{2\pi} \hat{u}_1 \left|\sin(\omega t)\right| \mathrm{d}\omega t = \ldots = \frac{2}{\pi}\hat{u}_1. \tag{10.16}$$

The Fourier coefficients of the output voltage $u_2(t)$ are analogous to the M2U case, compare (10.14) with appropriate scaling considering the lack of the center-tapped transformer.

B2U uncontrolled rectifier circuit with capacitive output filtering

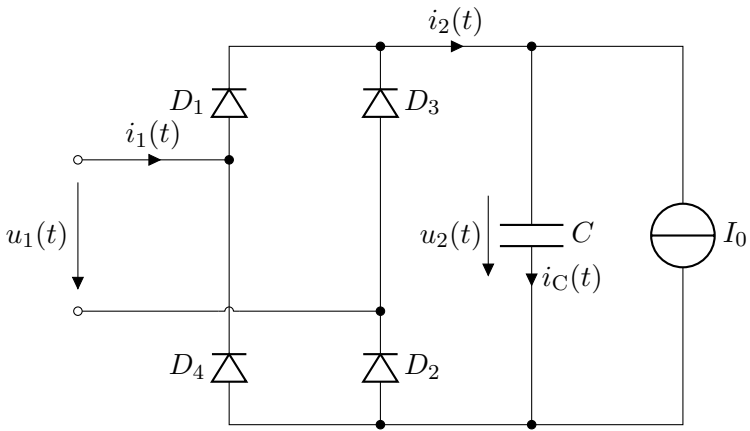

Fig. 10.11: B2U topology with output capacitor and constant load

B2U uncontrolled rectifier circuit with capacitive output filtering (cont.)

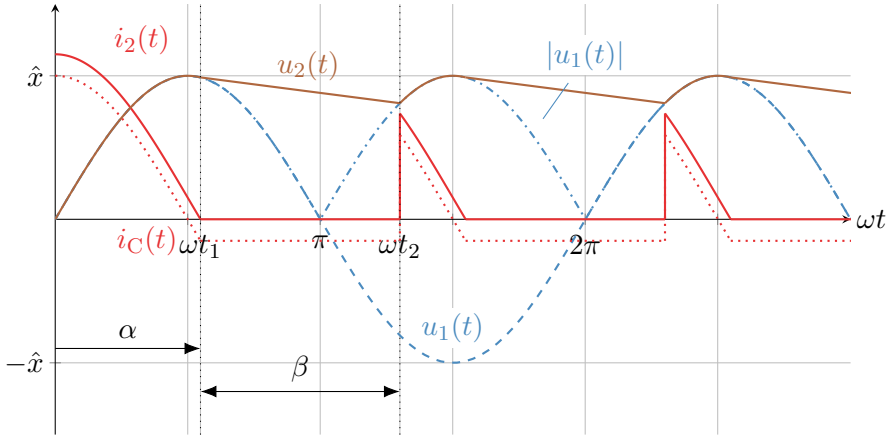

Fig. 10.12: Typical signal curves for B2U topology with output capacitor and constant load

B2U uncontrolled rectifier circuit with capacitive output filtering (cont.)

The filter capacitor current $i_{\mathrm{C}}(t)$ is

$$i_{\mathrm{C}}(t) = \begin{cases} -I_0, & i_2(t) = 0, \\ C\frac{\mathrm{d}}{\mathrm{d}t}u_2(t), & i_2(t) > 0, \end{cases} \tag{10.17}$$

that is, if the output current $i_2(t)$ is zero, the diode bridge blocks and the capacitor discharges via the load. Contrary, if the output current is positive, the diodes conduct and the capacitor voltage is determined by the rectified input voltage.The output current is given by

$$i_2(t) = i_{\mathrm{C}}(t) + I_0. \tag{10.18}$$

Inserting (10.17) in (10.18) delivers the output current during the conduction phase:

$$i_2(t) = C\omega\hat{u}_1 \cos(\omega t) + I_0, \quad 0 \leq \omega t < \omega t_1. \tag{10.19}$$

B2U uncontrolled rectifier circuit with capacitive output filtering (cont.)

The conduction phase lasts until $\omega t_1 = \alpha$ which can be determined from (10.19):

$$\alpha = \arccos\left(-\frac{I_0}{C\omega\hat{u}_1}\right). \tag{10.20}$$

For $\alpha < \omega t < \omega t_2$ the capacitor discharges via the load:

$$\begin{aligned} u_2(t) &= u_2(\omega t_1) + \int_{t_1}^{t} -\frac{I_0}{C}\mathrm{d}\tau = u_2(\alpha) + \int_{\alpha}^{\omega t} -\frac{I_0}{\omega C}\mathrm{d}\omega\tau \\ &= u_2(\alpha) - \frac{I_0}{\omega C}(\omega t - \alpha), \quad \omega t_1 \leq \omega t < \omega t_2. \end{aligned} \tag{10.21}$$

The blocking phase lasts until $\omega t_2 = \alpha + \beta$, that is, the rectified input voltage is equal to the capacitor voltage (note: not solvable for ωt_2 in closed-form, requires numerical methods):

$$u_2(\omega t_2) = u_2(\alpha) - \frac{I_0}{\omega C}(\omega t_2 - \alpha) \stackrel{!}{=} \hat{u}_1|\sin(\omega t_2)| = |u_1(\omega t_2)|. \tag{10.22}$$

B2U rectifier with capacitive output filtering and grid impedance

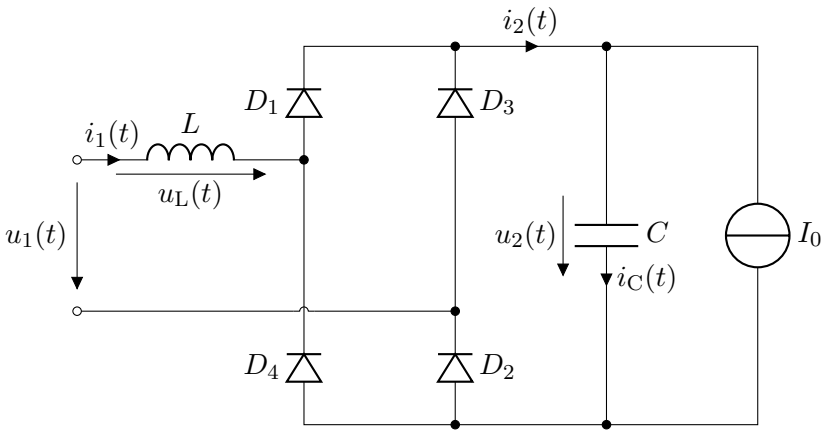

Fig. 10.13: B2U topology considering an output capacitor, constant load, and grid impedance

B2U rectifier with capacitive output filtering and grid impedance (cont.)

For the modified scenario form (10.13) we assume an infinite capacitance capacitor, i.e.,

$$u_2(t) \approx U_2$$

to keep the analysis simple. Like before, the diode bridge conduction is determined by the output current $i_2(t)$:

- $i_2(t) > 0$: diode bridge conducts, $u_{\mathrm{L}}(t) = |u_1(t)| - U_2$,
- $i_2(t) = 0$: diode bridge blocks, $u_{\mathrm{L}}(t) = \max\{0, |u_1(t)| - U_2\}$.

Hence, the B2U rectifier behavior is driven by the grid impedance current and the dynamics introduced by L. Similar to the previous analysis on DC-DC converters, the discontinuous conduction mode (DCM) and the boundary conduction mode (BCM) will be differentiated in the following.

B2U rectifier with capacitive output filtering and grid impedance (cont.)

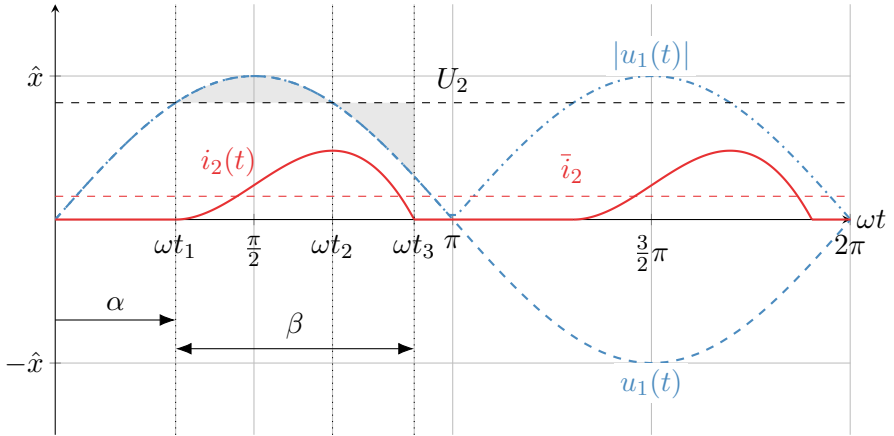

Fig. 10.14: Typical signal curves for B2U topology feeding a constant load from the grid and an infinite output capacitance in DCM

B2U rectifier with capacitive output filtering and grid impedance (cont.)

In steady-state DCM the output current is zero for

$$i_2(\omega t) = 0, \quad 0 \leq \omega t < \omega t_1. \tag{10.23}$$

Until then the diode bridge is in blocking mode and disconnects the input from the output. At $\omega t_1 = \alpha$ the diodes start conducting since the input voltage exceeds the output voltage:

$$u_1(\omega t_1 = \alpha) = \hat{u}_1 \sin(\alpha) \stackrel{!}{=} U_2 \quad \Leftrightarrow \quad \alpha = \arcsin\left(\frac{U_2}{\hat{u}_1}\right). \tag{10.24}$$

At this point, the output current is rising due to the positive inductor voltage:

$$\begin{aligned} i_2(\omega t) &= \frac{1}{L}\int_{t_1}^{t} u_1(t) - U_2 \mathrm{d}\tau = \frac{1}{\omega L}\int_{\omega t_1}^{\omega t} u_1(\omega\tau) - U_2 \mathrm{d}\omega\tau = \frac{1}{\omega L}\int_{\omega t_1}^{\omega t} \hat{u}_1 \sin(\omega\tau) - U_2 \mathrm{d}\omega\tau \\ &= \frac{\hat{u}_1}{\omega L}\left(\cos(\alpha) - \cos(\omega t) - \frac{U_2}{\hat{u}_1}(\omega t - \alpha)\right), \quad \omega t_1 \leq \omega t < \omega t_3. \end{aligned} \tag{10.25}$$

B2U rectifier with capacitive output filtering and grid impedance (cont.)

At $\omega t_2 = \alpha + \beta$ the current reaches zero again and the diode bridge blocks again:

$$\begin{aligned} i_2(\omega t_2) &= \frac{\hat{u}_1}{\omega L}\left(\cos(\alpha) - \cos(\omega t_2) - \frac{U_2}{\hat{u}_1}(\omega t_2 - \alpha)\right) \stackrel{!}{=} 0 \\ &\Leftrightarrow \cos(\alpha) - \cos(\alpha+\beta) - \beta\sin(\alpha) = 0. \end{aligned} \tag{10.26}$$

For a given α, this equation is not solvable in closed-form w.r.t. β and requires numerical methods. However, if β is known, α can be determined leading to

$$\alpha = \arctan\left(\frac{1-\cos(\beta)}{\beta - \sin(\beta)}\right). \tag{10.27}$$

The average output current in DCM is

$$\bar{i}_2 = \frac{1}{T}\int_0^T i_2(t)\mathrm{d}t = \frac{1}{\pi}\int_\alpha^{\alpha+\beta} i_2(\omega t)\mathrm{d}\omega t = \ldots = \frac{\hat{u}_1}{\pi\omega L}\left(\frac{\hat{u}_1}{U_2}(1-\cos(\beta)) - \frac{U_2}{\hat{u}_1}\frac{\beta^2}{2}\right). \tag{10.28}$$

B2U rectifier with capacitive output filtering and grid impedance (cont.)

For a better representation in the following, the average current is normalized:

$$\bar{i}_2' = \frac{\bar{i}_2}{\frac{2}{\pi}\frac{\hat{u}_1}{\omega L}} = \frac{1}{2}\left(\frac{\hat{u}_1}{U_2}(1-\cos(\beta)) - \frac{U_2}{\hat{u}_1}\frac{\beta^2}{2}\right). \tag{10.29}$$

Here, the denominator $2/\pi \cdot \hat{u}_1/\omega L$ is the absolute average value of the inductor current in case of a grid short circuit.

Based on the correlations found, the operating characteristics in DCM of the rectifier can be visualized, which has been implemented in Fig. 10.16 (left part):

- In DCM, $\beta \in [0, \pi[$ holds, i.e., the diode bridge is conducting for $0 \ldots 100\,\%$ per half cycle.
- At $\beta = \pi$ the diode bridge is conducting for the full half cycle (i.e., entering BCM).
- In order to achieve a commutation of the current between the diode pairs D1/D4 and D2/D3, the current gets zero (for a short time) so that the rectifier operates in BCM.

B2U rectifier with capacitive output filtering and grid impedance (cont.)

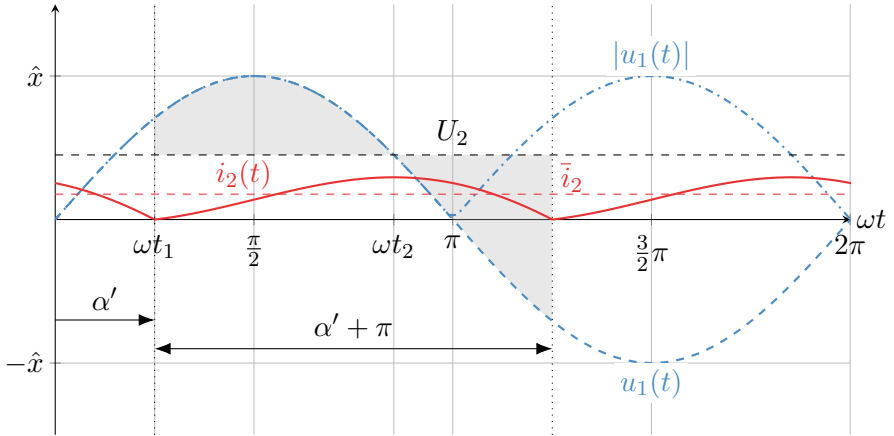

Fig. 10.15: Typical signal curves for B2U topology feeding a constant load from the grid and an infinite output capacitance in BCM

B2U rectifier with capacitive output filtering and grid impedance (cont.)

In steady-state BCM, the output current is analogous to the DCM as from (10.25) leading to

$$i_2(\omega t) = \frac{\hat{u}_1}{\omega L}\left(\cos(\alpha') - \cos(\omega t) - \frac{U_2}{\hat{u}_1}(\omega t - \alpha')\right), \quad \alpha' \leq \omega t < \alpha' + \pi \tag{10.30}$$

with α' being the phase angle at which the diodes start conducting in BCM – cf. Fig. 10.15. After a half cycle, the current reaches zero for a short moment enabling the diode bridge to commutate the current between the diode pairs:

$$i_2(\omega t = \alpha' + \pi) = 0 \quad \Leftrightarrow \quad \cos(\alpha') - \cos(\alpha' + \pi) - \frac{U_2}{\hat{u}_1}\pi = 0 \tag{10.31}$$

from which

$$\frac{U_2}{\hat{u}_1} = \frac{2}{\pi}\cos(\alpha') \tag{10.32}$$

follows after some intermediate calculation steps.

B2U rectifier with capacitive output filtering and grid impedance (cont.)

The average output current in BCM follows as

$$\begin{aligned}\bar{i}_2 &= \frac{1}{T}\int_0^T i_2(t)\mathrm{d}t = \frac{1}{\pi}\int_{\alpha'}^{\alpha'+\pi} i_2(\omega t)\mathrm{d}\omega t = \ldots \\ &= \frac{2}{\pi}\frac{\hat{u}_1}{\omega L}\sin(\alpha').\end{aligned} \tag{10.33}$$

Applying the same normalization as (10.29) leads to

$$\bar{i}_2' = \frac{\bar{i}_2}{\frac{2}{\pi}\frac{\hat{u}_1}{\omega L}} = \sin(\alpha'). \tag{10.34}$$

Combining (10.32) and (10.34) reveals

$$\frac{U_2}{\hat{u}_1} = \frac{2}{\pi}\cos(\arcsin(\bar{i}_2')). \tag{10.35}$$

The resulting load curve for the BCM is also depicted in Fig. 10.16 (right part).

B2U rectifier with capacitive output filtering and grid impedance (cont.)

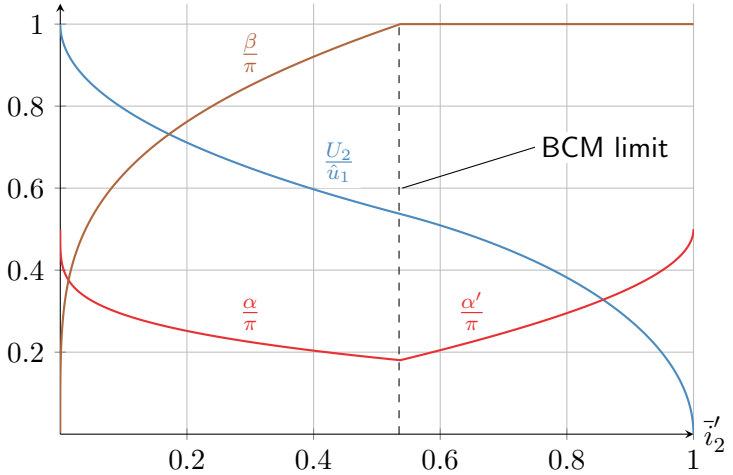

Fig. 10.16: Load curve of the B2U rectifier with capacitive output filtering and grid impedance

B2U rectifier with capacitive output filtering and grid impedance (cont.)

Assuming DCM, the input current of the B2U rectifier is

$$i_1(t) = \begin{cases} i_2(t), & \alpha \leq \omega t < \alpha + \beta, \\ -i_2(t), & \pi + \alpha \leq \omega t < \pi + \alpha + \beta. \end{cases} \tag{10.36}$$

The minus sign during the second half-cycle results from the conducting diodes D3/D4 reversing the current direction in the inductor – cf. Fig. 10.13. The input current can be decomposed into its fundamental and harmonic components:

$$i_1(t) = \underbrace{a_1 \cos(\omega t) + b_1 \sin(\omega t)}_{=i_1^{(1)}(t)} + \underbrace{\sum_{k=2}^{\infty} \Big(a^{(k)} \cos(k\omega t) + b^{(k)} \sin(k\omega t) \Big)}_{i_1^{(\mathrm{h})}(t)}, \quad k \in \mathbb{N}. \tag{10.37}$$

As will be discussed in the following, the harmonic components $i_1^{(\mathrm{h})}(t)$ are considered distortions negatively impacting the grid quality.

B2U rectifier with capacitive output filtering and grid impedance (cont.)

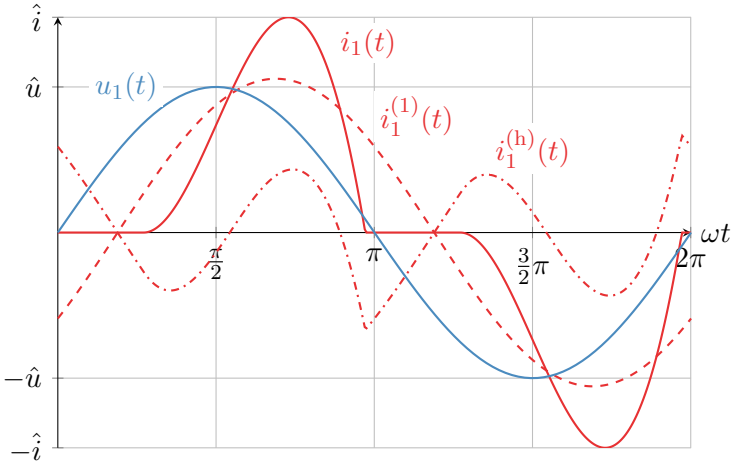

Fig. 10.17: Input current decomposition of the B2U rectifier with $i_1^{(1)}(t)$ being the fundamental and $i_1^{(\mathrm{h})}(t)$ harmonic components

Recap: active, reactive, and apparent power in sinusoidal steady-state

The complex power is defined as

$$\underline{S} = \underline{U} \cdot \underline{I}^* = P + \mathrm{j}Q = Se^{\mathrm{j}\varphi}, \tag{10.38}$$

with the active power P, the reactive power Q, and the apparent power S as well as $\underline{U}$ and $\underline{I}$ being the complex voltage and current phasors.From (10.38) directly follows:

$$S = |\underline{S}| = \sqrt{P^2 + Q^2}. \tag{10.39}$$

The power factor λ is defined as

$$\lambda = \cos(\varphi) = \frac{P}{S}. \tag{10.40}$$

Typically, one tries to operate power converters with a unity power factor $\lambda \approx 1$ to avoid reactive power transfer (i.e., additional reactive currents leading to more losses in the grid).

Active power transfer considering harmonics

The active power can be alternatively expressed as the average of the instantaneous power:

$$P = \frac{1}{T}\int_0^T p(t)\mathrm{d}t = \frac{1}{2\pi}\int_0^{2\pi} u(\omega t)i(\omega t)\mathrm{d}\omega t. \tag{10.41}$$

To generalize the analysis for arbitrary voltage and current harmonics, we consider both Fourier decompositions

$$u(\omega t) = \overline{u} + \sum_{k=1}^{\infty} \hat{u}^{(k)} \cos(k\omega t - \varphi_u^{(k)}), \quad i(\omega t) = \overline{i} + \sum_{k=1}^{\infty} \hat{i}^{(k)} \cos(k\omega t - \varphi_i^{(k)}) \tag{10.42}$$

with $\overline{u}$ and $\overline{i}$ being the DC components, $\hat{u}^{(k)}$ and $\hat{i}^{(k)}$ the amplitudes of the k-th harmonic and $\varphi_u^{(k)}$ and $\varphi_i^{(k)}$ the phase angles of the voltage and current harmonics.This amplitude-phase representation is analogous to (10.1) with the relations:

$$\hat{x}^{(k)} = \sqrt{(a^{(k)})^2 + (b^{(k)})^2}, \quad \varphi_x^{(k)} = -\arccos\left(\frac{a^{(k)}}{\hat{x}^{(k)}}\right) \cdot \mathrm{sign}\left(b^{(k)}\right). \tag{10.43}$$

Active power transfer considering harmonics (cont.)

Substituting the Fourier series of $u_1(\omega t)$ and $i_1(\omega t)$ into the instantaneous power expression delivers:

$$\begin{aligned} p(t) &= u(\omega t) i(\omega t) \\ &= \left(\overline{u} + \sum_{k=1}^{\infty} \hat{u}^{(k)} \cos(k\omega t - \varphi_u^{(k)}) \right) \left(\overline{i} + \sum_{m=1}^{\infty} \hat{i}^{(m)} \cos(m\omega t - \varphi_i^{(m)}) \right). \end{aligned}$$

Expanding this product yields:

$$\begin{aligned} p(t) = \overline{u}\overline{i} &+ \overline{u} \sum_{m=1}^{\infty} \hat{i}^{(m)} \cos(m\omega t - \varphi_i^{(m)}) + \overline{i} \sum_{k=1}^{\infty} \hat{u}^{(k)} \cos(k\omega t - \varphi_u^{(k)}) \\ &+ \sum_{k=1}^{\infty} \sum_{m=1}^{\infty} \hat{u}^{(k)} \hat{i}^{(m)} \cos(k\omega t - \varphi_u^{(k)}) \cos(m\omega t - \varphi_i^{(m)}). \end{aligned}$$

Active power transfer considering harmonics (cont.)

Using the trigonometric identities the last term becomes:

$$\sum_{k=1}^{\infty}\sum_{m=1}^{\infty}\hat{u}^{(k)}\hat{i}^{(m)}\cos(k\omega t-\varphi_u^{(k)})\cos(m\omega t-\varphi_i^{(m)})$$
$$=\sum_{k=1}^{\infty}\sum_{m=1}^{\infty}\hat{u}^{(k)}\hat{i}^{(m)}\frac{1}{2}\left[\cos((k-m)\omega t+\varphi_i^{(k)}-\varphi_u^{(m)})+\cos((k+m)\omega t-\varphi_u^{(k)}-\varphi_i^{(m)})\right].$$

Hence, we receive integral terms of the form

$$\int_0^{2\pi}\cos(n\omega t+\varphi)\mathrm{d}\omega t=\begin{cases}2\pi\cos(\varphi), & n=0,\\ 0 & n\neq 0\end{cases}$$

with $n=k-m\in\mathbb{Z}$ or $n=k+m\in\mathbb{Z}$, respectively. Due to the periodicity and symmetry of the cosine function, the integral over a full period is zero for $n\neq 0$.

Conclusion: Cross-frequency terms ($k\neq m$) cancel due to their oscillatory nature, leaving only contributions from voltage and current harmonics of the same order ($k=m$).

Active power transfer considering harmonics (cont.)

Summarizing the previous considerations, the active power can be expressed as:

$$P = \frac{1}{T}\int_0^T p(t)\,\mathrm{d}t = \sum_{k=1}^{\infty} \frac{\hat{u}^{(k)}\hat{i}^{(k)}}{2}\cos(\varphi_i^{(k)} - \varphi_u^{(k)}). \tag{10.44}$$

Inserting the B2U ideal input voltage assumption $u(t) = u_1(t) = \hat{u}_1 \sin(\omega t)$, this boils down to:

$$P = \frac{\hat{u}_1\hat{i}_1^{(1)}}{2}\cos(\varphi_i^{(1)} - \varphi_u^{(1)}) = U_1 I_1^{(1)}\cos(\varphi_i^{(1)} - \varphi_u^{(1)}) \tag{10.45}$$

with U_1 and $I_1^{(1)}$ being the RMS values of the fundamental voltage and current component and $\varphi_i^{(1)}$ the phase angle between the fundamental voltage and current component. The power factor results in

$$\lambda = \frac{P}{S} = \frac{U_1 I_1^{(1)}}{U_1 I_1}\cos(\varphi_i^{(1)} - \varphi_u^{(1)}) = \frac{I_1^{(1)}}{I_1}\cos(\varphi_i^{(1)} - \varphi_u^{(1)}). \tag{10.46}$$

i.e., the harmonics increase the apparent power S but do not contribute to the active power P. Consequently, the B2U's power factor is typically limited to $70\,\%$ or lower.

Total harmonic distortion (THD)

Another important measure for the quality of the input current is the total harmonic distortion (THD):

$$\mathrm{THD}(i_1) = \frac{\sqrt{\sum_{k=2}^{\infty} \left(I_1^{(k)}\right)^2}}{I_1^{(1)}} = \frac{I_1^{(\mathrm{h})}}{I_1^{(1)}}. \tag{10.47}$$

The THD quantifies the ratio of the RMS value of the harmonic components to the RMS value of the fundamental component.Rewriting the decomposition (10.37) in the RMS form

$$I_1^2 = \left(I_1^{(1)}\right)^2 + \left(I_1^{(\mathrm{h})}\right)^2, \tag{10.48}$$

and inserting (10.47) in the power factor expression (10.46) leads to

$$\lambda = \frac{1}{\sqrt{1 + \mathrm{THD}^2(i_1)}} \cos(\varphi_i^{(1)} - \varphi_u^{(1)}). \tag{10.49}$$

Hence, the larger the THD, the more the power factor deviates from unity.

B2U rectifier: THD and power factor

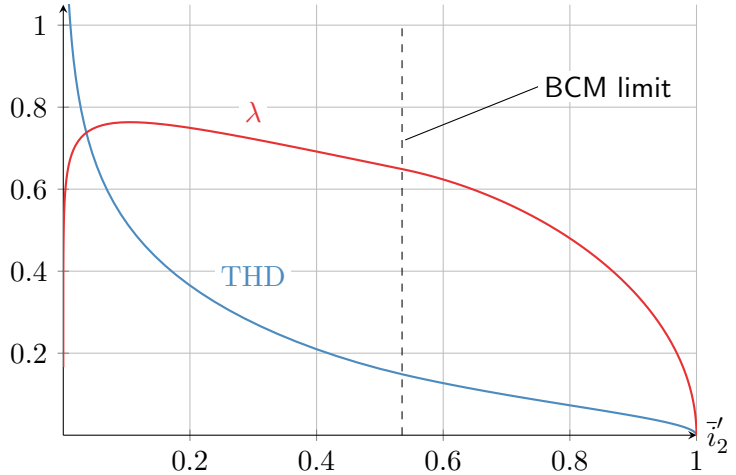

Fig. 10.18: THD and power factor of the B2U rectifier with capacitive output filtering and grid impedance

B2U rectifier impact on the grid voltage

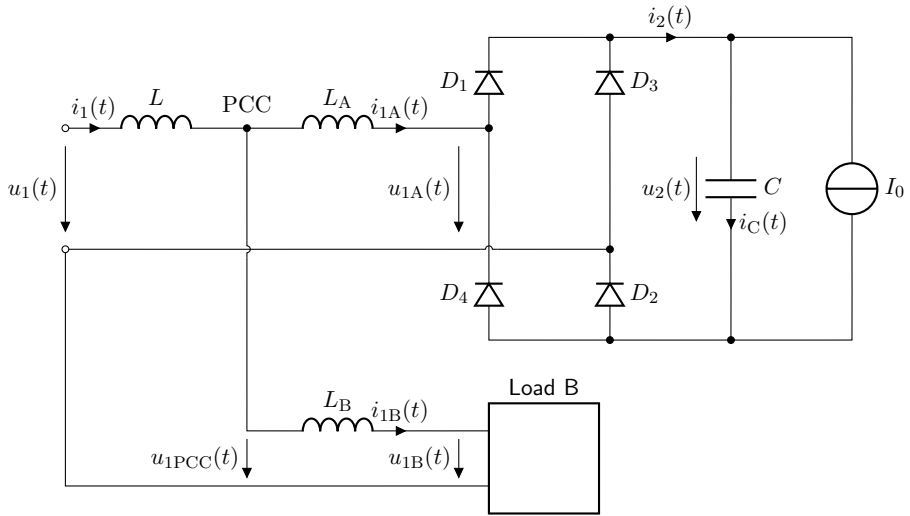

Fig. 10.19: B2U rectifier and a second load connected to the grid

B2U rectifier impact on the grid voltage (cont.)

In Fig. 10.19 the B2U rectifier and a second load are connected to the grid $u_1(t)$ with

- L being the grid inductance (at the point of common coupling – PCC),
- L_A being the inductance of the cable connecting the B2U rectifier to the PCC,
- L_B being the inductance of the cable connecting the second load to the PCC.

Assuming $i_{1\mathrm{B}}(t) = 0$ for the sake of simplicity, the inductive voltage divider rule yields

$$\frac{u_1(t) - u_{1\mathrm{PCC}}(t)}{u_1(t) - u_{1\mathrm{A}}(t)} = \frac{L}{L + L_\mathrm{A}} \tag{10.50}$$

and, therefore, the voltage at the second load's PCC $u_{1\mathrm{PCC}}(t)$ is

$$u_{1\mathrm{PCC}}(t) = u_1(t) - \frac{L}{L + L_\mathrm{A}}(u_1(t) - u_{1\mathrm{A}}(t)). \tag{10.51}$$

B2U rectifier impact on the grid voltage (cont.)

Assuming again a constant output voltage $u_2(t) = U_2$ (due to an infinite filter capacitance), the B2U's input voltage is

$$u_{1\mathrm{A}}(t) = \begin{cases} u_1(t), & i_{1\mathrm{A}}(t) = 0 \\ \mathrm{sign}(i_2(t)) \cdot U_2, & i_{1\mathrm{A}}(t) \neq 0. \end{cases} \tag{10.52}$$

Hence, the voltage at the second load's PCC is

$$u_{1\mathrm{PCC}}(t) = \begin{cases} u_1(t), & i_{1\mathrm{A}}(t) = 0 \\ u_1(t)\left(1 - \frac{L}{L+L_\mathrm{A}}\right) + \frac{L}{L+L_\mathrm{A}}\mathrm{sign}(i_2(t)) \cdot U_2, & i_{1\mathrm{A}}(t) \neq 0. \end{cases} \tag{10.53}$$

As on can see on the next slide, the B2U rectifier operation leads to a distorted grid voltage $u_{1\mathrm{PCC}}(t)$ which might impair the operation of the second load. Increasing the input inductance L_A by an explicit filter inductor can mitigate this issue, however, at the expense of volume, weight and cost as well as voltage drop associated with the input filter inductor.

B2U rectifier impact on the grid voltage (cont.)

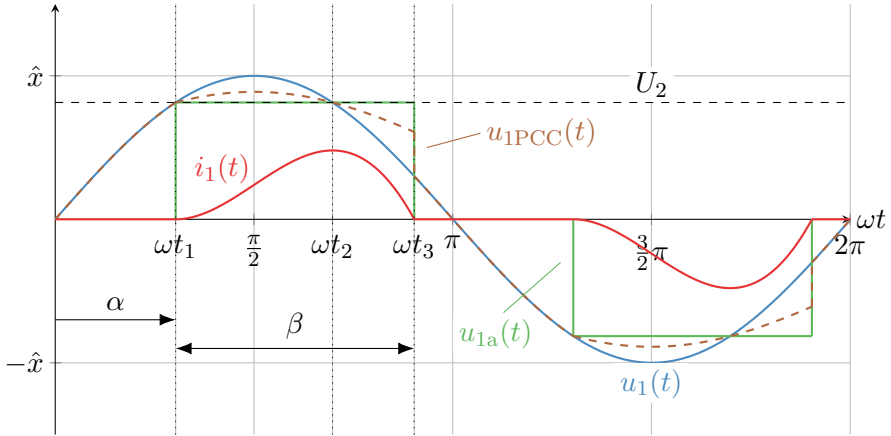

Fig. 10.20: Relevant signals of the scenario from (10.19) with B2U in DCM

B2U rectifier impact on the neutral line in three-phase grid

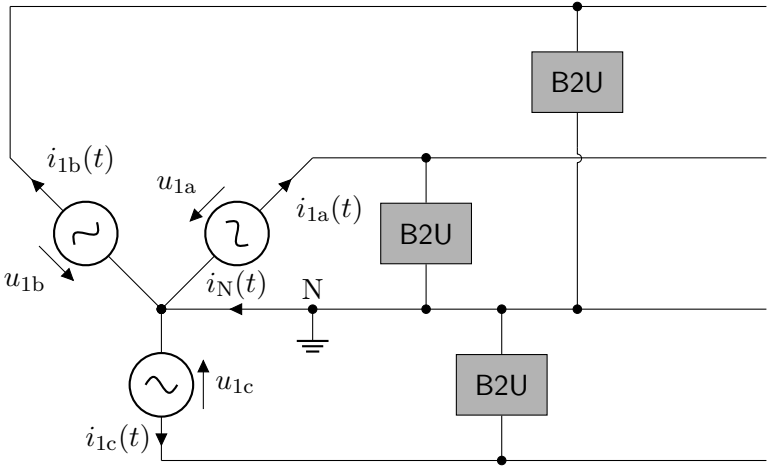

Fig. 10.21: Three-phase grid with single-phase rectifiers connected to neutral

B2U rectifier impact on the neutral line in three-phase grid (cont.)

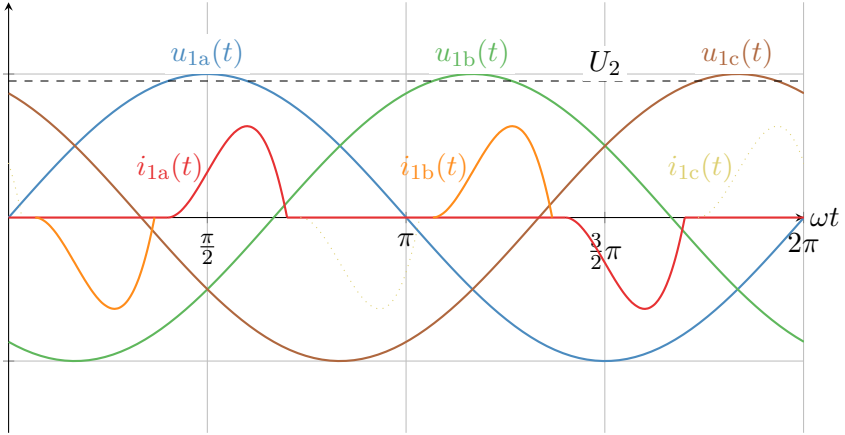

Fig. 10.22: Relevant signals of the scenario from (10.21) assuming identical operation conditions for all single-phase rectifiers

B2U rectifier impact on the neutral line in three-phase grid (cont.)

The neutral conductor current is the sum of the phase currents:

$$i_{\mathrm{N}}(t) = i_{\mathrm{1a}}(t) + i_{\mathrm{1b}}(t) + i_{\mathrm{1c}}(t). \tag{10.54}$$

In the example from Fig. 10.22 the neutral conductor current corresponds to the enveloping curve over the phase currents shown in the figure:

- The B2U rectifier represents a nonlinear load such that the three-phase currents do not cancel each other out.
- The neutral conductor current leads to power losses in the neutral conductor and can cause overheating.

Need for grid-friendly rectification

The shown analysis of the B2U rectifier highlights its negative impact on the grid, especially if multiple B2U rectifiers are connected to the same grid. Therefore, grid-friendly rectification alternatives are essential to ensure the stable operation of the grid and the connected loads.

Table of contents

General PFC circuit structure

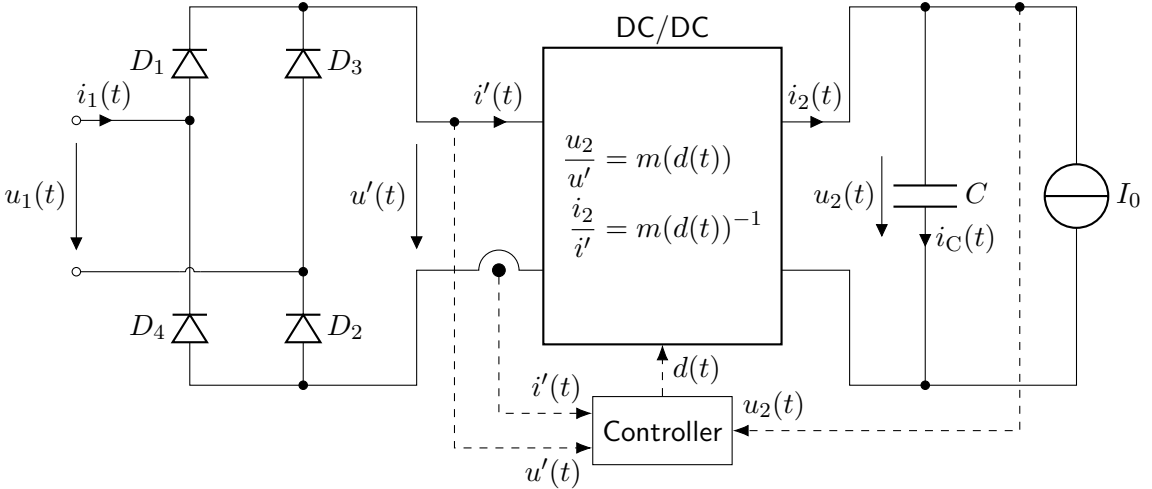

Fig. 10.23: Rectifier with power factor correction (PFC) realized as a combination of a single-phase diode bridge and a cascaded DC/DC converter with voltage / current transfer ratio $m(t)$

Idealized PFC rectifier signals in the time domain (steady state)

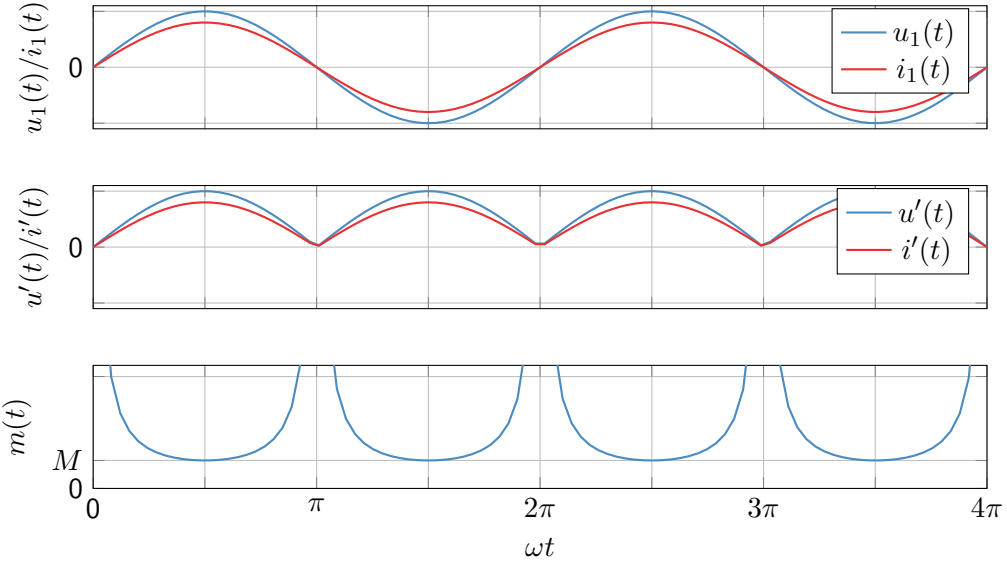

Operation concept and assumptions for the PFC rectifier

Main idea: utilize a DC/DC converter to control the input current $i_1(t)$ such that it follows the input voltage $u_1(t)$ in phase:

$$i_1(t) = \hat{i}_1 \sin(\omega t) \sim \hat{u}_1 \sin(\omega t) = u_1(t). \tag{10.55}$$

Assumptions for the following PFC rectifier analysis:

- The input voltage $u_1(t)$ is an ideal sinusoidal signal with amplitude $\hat{u}_1$ and frequency ω.
- The output voltage is considered constant: $u_2(t) \approx U_2$.
- The grid impedance is neglected for the sake of simplicity.
  - The grid impedance as in Fig. 10.13 would (mainly) introduce a phase shift between $|u_1(t)|$ and $u'(t)$ which can be compensated by the control setup.

Based on these assumptions and the objective (10.55), the voltages and currents in front of the DC/DC converter must be proportional to each other (to achieve unity power factor):

$$\frac{u_1(t)}{i_1(t)} = \frac{u'(t)}{i'(t)}. \tag{10.56}$$

Voltage transfer ratio

Considering an ideal DC/DC converter with a voltage transfer ratio $m(t)$, the converter must deliver a rectified-sinusoidal $u'(t)$ given some constant U_2:

$$u'(t) = \frac{U_2}{m(t)} \quad \Leftrightarrow \quad \hat{u}_1 |\sin(\omega t)| = \frac{U_2}{m(t)}. \tag{10.57}$$

Hence, the voltage transfer ratio $m(t)$ is given by

$$m(t) = \frac{U_2}{u'(t)} = \frac{U_2}{\hat{u}_1 |\sin(\omega t)|} \tag{10.58}$$

which varies between

$$\begin{aligned} \max_{u'}\{m(t)\} &= \infty, & \arg\max_{u'}\{m(t)\} &= 0, \\ \min_{u'}\{m(t)\} &= \frac{U_2}{\hat{u}_1} = M, & \arg\min_{u'}\{m(t)\} &= \hat{u}_1. \end{aligned} \tag{10.59}$$

One can conclude that the DC/DC converter must be able to deliver a voltage transfer ratio of

$$m(t) \in [M, \ldots, \infty].$$

Voltage transfer ratio (cont.)

The above voltage transfer ratio range restricts the possible topologies accordingly, e.g.:

- Standard boost converter: $m(t) = {}^{1}/_{(1-d(t))}$,
- Buck-boost converter or SEPIC: $m(t) = {}^{d(t)}/_{(1-d(t))}$.

Due to its simplicity and low component count, the boost converter is the most common choice for PFC applications leading to the reference duty cycle (assuming CCM operation):

$$d(t) = \frac{U_2 - \hat{u}_1 |\sin(\omega t)|}{U_2} = 1 - \frac{1}{M} |\sin(\omega t)|. \tag{10.60}$$

Remark on nomenclature and steady state

In contrast to the previous DC/DC converter section, the duty cycle $d(t)$ is now a function of time and not a constant (small d instead of capital D). However, the voltage transfer to duty cycle ratio was derived in steady state, i.e., (10.60) only holds approximately for $f_s >> f = {}^{\omega}/_{2\pi}$ (so-called quasi steady state).

PFC rectifier with boost converter

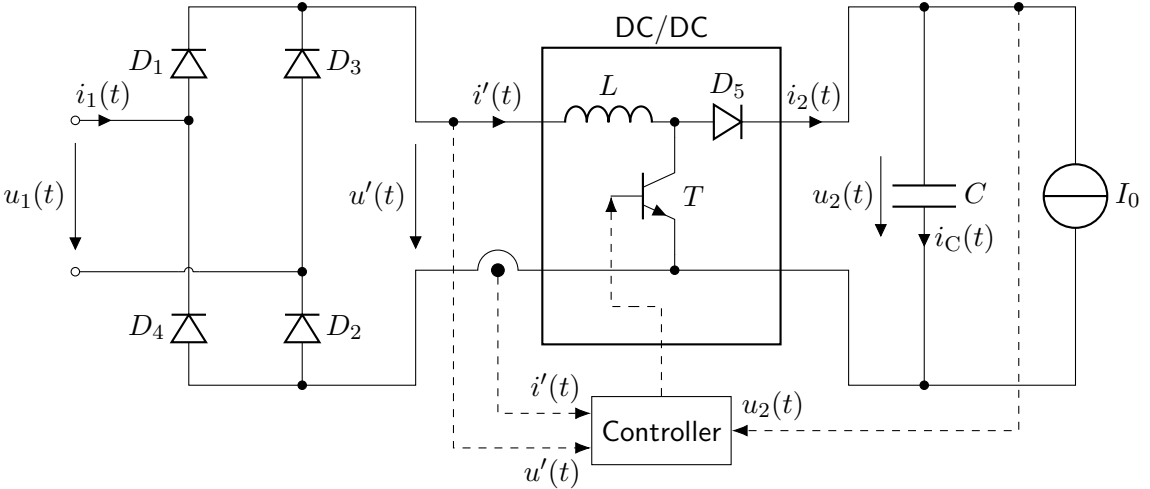

Fig. 10.24: PFC rectifier realized as a combination of a single-phase diode bridge and a cascaded DC/DC boost converter

PFC rectifier with boost converter (cont.)

The duty cycle from (10.60) does not consider the inner voltage demand of the boost converter, in particular of its filter inductor L:

$$\begin{aligned} u_{\mathrm{L}}(t) &= L\frac{\mathrm{d}}{\mathrm{d}t}i'(t) = L\frac{\mathrm{d}}{\mathrm{d}t}\left(\hat{i}_1|\sin(\omega t)|\right) \\ &= \hat{i}_1\omega L\cos(\omega t)\mathrm{sgn}(\sin(\omega t)). \end{aligned} \tag{10.61}$$

Within one switching period of the boost converter the voltage balance must hold:

$$\begin{aligned} & u'(t) = u_{\mathrm{L}}(t) + U_2(1-d(t)) \\ \Leftrightarrow \quad & \hat{u}_1|\sin(\omega t)| = \hat{i}_1\omega L\cos(\omega t)\mathrm{sgn}(\sin(\omega t)) + M\hat{u}_1(1-d(t)). \end{aligned} \tag{10.62}$$

Rearranging towards the duty cycle $d(t)$ yields

$$d(t) = 1 - \frac{1}{M}|\sin(\omega t)| + \frac{\hat{i}_1\omega L}{M\hat{u}_1}\cos(\omega t)\mathrm{sgn}(\sin(\omega t)). \tag{10.63}$$

PFC rectifier with boost converter (cont.)

Evaluating (10.63) for $\omega t = \varepsilon$ with $\varepsilon \in \mathbb{R} > 0$ being an infinitesimally small value, one obtains

$$d(\varepsilon/\omega) = 1 - \sin(\varepsilon) + \frac{\hat{i}_1 \omega L}{M \hat{u}_1} \cos(\varepsilon) \mathrm{sgn}(\sin(\varepsilon)) \approx 1 + \frac{\hat{i}_1 \omega L}{M \hat{u}_1} > 1.$$

Hence, the additional voltage demand of the boost converter inductor L leads to a duty cycle exceeding unity, that is, exceeding the feasible range and, therefore, the boost converter is not able to deliver the required voltage transfer ratio $m(t)$:

- The boost converter is not able to exactly track the input current reference $i_1(t) = \hat{i}_1 \sin(\omega t)$ (especially at the beginning and end of a half period).
- The lower L the less the negative impact of the inductor voltage demand.
- Consequently, one wants to keep the inductance L as low as possible which on the other hand requires a high switching frequency f_s to keep the current ripple within acceptable bounds.

Pulse width modulation (PWM)

As seen on the previous slides, the duty cycle $d(t)$ is a function of time. To generate a switching signal $s(t)$ for the boost converter, a pulse width modulation (PWM) scheme is used:

$$s(t) = \begin{cases} 1 & \text{(transistor } T \text{ on)}, \quad \text{if } d(t) > c(t), \\ 0 & \text{(transistor } T \text{ off)}, \quad \text{otherwise} \end{cases} \tag{10.64}$$

with a (high frequency) carrier signal $c(t)$, e.g., a triangular or sawtooth signal.

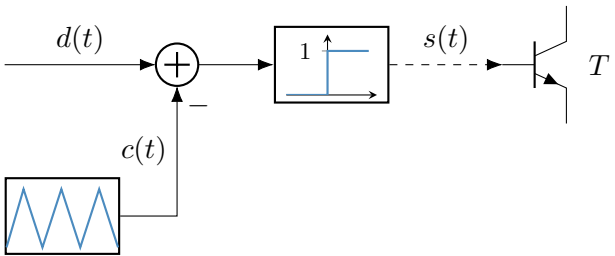

Fig. 10.25: Pulse width modulation with triangular carrier to actuate a transistor

PWM-based switching signals

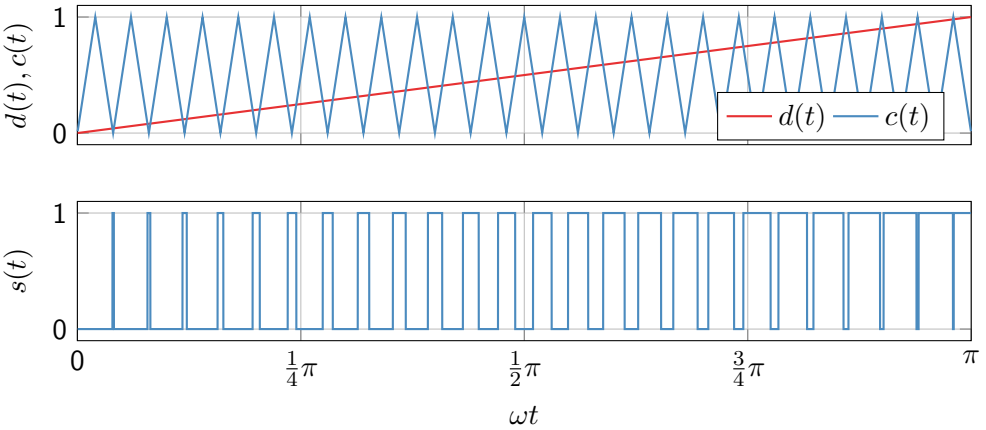

Fig. 10.26: Qualitative illustration of a PWM-based switching signal with a triangular carrier signal

PWM-based switching signals (cont.)

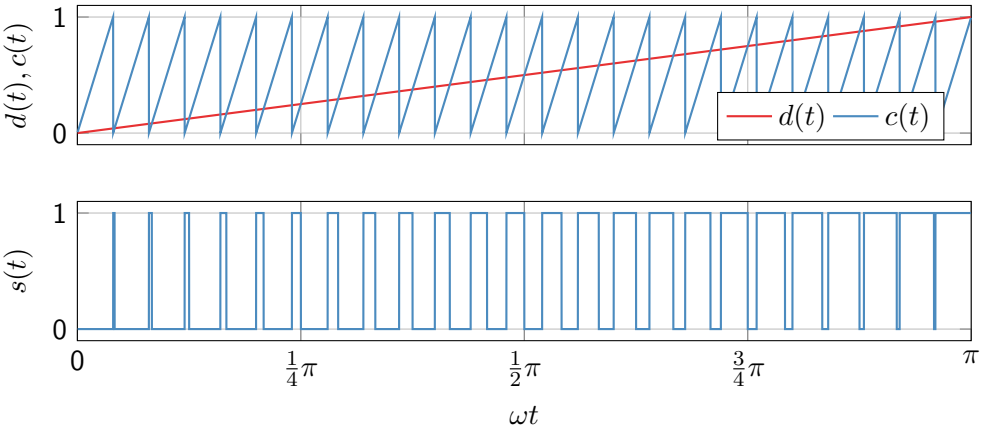

Fig. 10.27: Qualitative illustration of a PWM-based switching signal with a sawtooth carrier signal

PWM-based open-loop control of the boost converter PFC rectifier

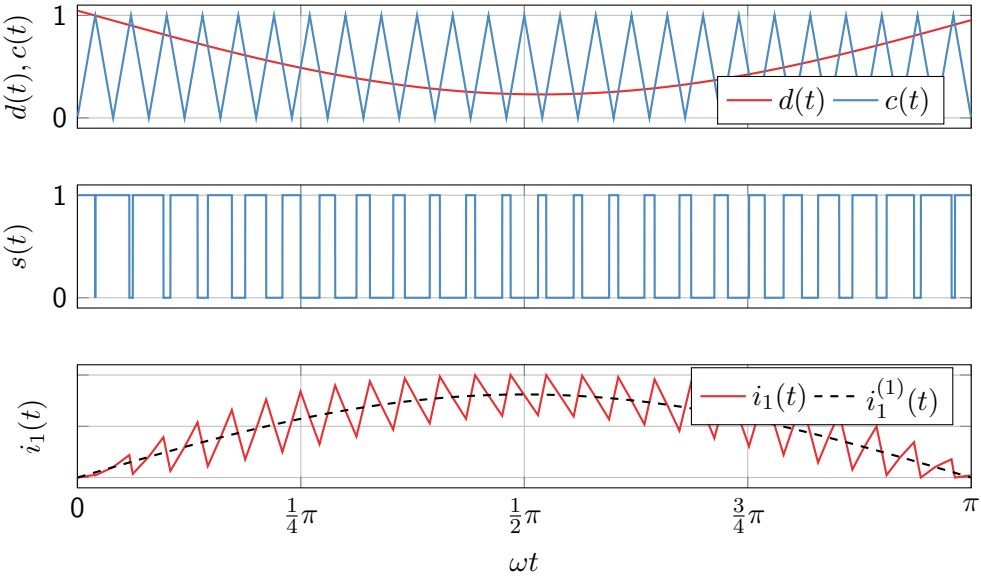

PWM-based PFC rectifier current ripple

Due to the switching behavior of the boost converter, the input current $i_1(t)$ exhibits a current ripple. The boost inductor voltage during a switching period is:

$$u_{\mathrm{L}}(t) = \begin{cases} \hat{u}_1 \sin(\omega t), & 0 < t \leq dT_{\mathrm{s}} \\ \hat{u}_1 \sin(\omega t) - U_2, & dT_{\mathrm{s}} < t \leq T_{\mathrm{s}}. \end{cases} \tag{10.65}$$

We assume that

$$T_{\mathrm{s}} << {}^{2\pi}/_{\omega}$$

such that the input voltage and duty cycle are approximately constant within one switching period.The ripple current envelope $\Delta i_1(t)$ is then defined as the moving difference between the actual input current $i_1(t)$ and its fundamental component $i_1^{(1)}(t)$:

$$\Delta i_1(t) = \pm \frac{1}{2} \max_{\tau \in [t \pm \frac{T_{\mathrm{s}}}{2}]} |i_1(\tau) - i_1^{(1)}(\tau)|. \tag{10.66}$$

One should note that this ripple definition is different from the one used in the previous DC/DC converter section.

PWM-based PFC rectifier current ripple (cont.)

Assuming CCM operation and a sufficiently small switching time interval T_s, the ripple current can be approximated by the current rise during the on-time of the boost converter:

$$\begin{aligned}\Delta i_1(t) &= \pm\frac{1}{2L}\int_0^{dT_\mathrm{s}} u_\mathrm{L}(\tau)\mathrm{d}\tau = \pm\frac{1}{2L}\int_0^{dT_\mathrm{s}} \hat{u}_1\sin(\omega t)\mathrm{d}\tau \\ &\approx \pm\frac{\hat{u}_1\sin(\omega t)}{2L}\int_0^{dT_\mathrm{s}} 1\mathrm{d}\tau = \pm\frac{\hat{u}_1\sin(\omega t)}{2L}dT_\mathrm{s}.\end{aligned} \tag{10.67}$$

Inserting $d(t)$ from (10.63) in a quasi steady-state fashion yields

$$\Delta i_1(t) = \pm\frac{\hat{u}_1 T_\mathrm{s}\sin(\omega t)}{2L}\left(1 - \frac{1}{M}|\sin(\omega t)| + \frac{\hat{i}_1\omega L}{M\hat{u}_1}\cos(\omega t)\mathrm{sgn}(\sin(\omega t))\right). \tag{10.68}$$

Due to the varying input voltage and duty cycle, the ripple current is not constant but also varies with time (cf. next slide).

PWM-based PFC rectifier current ripple (cont.)

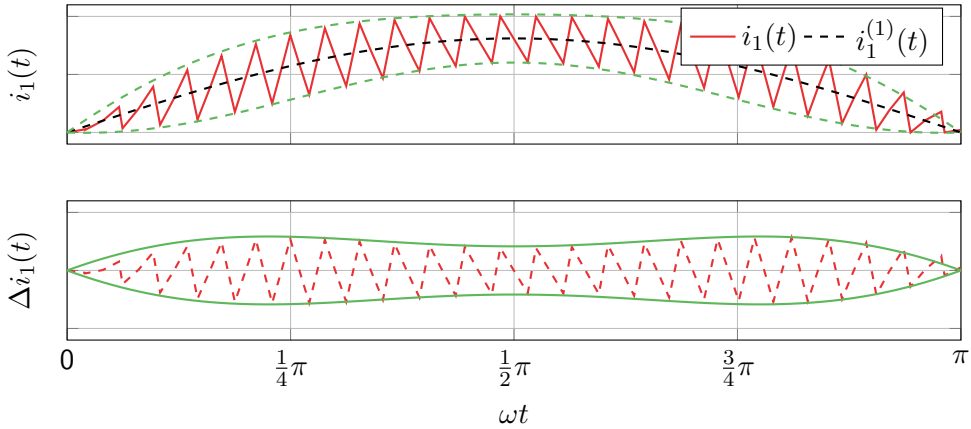

PFC rectifier with boost converter: closed-loop control structure

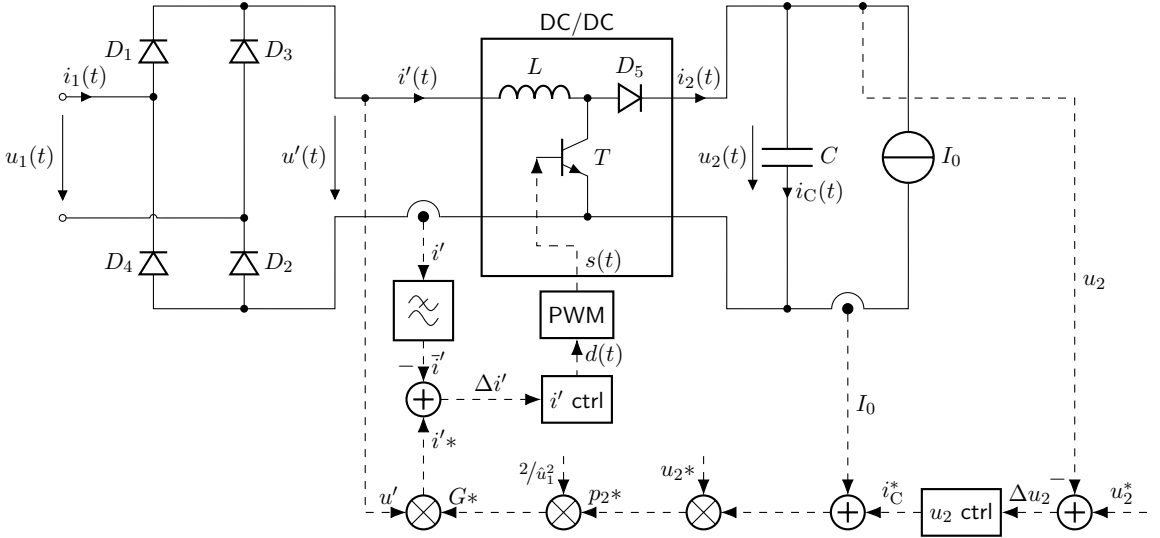

Fig. 10.28: Control structure of PFC rectifier with boost DC/DC converter

PFC rectifier with boost converter: closed-loop control structure (cont.)

Reasons for closed-loop control:

- Mismatches between the actual system and the plant model behavior result in (steady-state) control errors.
- Faster transient response to load changes.
- Robustness against further disturbances (e.g., input voltage variations).

Central idea of the closed-loop control: given some required load power

$$p_2(t) = u_2(t) i_2(t) = u_2(t) \left(I_0 + i_{\mathrm{C}}(t) \right)$$

operate the boost converter such that the load power is represented by a (virtual) conductance at the input of the boost converter:

$$g(t) = \frac{p_1(t)}{\hat{u}_1^2} = \frac{p_2(t)}{\hat{u}_1^2} = \frac{U_2 \left(I_0 + i_{\mathrm{C}}(t) \right)}{\hat{u}_1^2}.$$

PFC rectifier with boost converter: closed-loop control structure (cont.)

The required conductance $g(t)$ is calculated by the outer voltage controller:

- If $u_2(t) < U_2^*$: increase $p_2(t)$ by increasing the conductance $g(t)$.
- If $u_2(t) > U_2^*$: decrease $p_2(t)$ by decreasing the conductance $g(t)$.

With

$$\hat{i}'(t) = \hat{u}_1 g(t)$$

the required reference input current for the inner current controller can be calculated.

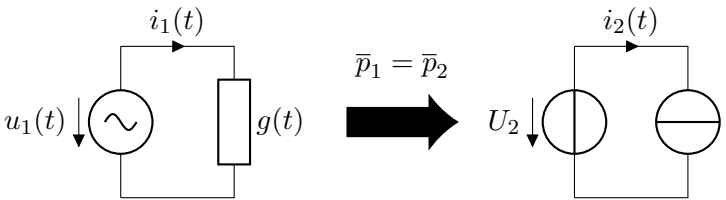

Fig. 10.29: Interpretation of the closed-loop control of a PFC rectifier as a variable conductance tuning

PFC rectifier with boost converter: capacitor sizing

Based on the previous assumption $u_2(t) \approx U_2$ the question is raised how the output capacitor C of the boost converter must be sized to keep the output voltage ripple within acceptable bounds justifying the assumption. For a lossless converter, the instantaneous power is:

$$p_2(t) = p_1(t) = u_1(t) i_1(t).$$

Assuming that the input voltage and current are both ideally sinusoidal and in phase (i.e., the PFC rectifier operates perfectly), the instantaneous power is:

$$p_2(t) = \hat{u}_1 \hat{i}_1 \sin(\omega t) \sin(\omega t) = \frac{\hat{u}_1 \hat{i}_1}{2} \left(1 - \cos(2\omega t)\right). \tag{10.69}$$

Hence, we can decompose the instantaneous power into a constant term and a harmonic term with twice the frequency of the input voltage/current:

$$p_2(t) = \underbrace{\frac{\hat{u}_1 \hat{i}_1}{2}}_{\overline{p}_2} \underbrace{- \frac{\hat{u}_1 \hat{i}_1}{2} \cos(2\omega t)}_{p_2^{(\mathrm{h})}(t)}. \tag{10.70}$$

PFC rectifier with boost converter: capacitor sizing (cont.)

The resulting harmonic output current component is (approximately)

$$i_2^{(\mathrm{h})}(t) \approx \frac{p_2^{(\mathrm{h})}(t)}{\overline{u}_2} = -\frac{\hat{u}_1 \hat{i}_1}{2\overline{u}_2}\cos(2\omega t) = -\frac{\overline{p}_2}{\overline{u}_2}\cos(2\omega t). \tag{10.71}$$

If the load current I_0 is (approximately) constant, the harmonic current is entirely flowing into the output capacitor $i_2^{(\mathrm{h})}(t) = i_\mathrm{C}(t)$ leading to the voltage ripple:

$$\Delta u_2(t) = \frac{1}{C}\int i_\mathrm{C}(t)\mathrm{d}t = -\underbrace{\frac{\overline{p}_2}{\overline{u}_2}\frac{1}{2\omega C}}_{\Delta\hat{u}_2}\sin(2\omega t). \tag{10.72}$$

To limit the output voltage ripple to a certain amplitude value $\Delta\hat{u}_2$, the output capacitor C must exhibit a minimal capacitance value:

$$C > \frac{\overline{p}_2}{\overline{u}_2}\frac{1}{2\omega\Delta\hat{u}_2}. \tag{10.73}$$

PFC rectifier with boost converter: capacitor sizing (cont.)

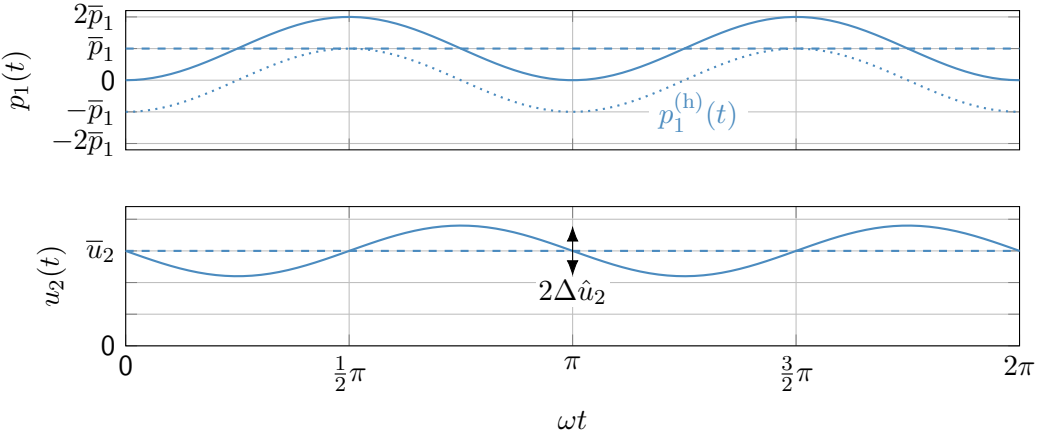

Fig. 10.30: Power and voltage oscillations in the PFC rectifier in quasi steady-state operation

Table of contents

M3U uncontrolled rectifier circuit

The M3U rectifier addresses three-phase systems and typically utilizes an input transformer to mitigate offset phase currents and further harmonics (compare Fig. 10.5). To simplify things, we assume that the input transformer delivers an ideal three-phase voltage source:

$$u_{1a}(t) = \hat{u}_1 \sin(\omega t), \quad u_{1b}(t) = \hat{u}_1 \sin(\omega t - 2\pi/3), \quad u_{1c}(t) = \hat{u}_1 \sin(\omega t + 2\pi/3).$$

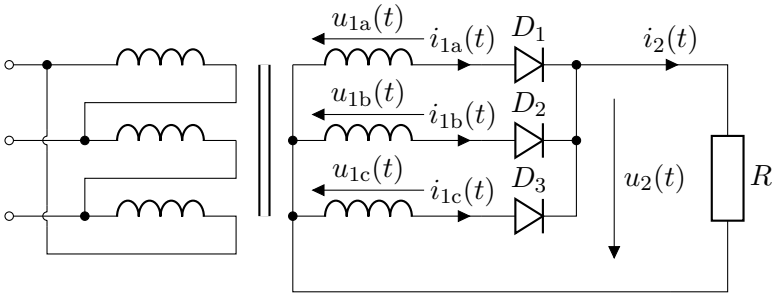

Fig. 10.31: M3U topology (aka three-pulse mid-point rectifier) with an input three-phase transformer and a resistive load

M3U rectifier resistive load operation

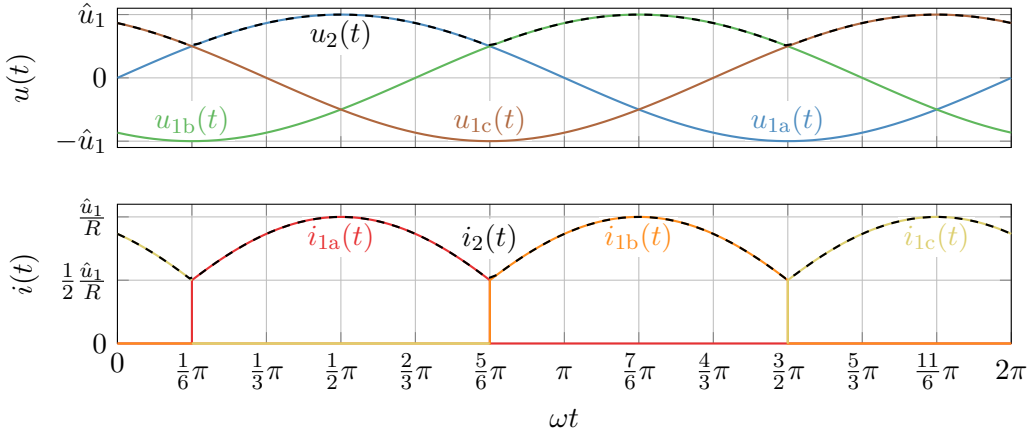

Fig. 10.32: M3U characteristic voltage and current curves for a resistive load

M3U rectifier resistive load operation: average output voltage

With a resistive load, the M3U rectifier's output is always determined by the transformer phase with the highest voltage:

$$u_2(t) = \max\left\{u_{1\mathrm{a}}(t), u_{1\mathrm{b}}(t), u_{1\mathrm{c}}(t)\right\}. \tag{10.74}$$

- Assume $u_{1\mathrm{a}}(t)$ has the highest voltage for some time t.
- Hence, there is a negative voltage difference between the phases b-a and c-a.
- These can be only compensated by the diodes D_2 and D_3, which are in blocking mode while D_1 is conducting.

The average output voltage can be found by evaluating the conduction interval of one phase, e.g., $u_{1\mathrm{a}}(t)$:

$$\bar{u}_2 = \frac{3}{2\pi}\int_{\frac{1}{6}\pi}^{\frac{5}{6}\pi} \hat{u}_1 \sin(\omega t)\mathrm{d}\omega t = \frac{3}{2\pi}\left[-\hat{u}_1\cos(\omega t)\right]_{\frac{1}{6}\pi}^{\frac{5}{6}\pi} = \frac{3}{2\pi}\hat{u}_1 2\frac{\sqrt{3}}{2} = \frac{3\sqrt{3}}{2\pi}\hat{u}_1. \tag{10.75}$$

M3U rectifier with output filter

To filter both the output voltage and current, an output filter can be added to the M3U rectifier circuit (Fig. 10.33). The filter consists of a series inductor L and a capacitor C in parallel. In steady state

$$\overline{u}_{\mathrm{C}} = \overline{u}_2 = \frac{3\sqrt{3}}{2\pi}\hat{u}_1 \tag{10.76}$$

holds as the average inductor voltage must be zero to prevent a current run away.

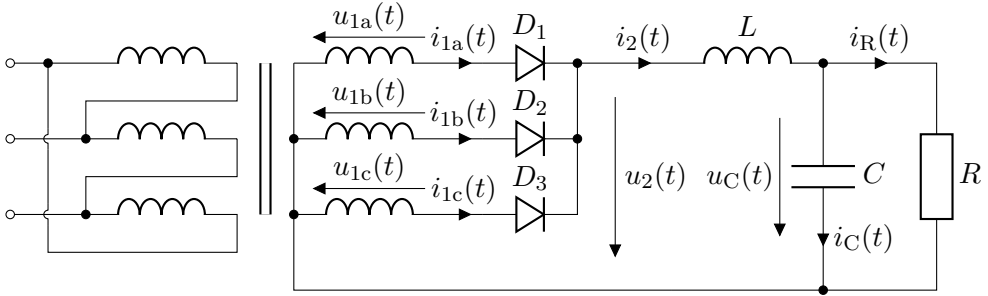

Fig. 10.33: M3U topology with an input three-phase transformer, a resistive load and output filter

M3U rectifier with output filter (cont.)

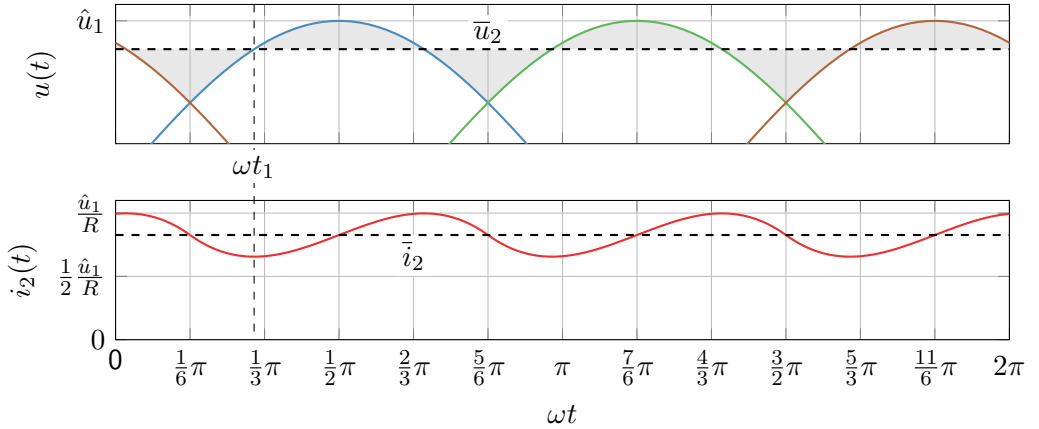

Fig. 10.34: M3U characteristic voltage and current curves considering an idealized output filter with $u_C(t) = \overline{u}_2 = \text{const.}$

M3U rectifier with output filter (cont.)

From Fig. 10.34 one can observe that

$$u_2(t) = u_{1a}(t) = \hat{u}_1 \sin(\omega t), \quad \omega t \in \left[\frac{1}{6}\pi, \frac{5}{6}\pi\right] \tag{10.77}$$

holds. At $\omega t = \omega t_1$ the phase voltage $u_{1a}(t)$ is equal to the average output voltage $\overline{u}_2$:

$$\overline{u}_2 = \frac{3\sqrt{3}}{2\pi}\hat{u}_1 = \hat{u}_1 \sin(\omega t_1) \quad \Leftrightarrow \quad \omega t_1 = \arcsin\left(\frac{3\sqrt{3}}{2\pi}\right). \tag{10.78}$$

Based on this, the current $i_2(t)$ can be calculated as

$$\begin{aligned} i_2(t) &= i_2(\omega t_1) + \frac{1}{\omega L}\int_{\omega t_1}^{\omega t} (u_2(\omega\tau) - \overline{u}_2)\,\mathrm{d}\omega\tau \\ &= i_2(\omega t_1) + \frac{1}{\omega L}\int_{\omega t_1}^{\omega t} (\hat{u}_1 \sin(\omega\tau) - \hat{u}_1 \sin(\omega t_1))\,\mathrm{d}\omega\tau, \quad \omega t \in \left[\frac{1}{6}\pi, \frac{5}{6}\pi\right] \end{aligned} \tag{10.79}$$

with $i_2(\omega t_1)$ being the initial (yet unknown) current at ωt_1.

M3U rectifier with output filter (cont.)

Solving the integral in (10.79) yields

$$\begin{aligned} i_2(t) &= i_2(\omega t_1) + \frac{\hat{u}_1}{\omega L}\left[-\cos(\omega\tau) - \omega\tau\sin(\omega t_1)\right]_{\omega t_1}^{\omega t} \\ &= i_2(\omega t_1) + \frac{\hat{u}_1}{\omega L}\left[-\cos(\omega t) + \cos(\omega t_1) - \sin(\omega t_1)\left(\omega t - \omega t_1\right)\right]. \end{aligned} \tag{10.80}$$

To determine the initial current $i_2(\omega t_1)$, one can utilize the fact that the average inductor current must be identical to the average load current since otherwise the output capacitor would be charged or discharged indefinitely:

$$\bar{i}_2 \stackrel{!}{=} \bar{i}_\mathrm{R} = \frac{\overline{u}_2}{R} = \frac{\hat{u}_1\sin(\omega t_1)}{R}. \tag{10.81}$$

M3U rectifier with output filter (cont.)

The average inductor current can be calculated as

$$\begin{aligned}\bar{i}_2 &= \frac{3}{2\pi}\int_{\frac{1}{6}\pi}^{\frac{5}{6}\pi} i_2(\omega\tau)\mathrm{d}\omega\tau = \frac{3}{2\pi}\int_{\frac{1}{6}\pi}^{\frac{5}{6}\pi} i_2(\omega t_1)\mathrm{d}\omega\tau \\ &+ \frac{3}{2\pi}\int_{\frac{1}{6}\pi}^{\frac{5}{6}\pi} \frac{\hat{u}_1}{\omega L}\left[-\cos(\omega\tau)+\cos(\omega t_1)-\sin(\omega t_1)\left(\omega\tau-\omega t_1\right)\right]\mathrm{d}\omega\tau \\ &= \dots \\ &= i_2(\omega t_1) + \frac{\hat{u}_1}{\omega L}\left[\cos(\omega t_1)+\sin(\omega t_1)(\omega t_1-\frac{\pi}{2})\right].\end{aligned} \tag{10.82}$$

Inserting into (10.81) and solving for $i_2(\omega t_1)$ yields

$$i_2(\omega t_1) = \frac{\hat{u}_1}{R}\sin(\omega t_1) - \frac{\hat{u}_1}{\omega L}\left[\cos(\omega t_1)+\sin(\omega t_1)(\omega t_1-\frac{\pi}{2})\right]. \tag{10.83}$$

With this result, the current $i_2(t)$ can be calculated using (10.80).

M3U rectifier with output filter: CCM vs. DCM

The previous analysis only holds for CCM as otherwise all diodes would be blocking simultaneously. From (10.80) one can find that the minimum current $i_2(t)$ is reached when $\omega t = \omega t_1$, i.e.,

$$\min\{i_2(t)\} = i_2(\omega t_1) = \frac{\hat{u}_1}{R}\sin(\omega t_1) - \frac{\hat{u}_1}{\omega L}\left[\cos(\omega t_1) + \sin(\omega t_1)(\omega t_1 - \frac{\pi}{2})\right]. \tag{10.84}$$

The boundary between CCM and DCM can be found by setting $\min\{i_2(t)\} = 0$ leading to $i_2(\omega t_1) = 0$. In this boundary case, the average output current is

$$\begin{aligned} \bar{i}_2 &= \frac{\hat{u}_1}{\omega L}\left[\cos(\omega t_1) + \sin(\omega t_1)(\omega t_1 - \frac{\pi}{2})\right] \\ &= \frac{\overline{u}_2}{\omega L}\left[\tan(\omega t_1) + \omega t_1 - \frac{\pi}{2}\right]. \end{aligned} \tag{10.85}$$

One can also reinterpret this result for designing the filter inductor L to ensure CCM operation:

$$L \geq \frac{\overline{u}_2}{\omega \bar{i}_2}\left[\tan(\omega t_1) + \omega t_1 - \frac{\pi}{2}\right]. \tag{10.86}$$

Table of contents

B6U uncontrolled rectifier circuit

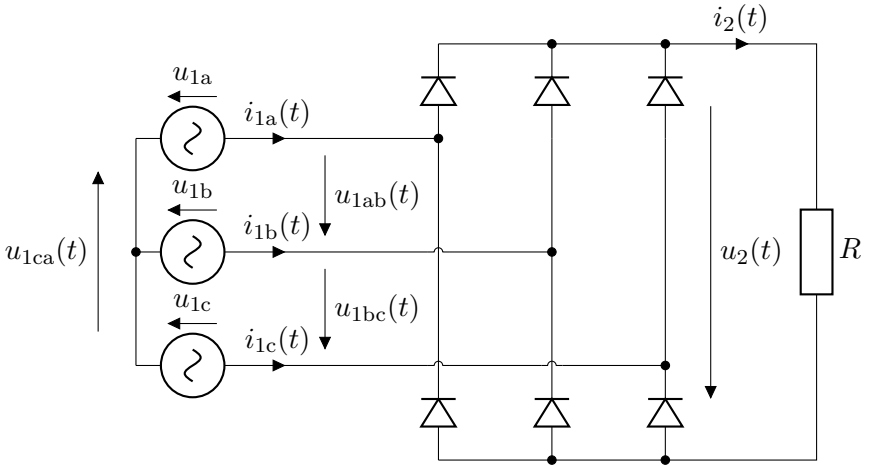

Fig. 10.35: B6U topology (aka six-pulse bridge rectifier) with resistive load

B6U rectifier resistive load operation

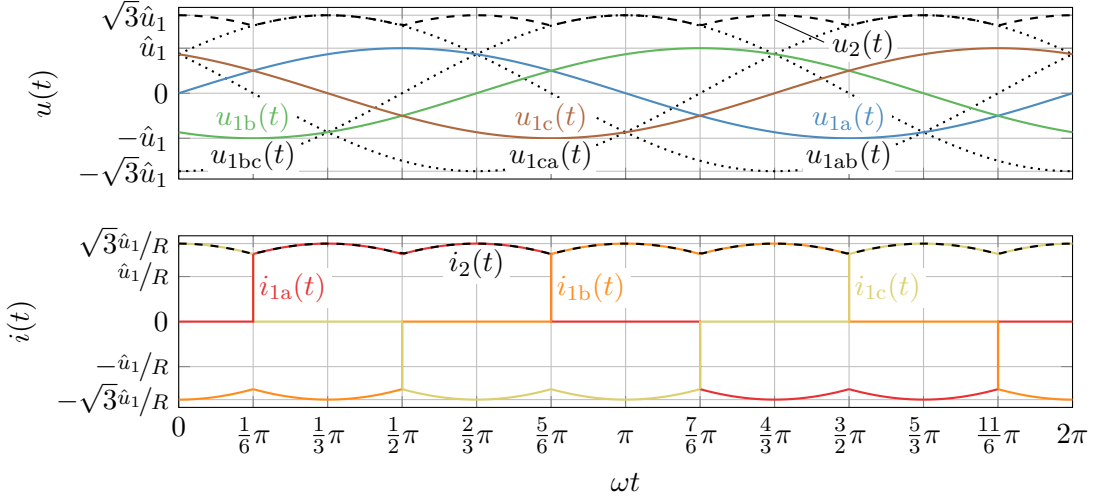

Fig. 10.36: B6U characteristic voltage and current curves for a resistive load

B6U rectifier resistive load operation (cont.)

In the B6U bridge with a resistive load the upper output potential is determined by the highest phase voltage while the lower output potential is determined by the lowest phase voltage. The output voltage $u_2(t)$ is given by

$$u_2(t) = \max\{u_{1a}(t), u_{1b}(t), u_{1c}(t)\} - \min\{u_{1a}(t), u_{1b}(t), u_{1c}(t)\}. \tag{10.87}$$

Alternatively, we can evaluate the line-to-line voltages

$$\begin{aligned} u_{1ab}(t) &= u_{1a}(t) - u_{1b}(t) & u_{1bc}(t) &= u_{1b}(t) - u_{1c}(t) & u_{1ca}(t) &= u_{1c}(t) - u_{1a}(t) \\ &= \sqrt{3}\hat{u}_1 \sin(\omega t + \frac{1}{6}\pi), & &= \sqrt{3}\hat{u}_1 \sin(\omega t - \frac{1}{2}\pi), & &= \sqrt{3}\hat{u}_1 \sin(\omega t + \frac{5}{6}\pi) \end{aligned}$$

and find that the B6U output voltage is given by

$$u_2(t) = \max\{u_{1ab}(t), u_{1bc}(t), u_{1ca}(t)\}. \tag{10.88}$$

B6U rectifier resistive load operation (cont.)

The average output voltage $\overline{u}_2$ is given by

$$\begin{aligned}\overline{u}_2 =& \frac{3}{\pi}\int_{\frac{1}{6}\pi}^{\frac{1}{2}\pi} u_{1\mathrm{ab}}(\omega t)\mathrm{d}\omega t = \frac{3}{\pi}\int_{\frac{1}{6}\pi}^{\frac{1}{2}\pi} \sqrt{3}\hat{u}_1 \sin(\omega t + \frac{1}{6}\pi)\mathrm{d}\omega t \\ =& \frac{3\sqrt{3}}{\pi}\hat{u}_1 \left[-\cos(\omega t + \frac{1}{6}\pi)\right]_{\frac{1}{6}\pi}^{\frac{1}{2}\pi} = \frac{3\sqrt{3}}{\pi}\hat{u}_1.\end{aligned} \tag{10.89}$$

Compared to the M3U rectifier average voltage from (10.75), the B6U average output voltage is doubled – this is an analogous finding to the single phase case where the B2U rectifier has a doubled average output voltage compared to the M2U rectifier.

Impact of further filter elements

The impact of filters elements, e.g., the line impedance from Fig. 10.13 or an LC output filter as in Fig. 10.33, can be analyzed in a similar manner for the B6U rectifier. While such filter elements are common in practice, they are not explicitly treated for the B6U rectifier in the following due to time constraints.

Table of contents

12-pulse rectifier: B6U-2S topology

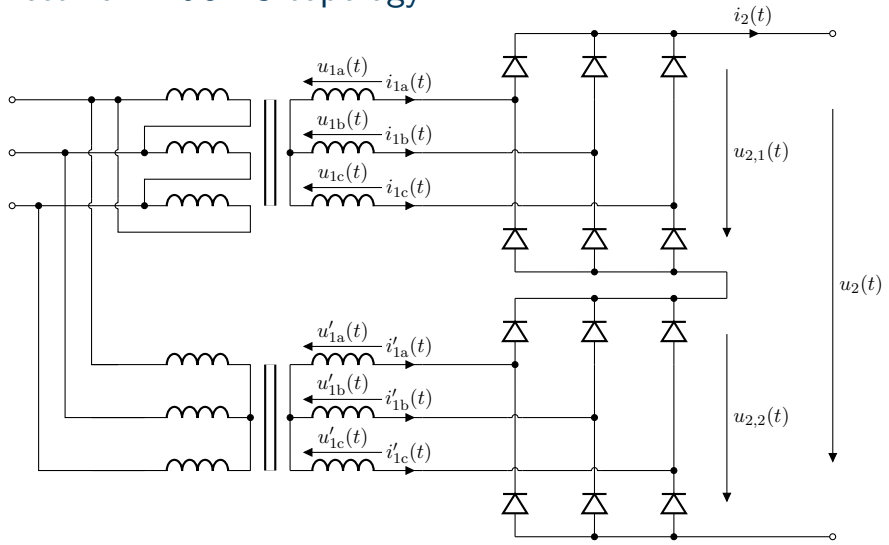

Fig. 10.37: 12-pulse recitifier with B6U-2S topology: two B6U rectifiers connected in series

12-pulse rectifier: B6U-2S topology (cont.)

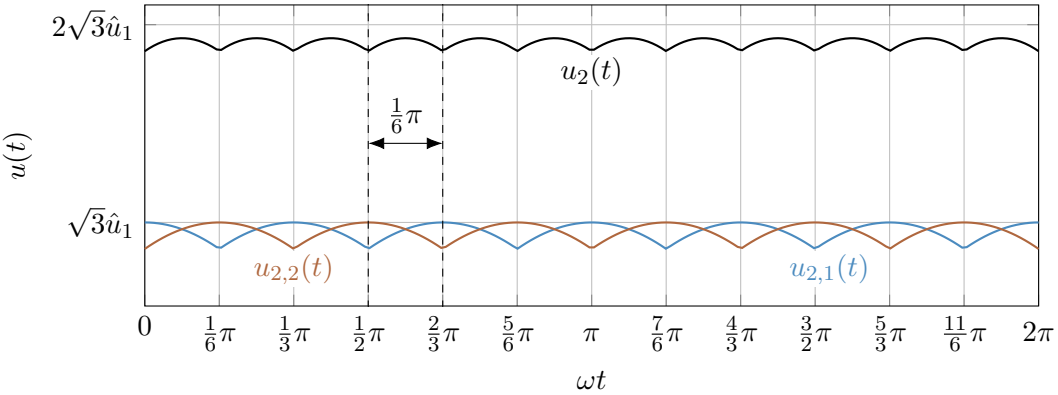

Fig. 10.38: B6U-2S output voltage characteristic: voltage output ripple is reduced by shifting the phase of the second rectifier by $1/6 \cdot \pi$ utilizing different transformer winding schemes at the input

12-pulse rectifier: B6U-2P topology

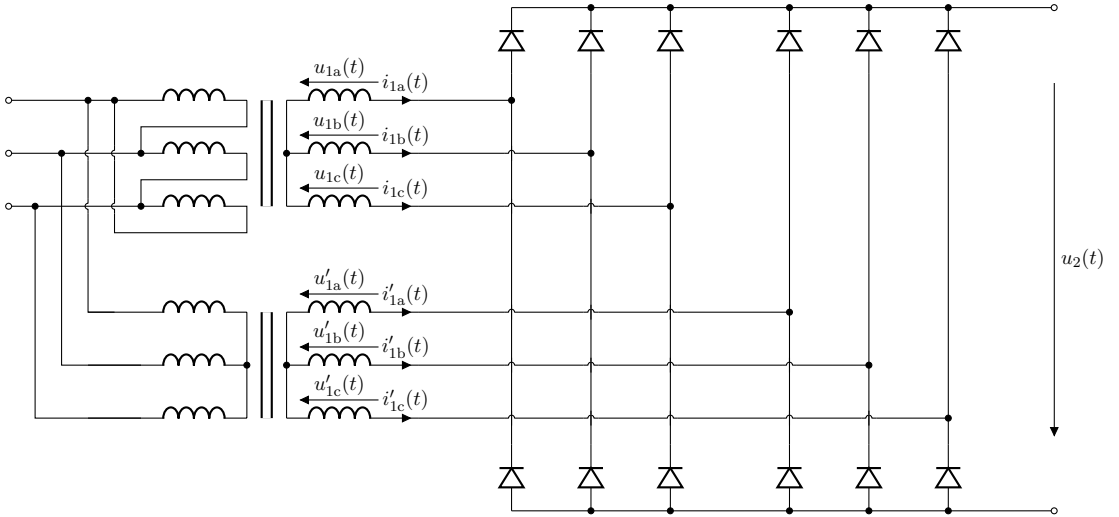

Fig. 10.39: 12-pulse recitifier with B6U-2P topology: two B6U rectifiers connected in parallel

12-pulse rectifier: B6U-2P topology (cont.)

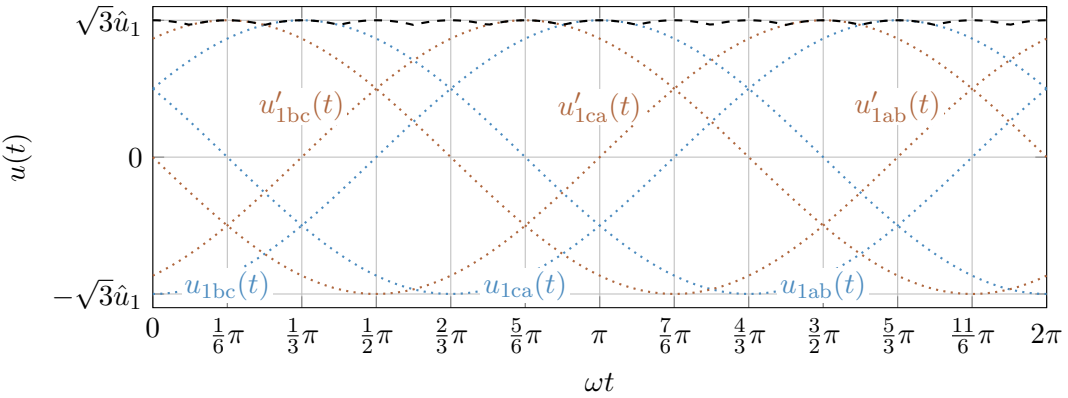

Fig. 10.40: B6U-2P output voltage characteristic: simplified representation as displacement currents between the transformers are not taken into account

Comparison of output voltage ripple characteristics

From the previous analyses of the considered three-phase rectifiers one can find

$$\Delta u_2 = \max\{u_2(t)\} - \min\{u_2(t)\} = \left(1 - \cos\left(\frac{\pi}{p}\right)\right)\hat{u}_2 \tag{10.90}$$

with p being the number of pulses. For the considered rectifiers, the output voltage is given by

$$\hat{u}_2 = \begin{cases} \hat{u}_1, & \text{for M3U,} \\ \sqrt{3}\hat{u}_1, & \text{for B6U and B6U-2P,} \end{cases} \quad \text{and} \quad \overline{u}_2 = \begin{cases} \frac{3\sqrt{3}}{2\pi}\hat{u}_1, & \text{for M3U,} \\ \frac{3\sqrt{3}}{\pi}\hat{u}_1, & \text{for B6U and B6U-2P} \end{cases}$$

leading to the normalized output voltage ripple being defined as

$$\frac{\Delta u_2}{\overline{u}_2} = \begin{cases} \frac{2\pi}{3\sqrt{3}}\left(1 - \cos\left(\frac{\pi}{3}\right)\right) = 60.46\,\%, & \text{for M3U,} \\ \frac{\pi}{3}\left(1 - \cos\left(\frac{\pi}{6}\right)\right) = 14.03\,\%, & \text{for B6U,} \\ \frac{\pi}{3}\left(1 - \cos\left(\frac{\pi}{12}\right)\right) = 3.57\,\%, & \text{for B6U-2P.} \end{cases} \tag{10.91}$$

Takeaway: the higher the recitifier's pulse number, the lower the output voltage ripple, that is, there is a trade-off between the number of semiconductors and the filter effort.

Section summary

This section provided an introduction to diode-based rectifiers. Not considering the active PFC extension, those are also coined passive rectifiers. The key takeaways are:

- All considered rectifiers operate exclusively unidirectional.
- There is a complex interaction between semiconductor effort and filter effort to provide a DC voltage with a certain signal quality.
- Without active PFC, any diode-based rectifier will introduce significant distortions at the primary side due to harmonics and phase shifts between input voltage and current.
- Active PFC can be used to provide a near-unity power factor, which is required in many applications due to industrial / legal regulations.

In addition, there are further topologies that are not covered in this course, such as

- M6U rectifier,
- very high pulse number rectifiers (e.g., 18 or 24-pulse rectifiers) requiring more complex transformer winding schemes to achieve the desired phase shift on the secondary side,
- three-phase rectifiers with an integrated PFC stage (e.g., Vienna rectifier).

Table of contents

Thyristor: an externally switchable power electronic component

- Can block voltage in both directions (when off)
  - Different to diode (only blocks reverse voltage)
- Can conduct current in only one direction (when on)
  - Identical to diode
- Turn-on: via gate signal
- Turn off: via current drop below holding current (i.e., depends on load characteristics and input voltage)

Application area

While transistors are used for high-frequency converters due to their favorable turn-on/off characteristics and have replaced thyristors in many cases, the latter are still used in low switching frequency applications (mostly energy grid) due to their favorable high voltage / current ratings.

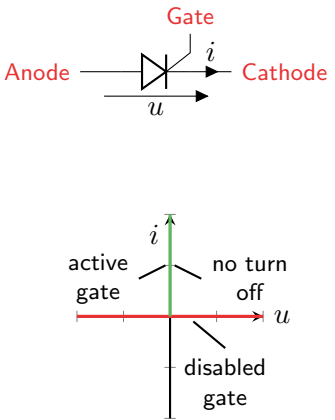

Fig. 11.1: Idealized thyristor characteristics and circuit symbol

Thyristor examples

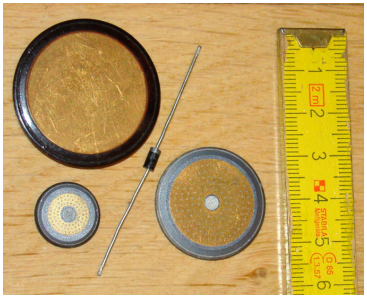

(a) Top left: $1000\,\mathrm{V}/200\,\mathrm{A}$ (diode); bottom left: $1500\,\mathrm{V}/20\,\mathrm{A}$; right: $1500\,\mathrm{V}/120\,\mathrm{A}$; 1N4007 (diode) (source: Wikimedia Commons, CC0 1.0)

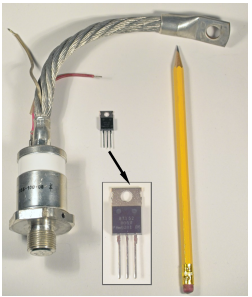

(b) Left: $800\,\mathrm{V}/100\,\mathrm{A}$; right: $800\,\mathrm{V}/13\,\mathrm{A}$ (source: Wikimedia Commons, Julo, CC0 BY-SA 3.0)

Fig. 11.2: Thyristor examples with different voltage and current ratings

M1 rectifier comparison

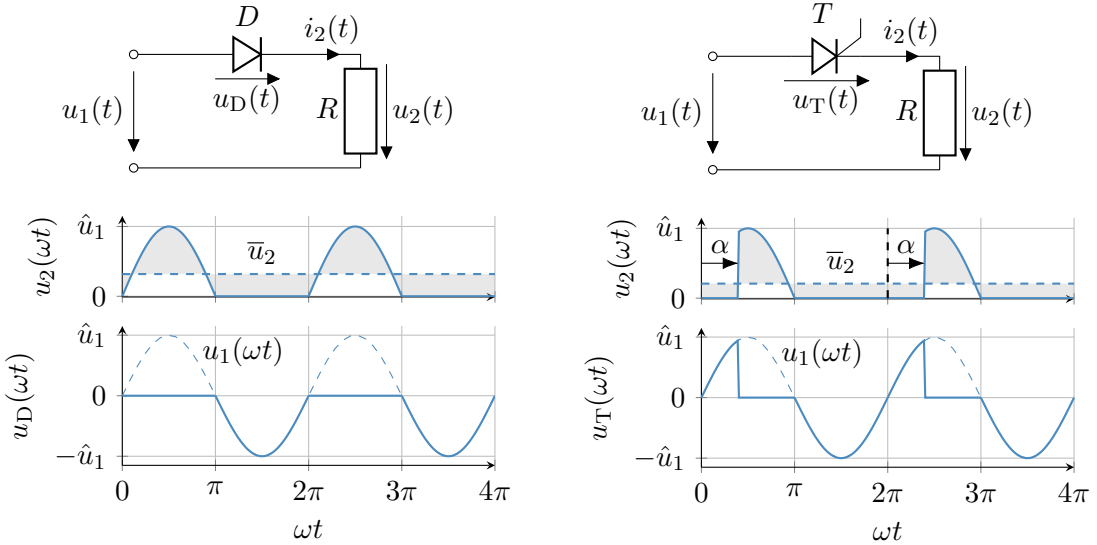

M1C rectifier

The average output voltage of the M1C circuit, i.e., the M1 rectifier with a thyristor, for a resistive load is given by

$$\overline{u}_2 = \frac{1}{2\pi}\int_{\alpha}^{\pi} \hat{u}_1 \sin(\omega t)\mathrm{d}\omega t = \frac{\hat{u}_1}{2\pi}\left[-\cos(\omega t)\right]_{\alpha}^{\pi} = \frac{\hat{u}_1}{2\pi}\left(1+\cos(\alpha)\right). \tag{11.1}$$

Here, α denotes the phase angle at which the thyristor is triggered (aka firing angle). In the M1C case, the feasible range for α is $[0, \pi]$ as the thyristor requires a positive forward voltage to start conducting, that is, if $u_{\mathrm{T}} < 0$ a firing impulse would not change its conduction state. The RMS value of the output voltage is given by

$$U_2 = \sqrt{\frac{1}{2\pi}\int_{\alpha}^{\pi} \hat{u}_1^2 \sin^2(\omega t)\mathrm{d}\omega t} = \ldots = \frac{\hat{u}_1}{2}\sqrt{\frac{\pi - \alpha + \sin(\alpha)\cos(\alpha)}{\pi}}. \tag{11.2}$$

In contrast to the M1U rectifier from (10.3), the M1C rectifier allows for controlling the output voltage by adjusting the firing angle α.

M1C rectifier: Fourier series

The Fourier coefficients of the output voltage $u_2(t)$ for the M1C converter are

$$
\begin{aligned}
a^{(0)} &= \frac{1}{\pi}\int_0^{2\pi} u_2(t)\mathrm{d}\omega t = \frac{1}{\pi}\int_\alpha^{\pi} \hat{u}_1 \sin(\omega t)\mathrm{d}\omega t = 2\overline{u}_2 = \frac{\hat{u}_1}{\pi}(1+\cos(\alpha)),\\
a^{(k)} &= \frac{1}{\pi}\int_0^{2\pi} u_2(t)\cos(k\omega t)\mathrm{d}\omega t = \frac{1}{\pi}\int_\alpha^{\pi} \hat{u}_1 \sin(\omega t)\cos(k\omega t)\mathrm{d}\omega t = \ldots\\
&= \begin{cases} \frac{\hat{u}_1}{\pi}\frac{2}{1-k^2}, & k=1\\ \frac{1}{2\pi}\left(\frac{\cos(\alpha(k-1))+\cos(k\pi)}{k-1} - \frac{\cos(\alpha(k+1))+\cos(k\pi)}{k+1}\right), & k\geq 2. \end{cases} \qquad (11.3)\\
b^{(k)} &= \frac{1}{\pi}\int_0^{2\pi} u_2(t)\sin(k\omega t)\mathrm{d}\omega t = \frac{1}{\pi}\int_\alpha^{\pi} \hat{u}_1 \sin(\omega t)\sin(k\omega t)\mathrm{d}\omega t = \ldots\\
&= \begin{cases} \frac{-\alpha+\pi+\cos(\alpha)\sin(\alpha)}{2\pi}, & k=1,\\ \frac{1}{2\pi}\left(\frac{\sin(\alpha(k-1))+\sin(k\pi)}{k-1} - \frac{\sin(\alpha(k+1))+\sin(k\pi)}{k+1}\right), & k\geq 2. \end{cases}
\end{aligned}
$$

In contrast to the M1U rectifier, one can observe additional harmonic components due to additional distortion of the output voltage caused by the thyristor switching.

Table of contents

M2C converter

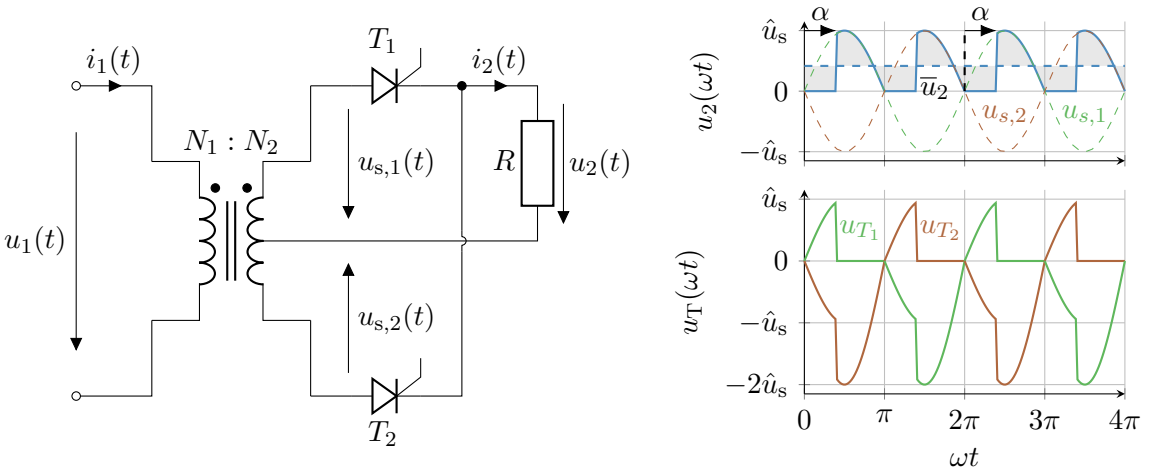

Fig. 11.3: M2C topology (aka two-pulse mid-point converter) with center-tapped transformer and a resistive load

M2C converter: resistive load

The average output voltage of the M2C converter for a resistive load is given by

$$\overline{u}_2 = \frac{1}{\pi}\int_{\alpha}^{\pi} \hat{u}_\mathrm{s}\sin(\omega t)\mathrm{d}\omega t = \frac{\hat{u}_\mathrm{s}}{\pi}\left[-\cos(\omega t)\right]_{\alpha}^{\pi} = \frac{\hat{u}_\mathrm{s}}{\pi}\left(1+\cos(\alpha)\right). \tag{11.4}$$

The RMS value of the output voltage results in

$$U_2 = \sqrt{\frac{1}{\pi}\int_{\alpha}^{\pi} \hat{u}_\mathrm{s}^2\sin^2(\omega t)\mathrm{d}\omega t} = \ldots = \frac{\hat{u}_\mathrm{s}}{\sqrt{2}}\sqrt{\frac{\pi-\alpha+\sin(\alpha)\cos(\alpha)}{\pi}}. \tag{11.5}$$

The primary to secondary voltage ratio of the center-tapped transformer yields

$$\frac{\hat{u}_\mathrm{s}}{\hat{u}_1} = \frac{1}{2}\frac{N_2}{N_1}.$$

It should be noted that in the case of a resistive load, the M2C's output voltage is always positive for the feasible firing angle range $\alpha \in [0, \pi]$.

M2C converter with an output filter

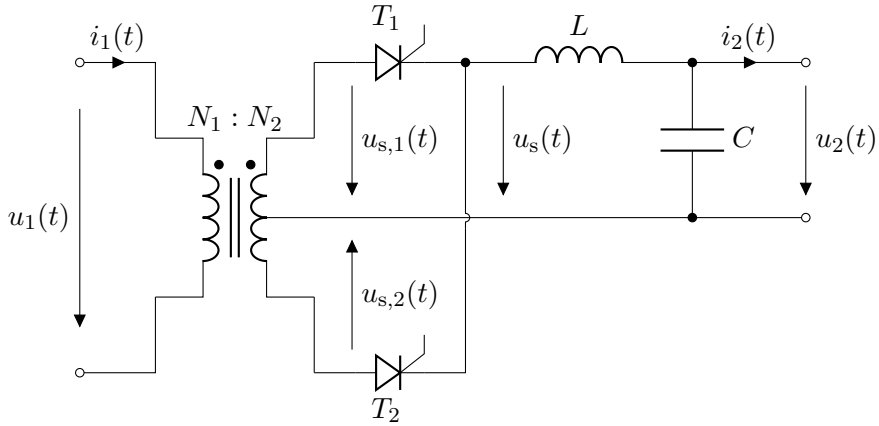

Fig. 11.4: M2C converter with an output filter assuming $u_2(t) = U_2 = \text{const.}$

M2C converter with an output filter (cont.)

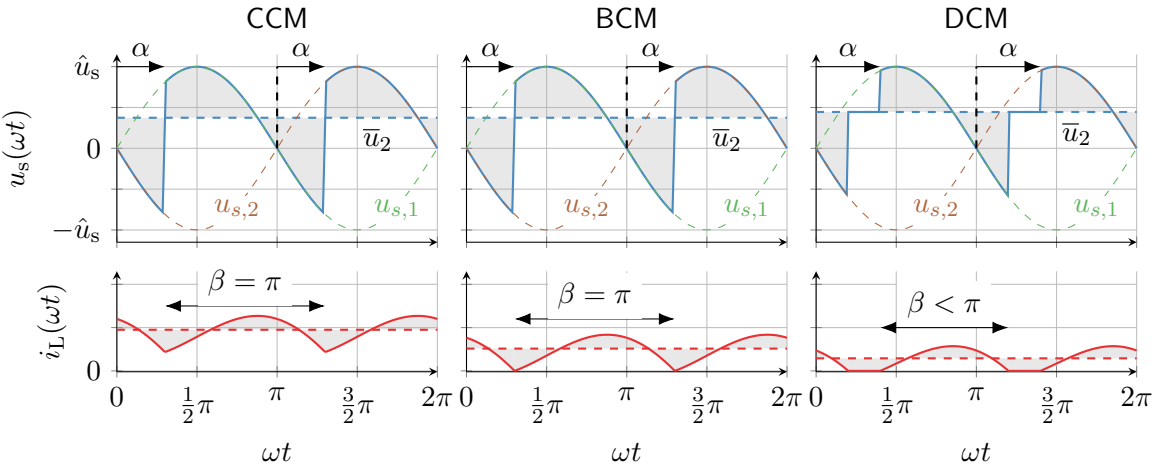

Fig. 11.5: M2C topology with an output filter and different average load currents

M2C converter with an output filter (cont.)

Due to the output filter, the secondary voltage $u_\mathrm{s}(t)$ can become negative since the current flow is maintained by the inductor and, therefore, a thyristor is remaining in the conducting state (until the next thyristor is triggered). The average output voltage in CCM (and BCM) is given by

$$\begin{aligned}\overline{u}_2 &= \frac{1}{\pi}\int_{\alpha}^{\alpha+\pi} \hat{u}_\mathrm{s}\sin(\omega t)\mathrm{d}\omega t = \frac{\hat{u}_\mathrm{s}}{\pi}\left[-\cos(\omega t)\right]_{\alpha}^{\alpha+\pi} = \frac{\hat{u}_\mathrm{s}}{\pi}\left(-\cos(\alpha+\pi)+\cos(\alpha)\right)\\ &= \hat{u}_\mathrm{s}\frac{2}{\pi}\cos(\alpha).\end{aligned} \tag{11.6}$$

In DCM the conduction interval β is less than π and the average output voltage is given by

$$\begin{aligned}\overline{u}_2 &= \frac{1}{\pi}\int_{\alpha}^{\alpha+\beta} \hat{u}_\mathrm{s}\sin(\omega t)\mathrm{d}\omega t = \frac{\hat{u}_\mathrm{s}}{\pi}\left[-\cos(\omega t)\right]_{\alpha}^{\alpha+\beta} = \frac{\hat{u}_\mathrm{s}}{\pi}\left(\cos(\alpha)-\cos(\alpha+\beta)\right)\\ &= \hat{u}_\mathrm{s}\frac{2}{\pi}\sin\left(\frac{\beta}{2}\right)\sin\left(\alpha+\frac{\beta}{2}\right).\end{aligned} \tag{11.7}$$

M2C converter with an active load

Analyzing (11.6) for the feasible firing angle range $\alpha \in [0, \pi]$ reveals

$$\overline{u}_2 \begin{cases} \geq 0, & \alpha \in [0, \pi/2], \\ < 0, & \alpha \in (\pi/2, \pi], \end{cases} \tag{11.8}$$

that is, the output voltage can become negative for $\alpha > \pi/2$ in CCM and BCM (analogous observation can be also made for DCM). Assuming an average output current $\overline{i}_2 > 0$, which can be only positive due to the thyristor unipolar current capability, the average output power is in the range of (for CCM and BCM)

$$\overline{p}_2 \begin{cases} \geq 0, & \alpha \in [0, \pi/2], \\ < 0, & \alpha \in (\pi/2, \pi]. \end{cases} \tag{11.9}$$

Hence, the M2C can transfer energy from the load to the source which requires an active load (e.g., battery or generator) to maintain this reversed energy flow. Consequently, the M2C can be used as a bidirectional energy transfer system operating both as a rectifier and an inverter.

M2C converter with an active load (cont.)

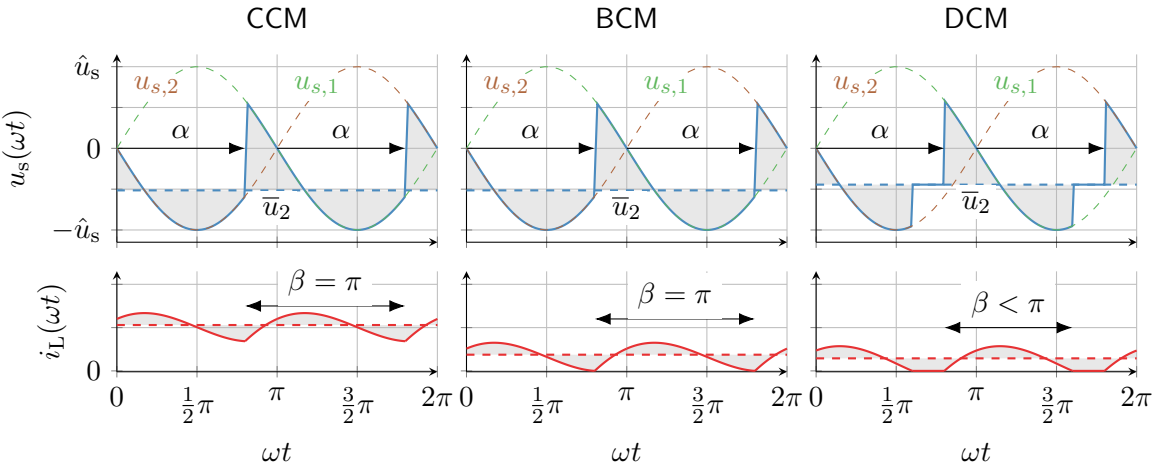

Fig. 11.6: M2C topology with a negative output voltage delivering energy to the source side

M2C output voltage overview

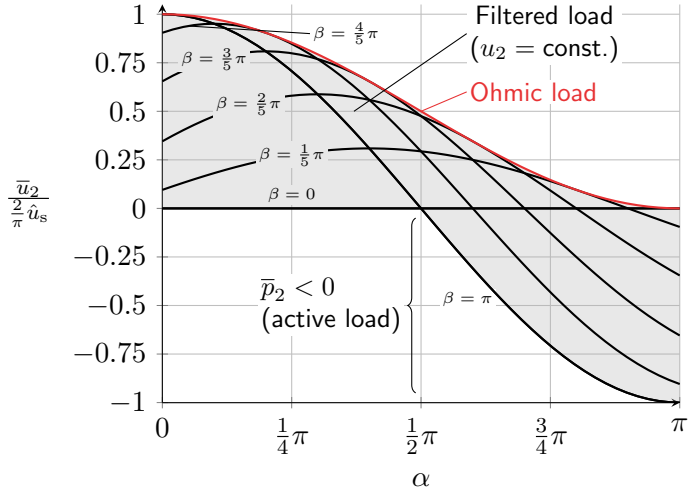

Fig. 11.7: M2C output voltage overview

Table of contents

M2C: complex power analysis

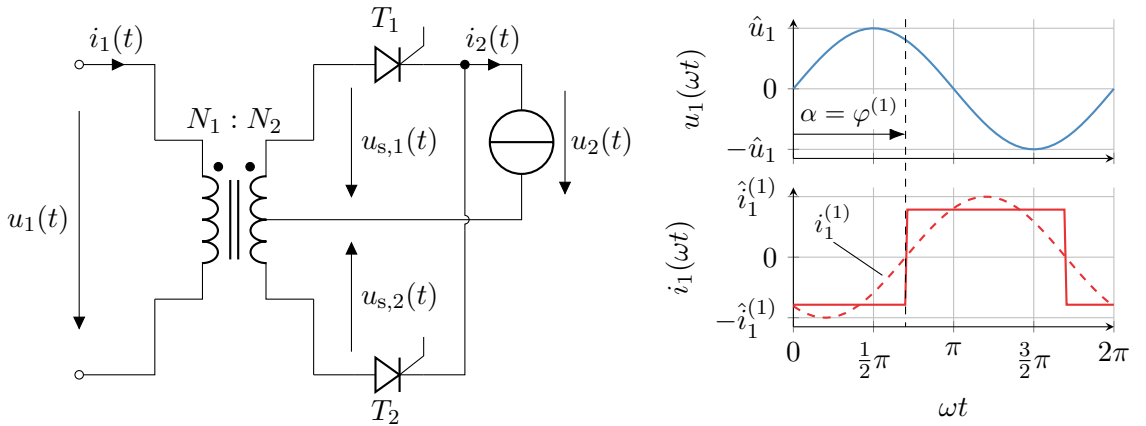

Fig. 11.8: Input voltage and current of the M2C converter with idealized filtered, constant output current (represented by a current source) and an idealized transformer

M2C: complex power analysis (cont.)

Based on the setup form Fig. 11.8 one can observe that the phase angle $\varphi^{(1)}$ between the input voltage $u_1(t)$ and the fundamental input current $i_1^{(1)}(t)$ is given by the firing angle α:

$$\varphi^{(1)} = \alpha.$$

Considering the center-tapped transformer, the input current fundamental amplitude is

$$i_1^{(1)} = \frac{4}{\pi}\frac{1}{2}\frac{N_2}{N_1}I_2 = \frac{2}{\pi}\frac{N_2}{N_1}I_2, \tag{11.10}$$

where I_2 is constant output current and $4/\pi$ represents the first Fourier coefficient of the square-shaped input current $i_1(t)$. The latter is formed by the thyristors applying the positive and negative output current to the transformer's secondary side. The RMS value of the fundamental component $I_1^{(1)}$ and the RMS value of the input current I_1 are

$$I_1^{(1)} = \frac{\sqrt{2}}{\pi}\frac{N_2}{N_1}I_2, \qquad I_1 = \frac{1}{2}\frac{N_2}{N_1}I_2. \tag{11.11}$$

The latter can be found by considering that the RMS value of a symmetrical block-shaped signal is its amplitude.

M2C: complex power analysis (cont.)

Assuming an ideal sinusoidal input voltage, the active power is only transferred based on its fundamental component

$$P_1 = P_1^{(1)} = I_1^{(1)} U_1 \cos(\varphi^{(1)}) \tag{11.12}$$

with U_1 being the RMS value of the input voltage – compare (10.45). Assuming idealized, lossless components the active input power must be equal to the average output power

$$P_1 = \overline{p}_2 = I_2 \overline{u}_2 = I_2 \hat{u}_\mathrm{s} \frac{2}{\pi} \cos(\alpha) = I_2 \hat{u}_{\mathrm{s}0} \cos(\alpha) \tag{11.13}$$

with $\hat{u}_{\mathrm{s}0} = \hat{u}_\mathrm{s} \cdot 2/\pi$ being the maximum reachable output voltage (for $\alpha = 0$). From (11.12) the fundamental reactive power can be determined as

$$Q_1^{(1)} = I_1^{(1)} U_1 \sin(\varphi^{(1)}) = I_2 \hat{u}_{\mathrm{s}0} \sin(\alpha) \tag{11.14}$$

and the fundamental apparent power is given by

$$S_1^{(1)} = I_1^{(1)} U_1 = I_2 \hat{u}_{\mathrm{s}0} = \text{const.} \tag{11.15}$$

M2C: reactive power diagram

Rewriting the fundamental apparent power in terms of the active and reactive power yields:

$$\left(S_1^{(1)}\right)^2 = \left(P_1\right)^2 + \left(Q_1^{(1)}\right)^2 = I_2^2 \hat{u}_{\mathrm{s0}}^2 \quad \Leftrightarrow \left(\frac{Q_1^{(1)}}{I_2 \hat{u}_{\mathrm{s0}}}\right)^2 + \left(\frac{P_1^2}{I_2 \hat{u}_{\mathrm{s0}}}\right)^2 = 1. \tag{11.16}$$

Inserting $P_1 = I_2 \hat{u}_{\mathrm{s0}} \cos(\alpha)$ from (11.13) finally yields the following circular equation

$$\left(\frac{Q_1^{(1)}}{I_2 \hat{u}_{\mathrm{s0}}}\right)^2 + \left(\cos(\alpha)\right)^2 = 1 \quad \Leftrightarrow \quad \left(\frac{Q_1^{(1)}}{S_1^{(1)}}\right)^2 + \left(\frac{\overline{u}_2}{\hat{u}_{\mathrm{s0}}}\right)^2 = 1 \tag{11.17}$$

which can be visualized as a reactive power diagram of the M2C converter – compare the upcoming Fig. 11.9.

M2C: reactive power diagram (cont.)

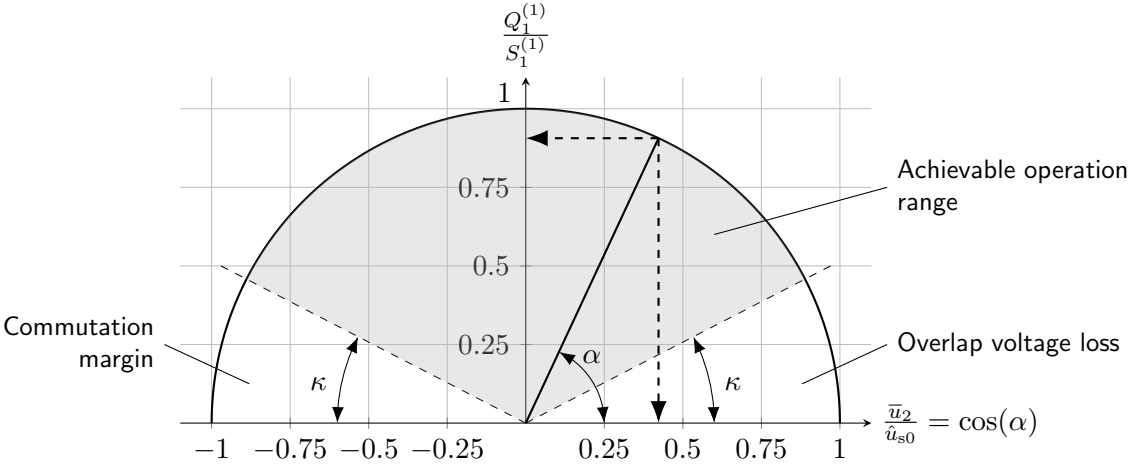

Fig. 11.9: Fundamental reactive power demand at some constant output current

M2C: complex power analysis incl. harmonics

Extending the previous analysis of the complex power fundamental components to the total complex power, one can determine the total apparent power as

$$S_1 = I_1 U_1 = \frac{1}{2}\frac{N_2}{N_1} I_2 U_1 = \frac{\pi}{2\sqrt{2}} S_1^{(1)} \approx 1.11 \cdot S_1^{(1)}. \tag{11.18}$$

Interestingly, the apparent power is independent of the firing angle α. The total reactive power is given by

$$Q_1 = \sqrt{S_1^2 - P_1^2} = S_1^{(1)} \sqrt{\frac{\pi^2}{8} - \cos^2(\alpha)} = \frac{\sqrt{2}}{\pi}\frac{N_2}{N_1} I_2 U_1 \sqrt{\frac{\pi^2}{8} - \cos^2(\alpha)}. \tag{11.19}$$

Alternatively, one could also determine the harmonic reactive power

$$Q_1^{(\mathrm{h})} = \sqrt{\left(S_1\right)^2 - \left(S_1^{(1)}\right)^2} = S_1^{(1)} \sqrt{\frac{\pi^2 - 8}{8}} = \frac{\sqrt{2}}{\pi}\frac{N_2}{N_1} I_2 U_1 \sqrt{\frac{\pi^2 - 8}{8}}. \tag{11.20}$$

first and then determine the total reactive power as

$$Q_1 = \sqrt{\left(Q_1^{(1)}\right)^2 + \left(Q_1^{(\mathrm{h})}\right)^2} = S_1^{(1)} \sqrt{\sin^2(\alpha) + \frac{\pi^2 - 8}{8}} = \frac{\sqrt{2}}{\pi}\frac{N_2}{N_1} I_2 U_1 \sqrt{\sin^2(\alpha) + \frac{\pi^2 - 8}{8}}.$$

Table of contents

Commutation

Idealized, instantaneous commutation

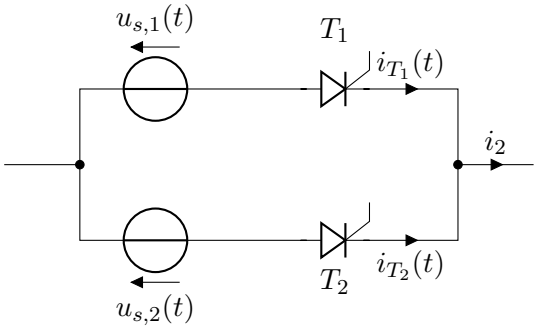

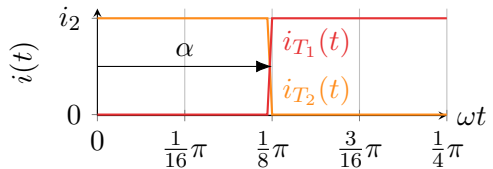

Actual commutation (with overlap)

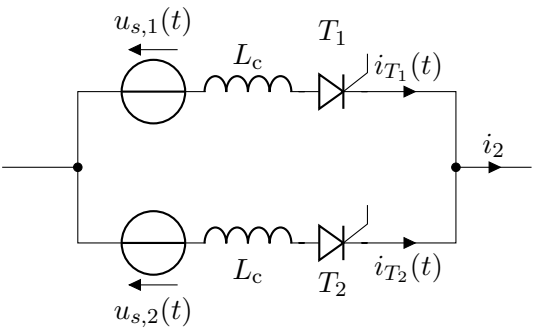

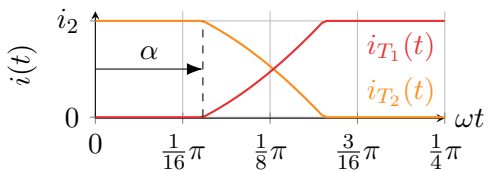

Commutation (cont.)

So far we have considered an idealized, instantaneous commutation of the thyristors. In practice, the commutation process is not instantaneous and the thyristors overlap for a certain period due to the commutation inductance L_c, which can originate from:

- Stray inductance of the feeding transformer,
- Parasitic inductance of the thyristor package,
- Parasitic inductance of the circuit layout.

Kirchhoff's voltage law for the commutation loop yields

$$u_\mathrm{c}(t) = u_{\mathrm{s},1}(t) - u_{\mathrm{s},2}(t) = 2L_\mathrm{c}\frac{\mathrm{d}}{\mathrm{d}t}i_{T_2}(t) = -2L_\mathrm{c}\frac{\mathrm{d}}{\mathrm{d}t}i_{T_1}(t) \tag{11.21}$$

with the commutation voltage $u_\mathrm{c}(t)$ and the thyristor currents $i_{T_1}(t)$ and $i_{T_2}(t)$.

Commutation (cont.)

From (11.21) the thyristor currents can be expressed as

$$i_{T_1}(t) = i_{T_1}(k\pi+\alpha) - \frac{1}{2L_\mathrm{c}\omega}\int_{k\pi+\alpha}^{\omega t} u_\mathrm{c}(\tau)\mathrm{d}\tau = i_{T_1}(k\pi+\alpha) + \frac{u_\mathrm{s}}{L_\mathrm{c}\omega}\left(\cos(k\pi+\alpha) - \cos(\omega t)\right),$$

$$i_{T_2}(t) = i_{T_2}(k\pi+\alpha) + \frac{1}{2L_\mathrm{c}\omega}\int_{k\pi+\alpha}^{\omega t} u_\mathrm{c}(\tau)\mathrm{d}\tau = i_{T_2}(k\pi+\alpha) - \frac{u_\mathrm{s}}{L_\mathrm{c}\omega}\left(\cos(k\pi+\alpha) - \cos(\omega t)\right).$$

Here, $i_{T_1}(k\pi+\alpha)$ and $i_{T_2}(k\pi+\alpha)$ are the thyristor currents at the beginning of the commutation process during the k-th half cycle. One can distinguish two cases:

$$i_{T_1}(k\pi+\alpha) = 0, \quad i_{T_2}(k\pi+\alpha) = i_2, \quad \text{commutation from } T_2 \text{ to } T_1,$$
$$i_{T_1}(k\pi+\alpha) = i_2, \quad i_{T_2}(k\pi+\alpha) = 0, \quad \text{commutation from } T_1 \text{ to } T_2.$$

The commutation process ends when the thyristor currents reach i_2 and zero, respectively.

Commutation: overlap angle and feasible firing angle range

To determine the commutation overlap angle κ, we consider $k = 0$ and the commutation from T_2 to T_1, that is, $i_{T_1}(\alpha) = 0$. The commutation ends when $i_{T_1}(\alpha + \kappa) = i_2$, which yields

$$i_{T_1}(\alpha + \kappa) = i_2 \stackrel{!}{=} \frac{u_\mathrm{s}}{L_\mathrm{c}\omega} \left(\cos(\alpha) - \cos(\alpha + \kappa)\right). \tag{11.22}$$

Solving for the overlap angle κ results in

$$\kappa = \arccos\left(\cos(\alpha) - \frac{i_2 L_\mathrm{c}\omega}{u_\mathrm{s}}\right) - \alpha. \tag{11.23}$$

To ensure a successful commutation $\alpha + \kappa < \pi$ must hold: Otherwise the commutation voltage changes its sign and the commutation fails. Hence, the achievable firing angle is determined by

$$\alpha + \kappa < \pi \quad \Leftrightarrow \quad \arccos\left(\cos(\alpha) - \frac{i_2 L_\mathrm{c}\omega}{u_\mathrm{s}}\right) < \pi \tag{11.24}$$

leading to

$$\alpha < \arccos\left(\frac{i_2 L_\mathrm{c}\omega}{u_\mathrm{s}} - 1\right). \tag{11.25}$$

Commutation: successful and unsuccessful examples

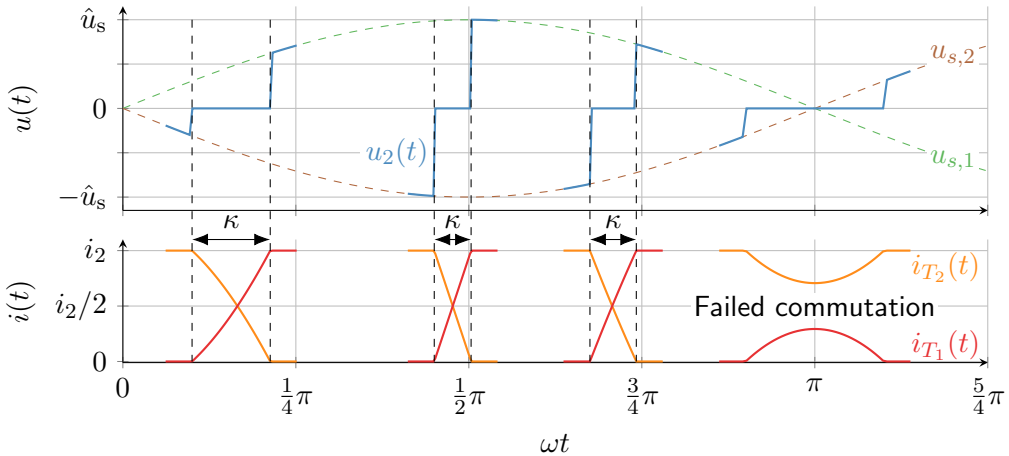

Fig. 11.10: Commutation process for different firing angles α

Commutation: output voltage deviation

As seen in Fig. 11.10, the output voltage of the thyristor stage is zero during the commutation process as the transformer's secondary side is temporarily short-circuited during the overlap period (since both thyristors are conducting):

$$u_{\mathrm{s}}(\omega t) = 0, \qquad \omega t \in [k\pi + \alpha, k\pi + \alpha + \kappa]. \tag{11.26}$$

The output voltage loss due to commutation corresponds to

$$\Delta u = \frac{1}{\pi}\int_{\alpha}^{\alpha+\kappa} \hat{u}_{\mathrm{s}} \sin(\omega t)\mathrm{d}(\omega t) = \frac{\hat{u}_{\mathrm{s}}}{\pi}\left[-\cos(\omega t)\right]_{\alpha}^{\alpha+\kappa} = \frac{\hat{u}_{\mathrm{s}}}{\pi}\left[\cos(\alpha) - \cos(\alpha+\kappa)\right]. \tag{11.27}$$

Inserting (11.23) for κ yields

$$\begin{aligned}\Delta u &= \frac{\hat{u}_{\mathrm{s}}}{\pi}\left[\cos(\alpha) - \cos\left(\alpha + \arccos\left(\cos(\alpha) - \frac{i_2 L_{\mathrm{c}}\omega}{\hat{u}_{\mathrm{s}}}\right) - \alpha\right)\right] \\ &= \frac{i_2 L_{\mathrm{c}}\omega}{\pi}.\end{aligned} \tag{11.28}$$

Hence, the average output voltage is deviating by Δu due to the commutation process.

Table of contents

M3C converter

The previous diode-based rectifiers with higher-pulse numbers can be directly transferred to their controlled counterparts using thyristors, such as the 3-pulse converter shown in Fig. 11.11.

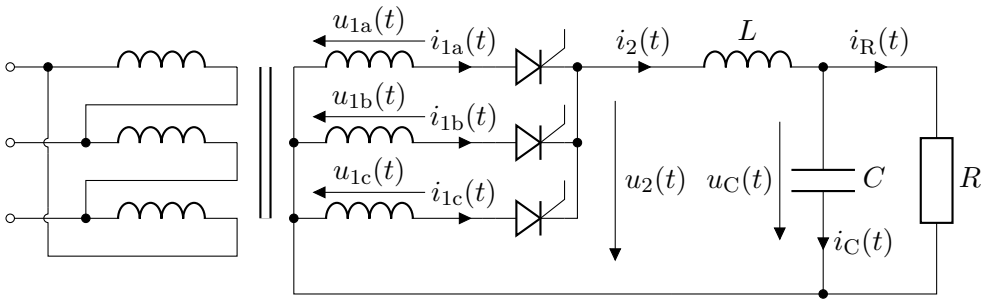

Fig. 11.11: M3C topology with an input three-phase transformer, a resistive load and output filter

M3C converter (cont.)

The M3C converter's firing angle α starts at the crossing of two adjacent input voltages, that is, where the voltage over the next thyristor becomes positive. For CCM and neglecting commutation and other parasitic effects, the M3C's average output voltage is

$$\begin{aligned}\overline{u}_2 &= \frac{3}{2\pi}\int_{\frac{1}{6}\pi+\alpha}^{\frac{5}{6}\pi+\alpha} \hat{u}_1 \sin(\omega t)\mathrm{d}\omega t \\ &= \frac{3}{2\pi}\hat{u}_1 \left[-\cos(\omega t)\right]_{\frac{1}{6}\pi+\alpha}^{\frac{5}{6}\pi+\alpha} = \dots \\ &= \frac{3\sqrt{3}}{2\pi}\hat{u}_1 \cos(\alpha).\end{aligned} \tag{11.29}$$

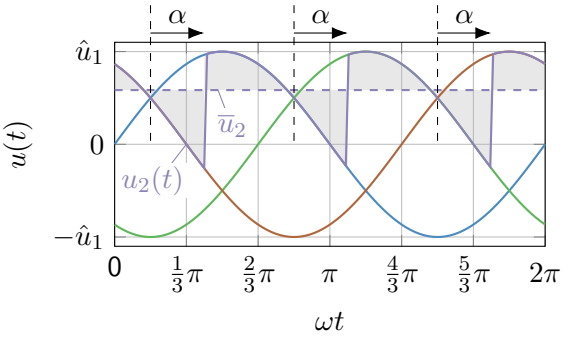

Fig. 11.12: Examplary firing angle for the M3C converter

B6C converter

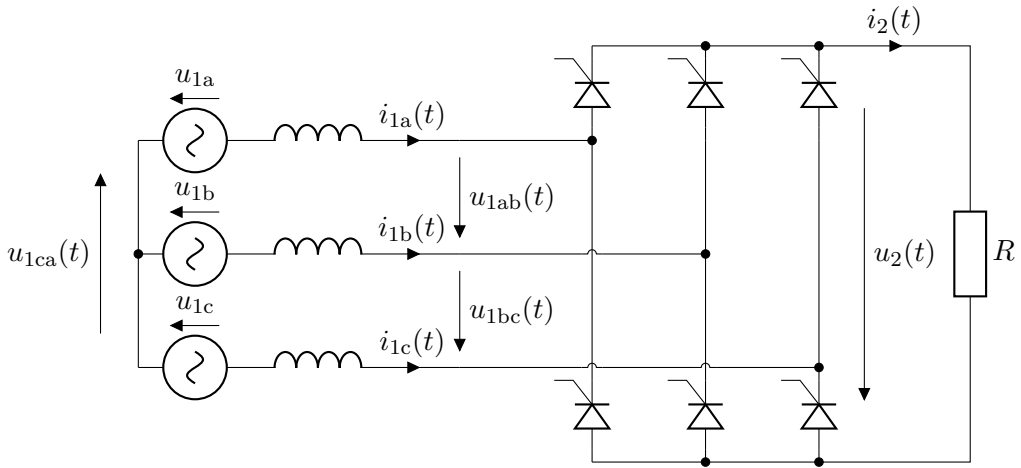

Fig. 11.13: B6C topology with line chokes and a resistive load

Output voltage of a thyristor bridge converter with p pulses

The average output voltage (under idealized CCM operation) of a thyristor bridge converter with p pulses is given by

$$\begin{aligned}\overline{u}_2 &= \frac{p}{2\pi}\int_{\alpha-\frac{\pi}{p}}^{\alpha+\frac{\pi}{p}} \hat{u}\cos(\omega t)\mathrm{d}\omega t \\ &= \hat{u}\frac{p}{2\pi}\left[\sin\left(\alpha+\frac{\pi}{p}\right)-\sin\left(\alpha-\frac{\pi}{p}\right)\right] \\ &= \hat{u}\frac{p}{\pi}\sin\left(\frac{\pi}{p}\right)\cos(\alpha). \qquad (11.30)\end{aligned}$$

Here, the maximum achievable voltage

$$\max_{\alpha}\overline{u}_2 = \hat{u}\frac{p}{\pi}\sin\left(\pi/p\right) \qquad (11.31)$$

increases with the number of pulses p.

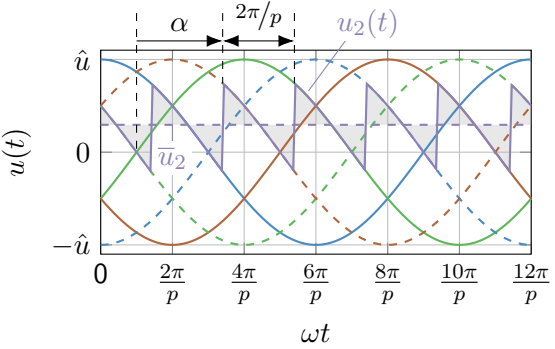

Fig. 11.14: Generalized firing angle representation for a thyristor bridge converter with p pulses and $\hat{u}$ being the line-to-line voltage amplitude

Section summary

This section provided an introduction to thyristor-based converters. The key takeaways are:

- In contrast to diode-based rectifiers:
  - Are controllable by varying the firing angle α (within its feasible range).
  - Can transfer power in both directions (rectifier and inverter operation).
- Likewise diode-based rectifiers:
  - Introduce harmonics in the output voltage and input current (i.e., require filters).
  - Typically, do not operate at unity power factor (require reactive power).
  - Are line-commutated, as the external grid voltage is required to achieve the commutation.

Previous analyses based on diodes or thyristor-based converters were dealt with in varying detail level, but as they can be transferred analogously they are not explicitly shown due to time constraints. In addition, there are further interesting thyristor-based applications such as

- four quadrant thyristor converters (e.g., cycloconverters) covering both voltage and current polarities,
- specialized stacked topologies for high-voltage DC transmission.

Table of contents

Transistor-based AC/DC converters: self-commutated converters

Up to now:

- Diode-based converters
  - Rectification only
  - No control
- Thyristor-based converters
  - Rectification and inversion
  - Limited control / line commutation

Extension in this section:

- Transistor-based converters
  - Rectification and inversion
  - Fully controllable / self-commutated

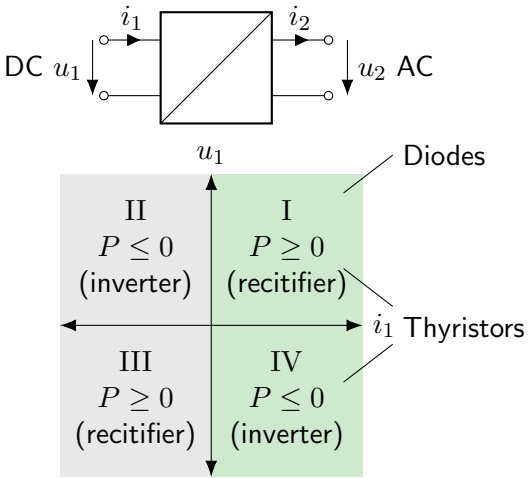

Idealized switch representation of a single-phase AC/DC bridge converter

Define switching function:

$$s_i(t) = \begin{cases} +1 & \text{upper position,} \\ -1 & \text{lower position.} \end{cases} \tag{12.1}$$

Output voltage considering a voltage source at the input is:

$$u_2(t) = \underbrace{\frac{1}{2}\left(s_1(t) - s_2(t)\right)}_{s(t)} u_1(t). \tag{12.2}$$

Input current assuming a current source at the output results in:

$$i_1(t) = s(t) i_2(t). \tag{12.3}$$

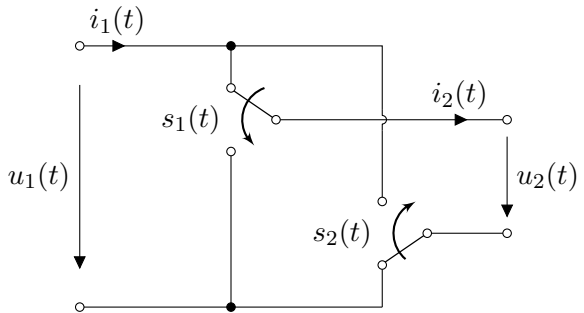

Fig. 12.1: Idealized switch representation of a single-phase AC/DC bridge converter

Circuit realization

- Remember: complementary switching of $\{T_1, T_2\}$ and $\{T_3, T_4\}$ to prevent a DC-link short-circuit.
- Possible (allowed) switching states:

T_1	T_2	T_3	T_4	s_1	s_2	s
on	off	off	on	$+1$	-1	$+1$
off	on	on	off	-1	$+1$	-1
on	off	on	off	$+1$	$+1$	0
off	on	off	on	-1	-1	0

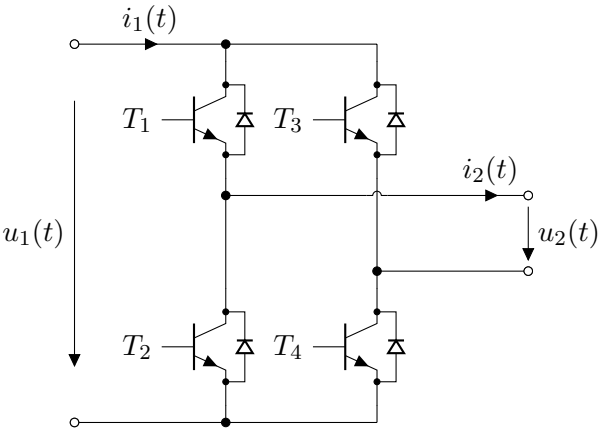

Fig. 12.2: Full-bridge single-phase AC/DC converter (identical to the one used in the DC/DC section in Fig. 8.42)

Pulse width modulation (PWM) options

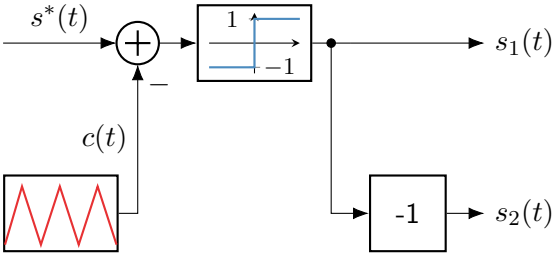

Fig. 12.3: PWM with complementary switching

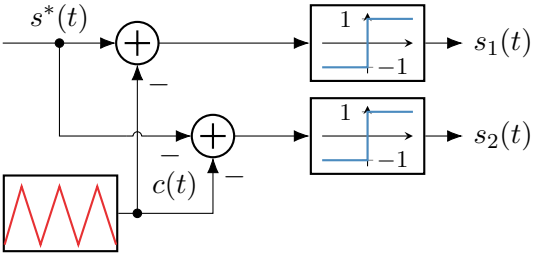

Fig. 12.4: PWM with interleaved switching

PWM example with complementary switching

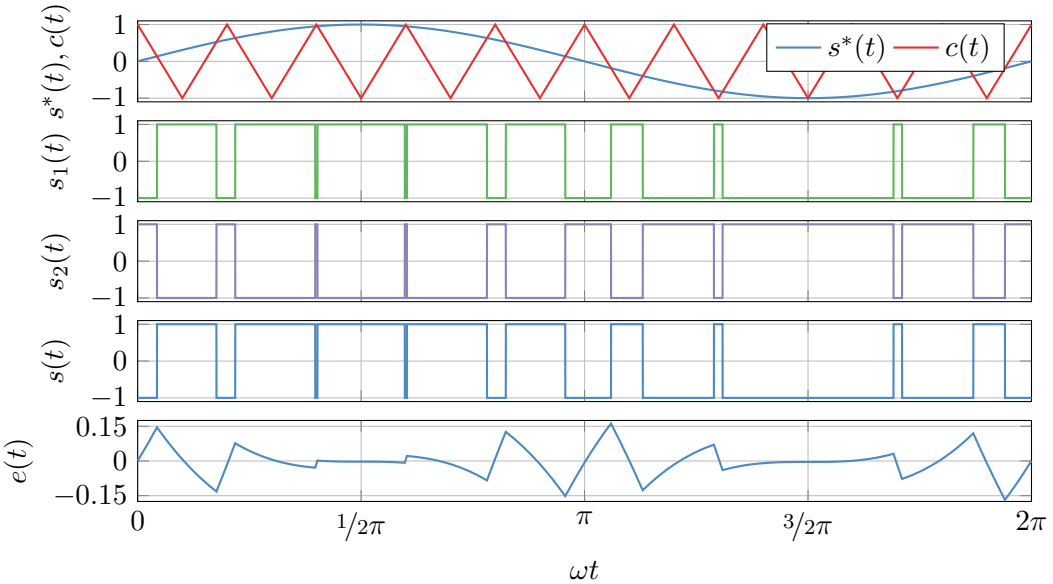

PWM example with interleaved switching

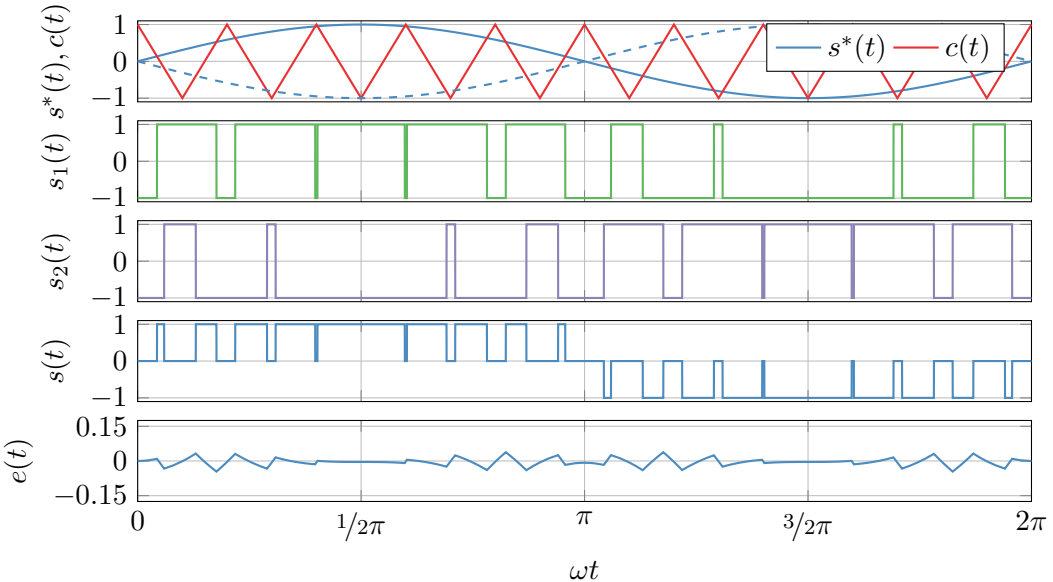

PWM approximation error analysis

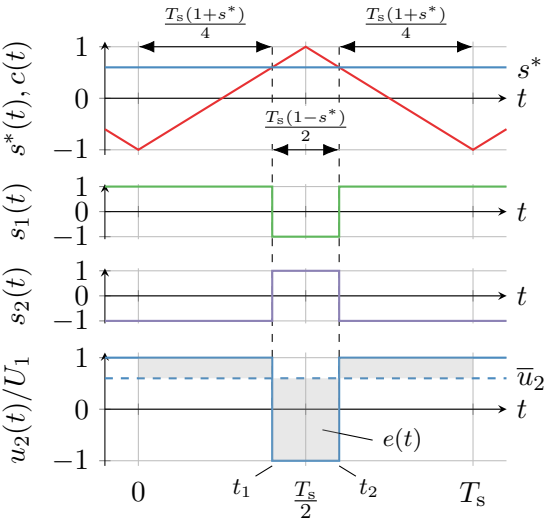

Fig. 12.5: Pulse pattern for complementary PWM

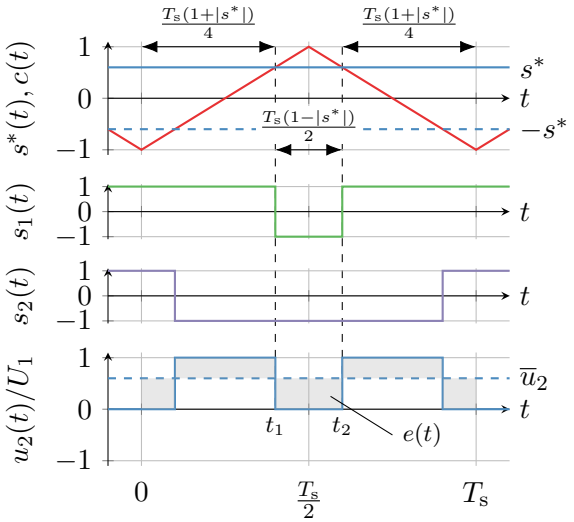

Fig. 12.6: Pulse pattern for interleaved PWM

PWM approximation error analysis (cont.)

To evaluate the error between the reference $s^*(t)$ and the switched output voltage $u_2(t)$, we introduce the following normalized integral difference:

$$e(t) = \frac{1}{T_\mathrm{s}} \int_{t_0}^{t} \left(s^*(\tau) - s(\tau)\right) \mathrm{d}\tau. \tag{12.4}$$

This error can be interpreted as the resulting current ripple assuming a pure inductive load L at a constant input voltage $u_1(t) = U_1$:

$$\Delta i_2(t) = \frac{T_\mathrm{s} U_1}{2L} \left|e(t)\right|. \tag{12.5}$$

For a constant reference $s^*(t) = s^*$, the biggest error corresponds to the integral over the time interval $[t_1, t_2]$ as can be seen in Fig. 12.5 and Fig. 12.6:

$$\begin{aligned} &\text{complimentary switching (cs):} && \max_t e_\mathrm{cs}(t) = \frac{1}{T_s} \left(s^* + 1\right) \left(t_2 - t_1\right) = \frac{1}{2} \left(s^* + 1\right) \left(1 - s^*\right), \\ &\text{interleaved switching (is):} && \max_t e_\mathrm{is}(t) = \frac{1}{T_s} \left|s^*\right| \left(t_2 - t_1\right) = \frac{1}{2} \left|s^*\right| \left(1 - \left|s^*\right|\right). \end{aligned} \tag{12.6}$$

PWM approximation error analysis (cont.)

Further, analyzing (12.6)

$$\frac{\mathrm{d}}{\mathrm{d}s^*}\left(\max_t e_{\mathrm{cs}}(t)\right) = -2s^*, \qquad \frac{\mathrm{d}}{\mathrm{d}s^*}\left(\max_t e_{\mathrm{is}}(t)\right) = \mathrm{sgn}(s^*) - 2s^* \tag{12.7}$$

reveals the worst case deviation at a switching reference of:

$$\arg\max_{s^*}\left\{\max_t e_{\mathrm{cs}}(t)\right\} = 0, \qquad \arg\max_{s^*}\left\{\max_t e_{\mathrm{is}}(t)\right\} = \pm\frac{1}{2}. \tag{12.8}$$

Inserting this finding into (12.5) delivers

$$\begin{aligned} \Delta i_{2,\mathrm{cs}} &= (1-s^*)(1+s^*)\Delta i_{2,\mathrm{cs,max}} \quad \text{with} \quad \Delta i_{2,\mathrm{cs,max}} = \frac{T_{\mathrm{s}}U_1}{2L}, \\ \Delta i_{2,\mathrm{is}} &= 4\,|s^*|\,(1-|s^*|)\Delta i_{2,\mathrm{is,max}} \quad \text{with} \quad \Delta i_{2,\mathrm{is,max}} = \frac{T_{\mathrm{s}}U_1}{8L}. \end{aligned} \tag{12.9}$$

Hence, the current ripple of the interleaved PWM is only $1/4$ of the complementary PWM.

PWM approximation error analysis (cont.)

Reasons for current ripple reduction of interleaved vs. complimentary PWM:

- Effective pulse number doubled:
  - CS: $f_\mathrm{p} = f_\mathrm{s}$
  - IS: $f_\mathrm{p} = 2f_\mathrm{s}$
- Output voltage steps halved:
  - CS: $\Delta u_2 = \pm 2U_1$
  - IS: $\Delta u_2 = \pm U_1$

Note on applicability

This analysis only holds for $s^* = \mathrm{const.}$ and can be transferred only approximately for $s^*(t) = f(\omega)$ if $T_s << \frac{2\pi}{\omega}$.

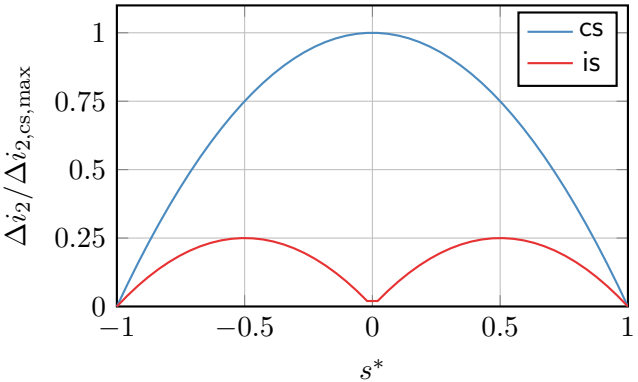

Fig. 12.7: Current ripple as a function of the single-phase AC/DC normalized reference output voltage s^*

Overmodulation

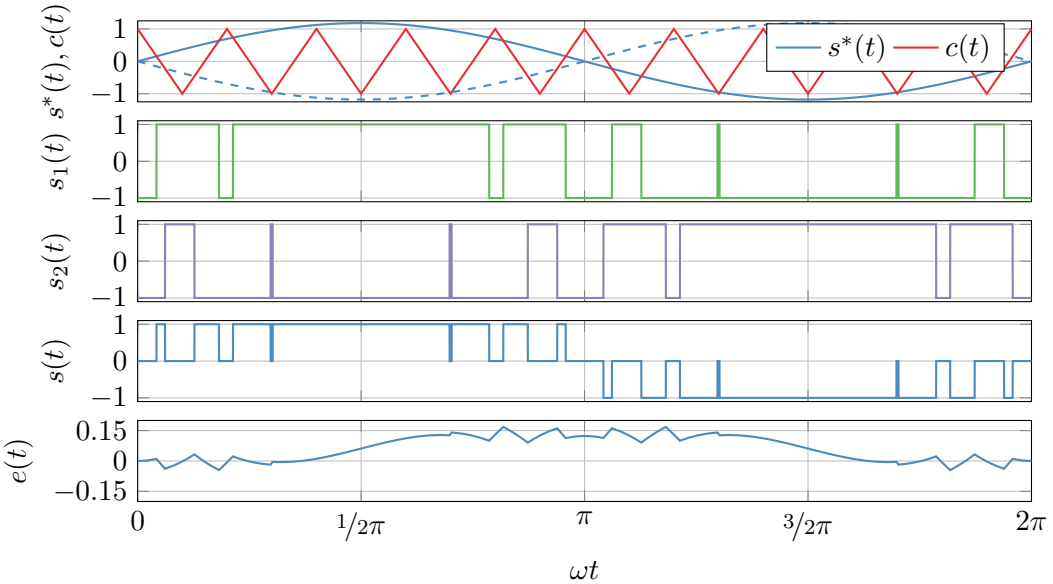

Overmodulation (cont.)

Considering a normalized input reference

$$s^*(t) = m \sin(\omega t) = \frac{\hat{u}_2^*}{U_1} \sin(\omega t)$$

with the modulation ratio m one can distinguish two PWM operation areas:

- $m \leq 1$: linear modulation,
- $m > 1$: overmodulation.

Harmonics

While the normalized output voltage fundamental can be increased beyond unity via overmodulation, increased voltage harmonics must be accepted.

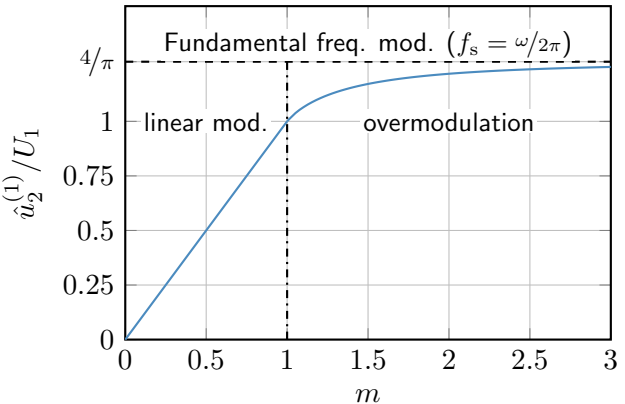

Fig. 12.8: Reference amplitude to output voltage fundamental amplitude

Overmodulation (cont.)

Due to the converter's constraints, the reference voltage is limited to

$$s^*_{\lim}(t) = \begin{cases} 1 & \text{if } s^*(t) > 1, \\ s^*(t) & \text{if } -1 \leq s^*(t) \leq 1, \\ -1 & \text{if } s^*(t) < -1. \end{cases}$$

Hence, from ωt_0 to ωt_1 the converter's output voltage is clipped for $m > 1$. With

$$m \sin(\omega t_0) \stackrel{!}{=} 1$$

one can find

$$\omega t_0 = \arcsin\left(\frac{1}{m}\right). \tag{12.10}$$

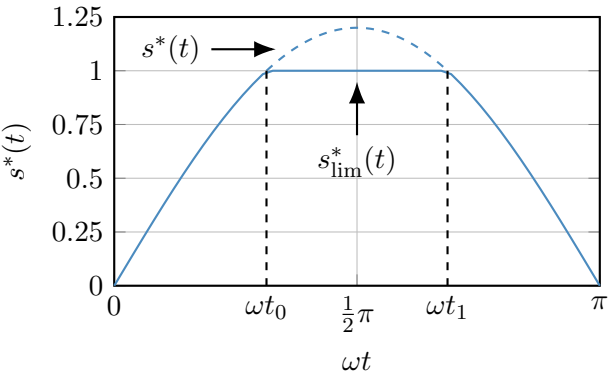

Fig. 12.9: Exemplary time series between average reference and actual voltage in the overmodulation range

Overmodulation (cont.)

To calculate the resulting fundamental output voltage during overmodulation, a Fourier analysis is performed while utilizing the quarter-wave symmetry of the output voltage signal:

$$\begin{aligned}\frac{u_2^{(1)}}{U_1} &= \frac{1}{\pi}\int_0^{2\pi} s_{\text{lim}}^*(\omega\tau)\sin(\omega\tau)\mathrm{d}\omega\tau \\ &= \frac{4}{\pi}\left(\int_0^{\omega t_0} m\sin^2(\omega\tau)\mathrm{d}\omega\tau + \int_{\omega t_0}^{\frac{\pi}{2}} 1\sin(\omega\tau)\mathrm{d}\omega\tau\right) \\ &= \frac{4}{\pi}\left[\frac{m}{2}\left(\omega t_0 - \frac{1}{2}\sin(2\omega t_0)\right) + \cos(\omega t_0)\right].\end{aligned} \tag{12.11}$$

Inserting ωt_0 from (12.10) and applying trigonometric identities yields:

$$\frac{u_2^{(1)}}{U_1} = \frac{2}{\pi}\left[m\arcsin\left(\frac{1}{m}\right) + \sqrt{1-\frac{1}{m^2}}\right] \in \left[1, \frac{4}{\pi}\right] \quad \text{for} \quad m \geq 1. \tag{12.12}$$

Fundamental frequency modulation (aka square wave modulation)

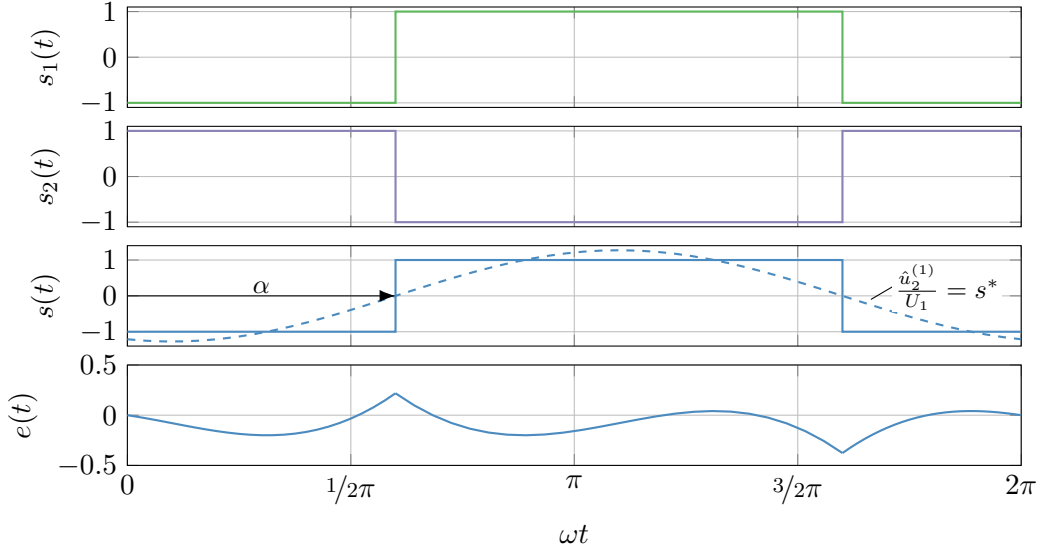

Fundamental frequency modulation (cont.)

The fundamental frequency modulation leads to a pulse pattern synchronized with the fundamental output voltage $\hat{u}_2^{(1)}(t)$, i.e., the switching frequency matches the fundamental voltage frequency

$$f_\mathrm{s} = \frac{\omega}{2\pi}.$$

The fundamental output voltage amplitude can be derived from the corresponding Fourier coefficient

$$\begin{aligned}\frac{u_2^{(k)}}{U_1} &= \frac{1}{\pi}\int_\alpha^{\alpha+\pi} \frac{u_2(t)}{U_1}\sin(k(\omega t-\alpha))\mathrm{d}\omega t = \frac{2}{\pi}\int_0^{\pi/2}\sin(k\omega t)\mathrm{d}\omega t \\ &= \frac{2}{\pi}\left[-\frac{1}{k}\cos(k\omega t)\right]_0^{\pi/2} = \frac{2}{\pi}\left[\frac{1}{k}\left(\cos(0)-\cos(k\frac{\pi}{2})\right)\right] \\ &= \frac{4}{\pi}\frac{1}{k}, \quad k = 1,3,5,7,\ldots\end{aligned} \tag{12.13}$$

The fundamental output voltage amplitude is thus given by $\hat{u}_2^{(1)} = 4/\pi \cdot U_1$ which is fixed due to fundamental frequency modulation while only the phase angle α can be adjusted.

Blanking / interlocking time

When the i-th half bridge is actuated, i.e., changes it switching state, an interlocking / blanking time t_0 is introduced to avoid short-circuiting the DC link:

- First: turn off conducting transistor,
- Second: wait t_0 (ensure safe turn off),
- Third: turn on the other transistor.

Background

Signal delays or component tolerances lead to varying switch on/off times, which is why the interlock ensures an orderly switching process.

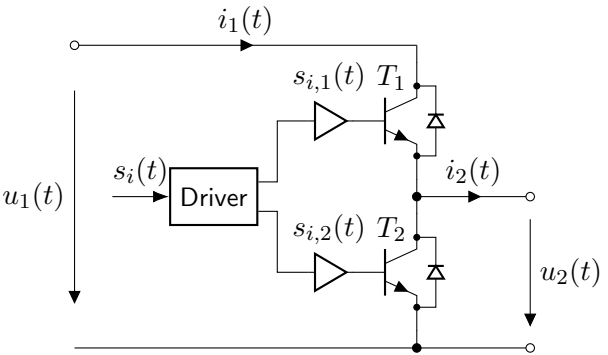

Fig. 12.10: Actuation of one half-bridge branch

Current paths depending on the switching state and current flow direction

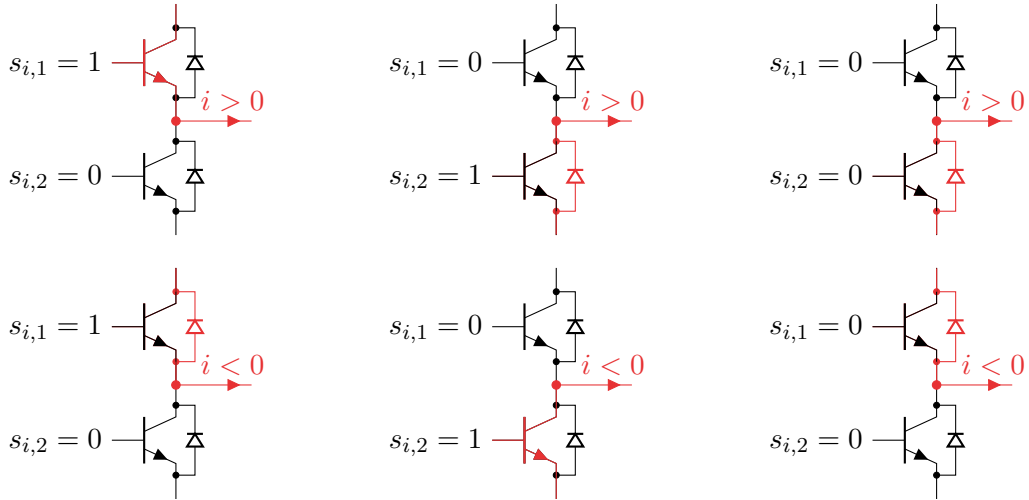

(a) Upper transistor on

(b) Lower transistor on

(c) Both transistors off

Blanking / interlocking time: positive load current

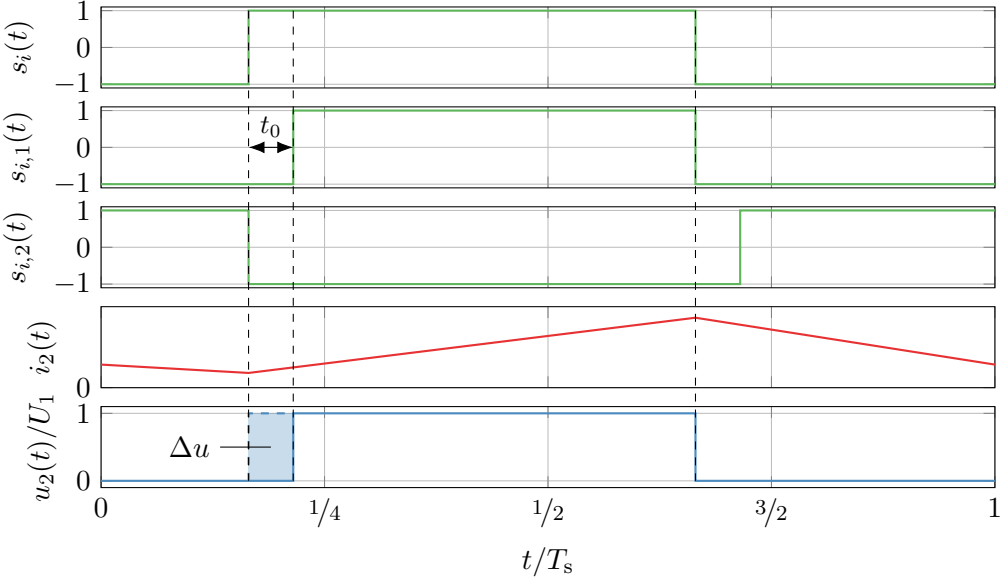

Blanking / interlocking time: negative load current

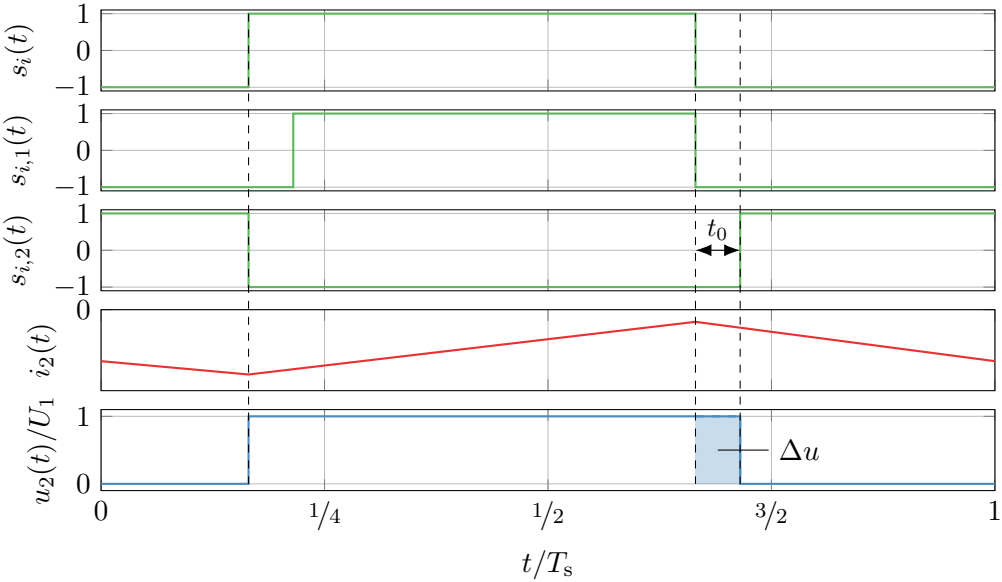

Blanking / interlocking time: discontinuous conduction

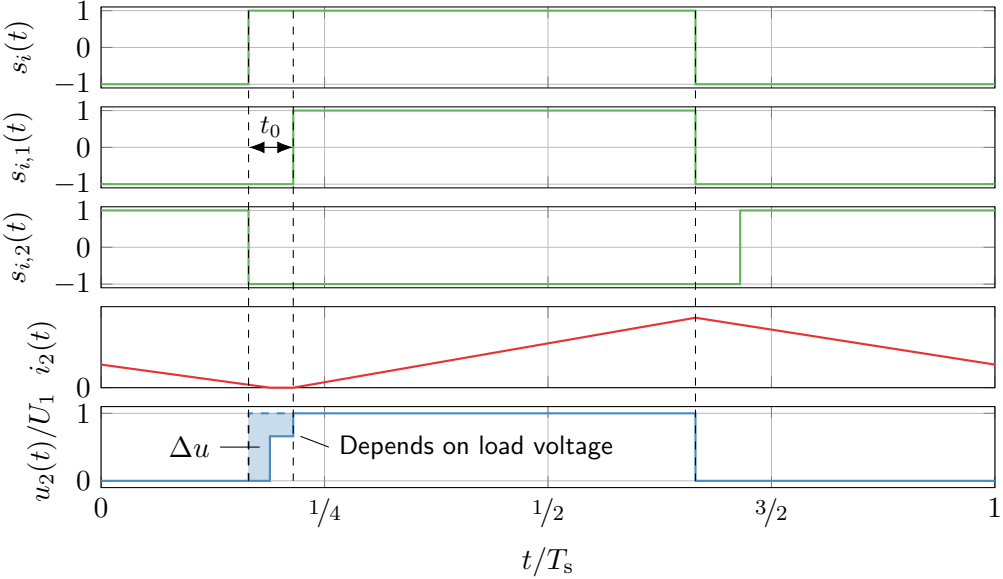

Blanking / interlocking time (cont.)

For the continuous conduction case, the voltage error Δu due to the interlocking time t_0 is given by

$$\Delta u = \overline{u}_2 - U_1 s^* = -\mathrm{sgn}(i_2)\frac{t_0}{T_\mathrm{s}}U_1 = -\mathrm{sgn}(i_2)t_0 f_\mathrm{s} U_1. \tag{12.14}$$

Hence, the error depends on the relative duration of the interlocking time t_0 compared to the switching period T_s which is a device-specific parameter (cf. below).

Device type	t_0	f_s
GTO	$10\,\mu\mathrm{s} - 30\,\mu\mathrm{s}$	$200\,\mathrm{Hz} - 500\,\mathrm{Hz}$
IGBT	$2\,\mu\mathrm{s} - 4\,\mu\mathrm{s}$	$5\,\mathrm{kHz} - 20\,\mathrm{kHz}$
MOSFET	$\leq 1\,\mu\mathrm{s}$	$20\,\mathrm{kHz} - 1000\,\mathrm{kHz}$

Tab. 12.1: Typical interlocking times and switching frequencies for different power semiconductor devices

Outlook: multi-level converters

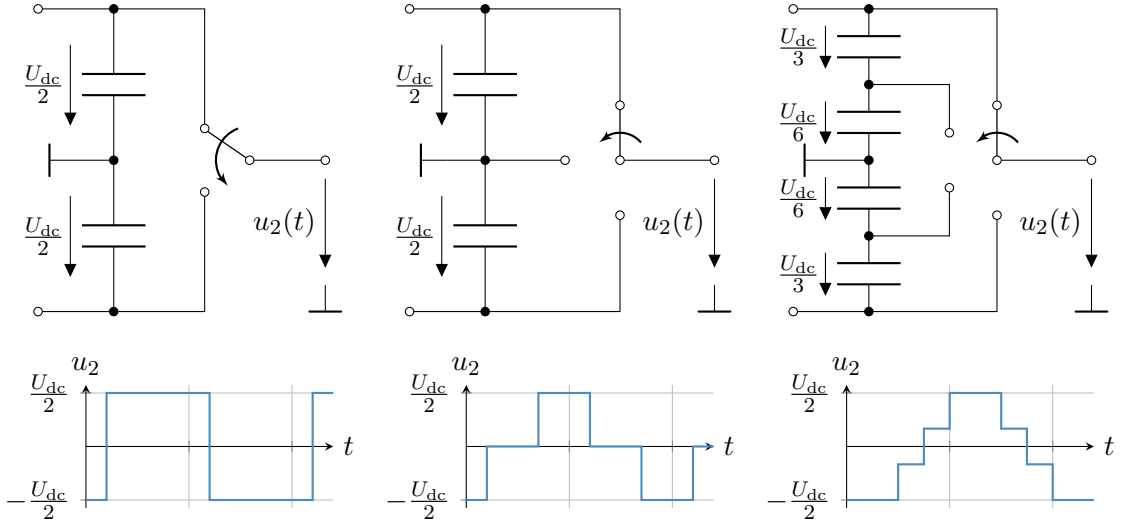

(a) 2-level half bridge (b) 3-level half bridge (c) 4-level half bridge

Table of contents

Rectifier application setup

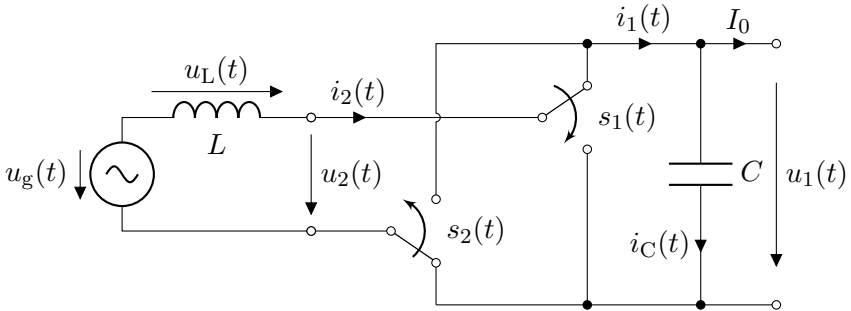

Fig. 12.13: Single-phase grid rectification: full bidirectional operation possible (e.g., for electrical rail vehicles with a $15\,\mathrm{kV}$, $16\frac{2}{3}\,\mathrm{Hz}$ grid). Note: converter topology is flipped to align u_2 with the AC grid side while u_1 is the DC output. Also known as active front end (AFE) rectifier.

Steady-state operation

Assuming steady state, the grid side input loop from Fig. 12.13 can be described with complex phasors:

$$\underline{\hat{u}}_2 = \underline{\hat{u}}_\mathrm{g} - \mathrm{j}\omega L \underline{\hat{i}}_2. \tag{12.15}$$

The converter's input voltage amplitude is

$$\hat{u}_2 = \sqrt{\hat{u}_\mathrm{g}^2 + \left(\omega L \hat{i}_2\right)^2}. \tag{12.16}$$

As the converter boosts the grid voltage towards the DC-link, the following condition must apply:

$$u_1(t) \approx U_\mathrm{dc} \geq \hat{u}_2 = \sqrt{\hat{u}_\mathrm{g}^2 + \left(\omega L \hat{i}_2\right)^2}. \tag{12.17}$$

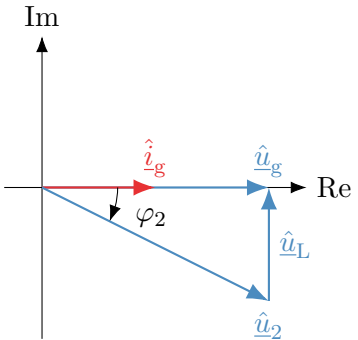

Fig. 12.14: Steady-state phasor diagram assuming $\cos(\varphi) = 1$ operation (enforced via some supervisory control)

Steady-state operation (cont.)

With the assumption of $\cos(\varphi) = 1$ operation and a lossless converter, the following relations hold:

$$P = P_1 = P_2 = P_\mathrm{g} = U_\mathrm{g} I_\mathrm{g} = \frac{1}{2} \hat{u}_\mathrm{g} \hat{i}_\mathrm{g}. \tag{12.18}$$

While there is no reactive power exchange with the grid, the converter needs to supply the reactive power Q_2 to compensate for the line inductance demand:

$$Q_2 = \omega L I_\mathrm{g}^2. \tag{12.19}$$

The resulting apparent power S_2 is

$$S_2 = \sqrt{P^2 + Q_2^2} = \sqrt{P^2 + \left(\omega L I_\mathrm{g}^2\right)^2} = \sqrt{P^2 + \left(\frac{\omega L}{U_\mathrm{g}^2} P^2\right)^2} = P \sqrt{1 + \left(\frac{\omega L}{U_\mathrm{g}^2} P\right)^2}. \tag{12.20}$$

Steady-state operation (cont.)

Neglecting the switching-induced current and voltage ripples, the instantaneous grid power is

$$p_{\mathrm{g}}(t) = u_{\mathrm{g}}(t) i_{\mathrm{g}}(t) = \hat{u}_{\mathrm{g}} \hat{i}_{\mathrm{g}} \cos^2(\omega t) = P + P\cos(2\omega t). \tag{12.21}$$

The instantaneous converter power at its AC input is

$$\begin{aligned} p_2(t) &= u_2(t) i_2(t) = \left(u_{\mathrm{g}}(t) + u_{\mathrm{L}}(t)\right) i_{\mathrm{g}}(t) = \left(u_{\mathrm{g}}(t) + L\frac{\mathrm{d}}{\mathrm{d}t} i_{\mathrm{g}}(t)\right) i_{\mathrm{g}}(t) \\ &= \hat{u}_{\mathrm{g}} \hat{i}_{\mathrm{g}} \cos^2(\omega t) + \omega L \hat{i}_{\mathrm{g}}^2 \sin(\omega t)\cos(\omega t) \\ &= P\left(1 + \cos(2\omega t)\right) + Q_2 \sin(2\omega t) = P + S_2 \cos(2\omega t - 2\varphi_2) \end{aligned} \tag{12.22}$$

with φ_2 being the phase angle between $i_2(t)$ and $u_2(t)$. Hence, the converter power oscillates at twice the grid frequency with an amplitude of S_2. As $S_2 > P$ applies, the instantaneous output power gets temporarily negative as a result of the reactive power compensation on the grid input side.

Steady-state operation (cont.)

Assuming a nearly constant DC-link voltage $u_1(t) \approx U_{\mathrm{dc}}$, the converter DC-side current $i_1(t)$ oscillates as well:

$$i_1(t) = \frac{p_1(t)}{U_{\mathrm{dc}}} = \frac{p_2(t)}{U_{\mathrm{dc}}} = \frac{P}{U_{\mathrm{dc}}} + \frac{S_2}{U_{\mathrm{dc}}} \cos(2\omega t - 2\varphi_2). \tag{12.23}$$

For a constant load current

$$I_0 = \frac{P}{U_{\mathrm{dc}}},$$

the converter's output current can be rewritten as

$$i_1(t) = I_0 \left(1 + \sqrt{1 + \left(\frac{\omega L U_{\mathrm{dc}}}{U_{\mathrm{g}}^2} \right)^2} \cos(2\omega t - 2\varphi_2) \right). \tag{12.24}$$

Consequently, the DC-link capacitor carries the harmonic current content:

$$i_{\mathrm{C}}(t) = i_1(t) - I_0 = I_0 \sqrt{1 + \left(\frac{\omega L U_{\mathrm{dc}}}{U_{\mathrm{g}}^2} \right)^2} \cos(2\omega t - 2\varphi_2). \tag{12.25}$$

Steady-state operation (cont.)

Assuming that the voltage ripple of the DC-link capacitor does not significantly affect the output current, the voltage oscillation amplitude can be approximated as:

$$\hat{u}_{\mathrm{C}} = \hat{u}_1 \approx \frac{\hat{i}_1}{2\omega C} = \frac{I_0}{2C}\sqrt{1 + \left(\frac{\omega L U_{\mathrm{dc}}}{U_{\mathrm{g}}^2} I_0\right)^2}. \tag{12.26}$$

This relation results from the complex phasor analysis of the capacitor's impedance given the current ripple (12.25). From (12.26) one can

- derive the required DC-link capacitance for a given voltage ripple,
- estimate the voltage ripple for a given DC-link capacitance.

Steady-state operation (cont.)

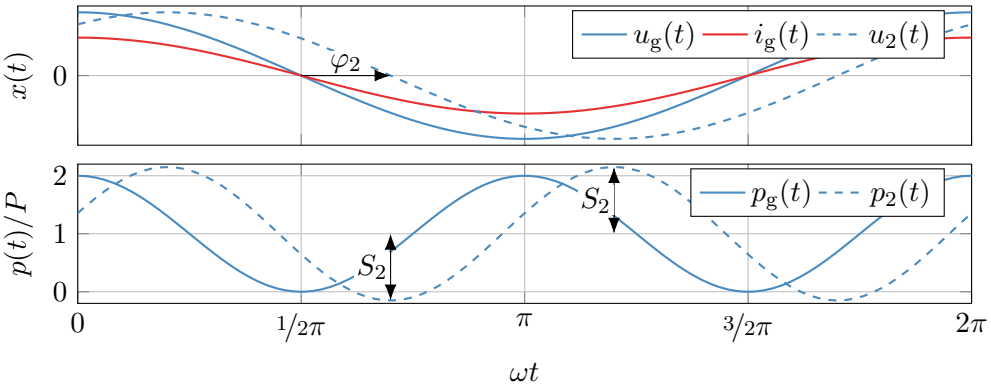

Fig. 12.15: Steady-state operation of the single-phase four-quadrant rectifier: (top) individual signals and (bottom) power oscillations at twice the grid frequency

Table of contents

Idealized switch representation of a three-phase AC/DC bridge converter

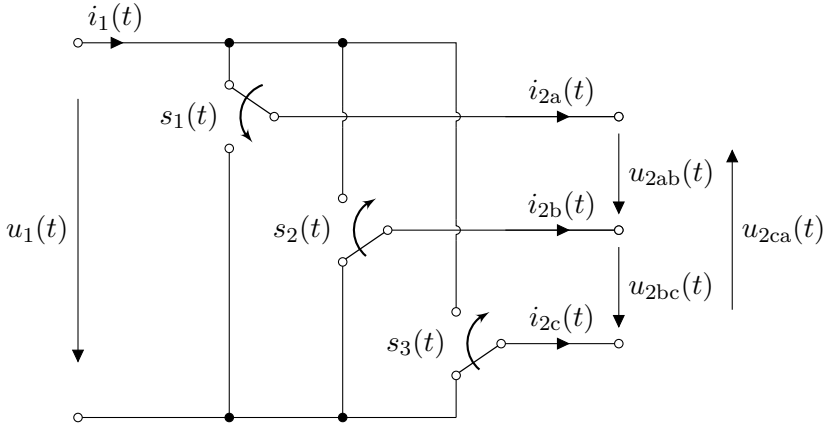

Fig. 12.16: Idealized switch representation of a three-phase two-level AC/DC bridge converter

Circuit realization

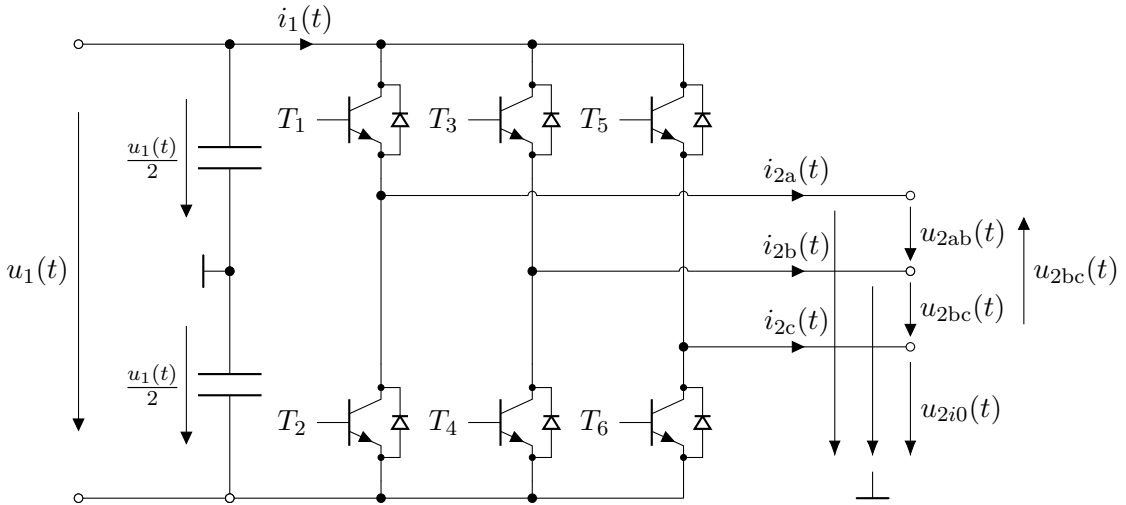

Fig. 12.17: Three-phase two-level AC/DC converter

Switching states and load-independent output voltages

Reutilizing the switching function definition (12.1), the line-to-line voltages can be expressed as

$$\begin{aligned} u_{2\mathrm{ab}}(t) &= \frac{1}{2}\left(s_{\mathrm{a}}(t) - s_{\mathrm{b}}(t)\right) u_1(t), \\ u_{2\mathrm{bc}}(t) &= \frac{1}{2}\left(s_{\mathrm{b}}(t) - s_{\mathrm{c}}(t)\right) u_1(t), \\ u_{2\mathrm{ca}}(t) &= \frac{1}{2}\left(s_{\mathrm{c}}(t) - s_{\mathrm{a}}(t)\right) u_1(t). \end{aligned} \tag{12.27}$$

The line-to-ground voltages are given by

$$\begin{aligned} u_{2\mathrm{a0}}(t) &= \frac{1}{2} s_{\mathrm{a}}(t) u_1(t), \\ u_{2\mathrm{b0}}(t) &= \frac{1}{2} s_{\mathrm{b}}(t) u_1(t), \\ u_{2\mathrm{c0}}(t) &= \frac{1}{2} s_{\mathrm{c}}(t) u_1(t). \end{aligned} \tag{12.28}$$

Three-phase converter with symmetric load in star connection

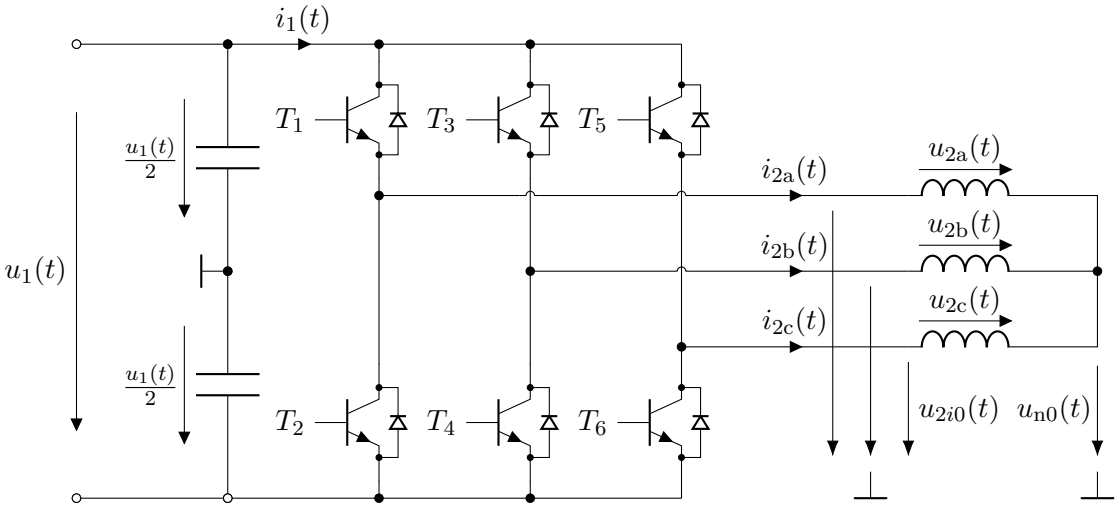

Fig. 12.18: Three-phase two-level AC/DC converter with symmetric load in star connection

Three-phase converter with symmetric load in star connection (cont.)

Assuming a star-connected load, the three-phase currents sum up to zero:

$$i_{2\mathrm{a}}(t) + i_{2\mathrm{b}}(t) + i_{2\mathrm{c}}(t) = 0. \tag{12.29}$$

If the star point is not connected to ground, $u_{\mathrm{n}0}(t) \neq 0$ may occur leading to a load voltage of

$$u_{2\mathrm{a}}(t) = u_{2\mathrm{a}0}(t) - u_{\mathrm{n}0}(t), \quad u_{2\mathrm{b}}(t) = u_{2\mathrm{b}0}(t) - u_{\mathrm{n}0}(t), \quad u_{2\mathrm{c}}(t) = u_{2\mathrm{c}0}(t) - u_{\mathrm{n}0}(t). \tag{12.30}$$

To calculate $u_{\mathrm{n}0}(t)$ one can utilize the load equation (assuming an inductive load):

$$u_{2i}(t) = L\frac{\mathrm{d}}{\mathrm{d}t} i_{2i}(t) + u_{\mathrm{n}0}(t) \tag{12.31}$$

summing up to

$$3u_{\mathrm{n}0}(t) + L\frac{\mathrm{d}}{\mathrm{d}t}\left(i_{2\mathrm{a}}(t) + i_{2\mathrm{b}}(t) + i_{2\mathrm{c}}(t)\right) = u_{2\mathrm{a}0}(t) + u_{2\mathrm{b}0}(t) + u_{2\mathrm{c}0}(t) \tag{12.32}$$

and finally delivering the star-to-ground voltage as

$$u_{\mathrm{n}0}(t) = \frac{1}{3}\left(u_{2\mathrm{a}0}(t) + u_{2\mathrm{b}0}(t) + u_{2\mathrm{c}0}(t)\right). \tag{12.33}$$

Three-phase converter with symmetric load in star connection (cont.)

No.	s_a	s_b	s_c	$\frac{u_{2a0}}{u_1}$	$\frac{u_{2b0}}{u_1}$	$\frac{u_{2c0}}{u_1}$	$\frac{u_{2a}}{u_1}$	$\frac{u_{2b}}{u_1}$	$\frac{u_{2c}}{u_1}$	$\frac{u_{ab}}{u_1}$	$\frac{u_{bc}}{u_1}$	$\frac{u_{ca}}{u_1}$	$\frac{u_{n0}}{u_1}$
0	-1	-1	-1	$-\frac{1}{2}$	$-\frac{1}{2}$	$-\frac{1}{2}$	0	0	0	0	0	0	$-\frac{1}{2}$
1	$+1$	-1	-1	$+\frac{1}{2}$	$-\frac{1}{2}$	$-\frac{1}{2}$	$+\frac{2}{3}$	$-\frac{1}{3}$	$-\frac{1}{3}$	$+1$	0	-1	$-\frac{1}{6}$
2	$+1$	$+1$	-1	$+\frac{1}{2}$	$+\frac{1}{2}$	$-\frac{1}{2}$	$+\frac{1}{3}$	$+\frac{1}{3}$	$-\frac{2}{3}$	0	$+1$	-1	$+\frac{1}{6}$
3	-1	$+1$	-1	$-\frac{1}{2}$	$+\frac{1}{2}$	$-\frac{1}{2}$	$-\frac{1}{3}$	$+\frac{2}{3}$	$-\frac{1}{3}$	-1	$+1$	0	$-\frac{1}{6}$
4	-1	$+1$	$+1$	$-\frac{1}{2}$	$+\frac{1}{2}$	$+\frac{1}{2}$	$-\frac{2}{3}$	$+\frac{1}{3}$	$+\frac{1}{3}$	-1	0	$+1$	$+\frac{1}{6}$
5	-1	-1	$+1$	$-\frac{1}{2}$	$-\frac{1}{2}$	$+\frac{1}{2}$	$-\frac{1}{3}$	$-\frac{1}{3}$	$+\frac{2}{3}$	0	-1	1	$-\frac{1}{6}$
6	$+1$	-1	$+1$	$+\frac{1}{2}$	$-\frac{1}{2}$	$+\frac{1}{2}$	$+\frac{1}{3}$	$-\frac{2}{3}$	$+\frac{1}{3}$	1	-1	0	$+\frac{1}{6}$
7	$+1$	$+1$	$+1$	$+\frac{1}{2}$	$+\frac{1}{2}$	$+\frac{1}{2}$	0	0	0	0	0	0	$+\frac{1}{2}$

Tab. 12.2: Switching states and resulting voltages of the three-phase two-level AC/DC converter with symmetric load in star connection (with $2^3 = 8$ possible switching states)

Three-phase fundamental frequency modulation (aka six-step mode)

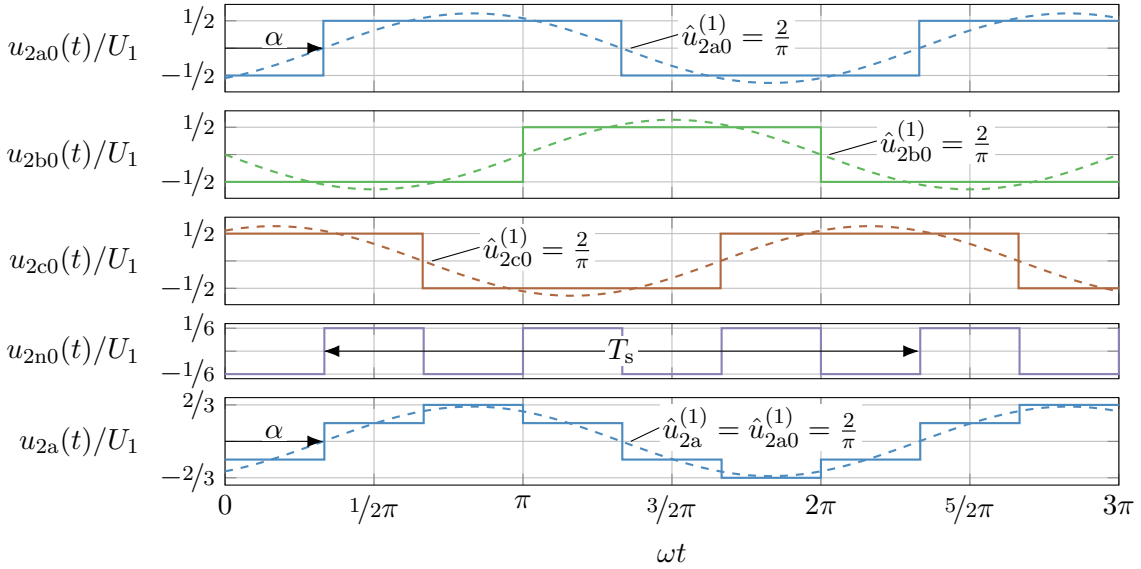

Three-phase fundamental frequency modulation (cont.)

From the previous figure and voltage equations, we can summarize the following observations:

- Due to the fundamental frequency modulation, the switching frequency of the inverter is identical to the fundamental frequency: $f_{\mathrm{s}} = \omega/2\pi$.
- The star-to-ground voltage $u_{\mathrm{n}0}(t)$ shows a rectangular signal pattern with triple fundamental frequency.
- Consequently, it does not influence the fundamental output voltage, that is, the fundamental components of the line-to-ground voltage $u_{2i0}(t)$ as well as the load voltage $u_{2i}(t)$ are identical: $\hat{u}_{2i0}^{(1)} = \hat{u}_{2i}^{(1)}$.

Note on the star point

The previous analysis assumed a non-connected star point, which comes with certain advantages, e.g., on the rejection of current harmonics. If, however, the star point would be connected, the three-phase converter can be interpreted and analyzed as three independent single-phase converters (each driven by a half bridge).

Three-phase pulse width modulation (PWM)

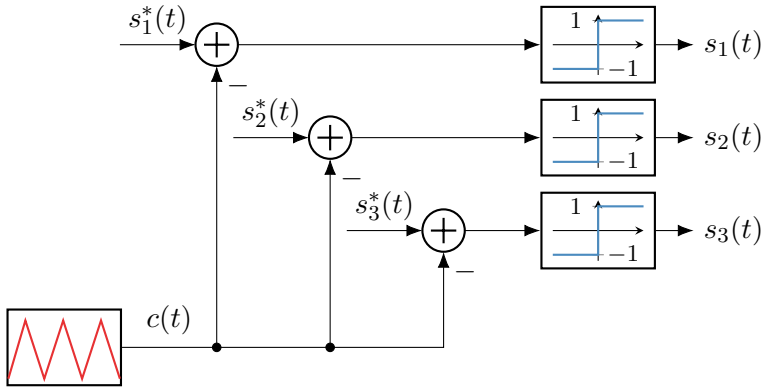

Fig. 12.19: Three-phase PWM (note: a distinction between interleaved and complementary PWM is not relevant here, as the three-phase converter operates on a half-bridge basis while the previously considered single-phase converter was based on a full bridge. While independent and phase-shifted carriers per phase could be also used in the three-phase converter, this is typically not utilized due to increasing current harmonics.)

Three-phase PWM example (with ref. modulation index $m = 0.5$)

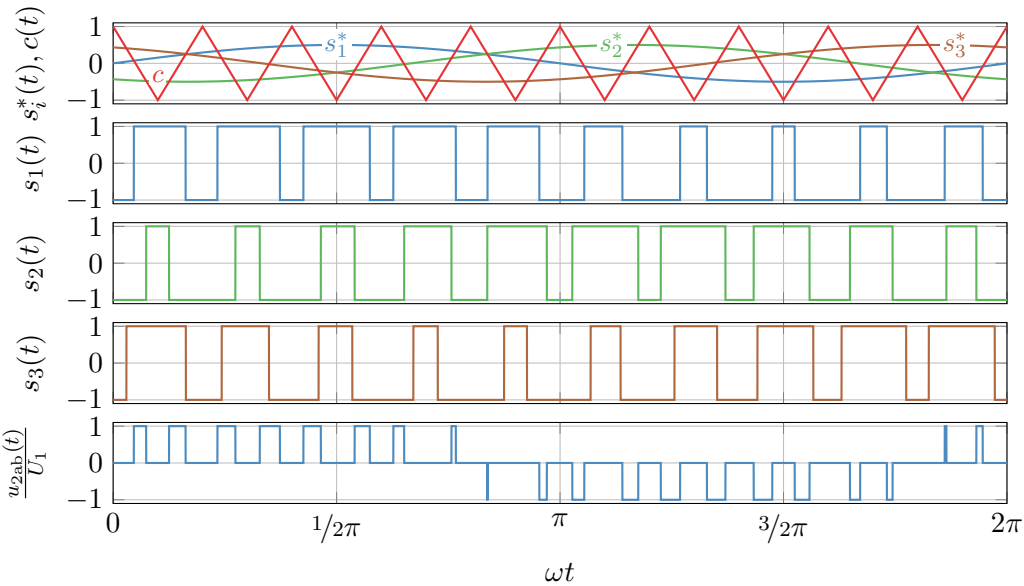

Three-phase PWM example (with ref. modulation index $m = 1$)

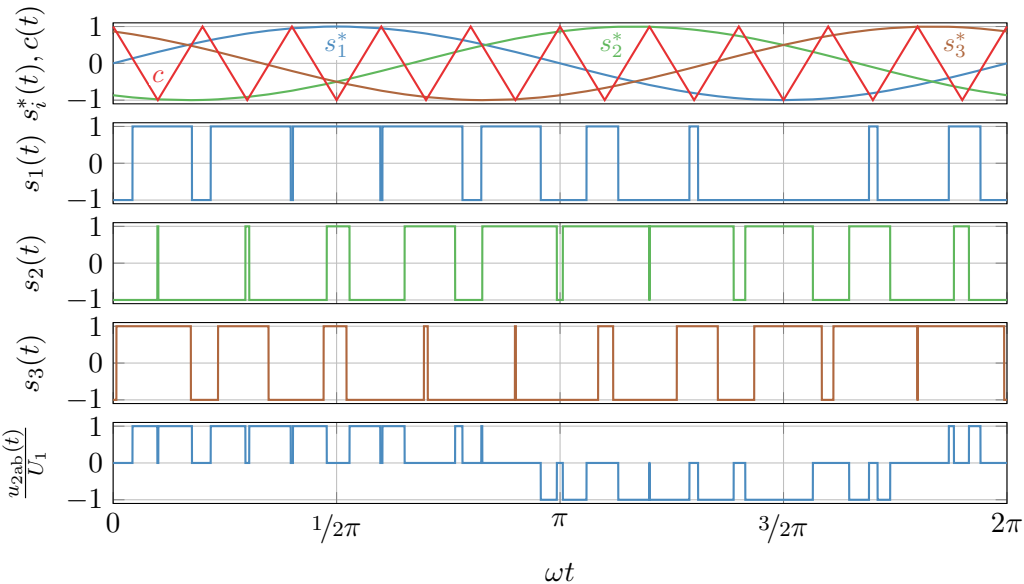

Three-phase PWM example (with ref. modulation index $m = 1.18$)

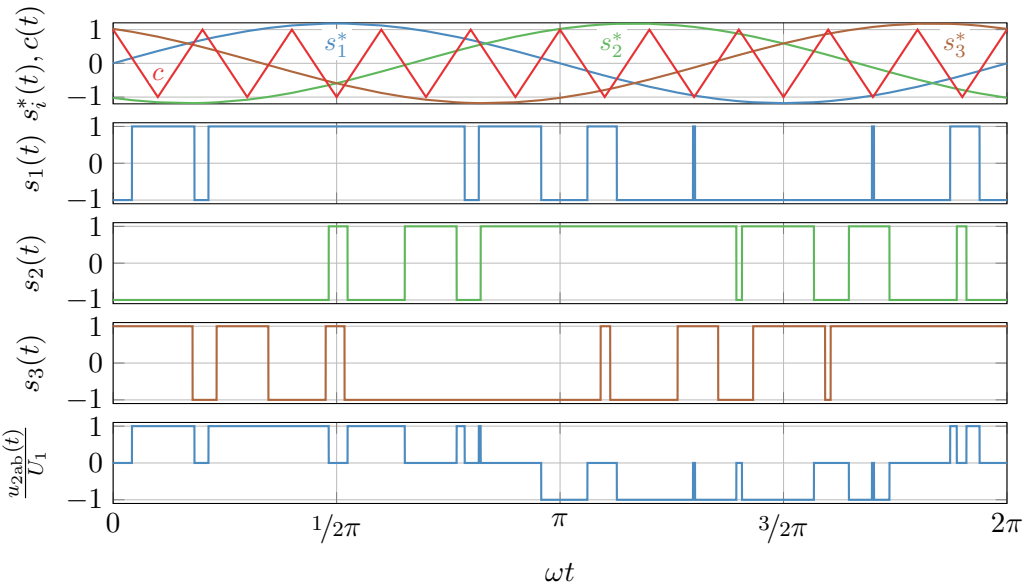

Section summary

This section provided an introduction to transistor-based AC/DC converters. The key takeaways are:

- They render themselves (half/full) bridge topologies as already known from the DC/DC converter context.
- Can transfer power in both directions and handle all four quadrants on the AC side.
- Require modulation strategies to generate the desired output voltage:
  - High switching frequency PWM (low harmonics, below maximum conv. utilization) or
  - Low switching frequency fundamental modulation (max. utilization, but high harmonics).
- The output voltage amplitude and phase angle can be adjusted to achieve arbitrary power factors for grid operation or to supply various loads such as DC or AC motors.

While this section only covered a very brief overview about these self-commutated converters, the following aspects are, among other, important for practical applications:

- closed-loop control,
- Further modulation strategies (e.g., space vector modulation or optimized pulse pattern),
- converters with a current source (instead of voltage source) within the DC link.

English-German dictionary

Bikash Sah

English-German dictionary I

AC machine	Wechselstrommaschine
acceleration	Beschleunigung
active power	Wirkleistung
air gap	Luftspalt
angle	Winkel
apparent power	Scheinleistung
armature	Anker / Läufer
autotransformer	Spartransformator
braking	bremsend
brush	Bürste
brushless	bürstenlos

English-German dictionary II

capacitance	Kapazität [Größe]
capacitor	Kondensator [Bauelement]
circuit	Schaltkreis
commutation	Kommutierung
compensation winding	Kompensationswicklung
conductance	Leitwert
conductivity	Leitfähigkeit
control	Regelung
copper	Kupfer
current	Strom
damper winding	Dämpferwicklung
DC machine	Gleichstrommaschine

English-German dictionary III

differential equation	Differentialgleichung
displacement	Verschiebung
displacement current	Verschiebestrom
displacement field	Elektrische Flussdichte
drive	Antrieb
driving	antreibend
eddy currents	Wirbelströme
efficiency	Wirkungsgrad
energy	Energie
equivalent circuit diagram	Ersatzschaltbild
excitation	Erregung
fan	Lüfter

English-German dictionary IV

fed-in winding	Träufelwicklung
field	Feld
field weakening	Feldschwächung
field winding	Erreger(-wicklung)
flux	Fluss
flux linkage	Flussverkettung
force	Kraft
form-wound winding	Formspulenwicklung
frequency	Frequenz
friction	Reibung
fundamental wave	Grundwelle
heat	Wärme

English-German dictionary V

inductance	Induktivität [Größe]
induction machine	Asynchronmaschine
inductor	Spule [Bauelement]
innere voltage	Polradspannung
interpoles	Wendepolwicklung
inverter	Wechselrichter
iron	Eisen
jerk	Ruck
lap winding	Schleifenwicklung
leakage	Streuung
load	Last / Belastung
losses	Verluste

English-German dictionary VI

machine	Maschine
magnetic domain	Weiss-Bezirk
magnetomotive force	magnetische Spannung
mass	Masse
momentum	Impuls
nameplate	Typenschild
oscillation [quantity depending on time]	Schwingung [Größe in Zeit]
permanent magnet	Permanentmagnet
permeance	Permeanz
phasor	Zeitunabh. komplexer Zeiger
power	Leistung
power electronics	Leistungselektronik

English-German dictionary VII

power factor	Leistungsfaktor
reactive power	Blindleistung
rectifier	Gleichrichter
reluctance	Reluktanz
resistance	Widerstand [Größe]
resistor	Widerstand [Bauelement]
root mean square	Effektivwert
rotor	Rotor
salient pole rotor	Schenkelpolläufer
saturation	Sättigung
separately excited DC machine	Fremderregte Gleichstrommaschine
series DC machine	Reihenschlussmaschine

English-German dictionary VIII

shaft	Welle
shut DC machine	Nebenschlussmaschine
slip	Schlupf
slip ring	Schleifring
slot	Nut
slot wedge	Nutkeil
speed	Geschwindigkeit
squirrel cage	Käfigläufer
starting torque	Anlaufdrehmoment
stator	Stator
steady state	Stationärer Zustand
steel	Stahl

English-German dictionary IX

synchronous machine	Synchronmaschine
tap	Anzapfung
terminal	Anschlussfeld
three phase machine	Drehstrommaschine
torque	Drehmoment
transformer	Transformator
transient	Transienter Zustand
turn	Windung
unit	Maßeinheit
velocity	Geschwindigkeit
voltage	Spannung
wave [quantity depending on time and space]	Welle [Größe in Zeit und Raum]

English-German dictionary X

wave winding . . . . . Wellenwicklung

windage . . . . . Luftwiderstand

work . . . . . Arbeit

yoke . . . . . Joch